THÈSE

En vue de l'obtention du

DOCTORAT DE L'UNIVERSITÉ DE TOULOUSE

Délivré par :

Université Toulouse 3 Paul Sabatier (UT3 Paul Sabatier)

Présentée et soutenue par :
DINH THE MANH
le lundi 26 mai 2014

Titre :

Contribution au développement de béton de chanvre préfabriqué
utilisant un liant pouzzolanique innovant
Contribution to the development of precast hempcrete
using innovative pozzolanic binder

École doctorale et discipline ou spécialité :
ED MEGEP : Génie civil

Unité de recherche :
Laboratoire Matériaux et Durabilité des Constructions

Directeur(s) de Thèse :
Prof. Gilles ESCADEILLAS
Dr. Camille MAGNIONT
Dr. Marie COUTAND

Jury :

Prof. Sofiane AMZIANE	Polytech'Clermont-Ferrand	Président du jury
Prof. Luc COURARD	University of Liège	Rapporteur
Dr. Mohamed SONEBI	Queen's University Belfast	Rapporteur
Prof. Gilles ESCADEILLAS	Université de Toulouse III	Examinateur
Dr. Camille MAGNIONT	Université de Toulouse III	Examinateur
Dr. Marie COUTAND	Université de Toulouse III	Examinateur

ACKNOWLEDGEMENT

The research work reported in this thesis has been performed in the Laboratory of Materials and Durability of Constructions (LMDC) Toulouse, France.

Doing research and writing a thesis is the result of the efforts of not only one person, but many. Thus, I would like to thank all of them for their direct or indirect contribution to this work by providing guidance, constructive comments and technical support or encouragement and support.

First of all, I would like to express my sincere gratitude to Professor Gilles Escadeillas, Head of LMDC, for having given me the opportunity to work on this research work in LMDC, an excellent working environment with good facilities and nice colleagues.

I am deeply indebted to my supervisors Gilles Escadeillas, Camille Magniont and Marie Coutand for their suggestions, advices and for sharing their knowledge and research skills.

I would like to express my gratitude to the members of the thesis defense committee, Professor Sofiane Amziane from Polytech' Clermont-Ferrand, a school of Blaise Pascal University, Professor Luc Courard from University of Liège, Belgium and Senior lecturer Mohamed Sonebi from Queen's University Belfast, Northern Ireland, UK for their interest in my research work and the time and effort they put into reading this thesis.

I would like to thank to LMDC technical staffs for their good cooperation and devoted assistance throughout the experimental part of this study.

The Education and Training Ministry, Vietnam and LMDC are gratefully acknowledged for their financial support to this research study.

I would like to thank all of my colleagues – former and present - for the good work environment and the fruitful discussions we had during my time at LMDC Toulouse.

At a personal level, I wish to especially thank my parents for everything they have done to help me reach this point. I also wish to mention a special thanks to Nguyen Thi Minh Hai, my wife, for helping me with every single facet of this effort and showing constant patience throughout this journey.

REMERCIEMENTS

Ce travail a été accompli au sein du Laboratoire Matériaux et Durabilité des Constructions (LMDC) de Toulouse, France.

Réaliser un travail de recherche et rédiger une thèse est le résultat des efforts non seulement d'une personne, mais de plusieurs. Je tiens à remercier toutes ces personnes pour leur contribution directe ou indirecte à ce travail en fournissant des conseils, des commentaires constructifs et un support technique ou en apportant leur encouragement et leur soutien.

Tout d'abord, je tiens à exprimer ma sincère gratitude au Professeur Gilles Escadeillas, Directeur du LMDC, pour m'avoir donné l'occasion de travailler sur cette étude de recherche au sein du LMDC, un excellent environnement de travail avec de bonnes installations et de bons collègues.

Je suis également très reconnaissant envers mes superviseurs Gilles Escadeillas, Camille Magniont et Marie Coutand pour leurs suggestions, conseils, encouragements et pour le partage de leurs connaissances et de leurs compétences.

Je tiens à exprimer ma gratitude aux membres de jury, Professeur Sofiane Amziane de Polytech' Clermont-Ferrand, une école de Université Blaise Pascal, Professeur Luc Courard de Université de Liège, Belgique et Docteur Mohamed Sonebi de l'Université Queen's Belfast, Irlande du Nord, Royaume-Uni de leur intérêt pour mon travail de recherche, du temps et des efforts qu'ils ont consacrés à l'expertise de cette thèse.

Je tiens à remercier les personnels techniques du LMDC pour leur bonne coopération et assistance tout au long de la partie expérimentale de cette étude.

J'adresse toute ma reconnaissance au Ministère de l'Education et de la Formation du Vietnam et au LMDC de Toulouse pour le soutien financier accordé pour cette étude.

Je tiens à remercier tous mes collègues - anciens et actuels - pour le bon environnement de travail qu'ils ont créé et pour les discussions fructueuses que nous avons eues pendant mon séjour au LMDC.

Personnellement, je tiens à remercier tout particulièrement mes parents pour tout ce qu'ils ont fait pour m'aider à parvenir au point où j'en suis aujourd'hui. Je tiens également à adresser à NGUYEN Thi Minh Hai, ma femme, une attention toute spéciale pour m'avoir aidé et avoir fait preuve de patience constante tout au long de ce voyage.

ABSTRACT

This study is part of a project aiming to develop biosourced material that satisfies sustainable development in the construction area. The object of the study is to develop a new pozzolanic binder and to characterize the hempcrete fabricated from this binder and plant aggregates (hemp shives). Hemp shives are the ligneous particles extracted from hemp stem as a co-product of the process of hemp fiber extraction. The physical properties of the hemp shives, such as particle size distribution, water absorption, bulk density and thermal conductivity are assessed. The formulations of the new pozzolanic binder are based on a mix of hydraulic or slaked lime, flash metakaolin and some admixtures. The mechanical and thermal properties of the hempcrete composite are then tested.

The study concludes that the new pozzolanic binder not only presents high mechanical performance from an early age but can also be considered as an eco-material. The hempcrete made of hemp shives and pozzolanic matrix will also have considerable potential as an eco-material with the new properties achieved such as a reduction of water absorption, an improvement of mechanical performance and a good capacity of thermal insulation.

Résumé

Cette étude s'inscrit dans le cadre d'un projet visant à développer un matériau biosourcé satisfaisant aux critères du développement durable dans le domaine de la construction. L'objectif de cette étude est de développer un nouveau liant pouzzolanique et de caractériser le béton de chanvre fabriqué à partir de ce liant et de granulats végétaux (chènevotte). La chènevotte, qui correspond à la partie ligneuse extraite de la tige du chanvre, est un co-produit du processus d'extraction de la fibre de chanvre. Les propriétés physiques de la chènevotte, telles que la distribution granulométrique, l'absorption d'eau, la densité en vrac et la conductivité thermique ont été évaluées. Les formulations des nouveaux liants pouzzolaniques sont basées sur une combinaison de chaux hydraulique ou de chaux éteinte, de métakaolin flash et d'adjuvants. Les propriétés mécaniques et thermiques du béton de chanvre ont ensuite été testées.

L'étude conclut que le nouveau liant pouzzolanique présente non seulement de bonnes performances mécaniques à jeune âge, mais peut aussi être considéré comme un éco-matériau. Le béton de chanvre utilisant la chènevotte et cette matrice pouzzolanique a aussi un potentiel considérable en tant qu'éco-matériau avec de nouvelles propriétés comme la réduction de l'absorption d'eau, l'amélioration des performances mécaniques et une bonne capacité d'isolation thermique.

Table of content

GENERAL INTRODUCTION

In recent decades, we have been faced global environmental challenges including climate change, pollution, environmental degradation due to human activities on a global scale in different fields such as industry, energy, transport, construction etc. Thus, in order to protect environment, it is necessary to integrate all projects into an approach of sustainable development all over the world.

The construction sector has been known as a field that consumes the largest total energy in the world [BIN12] and emits the second largest global amount of CO_2 after industry [FRI06] in comparison with other activities. This demonstrates that construction sector is one of the fields that have caused the most negative impact on the environment. In the construction field, the production of building materials is considered as the much large CO_2 emission and energy consumption, especially Portland cement production; therefore, it is necessary to study to integrate the production of building materials into an approach of sustainable development. Thus, the new building materials need to be developed to replace the conventional materials. These new materials, whose productions need to satisfy conditions for environment and people's health, and for their properties must be improved as much as possible.

Moreover, plant co-products in general, and hemp shives in particular, have been used to fabricate new materials for wall thermal insulation, which not only provide good thermal insulation, but also a limited impact on the environment and a low cost. Previous studies [ARG10 & SAN11] also showed that flash metakaolin (MK) is considered as an eco-material because its production process consumes far less energy than that of cement and emits very little CO_2. Another study [MAG10b] showed the potential pozzolanic binder using high content of flash metakaolin and hydraulic lime, which was used to fabricate hempcrete with hemp shives, and the properties of this hempcrete were comparable with those found in literature.

Thanks to the important advantage of flash metakaolin (MK) and hempcrete for environment, the principal objective of this thesis is the development of eco-materials for construction. In this study, we will develop new pozzolanic binders using MK and fabricate hempcrete made of one of these new binders and hemp shives. For the new pozzolanic binders, we will optimize the mineral raw materials (MK and natural hydraulic lime - NHL3.5 or slaked lime). To improve the mechanical strength of these new binders at early age, some of admixtures (glycerol carbonate, K_2SO_4 and superplasticizer) will be

used. For the hempcrete, in order to reduce the water absorption capacity of hemp shives, hemp shives will be treated by the pozzolanic binder before fabrication of hempcrete. This can limit the drawback due to the soluble extractives from hemp shives, and may consequently improve the mechanical properties of hempcrete. On the other hand, the properties of our pozzolanic binder and our hempcrete will be compared with those of commercial binder and hempcrete using commercial binder respectively. This thesis is composed of four chapters as following.

In the literature review chapter, we will present the negative influences of the construction sector on the environment in order to show that the sustainable development is necessary in construction field, especially in the materials production. The perspective building materials will be also introduced. The following parts of this chapter review the use of binders being considered as eco-binders against Portland cement and of hemp shives in previous studies, and synthesize the recent works on the production methods and the properties of hempcrete. At the end of this chapter, the framework of this thesis will be presented.

The second chapter will first describe the methods used in this study in order to characterize the raw materials and the properties of hempcrete. The mineralogical components of natural hydraulic lime – NHL3.5, slaked lime and flash metakaolin will be analyzed, and their hydration mechanisms will be also described. Moreover, we will also present the characteristics of the admixtures (glycerol carbonate, potassium sulfate and superplasticizer), which are used to improve performances of pozzolanic binder. At the end of this chapter, the properties of hemp shives such as bulk density, thermal conductivity, water absorption and particle size distribution will be characterized.

The third chapter is composed of two parts to develop the new pozzolanic binders. In the first part, the raw materials for two kinds of pozzolanic binders will be optimized based on the mechanical properties. In the other part, we will study the influence of the admixtures on these pozzolanic binders in order to choose the new binders requiring not only improved mechanical properties, especially at early age, but also reduce their dimension variation. Moreover, the mechanisms of hydration of these binders will be characterized by X-ray diffraction and thermogravimetric analyses. Furthermore, the mechanical property of new pozzolanic binders will be compared with that of commercial binder. At the end of this chapter, the properties of standard mortars using new pozzolanic

binders will be tested and compared with those of mortar using commercial binder.

The last chapter will first present the study on the pretreatment of hemp shives and its impact on water absorption of hemp shiv. The following parts of this chapter will present the mechanical behaviors and thermal conductivity of different hempcrete formulations. Moreover, the properties and mineralogical analyses of these hempcretes will be compared with those of the hempcretes using commercial binder.

Finally, general conclusion will be presented to confirm the obtained results in this study, and the future works will be suggested to continuously complete this study as well as to develop other important directions.

INTRODUCTION GENERALE

Depuis quelques décennies, nous sommes confrontés à des enjeux environnementaux globaux tels que le changement climatique, la pollution, la dégradation de l'environnement due aux activités de l'homme, dans différents domaines tels que l'industrie, l'énergie, les transports, la construction, etc. Dorénavant, afin de protéger l'environnement, il est nécessaire d'intégrer tous les projets dans une démarche de développement durable.

Le secteur de la construction est reconnu comme une activité qui consomme la plus grande qualité d'énergie dans le monde [BIN12] et qui émet le deuxième plus grand taux de CO_2, après l'industrie [FRI06], en comparaison avec d'autres activités. Ceci montre que ce secteur de la construction est l'un des domaines qui nuit le plus à l'environnement. Dans le domaine de la construction, la production de matériaux représente une très grande part des émissions de CO_2 et de la consommation d'énergie, particulièrement pour la production de ciments Portland. Par conséquent, des études sont nécessaires pour intégrer la production de matériaux de construction dans une démarche de développement durable. Ainsi, de nouveaux matériaux de construction doivent être développés pour remplacer les matériaux conventionnels. La production de ces nouveaux matériaux devra respecter des critères environnementaux et de confort et santé des usagers. De même, leurs propriétés devront être améliorées autant que possible.

Par ailleurs, les sous-produits végétaux en général, et la chènevotte de chanvre en particulier, ont été utilisés pour fabriquer de nouveaux matériaux qui non seulement fournissent une bonne isolation thermique, mais ont aussi un impact limité sur l'environnement et un faible coût. Des études antérieures [ARG10 & SAN11] ont aussi montré que le métakaolin flash (MK) peut être considéré comme un éco-matériau parce que son processus de production consomme beaucoup moins d'énergie que celle du ciment et émet très peu de CO_2. Une autre étude [MAG10b] a montré le potentiel de liant pouzzolanique, en utilisant une haute teneur de métakaolin flash et de la chaux hydraulique, pour fabriquer un béton de chanvre avec chènevotte. Les propriétés de ce béton étaient comparables à celles trouvées dans la littérature.

Grâce à l'important avantage du métakaolin flash (MK) et du béton de chanvre pour l'environnement, l'objectif principal de cette thèse est le développement d'éco-matériaux pour la construction. Dans cette étude, nous allons développer de nouveaux liants pouzzolaniques utilisant du MK pour formuler un béton de chanvre à base de chènevotte.

Pour ces nouveaux liants pouzzolaniques, nous optimiserons les matières premières minérales (MK et chaux hydraulique naturelle - NHL3.5 ou chaux éteinte). Pour améliorer la résistance mécanique de ces nouveaux liants aux jeunes âges, des adjuvants (carbonate de glycérol, K_2SO_4 et superplastifiant) seront utilisés. De plus, afin de réduire leur capacité d'absorption d'eau, les particules de chènevotte seront traitées au liant pouzzolanique avant la fabrication du béton de chanvre. Cela pourrait aussi limiter l'inconvénient de la modification d'hydratation liée à la solubilisation de produits extractibles de la chènevotte, et devrait permettre d'améliorer les propriétés mécaniques du béton de chanvre. D'autre part, les propriétés de nos liants pouzzolaniques et bétons de chanvre seront comparés avec celles d'un liant commercial et de bétons de chanvre utilisant ce liant. Cette thèse est composée des quatre chapitres suivant.

Dans le chapitre *Etat de l'art*, nous allons présenter les influences négatives du secteur de la construction sur l'environnement afin de montrer que le développement durable est nécessaire au domaine de la construction, en particulier dans la production de matériaux. Les matériaux de construction en perspective de ce travail seront également présentés. Les sections suivantes de ce chapitre examineront l'utilisation de liants, considérés comme éco-liants vis-à-vis du ciment Portland, et de chènevotte, et feront la synthèse des travaux récents sur les méthodes de production et les propriétés des bétons de chanvre. À la fin de ce chapitre, le cadre de cette thèse sera présenté.

Le deuxième chapitre décrira d'abord les méthodes utilisées dans cette étude afin de caractériser les matières premières et les propriétés du béton de chanvre. Les composants minéraux de la chaux hydraulique naturelle (NHL3.5), de la chaux éteinte et du métakaolin flash seront analysés, et leurs mécanismes d'hydratation seront également décrits. En outre, nous présenterons également les caractéristiques des adjuvants (carbonate de glycérol, sulfate de potassium et superplastifiant) utilisés pour améliorer les performances des liants pouzzolaniques. À la fin de ce chapitre, les propriétés de la chènevotte, telles que la densité en vrac, la conductivité thermique, l'absorption d'eau et la granulométrie seront caractérisées.

Le troisième chapitre est composé de deux parties concernant le développement des nouveaux liants pouzzolaniques. Dans la première partie, les matières premières pour deux types de liants pouzzolaniques seront optimisées, en fonction des propriétés mécaniques. Dans la deuxième partie, nous étudierons l'influence des adjuvants sur ces liants

17

pouzzolaniques, afin d'améliorer non seulement leurs propriétés mécaniques, en particulier au jeune âge, mais aussi de réduire leurs variations de dimension. Par ailleurs, les produits d'hydratation de ces liants seront caractérisés par diffraction de rayons X et analyses thermogravimétriques. En outre, les propriétés mécaniques des nouveaux liants pouzzolaniques seront comparées avec celles d'un liant commercial. A la fin de ce chapitre, les propriétés des mortiers normalisés utilisant ces nouveaux liants pouzzolaniques seront déterminées et comparées avec celles de mortiers utilisant un liant commercial.

Le dernier chapitre présentera d'abord l'étude sur le prétraitement de la chènevotte, et son impact vis-à-vis de l'absorption d'eau. Les parties suivantes de ce chapitre présenteront les comportements mécaniques et les conductivités thermiques de différentes formulations de bétons de chanvre. En outre, les propriétés et analyses minéralogiques de ces bétons seront comparées à celles du béton de chanvre utilisant le liant commercial.

Enfin, une conclusion générale sera présentée pour rappeler les résultats obtenus dans le cadre de cette étude, et des perspectives seront suggérées afin de compléter cette étude et développer d'autres directions importantes.

Chapter 1:   Literature review

1.1 Introduction

This chapter presents the synthesis of existing literature on both technology and physico-chemical properties of cementitious materials and review the use of eco-binders. The manufacturing processes, the hydration reactions with mutual transfers will be discussed. The interaction between plant aggregates and binder will be reviewed base on previous studies. Moreover, the properties of hempcrete (mechanical, thermal and hygroscopic) will be reviewed. Lastly, we will give the specific conclusions of interest in order to design the experimental programme for this study.

Introduction

Ce chapitre présente la synthèse de la littérature existante sur la technologie et les propriétés physico-chimiques des matériaux cimentaires et sur l'utilisation des éco-liants. Les procédés de fabrication, les réactions d'hydratation avec les interactions entre composés cimentaires sont examinés. Les interactions entre les granulats végétaux et le liant sont aussi présentées sur la base d'études antérieures. En outre, les propriétés du béton de chanvre (mécanique, thermique et hygroscopique) sont examinées. Enfin, nous donnons des conclusions spécifiques permettant de définir le programme expérimental de cette étude.

1.2 Sustainable development in construction

1.2.1 Sustainable development

In the report of the World Commission on Environment and Development: Our Common Future [BRU87], Mrs Brundtland – the report's author gave the most widespread definition of sustainable development: "*Sustainable development is development that meets the needs of the present without compromising the ability of future generations to meet their own needs*". The sustainable development was described as enhancing quality of human life for present and future generations with a healthy environment and improved social, economic and environmental conditions.

United Nations held many conferences in order to give the action programs for sustainable development. The first conference of United Nations on environment and development in Rio de Janeiro in June 1992 adopted the program of action in sustainable development with the principle declaration: "*Human beings are at the centre of concerns*

for sustainable development. They are entitled to a healthy and productive life in harmony with nature", called "Rio Declaration" [UNC92]. The Earth Summit 2002 discussed about and proposed effective program of action for sustainable development. Especially, the one of the largest conference in history of United Nations took place in Rio de Janeiro, Brazil in June 2012 proposed the institutional framework for sustainable development [UNC12]. On the other hand, the Kyoto Protocol [KYO97] was adopted in Kyoto, Japan in December 1997 and entered into force in February 2005 to limit or reduce emission of greenhouse gases (carbon dioxide, methane, nitrous oxide, sulphur hexaflouride) and two groups of gases (hydrofluorocarbons and perfluorocarbons).

In conclusion, the sustainable development over the world is extremely necessary to protect and enhance environment. The United Nations, the international community and each country need to propose long-term environmental strategies, which take account of the interrelationships among people, resources, environment, and development. Thus, each area also needs to study to integrate the projects into an approach of sustainable development.

1.2.2   Influence of construction on environment

The report of "Our Common Future" [BRU87] showed threatens and challenges for all fields, which are population and human resources, food security, species and ecosystem, the choice of energy for environment and development, industry, and urbanization in developing countries.

We know that the construction sector has an impact on many other industries because of the use of various kinds of materials which are produced in various categories of industry, thus this sector has major impacts not only on economic and social life, but also on the natural and built environment. This area is one of the key consumers in nation's total energy and cause a significant amount of greenhouse gas emissions, mainly CO_2, altering our planet's climate. All the activities from production of building materials, construction, building operations, and decommissioning, directly or indirectly affect the environment.

In regard to energy consumption, previous studies showed that construction sector is responsible for a large share of the world's total energy consumption, it was estimated that buildings account for 30 - 50% of the worldwide energy use [BIN12, CON07, DES11

and UNE07]. The Figure 1.1 is an example, which shows the energy consumption of construction sector in comparison with other sectors in France in 2011.
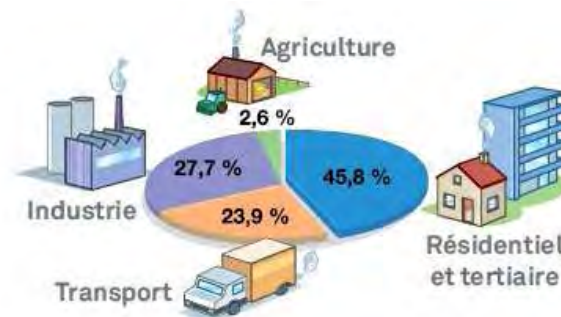
Figure 1.1: Final energy consumption by sector in France [DES11]

Concerning greenhouse gas emissions, carbon dioxide (CO_2) is one of principal greenhouse gases being responsible for global warming, it was estimated that CO_2 contributes about 50% to greenhouse gases [DIN99]. The Environmental Protection Agency of United State [EPA07] showed that greenhouse gas emissions in construction sector appear to come mostly from energy use. Price et al [PRI06] also indicated that construction sector is the second largest global CO_2 emitter after industry, representing approximately 33% of the total, in which around 36% in Europe [BPI11] and 39% in United State [USG04].

In building operations, the production and delivery processes of building materials include discovering raw materials in nature as well as extracting, manufacturing, packaging, and transportation to a building site. These processes can consume much large energy and emit large CO_2 amount, consequently cause the much important damage for environment. Nowadays, cement concrete is the most widespread building material because of excellent mechanical and durability properties, geometrical adaptability, its high level of fire resistance, and decrease of unwanted noise. Portland cement is the key ingredient in cement concrete, it is known that the production of each ton of Portland cement releases almost one ton of carbon dioxide into the atmosphere. Worldwide, the cement industry alone is estimated to be responsible for about 7% of all CO_2 generated [MAH00]; in Western European, it is approximately 8-12% of total CO_2 emission [GIE97]. Furthermore, production and exploitation processes of other building materials such as steel, aggregates, plaster etc. also significantly impact environment.

In conclusion, it is clear that construction sector has major impact on environment due to consume a large amount worldwide energy and cause a significant amount of

greenhouse gas emissions, which considerably contributes alter our planet's climate. Thus, it is necessary to reduce greenhouse gases emission into the atmosphere in order to control adverse environmental impacts. Therefore, selection of materials and technologies for the building construction should satisfy the felt needs of the user as well as the development needs of the society, without causing any adverse impact on environment.

1.2.3   *Perspective building materials for future*

The previous paragraphs showed that it is necessary to choose the materials that can contribute to considerably limit the negative impact on environment, this means the use of materials with low embodied energy and toxicity. Escadeillas [ESC06] also indicated that it should choose eco-materials, or research and develop new materials whose manufacturing and implementation would generate less gas emissions while keeping and improving as much as possible the performances (mechanical, thermal and durable properties …). Thus the use of a low CO_2 binder including plant aggregates could be a solution for the development of innovative and low impact building materials in the future.

1.2.3.1 Low CO_2 binders

In cement manufacture field, European Commission [EUR11] point out that the use of renewable energy sources and improving technologies could reduce the emissions of CO_2. In an other study, Benhelal et al [BEN12a] showed that global strategies should be considered in cement industry which are energy saving approach, carbon separation and storage approaches.

Many studies have mentioned the reduction of energy consumption and CO_2 emission in cement production (around 1 ton CO_2 per 1 ton cement in traditional cement production). For the replacement of clinker, Martín-Sedeño et al [MAR10] indicated that the use of belite sulfoaluminate clinker reduced 35% CO_2 emission and energy consumption in cement production in comparison with ordinary Portland cements because this clinker production needed less calcite and calcinations temperature than the clinker production of ordinary Portland cements did. Furthermore, the use of alternative low CO_2 cements such as pozzolan-based cements, calcium (sulfo)aluminate-based cements and calcium sulfate-based cements [GAR04] and the improvement of the efficiency of cement use also contribute to reduce CO_2 emission [DAM10].

For the technology of cement production, the novel technologies not only bring the remarkable environmental advantages, but also reduce the total cost of cement such as the

technologies of pyro-processing [BEN12b], the calcium looping [DEA11] and the NH_3 scrubbing [DON12].

In regard to other low CO_2 binders for the low strength structures, natural hydraulic lime (NHL) is considered as a more environmentally-friendly hydraulic binder, because its production needs lower energy than Portland cement do thanks to lower temperature of raw materials' calcinations, for example a product of Saint Astier emits totally around 650 kg CO_2 per ton of NHL5 [SAI06]. On the other hand, flash metakaolin (MK) is also an eco-material because its production is not only rapid (within several tenths of a second) but also emits little CO_2 [ARG10]. In previous studies, flash calcined metakaolin was used to replace partial cement in mortar and concrete. Magniont [MAG10b] illustrated that an alternative binder using 50% MK and 50% NHL5 can be used to produce concrete including hemp particles, a kind of plant aggregates. San Nicolas [SAN11] showed the development of mechanical performances and durability of concrete using flash metakaolin up to 25% for substitution of CEMI cement. Trinh [TRI12] indicated that MK can be effectively used in grout intended for soil nailing applications. His results demonstrated that the use up to 60% MK for replacement of cement in soil nailing is not only compatible with this application but also significantly reduces the CO_2 emission during production of binders intended for injection grouting.

In conclusion, there are many kind of low CO_2 binder mentioned. They can be obtained through different ways: replacement of clinker in cement manufacture, low CO_2 cements, improvement in the efficiency of cement use, use novel design such as reduction of fuel consumption and calcium looping, and use other low CO_2 binder as natural hydraulic lime and flash metakaolin.

1.2.3.2 Plant aggregates

Nowadays, there are many researches into plant concrete for insulation structures, a kind of materials used plant aggregates from vegetable resources (wood, straw, hemp, flax, …) because these aggregates have not only good thermal and acoustic insulation but also low cost and low environmental impact (they contribute to significantly limit greenhouse gas emissions, [NGU10]). Plant aggregates based concrete was studied with lime-based binders used in construction for roof insulation, filling of self bearing structure, realization of insulating screeds and decorative coats [CER05], [ELF08], [NGU10]. Hemp and sunflower stems were used as aggregates of plant concrete in previous studies with

different binders such as lime [NGU10], pozzolanic binder [MAG10b & NOZ12], and starch [TRA10]. Arnaud [ARN08] indicated that hemp shives is environment-friendly and economic material because hemp is an annual plant (around 4 months for harvesting) requiring no herbicides and no pesticides in growth.

1.2.4 Conclusion

The building sector has negatively impacted on environment and people health due to high consumption of energy as well as significant emission of CO_2 from material production and large consumption of non renewable raw materials. It is therefore necessary to develop new products that not only satisfy the same technical criteria, but also have enhanced qualities in term of the environment, people health and comfort. Thus, it is necessary to develop and fabricate the eco-materials for construction, and thereby encourage construction professionals to use them.

1.3 Binders and admixtures

Binders always play an important role in building materials. Various binders have been used to fabricate concrete using plant aggregates. From sustainable development standpoint, the economic and environmental factors are also considered as criteria for binder selection.

Among the most commonly used materials, previous studies showed that lime is widespread to fabricate plant aggregates based concrete, especially lime-hempcrete [NGU10]. On the other hand, pozzolanic binder was considered as a potential binder for hemp concrete [MAG10b & NOZ12]. The results demonstrated that hemp concrete using pozzolanic binder from lime and pozzolanic admixture not only satisfies mechanical and thermal properties but also reduces its impact on environment. In the next parts, we will present the properties of some kinds of materials which will be used in this study to fabricate new pozzolanic binders for fabrication of hemp concrete.

1.3.1 Lime

1.3.1.1 General

Lime has been largely used in construction area as an ingredient in mortars. In recent decades, it has been used to fabricate hemp concrete. It is obtained by calcination and decarbonation of a limestone rock according to (1.1) equation below.

$$CaCO_3 \xrightarrow{800^o C - 1200^o C} CaO + CO_2 \qquad (1.1)$$
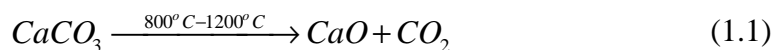
The lime (CaO) thus obtained is called quick lime. Depending on the nature of limestone used, there are different types of limes: aerial lime resulting from pure limestone, magnesium lime coming from a mixture of limestone and magnesium carbonate, and hydraulic lime coming from clayey limestone.

Lime is used in construction in the form of slaked lime, which means that quick lime is slaked by water as (1.2) equation.

$$CaO + H_2O \rightarrow Ca(OH)_2 \qquad (1.2)$$

Depending on the amount of water, this slaked lime presents in form of a powder, limewater or lime paste.

1.3.1.2 Aerial lime

a. Production

Production process of aerial lime consists of extraction of limestone, crushing and calcination. Limestone is crushed to be compatible with the kiln (the 30 – 150 mm fraction in vertical kilns, 10 – 60 mm in horizontal kilns (chapter 3, [AMZ12]). The quick lime is obtained by calcination between 800 and 1200°C. After calcination, quick lime is crushed or slaked depending on the use.

b. Chemical and mineralogical composition

The major chemical composition of aerial lime is CaO (around 70%), the others are SiO_2, Al_2O_3, Fe_2O_3, MgO, K_2O, etc, the loss on ignition – LOI is around 25 - 27% (Table 1.1). The chemical compositions of some kinds of aerial lime used in the literature are presented in Table 1.1.

The principal mineralogical components of aerial lime are calcium hydroxide ($Ca(OH)_2$) and calcium carbonate ($CaCO_3$). Figure 1.2 and Table 1.2 present mineralogical composition detected by XRD and mineral content determined by thermogravimetry.

Figure 1.2 is an example of X-ray diffraction analysis (XRD) in the literature. It can be seen that the portlandite ($Ca(OH)_2$) is considered as the main phase, and calcite ($CaCO_3$) is also detected with some small peaks.

Table 1.1: Chemical composition of aerial lime

Literature	Content of Ingredients (% by weight)							
	SiO$_2$	Al$_2$O$_3$	Fe$_2$O$_3$	CaO	MgO	K$_2$O	SO$_3$	LOI
[AGG11]	0.17	0.18	0.07	70.06	2.35	-	0.77	25.60
[ARA05]			0.89	68.53	3.29	0.05	1.37	25.25
[BAK06]	0.17	0.18	0.07	70.06	2.35	-	0.77	25.60
[BIL11]	1.05	0.85	0.62	65.30	1.91	-	-	25.34
[CAR09]	-	0.68		70.90	0.31	-	0.16	26.90
	-	0.68		71.20	0.06	-	0.12	26.40
[FOR06]	0.39	0.16	0.24	72.10	-	-	-	26.46
[LAN05]	0.71	0.55		68.26	3.55	0.04	0.96	25.46
[LAW07]	0.08	0.018	0.02	74.46	0.20	0.002	0.033	24.78

P: Portlandite
Ca: Calcite
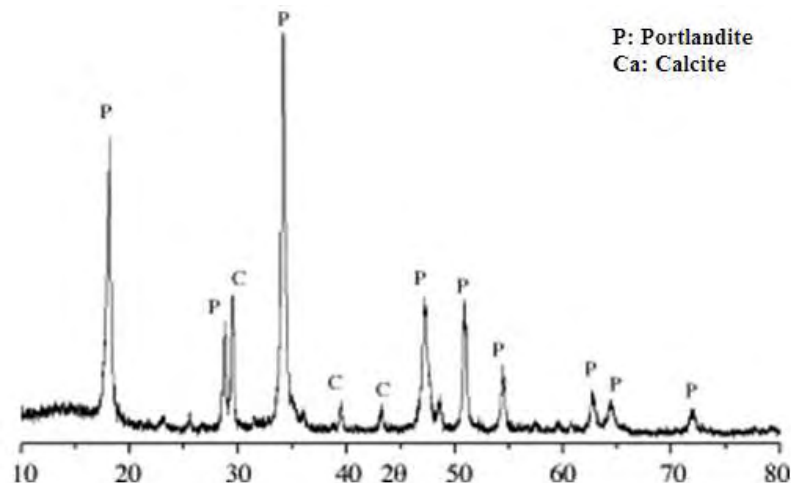
Figure 1.2: X-ray diffraction pattern of aerial lime [ARA05]

Table 1.2: Mineralogical composition of aerial lime from literature

Literature	Mineralogical compositions	
	Ca(OH)$_2$	CaCO$_3$
[AGG11]	89.00%	6.00%
[ARA05]	87.00%	10.00%
[BAK06]	89.00%	5.00%
[CAR09]	86.10%	8.90%
	88.40%	7.30%

Table 1.2 indicates that the portlandite content is very high (around 86.1 - 89%), while calcite content is low (around 5 -10%).

c. Mechanical properties

The mechanical performances of aerial limes are very poor, and the development of mechanical strength is very slow (chapter 3, [AMZ12]. Izaguirre et al [IZA11] showed that the maximum mechanical strength of aerial lime mortar is around 3.3 MPa after 182 days

curring in ambient laboratory condition (20°C, 60% RH), which is similar to Lanas et al.'s results [LAN03].

d. Thermal conductivity

The thermal conductivity of aerial lime paste and mortar is high. Previous studies showed that thermal conductivity value of aerial lime paste is 0.37 W/(m.K) in the dry state [NGU10], and that of aerial lime mortar is around 0.65 - 0.84 W/(m.K) in the dry state [CER06, VEJ12a & VEJ12].

1.3.1.3 Natural Hydraulic Limes

a. Production

According to standard of NF EN 459-1, Natural Hydraulic Lime (NHL) is produced by burning more or less argillaceous or siliceous limestones, with subsequent slaking, with or without final grinding. The calcination process is carried out with a maximum temperature of 1000°C (as opposed to 1450°C for the production of Portland cement), using very pure coal as the fuel (anthracite coal containing 92-95% carbon) (chapter 3, [AMZ12]). The amount of reactive silica depends on the method and temperature of the firing of the limestone, and the calcination temperature of 1000°C is generally considered to be insufficient to form C$_3$S (chapter 3 [AMZ12]). The slaking process is controlled to obtain dry product. The main reactions take place during calcination and slaking process following (1.3) and (1.4) equations respectively (chapter 3 [AMZ12]).

$$CaCO_3 + xSiO_2 \rightarrow (1-2x)CaO + x2CaO.SiO_2 + CO_2 \qquad (1.3)$$

$$(1-2x)CaO + x2CaO.SiO_2 + (1-2x)H_2O \rightarrow (1-2x)Ca(OH)_2 + x2CaO.SiO_2 \quad (1.4)$$
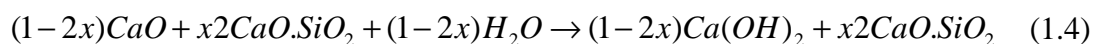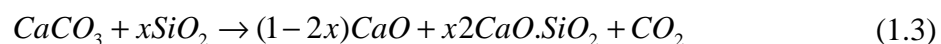
There are three kinds of NHL: NHL2, NHL3.5 and NHL5 which have different compressive strengths (NF EN 459-1).

b. Chemical and mineralogical composition

The chemical compositions of NHLs are mainly CaO (50%-70%) and SiO$_2$ (10%-20%); with other minor components as Al$_2$O$_3$, Fe$_2$O$_3$, MgO, K$_2$O, etc. The proportion of these components depends on the initial amount of clays and calcium hydroxide [ARN08]. The loss on ignition may vary from 15 to 24%. The chemical components of some kinds of NHLs are showed on the Table 1.3 below.

Table 1.3: Typical chemical composition of NHLs

Literature	*Content of Ingredients (% by weight)*								
	SiO$_2$	Al$_2$O$_3$	CaO	MgO	Fe$_2$O$_3$	Na$_2$O	K$_2$O	SO$_3$	LOI
NHL5 [GUA06]	15.60	4.40	49.30	1.57	2.32	0.27	1.19	2.6	22.20
NHL3.5 [GUA06]	18.80	2.65	56.10	2.31	0.93	0.15	0.47	1.55	16.60
NHL3.5 [GUA06]	12.50	1.36	63.30	1.51	0.45	0.12	0.20	0.80	19.30
NHL3.5 [DOM06]	19.04	2.69	51.86	2.04	1.04	0.48	0.75	0.90	17.72
NHL5 [LAN04]	12.57	5.42	54.26	7.65	1.16	0.34	1.35	2.13	15.00
NHL5 [MAG10b]	18.49	1.89	57.03	1.07	0.56	0.07	0.31	0.37	17.25
NHL2 [MER07]	11.49	2.74	56.12	2.22	1.12	0.17	0.99	0.30	24.00

As regards mineralogical composition of NHLs, the main phases are hydrated lime (Ca(OH)$_2$, noted CH), calcite (CaCO$_3$, noted Ca) and dicalcium silicate (2CaO.SiO$_2$, noted C$_2$S). Moreover, other hydraulic phases (3CaO.SiO$_2$, noted C$_3$S; 3CaO.Al$_2$O$_3$, noted C$_3$A; 4CaO.Al$_2$O$_3$.Fe$_2$O$_3$, noted C$_4$AF; 2CaO.A1$_2$O$_3$.SiO$_2$, noted C$_2$AS) and even calcium sulfate (CaSO$_4$, noted Cs) can be detected (less than 5%) (chapter 3, [AMZ12]). Figure 1.3 shows an example of XRD analysis of NHL5 from Saint-Astier [MAG10b]. Mineralogical compositions of some kinds of NHLs from the literature are shown on Table 1.4.
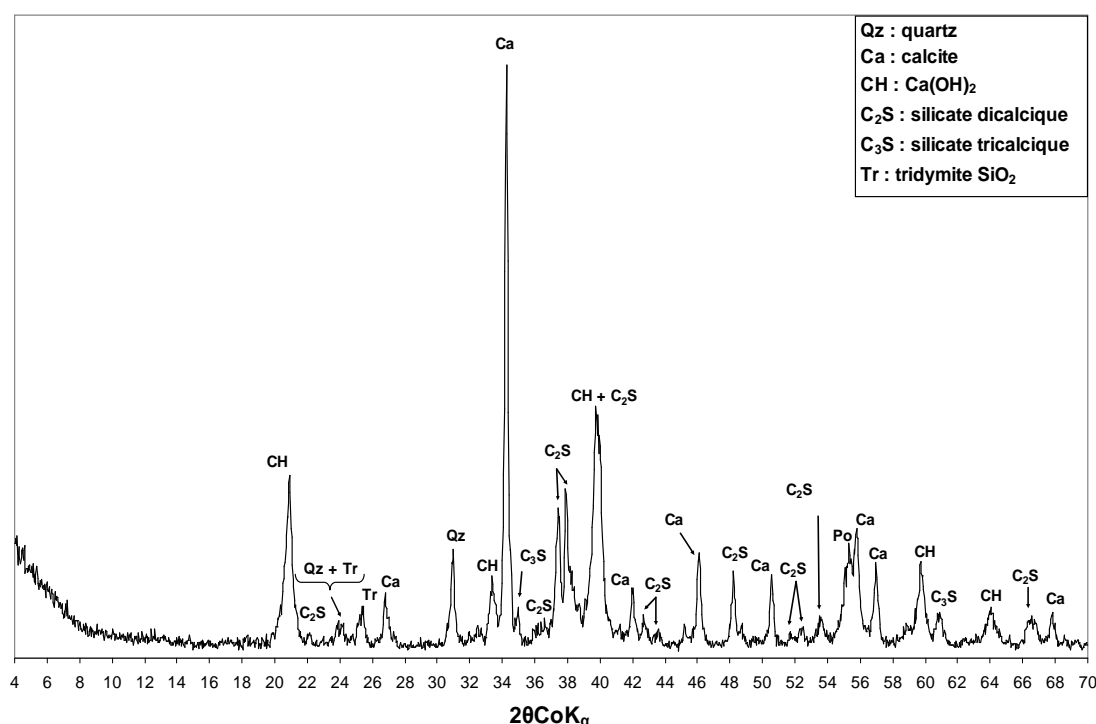
Figure 1.3: X-ray diffraction pattern of NHL5 from Saint Astier [MAG10b]

Figure 1.3 and Table 1.4 below demonstrated that CH, Ca and C$_2$S components predominate over other compositions.

Table 1.4: Typical mineralogical composition of NHLs

Literature	*Mineralogical ingredients*							
	CH	Ca	C_2S	C_3A	C_2AS	C_4AF	Cs	Insoluble
NHL3.5 [GUA06]	19.30	22.80	30.10	-	1.20	-	-	1.10
NHL3.5 [GUA06]	42.00	16.30	24.10	1.40	0.60	-	-	-
NHL3.5 [DOM06]	17.60	30.40	40.50	-	-	-	-	2.00
NHL5 [MAG10b]	22.00	23.00	43.00	0.70	1.30	0.70	0.70	5.60
NHL2 [MER07]	42.80	17.80	21.20	2.30	2.30	1.00	-	-

c. Setting mechanisms

When NHLs contact water, the setting of NHLs takes place in two stages. In the first stage, the rapid hydration of the hydraulic component of C_2S (as well as C_4AF, C_2AS and C_3A) forms calcium silicate hydrates (C-S-H) and calcium hydroxide as showed in (1.5) equation. The second phase, the carbonation of calcium hydroxide takes place on contact with the atmospheric CO_2 as presented by (1.6) equation (this process is a very slow hardening which can take several months).

$$2CaO.SiO_2 \xrightarrow{\quad H_2O \quad} Ca(OH)_2 + C-S-H \qquad (1.5)$$

$$Ca(OH)_2 \xrightarrow{\quad CO_2\,(humid\ milieu) \quad} CaCO_3 \qquad (1.6)$$
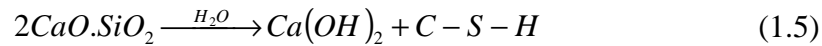
d. Mechanical properties

The mechanical strengths of NHLs pastes are very low, their compressive strengths vary from 2 to 15 MPa at 28 days depending on the kind of NHLs (NF EN 459-1). The mechanical strengths of NHLs mortars are very poor before seven days and develop gradually over time [AMZ12]. Indeed, Domede [DOM06] showed that the strength of NHL3.5 mortar is 1.1 MPa at 7 days, 3.6 MPa at 28 days (with a Young's modulus of 5200 MPa) and 3.9 MPa at 60 days. The compressive strength of NHL5 mortar obtained by [LAN04] at 28 days varies from 9 to 2.3 MPa depending on the NHL5 to sand ratios (from 1 to 5 respectively).

e. Thermal conductivity

The thermal conductivity of natural hydraulic lime paste and mortar is fairly high, which is similar to that measured for aerial lime paste and mortar [AMZ12]. Nguyen's measurement [NGU10] showed that the thermal conductivity of NHL2 and NHL3.5Z pastes are respectively 0.363 and 0.37 W/(m.K). Amziane et al [AMZ12] indicated that the thermal conductivity of NHLs mortars are from 0.3 to 1.0 W/(m.K).

f. Environmental impacts

In the production process of NHLs, the calcination temperature is much lower than that of Portland cement production (around 1000°C as compared to 1450°C for cement), its CO_2 emission thus reduces significantly in comparison with that of Portland cement production [AMZ12]. The data of Saint Astier company [SAI06] and Italcementi Group [ITA07] showed that the CO_2 emissions during the production of NHL5 are respectively 710 and 733 kg of CO_2 per ton of NHL5, which are significantly lower than the CO_2 emission of cement production (around 1000 kg of CO_2 per ton of Portland cement).

1.3.2 *Metakaolin*

1.3.2.1 Production

Metakaolin (MK) is a pozzolanic material obtained by firing kaolin at a temperature between 600 and 850°C. The production process is carried out by three stages: raw material selection and grinding, and calcination process [SAN13]. This calcination induces the dehydroxylation reaction ((1.7) equation), that does not emit any CO_2 contrary to the decarbonation of lime.

$$Al_2O_3.2SiO_2.2H_2O \longrightarrow Al_2O_3.2SiO_2 + 2H_2O$$
$$or \quad AS_2H_2 \longrightarrow AS_2 + 2H \tag{1.7}$$
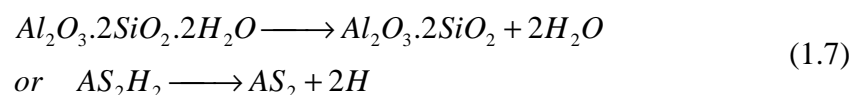
In the industrial scale, MK is calcined by two methods: rotary kiln and flash calcinations.

The rotary kiln calcination method is the most commonly-used method, kaolinite is calcined in rotary kilns (60-90m in length and 4-5m in diameter) being similar to production process of cement. The calcinations process is carried out around five hours at a temperature between 600 and 800°C with fairly pure material (kaolinite content of over 75%) [AMZ12]. The obtained MK particles are in form of pellets being 5 – 10 mm in diameter, which are then crushed to the desired finesse [SAN13].

The flash calcinations method is carried out by calcination of powdered clay [CAS07]. This powdery material turns around the flame (1000 - 1200°C) in only a few tenths of a second. The obtained MK (around 700°C) is quickly cooled to 100°C, then contained in silos to cool to ambient temperature before distribution for the construction sites [SAN13]. The energy consumption used for this technique is 80% less than the energy consumed during cement production [SAN11]. MK obtained by flash calcination

presents greater reactivity than that obtained by rotary kiln calcinations because the morphology of flash metakaolin particles are in form of vitreous balls [BIC05 & SAN11].

1.3.2.2 Chemical and mineralogical composition

Major chemical constituents of metakaolin are SiO_2 (50 – 70%) and Al_2O_3 (20 – 40%), which present more than 90% in total. The other components are around 10%: oxides iron, titanium, potassium, sodium, calcium, magnesium and so on (chapter 3, [AMZ12]). Typical chemical composition of some MK in literature is given in Table 1.5.

Table 1.5: Typical chemical composition of metakaolin

Literature	*Content of ingredients (% by weight)*									
	SiO_2	Al_2O_3	Fe_2O_3	CaO	MgO	K_2O	SO_3	TiO_2	Na_2O	LOI
[CAS07]	56.20	37.20	1.40	1.20	0.20	1.20	-	-	-	2.10
[VEL09]	62.62	28.63	1.07	0.06	0.15	3.46	-	0.36	1.57	2.00
	59.90	32.29	1.28	0.04	0.17	2.83	-	0.36	0.24	2.80
	62.48	28.72	1.01	0.03	0.13	3.55	-	0.34	2.45	1.20
[FOR06]	55.42	43.32	0.64	0.20	-	0.06	-	-	0.02	-
[MAG10b]	67.10	26.80	2.56	1.12	0.11	0.12	<LD	1.30	0.01	0.84
[MOF]	51.60	41.30	4.64	0.09	0.16	0.62	-	0.83	0.01	0.60
[BIL11]	48.74	34.85	2.07	0.03	0.09	1.29	-	4.26	0.01	4.84
[SID11]	51.52	40.18	1.23	2.0	0.12	0.53	0.00	2.27	0.08	2.01
	52.10	41.0	4.32	0.07	0.19	0.63	-	0.81	0.26	0.60
	58.10	35.14	1.21	1.15	0.20	1.05	0.03	-	0.07	1.85

Table 1.6: Typical mineralogical composition of metakaolin

Literature	*Mineralogical ingredients*						
	Quartz	Calcite	Mullite	Phyllite	Anatase	Kaolinite	Illite
[BIC05]	+++	-	-	-	+	-	-
[CAS07]	+++	-	-	-	-	+	+
[LAN04]	+++	-	-	-	-	-	+
[MAG10b]	+++	+	+	-	+	-	-
[BIL11]	+++	-	-	-	+	+	+
[SAN11]	+++	-	-	-	+	-	-
	+++	-	-	+	+	-	-

"+++": high quantity; "+": small quantity; "-": non-quantity

Metakaolin is mainly composed of a very reactive amorphous silicon-aluminates mineralogical form (aluminum - Al_2O_3 and silica - SiO_2) with a SiO_2 to Al_2O_3 ratio between 1.5 to 2.5 depending on the purity of raw material used in the production [SAN13]. This reactive amorphous phase is responsible for the pozzolanic activity of MK

which reacts with calcium hydroxide ($Ca(OH)_2$) to form C-S-H gel, calcium aluminate hydrates (C_4AH_{13} and C_3AH_6-Hydrogarnet) and calcium alumino-silicate hydrates (C_2ASH_8-Straetlingite) [FRI02]. Mineralogical compositions of some kinds of metakaolin are presented on the Table 1.6.

1.3.2.3 Pozzolanic reaction

MK is synthetic pozzolan with a very large specific surface. It reacts readily and quickly with calcium hydroxide (CH) at normal temperature in the presence of water, because its acidic oxide content is very high ($Al_2O_3 + SiO_2 > 90\%$) [CAS07, PER07 & RAF11]. This reaction forms additional cementitious C-S-H gel, together with crystalline products, which include calcium aluminate hydrates (C_2ASH_8, straetlingite) and alumino-silicate hydrates (C_4AH_{13} and C_3AH_6) [FRI02]. The crystalline products depend principally on the AS_2/CH ratio and reaction temperature [PER07]. The pozzolanic reaction is described as (1.8) equation [CAS07 & MAG10b].

$$AS_2 + 5CH + 5H \rightarrow C_5AS_2H_{10} \qquad (1.8)$$

$C_5AS_2H_{10}$ represents an average composition of the products of this reaction, which are hydrated silicates of calcium (C-S-H) and hydrated silico-aluminates of calcium, a majority of the straetlingite (C_2ASH_8) and possibly hydrogarnet (C_3ASH_6), and calcium aluminate hydrates (C_4AH_{13}) [CAS07, MAG10b].

1.3.2.4 Mechanical properties

Many studies investigated the effect of MK (for partial substitution of cement) on the mechanical properties of concretes or mortars. Siddique et al [SID11] showed that the cement-MK mortar and concrete reach the best compressive strength with the replacement of 20% Portland cement by MK. In other study, San Nicolas [SAN11 & SAN13] illustrated that the strength of cement-MK mortar with flash MK content of 25% is lower during the first 7 days, but higher after 28 days in comparison with those of cement mortar. The studies attributed the increase of cement-MK concrete and mortar strengths to the formation of additional C-S-H from the pozzolanic reaction between MK and $Ca(OH)_2$ produced during cement hydration induces [AMZ12, SAN11 & SAN13].

Morever, Eires et al. [EIR06] investigated the mechanical behavior of the MK – hydrated lime pastes with different ratios. The results showed that a mixture comprising

25% hydrated lime and 75% MK is the best compressive strength (8 MPa at 14 days and 10.5 MPa at 56 days). Magniont's study [MAG10b] also showed the compressive strength of the binder containing 50% MK and 50% NHL5 at 28 days is better in comparison with that of NHL5 according to requirement in NF EN 459-1 for (18 MPa versus 15 MPa).

1.3.2.5 Physical properties and thermal conductivity

MK presents a bulk density around 700 ± 100 kg/m^3 and the true density around 2600 ± 100 kg/m^3. Its fineness is higher than that of cement, its specific surface is from 12.5 to 30 m^2/g [AMZ12 & TRI12].

From the thermal conductivity point of view, Amziane et al. [AMZ12] showed that the partial substitution of the Portland cement by MK has no effect on its thermal conductivity.

1.3.2.6 Environmental impacts

Metakaolin is considered as an eco-material because the CO_2 emission and energy consumption during the production process of MK are far less than those for production of Portland cement and lime, especially for flash metakaolin [AMZ12]. For flash metakaolin, the energy consumption and CO_2 emission (equivalent kilos of CO_2 per ton of product) in manufacture process are respectively 4 times and 10 times less than those of CEM I 52.5R cement (Table 1.7).

Table 1.7: Environmental evaluation of flash metakaolin [SAN11]

	Flash MK	*CEM I 52.5R cement*
Energy consumption (MJ/t)	2211	7954
CO_2 emission (kg/t)	96	913.6

1.3.3 Admixtures

1.3.3.1 Glycerol carbonate

Glycerol is a co-product of oleochemistry generated by the industrial production of fatty acids (surface active agents), and through the production of biodiesel [KOS06]. Glycerol carbonate (GC) can be synthesized from glycerol according to a green process. GC can be used as a plasticizer for nail varnish formulations [BAN07]. It has various properties that are the subject of numerous patents defining its use as synthesis intermediate for the preparation of polyesters, polycarbonates and polyurethanes and as an

active ingredient for various applications in plant protection formulations, detergents, cosmetics and coatings [ROK05].

In building materials, GC has been previously used as a catalyst for the curing of cementitious mixtures [CLE05]. In a previous study, the GC was used by Nguyen [NGU06] as an additive for cement in order to reduce shrinkage. The first results showed that the GC contributed to a very fast hardening of the mortar and was consequently discarded from the study. The incorporation of GC in an innovative pozzolanic matrix leads to fast hardening of the paste, an improvement in compressive strength and the limitation of shrinkage [MAG10a & MAG10b].

1.3.3.2 Potassium sulfate

Potassium sulfate (PS) is a chemical activator that encourages ettringite (Aft phase) formation and so significantly enhances the strength of the paste [WIL98]. Moreover, Martinez-Aguilar et al [MAA10] demonstrated that PS not only improve strength but also stabilize dimension of the paste. In a previous study, Shi attributed increases in early pozzolanic reaction and formation of Aft phase to the concentration of SO_4^{-2} ion [SHI00]. The presence of Na_2SO_4 or K_2SO_4 in pozzolanic paste, Na_2SO_4 or K_2SO_4 reacts first $Ca(OH)_2$ to form gypsum as (1.9) equation, and ettringite is then formed according to (1.10) equations [ESC12 & SHI00].

$$Na_2SO_4(K_2SO_4) + Ca(OH)_2 + 2H_2O \; \rightarrow \; CaSO_4.2\,H_2O + 2NaOH(2KOH) \qquad (1.9)$$

$$2Al(OH)_4 + 3SO_4^{2-} + 6Ca^{2+} + 4OH^- + 26H_2O \rightarrow 3CaO.Al_2O_3.3CaSO_4.32H_2O \quad (1.10)$$
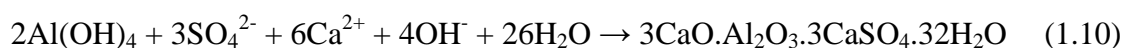
1.3.4 Conclusion

It can be seen that flash metakaolin can be considered as an eco-material. It can react readily and quickly with calcium hydroxide at normal temperature in the presence of water. Moreover, Magniont [MAG10b] showed a potential binder from natural hydraulic lime (NHL5) and flash metakaolin with organic admixture (GC) that is good binder for hempcrete. However, its mechanical behavior is too low at early age.

In our study, we will investigate new pozzolanic binders from two different limes and flash metakaolin with different ratios in order to optimize metakaolin to lime ratio. After that we will work on the improvement of mechanical performance at early age of this binder with organic admixture (GC) and/or mineral admixture (K_2SO_4).

1.4 Hemp shives

The hemp shives are the inner part of the fragmented stalk of hemp, derived from the mechanical defibering process (shives representing 40% to 60% by mass) [ARN08]. Hemp shives can have different origins, which means that they grew under different climates, had different harvests and different cuttings so their microstructure will be different. Historically, hemp shives were a by-product of the hemp fibre industry and were sold as horse bedding and for combustion [BRU08]. In the recent years, hemp shives have been used as aggregates to fabricate hemp concrete.

1.4.1 *Microstructure*

Figure 1.4 describes the cross section of hemp stem and hemp shiv. Figure 1.4a shows that woody part occupies a largest quantity of hemp stem. Hemp shives are extracted from this woody part after extraction of hemp fibers.

1: Fiber; 2: Woody core; 3: Hollow space
a) Cross section of hemp stem   *b) Cross section of hemp shiv*
Figure 1.4 Cross section of hemp stem and hemp shiv [NGU10]
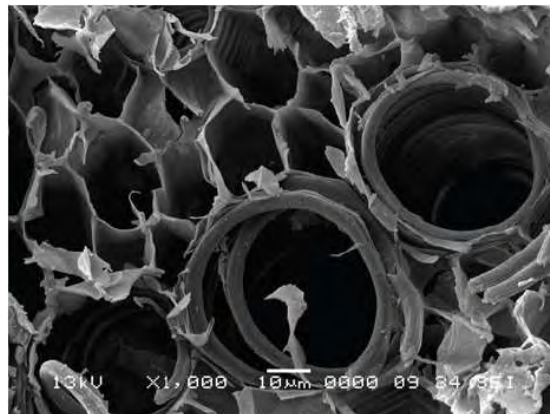
The observation by Scanning Electron Microscope (SEM) from previous studies [ARN08], [NGU10], [MAG10b] indicated that hemp shiv is an extremely high porous material which has therefore excellent capacity to absorb and retain water. These observations showed that shiv possesses capillaries with different size and oriented longitudinally. These capillaries are void in dry state, the diameters of capillaries are from 10 to 50 μm, as an example on Figure 1.4b.

1.4.2 *Chemical composition*

The analyses of previous studies showed that the main chemical components of hemp shiv are cellulose, hemicellulose, pectin, lignin and other items in very small content (waxes and ash). Table 1.8 synthesizes the chemical ingredients of hemp shiv.

Table 1.8: Chemical composition of hemp shiv

Literature	*Cellulose*	*Hemi-cellulose*	*Lignin*	*Pectin*	*Ash*	*Wax*
[ARN08]	48%	12%	28%	6%	2%	4%
[THO05]	34-44%	18-37%	19-28%	6%	1-2%	1%
[VIG96]	44%	18%	28%	4%	2%	1%

Table 1.8 shows that the major compositions are cellulose, hemicellulose and lignin (around 90% in total), the others are pectin, ash and wax (around 10% in total). Cellulose provides strength to the plant and hemicellulose provides linkage between cellulose, while lignin provides protection against attack by pathogens and consumption by herbivores, both insect and mammalian [THO05].

1.4.3 Bulk density and porosity

Table 1.9: Bulk density and porosity of hemp shives

Literature	*Bulk density* ρ_{vs} *(kg/m^3)*	*Total porosity* n_{total} *(%)*	*Inter-particles Porosity* n_{inter} *(%)*	*Intra-particles porosity* n_{intra} *(%)*
[ARN08]	110		57	
[ARN12]	112, 114, 119			
[EVR08]	100 - 120			
[CER05]	130	91.2	59.4	31.8
[MAG10b]	110 - 140			
[NOZ12]	114.2 ± 2.3	92.4±0.15	55.2±6.7	37.2±0.1
[NGU10]	102.83	92.98	59.90	33.08
[BRU08]	98			
[VER12]	148.3 ± 1.9			

The previous results indicated that hemp shiv is a plant aggregate characterized by a high porosity and its bulk density is therefore low. Porosity presents three types including total porosity (n_{total}), inter-particles porosity (n_{inter}) and intra-particles porosity (n_{intra}) [CER05], [NGU10]. Previous measurements illustrated that total porosity, inter-particles porosity and intra-particles porosity of hemp shiv are respectively around 90%, 60% and 30%, as Table 1.9.

Bulk density of hemp shiv is very low. It was measured from different origins by different methods such as using a bucket, a glass cylinder or pycnometer. The bulk density varies from 98 to 148.3 kg/m^3 depending on origin of hemp and the method applied as presented in Table 1.9.

1.4.4 Particles size distribution (PSD)

Until now, it has not been existed standard for the PSD of plant aggregates although numerous authors have studied this parameter. A previous study [ASS07] showed that the hemp particles have parallelepiped shape with 1 to 5 mm in width and 10 to 30 mm in length; less than 0.5 % by mass of passing inferior 0.5 mm sieve, about 90% by mass between 1 mm and 4 mm and less than 3% by mass above 4 mm.

Two methods have been previously employed to analyze PSD of hemp shiv: mechanical sieving and image analysis methods.

1.4.4.1 Mechanical sieve method
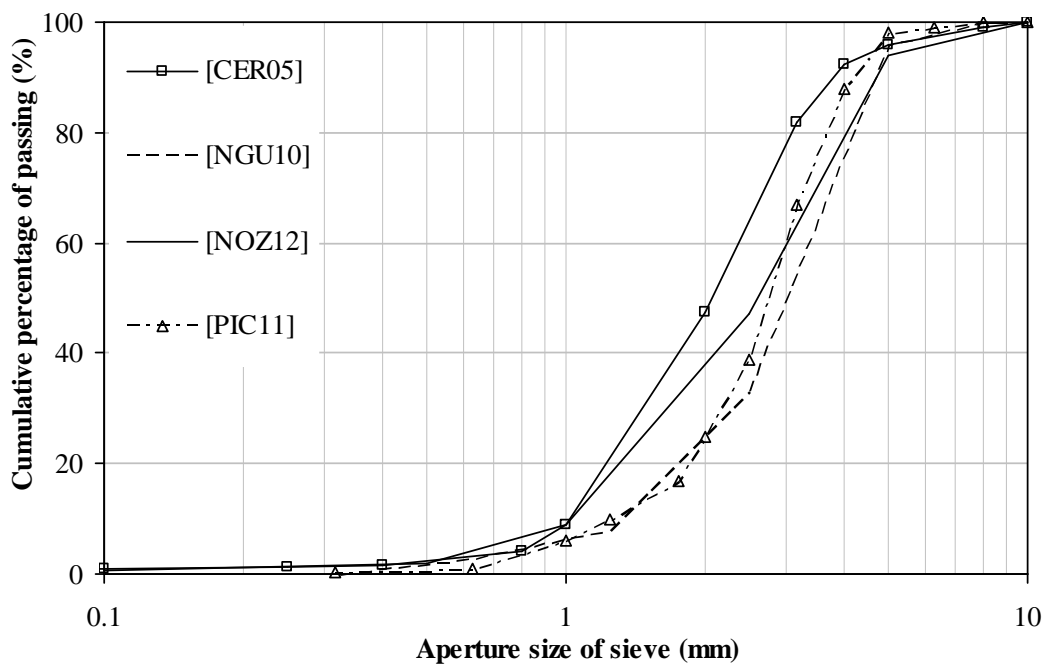
Figure 1.5: Grading curve by mechanical sieve in literature

As regards mechanical sieve method, the previous studies have been realized on the dry hemp shiv with different quantities of samples (up to 200 grams). Different sets of standard sieves were used (they had square mesh from 0.315 mm to 10 mm) [CER05, NGU10, NOZ12 & PIC11]. Figure 1.5 shows the grading curves obtained by mechanical sieve method from the literature.

The results in Figure 1.5 indicated that the size of particles varies from 0.1 to 10 mm, the cumulative percentage of passing by mass is around 6 - 9 % for 1 mm sieve, about 76 - 93 % for 4 mm sieving and 96 - 98 % for 5 mm sieve. However, Nguyen [NGU10]

indicated that this method cannot characterize the width and length of the parallelepiped form of hemp particles and is not exact to measure PSD of hemp shives because there were many hemp particles passing through a given sieve that had lengths much larger than the sieve aperture.

1.4.4.2 Image analysis method

In order to measure the width and length of the hemp particles, image analysis method using ImageTool or ImageJ software has been developed. This analysis measures PSD of hemp shives on samples of 2 to 5 grams. This method can determine number of parameters of hemp particles, which are area, perimeter, width and height of bounding rectangle, major and minor axes of best-fitting ellipse, angle of inclination of the major axis with the horizontal, and Feret's diameter as presented in Figure 1.6 below.
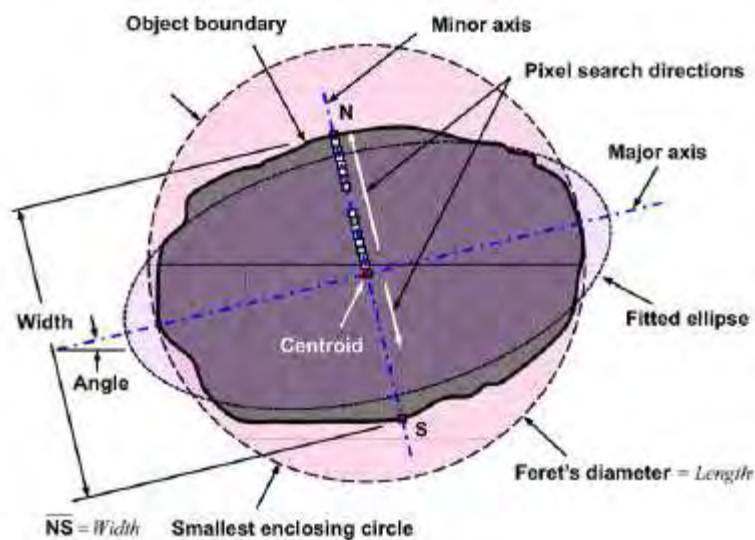
Figure 1.6: Length and width determination [IGA09]

Figure 1.6 shows the parameters which are analyzed by ImageJ software. The length dimension of particles is determined by using Feret's diameter, included in ImageJ as standard output. The Feret's diameter is the diameter of a smallest circle that encloses a particle outline, which actually signifies the particle's maximum dimension. The width dimension of particles is determined as minimum dimension of width and height of bounding rectangle [IGA09].

Several authors have determined PSD of hemp particles by image analysis method, the results were presented in Figure 1.7.
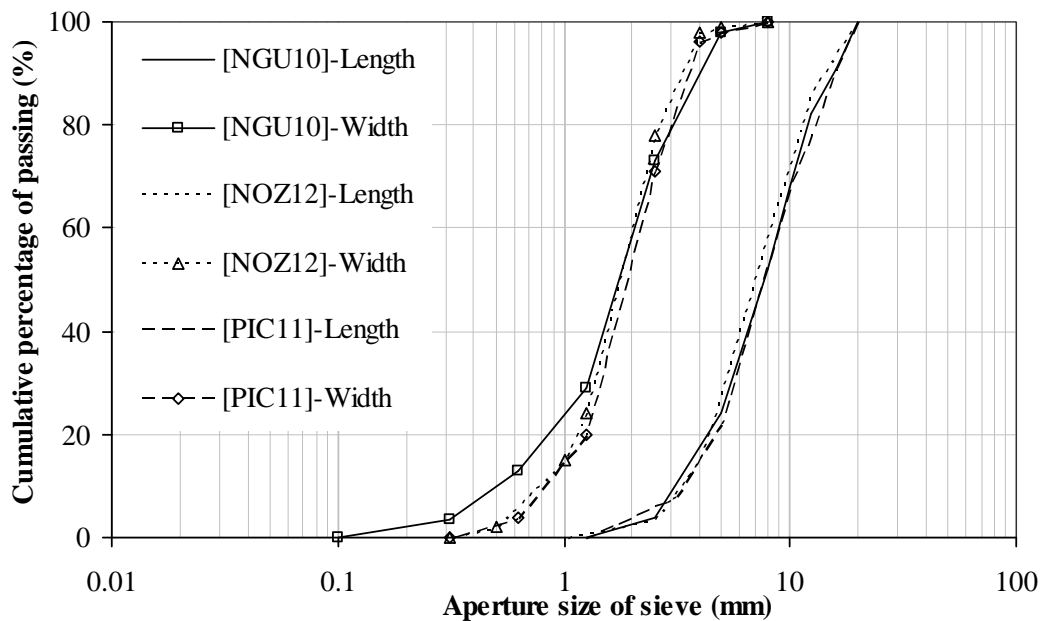
Figure 1.7: Grading curve by image analysis

Figure 1.7 shows grading curves by image analysis method for different measures. Nguyen [NGU10] carried out this test on different weight samples (2 g and 5 g) using ImageTool software. His results showed that hemp particle size was distributed from 0.35 mm to 8 mm and from 1.25 mm to 20 mm according to the width and length respectively. In Nozahic's study [NOZ12], the samples of 4 g were analyzed. The PSD was from 0.35 mm to 6.3 mm, from 1 to 20 mm, and from 1 to 9 mm according to the width, length and equivalent diameter respectively. Moreover, Nozahic also indicated that PSD of hemp particles according to the width is very close to the distribution obtained by the sieve method. This can demonstrate that the majority of the particles are oriented along with the diagonal of the mechanical sieves' aperture when they pass through the sieves.

The studies pointed out that the advantage of image analysis method in comparison with the mechanical sieve method is that the image analysis method can characterize complex particle morphology and heterogeneity. However, the drawback of this method is that the small particles and fibres cannot be detected.

1.4.5   Water absorption

High porosity and capillary structure of the shiv particles are responsible for a high water absorption and retention capacity [ARN08]. Numerous authors had measured water absorption capacity and kinetics of hemp shiv on dry samples weighing around 50-100 grams each. Figure 1.8 below synthesized measurements in the literature.

40
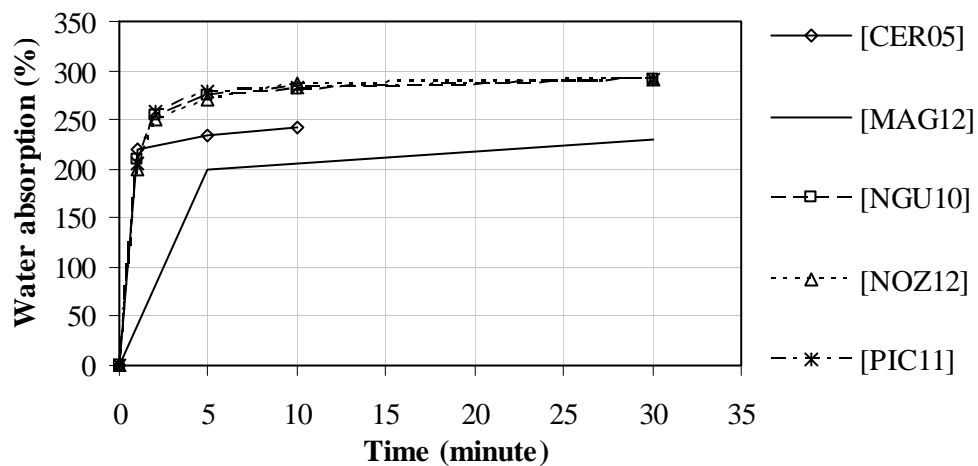
Figure 1.8: The capacity of water absorption of hemp shiv

Figure 1.8 shows the capacity of water absorption of different hemp shives in initial 30 minutes of immersion in literature. It can be seen that the water absorption increased very quickly during the first minute (around $200 \div 220\%$). After 5 minutes, the water absorption increased very slowly. This figure also shows that Magniont's result present the lowest water absorption, which is attributed to the different protocol applied because of the different method of superficial drying of hemp shiv before weighing. Moreover, the measurements in long time indicated that hemp shives can absorb water till three times and four times of its dry mass after 24 hours and 48 hours of immersion respectively [MAG12 & NGU10].

1.4.6   Thermal properties

Hemp particles are known as a high porosity material and their bulk density and thermal conductivity are therefore low because of the high immobile air content. In a previous study, Cordier [COR99] and Cerezo [CER05] showed the evolution of thermal conductivity of loose hemp shives in function of the bulk density (Figure 1.9).
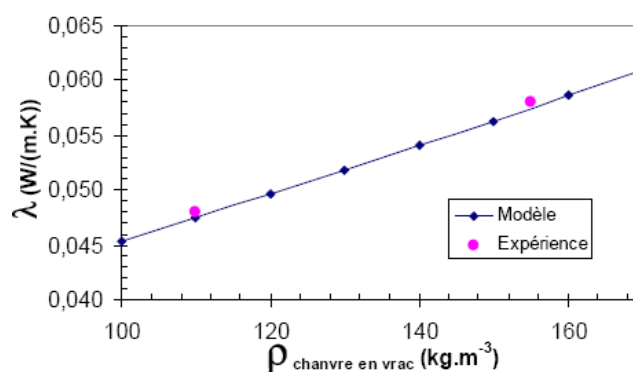
Figure 1.9: Thermal conductivity of hemp shiv in function of bulk density [CER05]

Table 1.10 presents the measurements of thermal conductivity corresponding to bulk density of dry hemp shives.

Table 1.10: Coefficient of thermal conductivity of hemp shiv

Order	Literature	Bulk density kg/m³	Thermal conductivity W/(m.K)
1	Cerezo [CER05]	110	0.048
2	Cerezo [CER05]	155	0.058
3	Magniont [MAG12]	134.8	0.055
4	Verdier [VER12]	148.3 ± 1.9	0.056

Table 1.10 showed that the thermal conductivity coefficient of loose hemp shiv is very low. It varies from 0.048 to 0.058 W/(m.K) corresponding the bulk densities from 110 to 155 Kg/m³.

1.4.7 Conclusion

Hemp shives are co-product of the process of hemp fibre extraction from hemp stems, and they are therefore very low cost. Hemp shives present very high porous structure, very low bulk density and thermal conductivity. Moreover, they are considered as an eco-material (paragraph 1.2.3.2). Thus, the use of hemp shives as aggregates for fabrication of plant concrete can not only bring the good thermal insulation and economic effect, but also limits the impact on environment.

However, due to the high water absorption rate of hemp shives, it is necessary to study the pre-treatment methods in order to limit negative influence of this property on the properties of materials fabricated from hemp shives.

1.5 Hemp concrete

Hemp concrete is also called "hempcrete", is defined as being a conglomerate constituted by hemp shives with a mineral binder and water. The different proportions between the shives and binder can provide different mechanical, thermal, and acoustic performances of hempcrete. Hempcrete can be used to make various surfaces in construction such as application in wall, roof, floor and rendering [ASS07].

1.5.1 Formulation

Many formulations of hempcrete have been studied by the different authors. The obtainable properties depend largely on these compositions, the nature of the binder as well

as the mode of implementation of the fresh material and the test methods. Table 1.11 summarizes these different parameters for a part of tested compositions from the different authors.

Table 1.11: Formulations of hempcrete mixtures

Mixture	Literature	Implementation method	Nature of binder	Mass of raw material (%)			W/B	S/B	ρ_{dry} (kg/m^3)
				Shiv	Binder	Water			
Wall	[ASS07]	Casted in place	T70	14.9	32.8	52.2	1.6	0.455	420
Floor			T70	11.4	31.4	57.1	1.8	0.364	500
Roof			T70	25.0	25.0	50.0	2.0	1	250
A3-2	[CER05]	Casted in place and compaction of 0.05MPa	T70	9.9	47.7	42.4	0.9	0.207	661
A3-1.5			T70	11.9	42.8	45.3	1.1	0.277	609
A4-1.5			T70	14.4	37.3	48.4	1.3	0.386	504
A3-1			T70	14.8	35.6	49.6	1.4	0.415	456
Wall			T70	16.5	33.7	49.8	1.5	0.489	391
A3-0.75			T70	16.9	30.5	52.6	1.7	0.553	385
A4-1			T70	17.3	29.9	52.8	1.8	0.579	356
Hempcrete	[COL04]		T70	16.4	34.1	49.6	1.5	0.48	425
Hempcrete	[EIR]	Casted in place and compaction	MK+L	20.5	39.8	39.76	1	0.515	-
Shotcrete	[ELF08]	Dry-mix shotcrete	T70	16	34	50	1.5	0.471	417-551
Wall	[EVR08]	Casted in place and compaction	T70	17	33	50	1.52	0.52	318
Roof		Precast hempcrete	T70	25	25	50	2	1	
A	[BRU09]	Vibrational table	L+HL	11.97	42.74	45.30	1.06	0.28	
B			L+HL	12.41	37.59	50.00	1.33	0.33	
C			L+HL+C	12.00	40.00	48.00	1.20	0.30	
D			L+HL+C	11.72	41.84	46.44	1.11	0.28	
E			C	10.43	47.39	42.18	0.89	0.22	
AAA	[NGU10]	Casted in place and variable compaction till 2.2 MPa	T70	36.7	40.8	22.4	0.55	0.90	612.2
BBB			T70	20.0	43.1	36.9	0.86	0.47	674.3
BBA			T70	26.2	47.6	26.2	0.55	0.55	-
BBC			T70	19.5	41.7	38.8	0.93	0.47	642.8
ABB			T70	32.7	36.3	31.0	0.86	0.90	-
CBB			T70	13.3	46.6	40.0	0.86	0.29	-
BAB			T70	20.0	43.1	36.8	0.85	0.46	768.6
BCB			T70	20.0	43.1	36.9	0.86	0.47	513.0
CCC			T70	12.6	43.7	43.7	1.00	0.29	-
BAA			T70	23.1	49.7	27.2	0.55	0.46	584.8
BAC			T70	19.4	41.8	38.8	0.93	0.47	506.2
BCA			T70	23.1	49.7	27.2	0.55	0.46	813.7
BCC			T70	19.4	41.7	38.8	0.93	0.47	712.6
AAC			T70	31.9	35.4	32.7	0.93	0.90	746.3
CAB			T70	13.4	46.6	40.0	0.86	0.29	574.6
CAA			T70	15.6	54.5	29.8	0.55	0.29	-
CAC			T70	13.0	45.0	42.0	0.93	0.29	492.5
CCA			T70	15.7	54.4	29.9	0.55	0.29	-
BBB			CPA	20.0	43.1	36.9	0.86	0.47	-

Mixture	Literature	Implementation method	Nature of binder	Mass of raw material (%)			W/B	S/B	ρ_{dry} (kg/m³)
				Shiv	Binder	Water			
BBB	[NGU10]	Casted in place and variable compaction till 2.2 MPa	NHL 2	20.0	43.1	36.9	0.86	0.47	-
BBB			NHL 3,5Z	20.0	43.1	36.9	0.86	0.47	-
BBB			T70	20.0	43.1	36.9	0.86	0.47	-
EL035			T70	21.2	58.4	20.4	0.35	0.36	-
EL045			T70	22.2	53.7	24.1	0.45	0.41	-
EL070			T70	24.2	44.6	31.2	0.70	0.54	-
Roof	CESA		BAT	24.2	30.3	45.5	1.5	0.8	
Floor				13.8	34.5	51.7	1.5	0.4	
CHEN10	[MAG10b]		MK+NHL5	5.8	58.8	35.4	0.6	0.1	
CHEN25				11.7	47.3	41.1	0.9	0.2	
CHEN32				13.7	43.4	42.9	1.0	0.3	
CHEN42				16.8	40.5	42.8	1.1	0.4	420
CHEN45				17.1	38.5	44.4	1.2	0.4	414
FORM5				11.7	47.3	41.1	0.9	0.25	
B-Ch-Ref	[NOZ12]		Pumice + CL90	19.5	39.1	42.2	1.06	0.5	485.3
B-Ch-Ca				19.5	39.1	42.2	1.06	0.5	497.2
PHC	[COL13a]		CaO+HL	22.81	35.09	42.11	0.65	1.2	460
SHC			T70	21.74	43.48	34.78	0.50	0.8	430
MHC			T70	16.13	32.26	51.61	0.50	1.6	430

Table 1.11 presents mass of raw materials by their mass proportions in the fresh state, moreover mass of water to mass of binder ratio (W/B) and mass of shives to mass of binder ratio (S/B) are also calculated for comparison. This table shows that different methods of implementation were tested: casted in place, shotcrete or precast hempcrete. The initial compaction was also different. The binders used were also diversified: Tradical 70 (T70), aerial lime (L), hydraulic lime (HL), cement CPA 52.5 (CPA), cement CEM II/A-L (C) metakaolin (MK), natural hydraulic lime (NHL2 and NHL 3.5Z), batichanvre (BAT), pumice and CL90 lime. The contents of raw materials were distinct from one study to the other: binder content varies from 25 to 58.8%, shiv content from 5.8 to 36.7%, and water to binder ratio from 0.35 to 2. Consequently, the variation of dry density was very large (from 250 to 813.7 kg/m³). This variation can be related to the shiv content as presented on Figure 1.10.

Figure 1.10 shows that the higher the shiv content of hempcrete is, the lower the dry density will be. This figure also shows that the Nguyen's results [NGU10] differed from the others: in comparison with the other authors' results, his samples gained a higher dry density in spite of their high shiv content. In fact, in Nguyen's work, a very high stress of compaction was applied for the fabrication of hempcrete samples (this stress was kept

during 48 hours until demoulding) leading to a decreased porosity and therefore increased density.
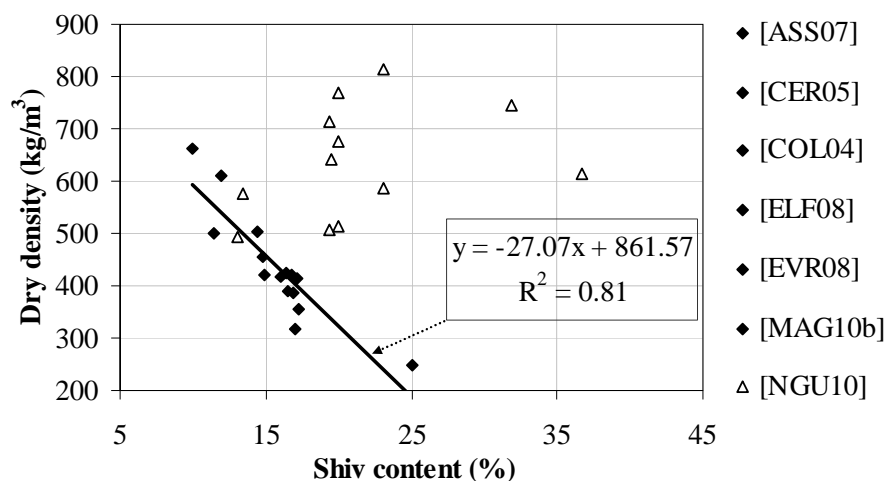
Figure 1.10: Dry density of hempcrete in function of shiv content

1.5.2 Mixing method, fabrication of specimens and curing condition

Different mixing methods were applied to mix hempcrete in the previous studies. These procedures are presented in Table 1.12.

Table 1.12: Process of mixing for hempcrete

Non-wetting hemp shiv *[ASS07, CHA08, ARN12]*	*Pre-wetting hemp shiv*	
	[ASS07]	*[CER05, NGU10 & NOZ12]*
1. Introduce water entirely	1. Introduce hemp shives	1. Introduce hemp shives
2. Introduce binder	2. Introduce 1/3 of mixing water quantity	2. Introduce water to wet hemp shives
3. Mixing until obtaining a homogeneous slurry	3. Introduce gradually the binder and the residual water.	3. Introduce binders
4. Introduce hemp shives		4. Introduce water to mix
5. Mixing until obtaining a homogeneous mixture	4. Mixing until obtaining a homogeneous mixture	5. Mixing until obtaining a homogeneous mixture

Table 1.12 shows two main methods: using non-wetted or wetted hemp shives. In other study, Bruijn et al. [BRU09] presented another method: wetting hemp particles and forming binder slurry in two separate mixers, after that the binder slurry was put in the mixer contained wetted shives and continually mixed to reach a homogeneous mixture of hempcrete. The authors [CER05, BRU09, NGU10 & MON11] indicated that the pre-

wetting of hemp particles limits the competition with mineral binder for water during the fabrication of hempcrete, therefore, improves interaction of binder and plant aggregates.
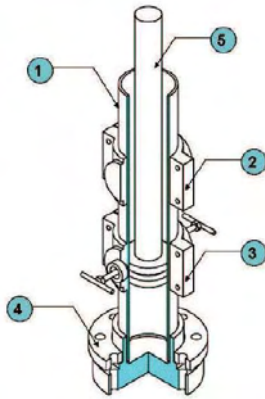
1 – PVC cylinder : H = 600 mm, Ø =100 mm

2 and 3 – PVC collar to reinforce

4 – Bottom slab

5 – Steel piston

Figure 1.11: Compaction device [NGU10]

For hempcrete casted in place, cylindrical and cubic moulds with different size were used. The mould was often coupled with a compaction system in order to ensure the good cohesion of materials during casting, for exemple the compaction device used by Nguyen [NGU10] is presented on Figure 1.11. Hempcrete samples were removed from the moulds after 1-2 days of curing at 20°C and 95% relative humidity, after that they were conserved in condition at 20°C and 50 - 95% relative humidity as presented in Table 1.13.

Table 1.13: Sample size and curing condition of hempcrete

Literature	Sample size	Curing condition		Demould
		Temperature	Relative humidity	
Arnaud [ARN12]	Ø=16 cm, H=32 cm	20°C	30 - 98%	Non
Bruijn [BRU09]	15x15x15 cm^3	20°C	75 - 95%	2 days
	Ø=15 cm, H=30 cm			
Cerezo [CER05]	Ø=16 cm, H=32 cm	20°C	50%	2 days
Nguyen [NGU10]	Ø=10 cm, H=20 cm	20°C	75%	2 days
Nozahic [NOZ12]	15x15x15 cm^3	20°C	35±5%	1 days
	Ø=11 cm, H=22 cm			
Verdier [VER12]	Ø=16 cm, H=32 cm	20°C	65 - 95%	2 days

For hempcrete using spraying method, samples were fabricated by cutting from the block of hempcrete. In Elfordy's study [ELF08], different samples were cut from hempcrete blocks of 30x60 cm^2 in section and 20 cm in height: cylindrical samples of 8 cm in diameter and 2.5 cm in thickness for the measurement of thermal conductivity, cube samples of 5x5x5 cm^3 for density measurement and compressive test, and blocks of 10x15x30 cm^3 for bending tests. In another study, Chamoin [CHA08] used cubic samples

of 5x5x5 cm^3 and cylindrical samples of 5 cm in diameter and 7 cm in height from blocks of 30x30 cm^2 in section and 16 cm in height. The samples were conserved at 20°C and 50% RH.

The results summarized in this section and section 1.5.1 evidently illustrate the diversity of formulations, casting methods, sample sizes and curing conditions for hempcrete. This can explain the variability found among the previous studies on hempcrete characteristics and the difficulty to compare their results. Thus, it is necessary to develop standardized testing methods.

1.5.3 Interaction between plant aggregates and binder

1.5.3.1 The problems

Plant aggregates in general and hemp shives in particular are strongly absorbent, porous, swelling, anisotropic and heterogeneous. These properties can cause multiplicity of problems for the interaction between mineral binder and these aggregates when they are used to fabricate plant concrete.

Due to great water absorption capacity of hemp particles, a competition with mineral binder for water occurred during the fabrication of hempcrete: the hemp particles tend to absorb the water that is needed to hydrate the binder [NGU10 & ARN12]. This phenomenon generates the chalking phenomenon of hydraulic binders at interface of shiv particle and binder [CER05]. Previous studies [ELF08, MOU09 and NGU10] indicated that the use of binders having strong capacity of carbonation, especially air lime – based binders, is often performed to resolve this problem, at least on the surface. Other previous studies [COU84, VIC99 and ROW05] showed that the swelling of the particles occurs at early age and the detachment between plant particle and matrix at interface takes place during dry process. This detachable phenomenon causes poor resistance to degradation for the bond of plant particles and matrix during drying process [MOH06 & SAV02]. Furthermore, the mechanical setting of the hempcrete can be disrupted due to a physico-chemical interaction between the binder and the shiv in high relative humidity [ARN12]. Thus, according to this author, the relative humidity of 50% is the most suitable curing condition for the mechanical setting of hempcrete.

The contact between plant particles and the high alkaline medium of mineral binder solution leads to solubilize the polysaccharide extractives and to the degradation of products of alkaline attack [GOV04 & SED07]. This can delay the setting of cement

[DIQ12, GOV04, RAT13 & SEM02]. Moreover, Diquelou's results [DIQ12] showed that water extractives from hemp shives extremely delay the formation of $Ca(OH)_2$ (0% after first day) and reduce of 25% the compressive strength of the Portland cement paste in comparison with that of paste using fresh water. The reduction of compressive strength of pozzolanic paste using water extractives of hemp shiv and lavender aggregates is also demonstrated in Ratiarisoa's results [RAT13]. For the interaction between hemp shiv and cement, Diquelou [DIQ12] concluded that the diffusion of water extractive from hemp shiv to cement paste causes non-hydrated, retarded and non-influence zones of cement paste around the shiv during the hardening process of cement paste. This leads to the rupture of cohesion between shiv and cement.

1.5.3.2 Improvement of interface between binder and plant aggregates

The paragraphs above indicate that the problems of the interaction between plant aggregates and mineral binder were generated due to the great water absorption capacity of plant particles. In order to tackle completely these problems, the plant particles could be enclosed by a substance to limit their water absorption.

For the treatment method of plant aggregates, we can find different methods in the literature. Khazma et al [KHA08] enclosed flax particles with a mixture of cement and sucrose. Flax concrete was fabricated with a cement and sucrose to flax particles ratio by mass of 1.5 and a conservation in humid condition (98% RH, 20°C) during 28 days before fabrication of concrete. Monreal et al [MON08 & MON11] enclosed beet pulp with different substances and different substance to aggregates ratios by mass (cement: C/P = 1, lime: L/P = 1.67, and linseed oil: O/P = 1). The aggregates treated by cement and lime were conserved at 20°C and 98% RH, and the aggregates treated by linseed oil were conserved at 50°C in 21 days. Nozahic [NOZ12] treated hemp particles by lime and linseed oil: for the treatment by lime, dry hemp aggregates were immerged in saturated calcium hydroxyl solution (40 g/l) in 2 hours then dried until constant mass; for treatment by linseed oil, dry hemp particles were mixed with linseed oil (oil to shiv ratio: 0.5) during 5 minutes and then conserved at 20°C and 35% RH during 20 days.

In regard to water absorption, the results showed a significant decrease in water absorption capacity of treated aggregates (from 40 to 80%) in comparison with that of untreated aggregates [KHA08, MON08, MON11 & NOZ12].

For the compressive strength of concrete, the results obtained in these different studies are more contrasting. The result of Khazma et al [KHA08] showed a significant

increase in compressive strength of concrete containing the treated aggregates (2.5 MPa in comparison with 0.44 MPa for concrete with untreated aggregates). This result is explained by the improvement of the cohesion between treated aggregates and matrix [KHA08]. On the contrary, Moreal et al [MON08] and Nozahic [NOZ12] indicated that the compressive strength of concrete with treated aggregates is lower than that of untreated aggregates concrete. These results show the reduction of interface's quality between plant particles and matrix [NOZ12].

In conclusion, the previous studies confirmed the extreme reducing effect of water absorption for treated plant aggregates with different treatment methods. However, these different treatment methods presented both positive and negative effects of mechanical performances of concrete. Thus, it will be necessary to follow the study of the treatment method of plant aggregates in order to improve mechanical performance of concrete.

1.5.4   Mechanical properties

Hempcrete possesses a high degree of porosity and its compressibility is therefore high. Many studies have been published on development of formulations and implementation methods of hempcretes using different binders and hemp shiv with different dosages in order to use it as a building material. The influence of the factors on the mechanical properties of hempcrete has also been studied.

1.5.4.1 Synthesis of mechanical test parameters and compressive strength

There is not standardized testing method for hempcrete, therefore, the previous studies had been carried out with different testing methods. The Table 1.14 synthesized the parameters of hempcrete tests from different studies.

Table 1.14: Parameters of mechanical test for hempcrete

Literature	*Sample size (cm)*	*Method of implementation*	*Timescale for demould*	*Condition of conservation*	*Timescale for test*	*Test speed (mm/min)*
[ARN12]	Φ16xH32	Very weak compaction (0.05MPa)	48 hours	20°C, 30-98%	21 days to 24 months	5
[BRU09]	15x15x15 Φ16xH32	Vibrational table	48 hours	20°C, 50-95%	18 weeks	No information
[CER05]	Φ16xH32	Very weak compaction (0.05MPa)	Conservation in moulds without top and bottom	20°C, 50%	21 days to 48 months	0.25 - 5
[ELF08]	5x5x5	Shotcrete	Conservation in moulds	No information	1 month	5
[MAG10b]	4x4x16	Manual	48 hours	20°C, 95%	9 days to	0.5

Literature	*Sample size (cm)*	*Method of implementation*	*Timescale for demould*	*Condition of conservation*	*Timescale for test*	*Test speed (mm/min)*
[ARN12]	Φ16xH32	Very weak compaction (0.05MPa)	48 hours	20°C, 30-98%	21 days to 24 months	5
[BRU09]	15x15x15 Φ16xH32	Vibrational table	48 hours	20°C, 50-95%	18 weeks	No information
		compaction		and external	12 months	
[MOU09]	30x30x16 30x15x16	Shotcrete or Vibration	1 week	20°C, 50%	9 days to 15 months	5
[NGU10]	Φ10xH20	Compaction until 2.5 MPa	48 hours	20°C, 75%	28 days 90 days	6
[NOZ12]	Φ11xH22	Compaction: 2 MPa	24 hours	20°C, 35±5%	60 days	11
	15x15x15		24 hours	20°C, 35±5%	60 days	7.5
[VER12]	Φ16xH32	Compaction 0.6 MPa	48 hours	20°C, 65-95%	28 days	5

Table 1.14 presents the diversity of the test parameters: the age of the test is variable (from 9 days to 48 months), the test speed varies from 0.25 to 11 mm/min. This can lead to a difficult comparison of mechanical behavior of hempcrete.

The figures from Figure 1.12 to Figure 1.16 present results of different studies investigating compressive strength of hempcrete.
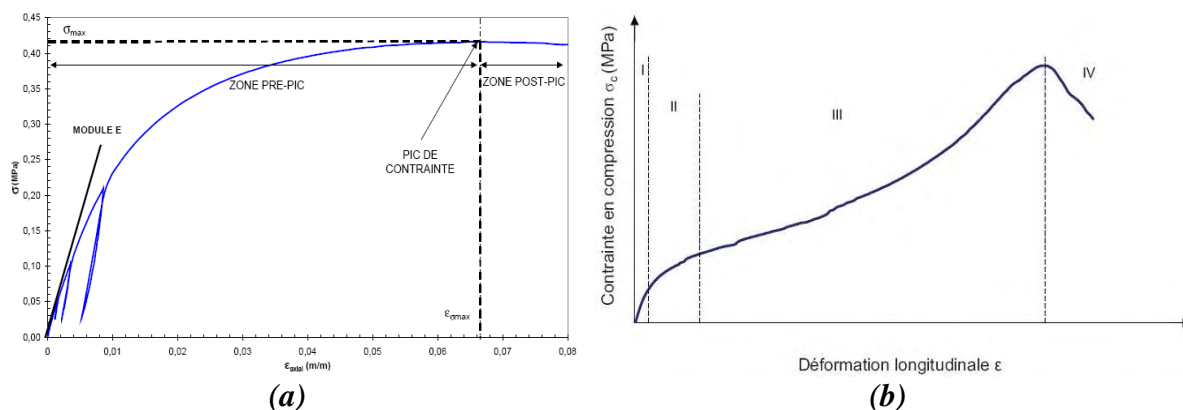
Figure 1.12: Compressive stress vs deformation, (a) - [CER05] and (b) – [NGU10]

The Figure 1.12 shows two different mechanical behaviors between Cerezo's and Nguyen's results. Cerezo's result in the Figure 1.12a indicates that three distinct zones can be distinguished in the mechanical behavior:

- At the beginning of the test, the first zone is likened to a linear elastic material,

- In a second time, this pre-peak zone presents a behavior as elasto-plastic material,

- Beyond the maximum stress, in the post-peak zone, the binder is totally degraded. The mechanical behavior of the particles becomes predominant. Their elastic module is much lower than that of the matrix, the strength decreases.

While Nguyen's result (Figure 1.12b) distinguished four zones in the mechanical behavior:

- Zone I presents a behavior as linear elastic material being the same as Cerezo's result,

- Zone II presents a behavior as elasco-plastic material being only the same as the beginning of pre-peak phase in Cerezo's result. This phase shows that development of damage to the binder and/or the interface between the hemp particles and the matrix,

- Zone III presents a constant increase of stress with the strain, the end point of this phase is the peak of stress. This zone is clearly different from the last of pre-peak zone in Cerezo's result. This phase indicated distribution of the stress into the hemp particles and beginning of their compaction,

- Zone IV is destructive phase of material being similar to the post-peak zone in Cerezo's results.

The difference of mechanical behavior between Cerezo and Nguyen can be attributed to the difference of initial compaction. The very high initial compaction induced the high prestressed hemp shiv which is better support, therefore, the compressive strength of hempcrete increases continuously when cohesion of binder and shiv was destroyed. That is why zone III was formed in Nguyen's result.
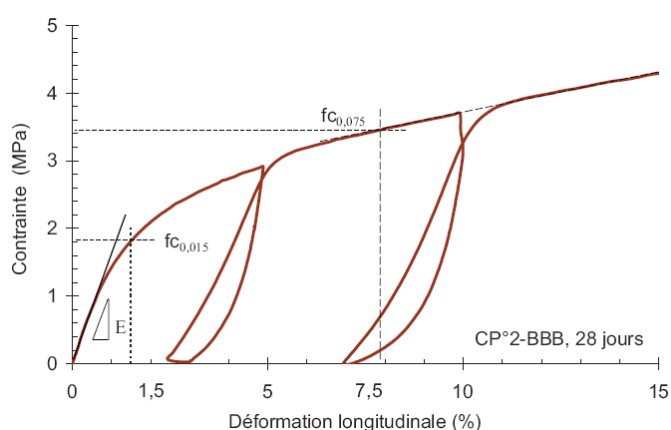
Figure 1.13: Compressive stress vs deformation, [NGU10]

Due to high compressibility of hempcrete, Nguyen [NGU10] chose to measure the stress corresponding to relative deformation of 1,5 and 7,5 % (Figure 1.13) to characterize the mechanical behavior of the material. Cerezo [CER05] characterized the mechanical

performance of hempcrete by maximum stress because Cerezo's hempcrete presented a more fragile behavior than Nguyen's hempcrete (Figure 1.12).
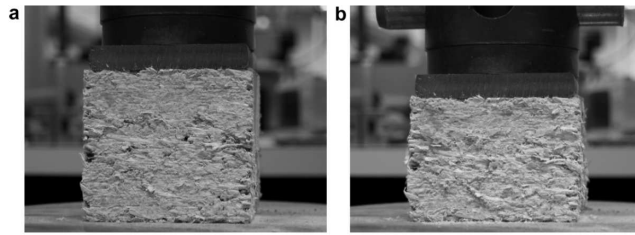
Figure 1.14: Illustration of the compaction of the material under compression: before (a) and after (b) compression test [ELF08]
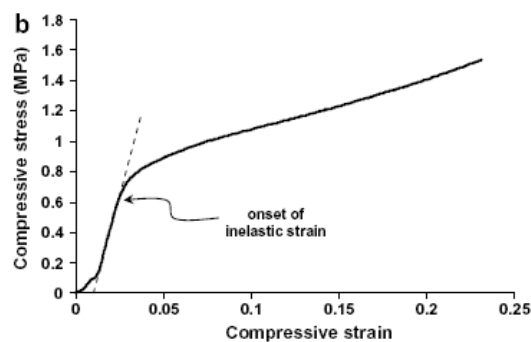
Figure 1.15: The compressive stress vs deformation [ELF08]

Figure 1.14 and Figure 1.15 present the mechanical behavior of sprayed hempcrete. The result shows a continuous increase of stress beyond the onset of inelastic strain and the samples is not break. This behavior indicates the ductile characteristic of hempcrete which is comparable with Nguyen's result in zone III.
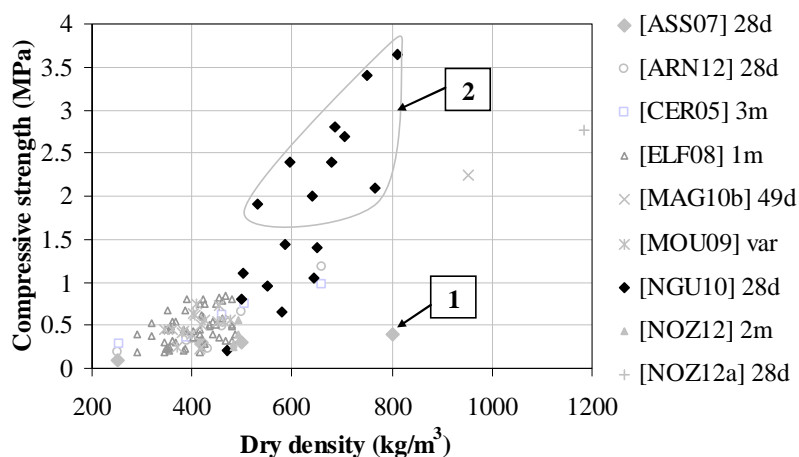
Figure 1.16: Rapport between compressive strength and dry density in literature

The Figure 1.16 synthesizes the values of compressive strength of different hempcrete formulations in function of their dry densities from previous studies. For global

trend, it is evidently seen that the higher the dry density of hempcrete is, the higher the compressive strength will be, except one result of [ASS07] and some results of Nguyen [NGU10], (N°1 & 2, Figure 1.16). One result of [ASS07], (N°1, Figure 1.16), has a very high density (800 kg/m^3), but its strength is very low (0.4 MPa). Some results of Nguyen [NGU10], (N°2, Figure 1.16), were very different from global trend, they presented much high strengths against others with the same densities. These much higher strengths can be attributed to the very high stress of compaction during fabrication (until demould time) of hempcrete samples. Moreover, this synthesis indicates that the values are very variable among these studies (the compressive strength varies from 0.06 to 3.65 MPa, when dry density range from 250 to 810 kg/m^3). This can be attributed to the influence of a lot of parameters on the mechanical behavior of hempcrete such as the dosage and nature of raw materials, the method of implementation (especially the initial compaction), timescale and speed of the test. Next parts will detail the influence of the distinct predominant parameter on mechanical behavior of hempcrete.

1.5.4.2 Influence of binder content and nature

As regards dosage of binder, several authors have studied its influence on mechanical properties of hempcrete. Table 1.15 and Figure 1.17 below show the results from literature.

Table 1.15: Mechanical characteristics of hempcrete versus binder content in literature

Literature	*Binder content (%)*	*σ_{max} (MPa)*	*E (MPa)*	*$\varepsilon_{\sigma max}$*
[ASS07]	25.0 – 57.1	0.10 – 0.40	3 – 25	–
[ARN12]	24.6 – 47.7	0.19 – 1.18	7 – 160	0.132 – 0.032
[CER05]	24.6 – 47.7	0.28 – 0.98	4 –160	0.140 – 0.029
[NGU10]	35.4 – 49.7	1.92 – 3.60	39 – 147	

The results presented in Table 1.15 and Figure 1.17 show that the more important the binder content is, the higher the stress level is and the higher the modulus of elasticity is. Indeed, the higher the concentration of binder in the mixture is, the closer to the mechanical behavior of the pure binder the mechanical behavior of the hempcrete is [ARN12]. Conversely, the more the hemp shiv content of hempcrete increases, the higher the deformability is – hence the presence of a ductile phase, observed by [CER05] and [ARN12]. For the Nguyen's results [NGU10], they show much higher values of strengths in comparison with others because the much higher initial compaction during 2 days before demould was applied when the samples were fabricated (see the section 1.5.4.4).
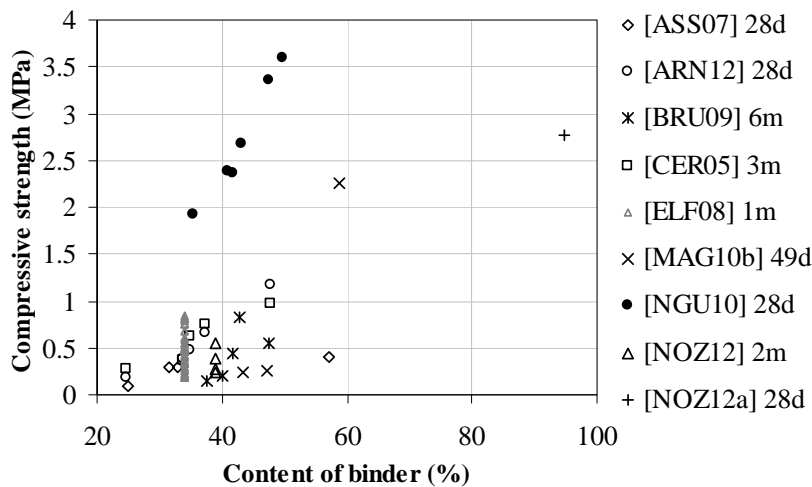
Figure 1.17: Compressive strength in function of binder content for hempcrete

In regards to the nature of binder, the different binders such as limes, cement, pozzolanic binder were used to fabricate hempcrete in the previous studies. The investigation showed that the mechanical behavior of hempcretes using different binders were different. Nguyen [NGU10] compared the compressive strengths of hempcretes fabricated with four different binders (cement CPA 52.5, NHL2, NHL3.5Z and Tradical 70) with the same content of raw materials, cast method and conservation condition. The results are presented in Figure 1.18 below.
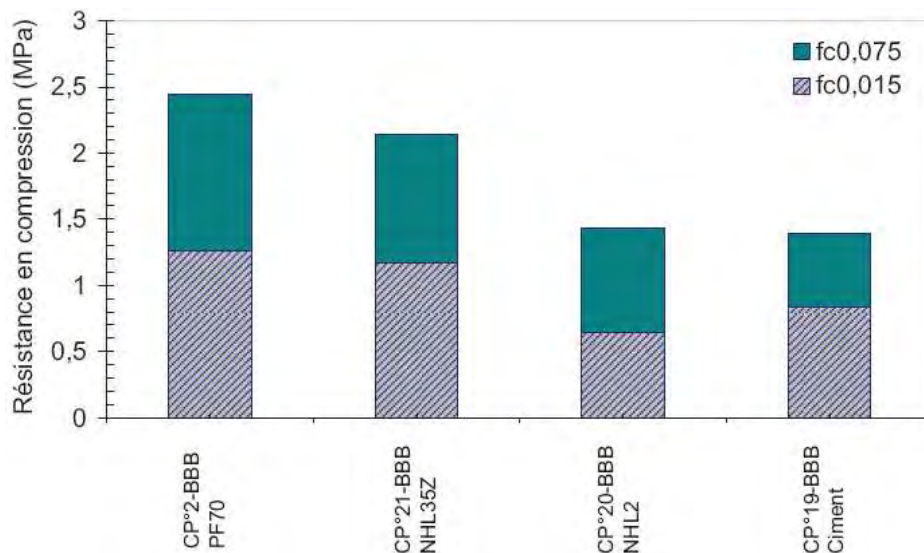
Figure 1.18: Compressive strength of samples fabricated by different binders [NGU10]

The Nguyen's results on Figure 1.18 illustrate that the samples fabricated with cement presented lower compressive strength than the others fabricated with natural hydraulic lime (NHL2) or binders containing pozzolan (T70 and NHL3.5Z). The author

54

attributed this result on one hand to the poor hydration and disturbance of water absorption of hemp shiv, and on the other hand to the more fragile behavior of cement that can lead to the lower strength.

Bruijn [BRU09] also showed the different compressive strengths of hempcretes using the different binders. In spite of the highest binder content (47.4% by weight), the hempcrete using only cement presented the significant lower compressive strength in comparison with the hempcrete using a binder made of 50% cement, 20% hydrated lime and 30% limes with a lower binder content (41.8% by weight).

1.5.4.3 Influence of test direction

In previous studies, the compressive strength of hempcrete was evaluated according to two test directions: the test direction according to the direction of compaction – called "parallel direction", and the test direction being perpendicular to the compaction direction – called "perpendicular direction". The authors showed difference of mechanical behavior between these two directions [ELF08, MOU09 & NOZ12]. Figure 1.19 below is an example presented the Nozahic's results of compressive tests according to two directions.
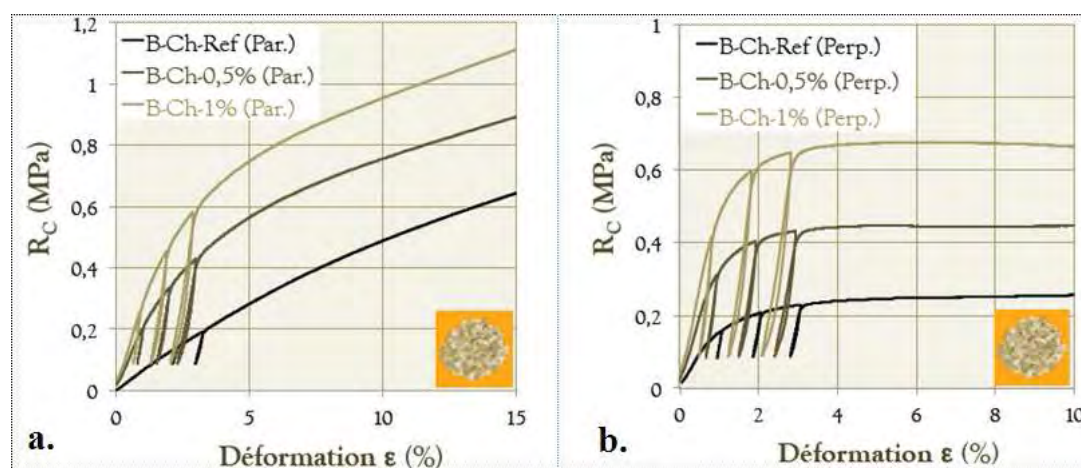
Figure 1.19: Compressive strength in function of parallel direction (a)

and perpendicular direction (b) with compaction direction of samples [NOZ12]

In the case of parallel direction, the mechanical behavior presented a continuous increase of stress (Figure 1.19a). Nozahic [NOZ12], Mounanga [MOU09] and Elfordy [ELF08] attributed this ductile behavior to the compressibility and the initial orientation of hemp particles. For the case of perpendicular direction, Figure 1.19b shows that hempcrete is more rigid than that of first case, and the stress curves gradually decrease after reaching the maximum value. Previous studies [ELF08, MOU09 & NOZ12] attributed this result to

the joints of binder around hemp shives. Moreover, Figure 1.19b presents the gradual decrease of stress curves after hempcrete rupture. Nozahic [NOZ12] attributed this phenomenon to the existence of friction among particles in spite of the rupture of the joints of binder.

1.5.4.4 Influence of initial compaction

The initial compaction is a load applying pressure to a hempcrete sample when it is manufactured. Figure 1.20 below shows Nguyen's results [NGU10] which present influence of the initial compaction on the mechanical performance of material.
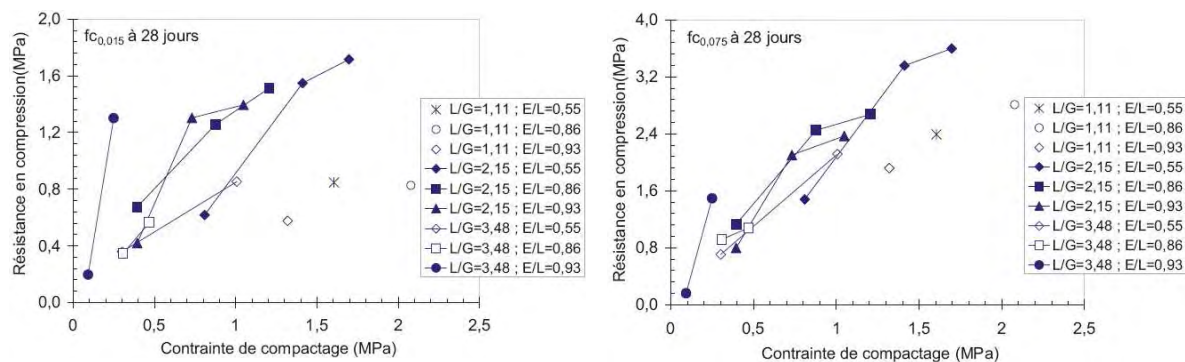
Figure 1.20: Compressive strength vs deformation of hempcrete at 28 days [NGU10]

In Figure 1.20, Nguyen [NGU10] presents the compressive strength results of hempcretes fabricated with different initial compaction (from 0.25 to 2.5 MPa), this initial compaction was remained during 2 days before demoulding. It can be seen that the higher the initial compaction is, the higher the compressive strength will get. Nguyen [NGU10] explained that the initial compaction decreases the hempcrete porosity, and the compressive resistance therefore augments.

1.5.4.5 Influence of curing condition

In the previous studies, various curing conditions were applied for conservation of hempcrete after casting. Magniont [MAG10b] and Arnaud et al [ARN12] presented two different studies of influence of curing condition on mechanical behavior of hempcrete. Magniont studied mechanical performance of hempcretes cured in climatic room (95% RH) and in outdoor conditions. While, Arnaud et al [ARN12] studied the compressive tests of the hempcrete samples preserved in their mould until the date of the test at 20°C and in four different conditions of relative humidity controlled using saturated saline solutions: 30%, 50%, 75% and 98% RH. Figure 1.21 and Figure 1.22 below presented the results of two authors.
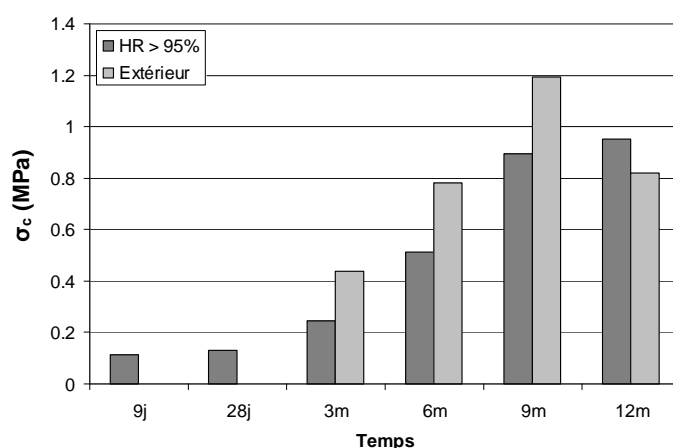
***Figure 1.21: Evolution of compressive strength of hempcrete for 1 year
in controlled and external curing conditions [MAG10b]***

The Magniont's results presented in Figure 1.21 show that the compressive strength of hempcrete conserved in external condition is 1.3 to 1.7 times higher than that of hempcrete conserved in climatic room until 9 months of age. Magniont [MAG10b & MAG12] attributed this result to the positive influence of the carbonation and the migration of hydration products into the pores of hemp shives improving their rigidity and consequently the mechanical properties of hempcrete. She also attributed the decrease of strength after 12 months to the experimental dispersion or the high water content of the samples at the time of the test, or to lixiviation phenomenon of matrix due to the degradation mechanism in long term in outdoor condition.
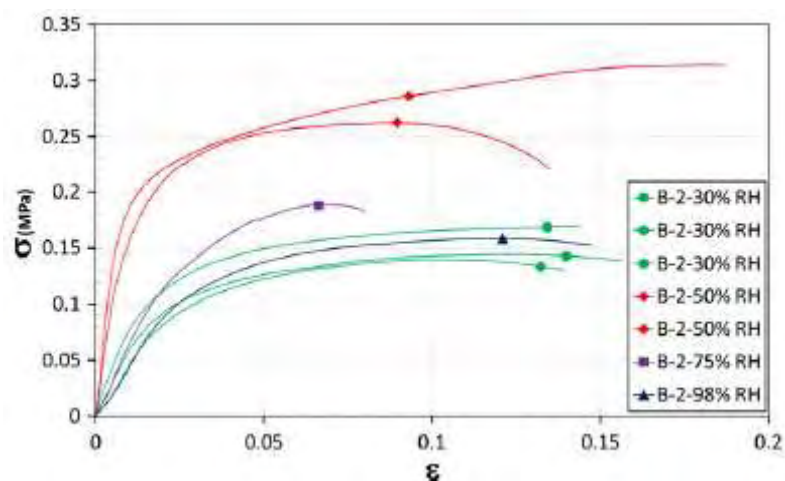
Figure 1.22: Compressive strength of hempcrete at 28 days [ARN12]

Figure 1.22 shows that the compressive strengths and Young's moduli of the hempcrete cured in 50% RH were much higher than those of hempcrete conserved in high relative humidity (75% and 98% RH) as well as in low relative humidity (30% RH). The

author explained that a humid environment (75% and 98% RH) slows down sharply the setting of the hempcrete because the diffusion of CO_2 from the air through the pores of a lime mortar is indeed hindered due to the very high internal relative humidity of the material.

1.5.4.6 Influence of particle size of hemp shiv

Hemp shives were supplied from different producers, the particle size distribution of shives is therefore different. Arnaud [ARN12] studied the mechanical properties of hempcrete based on three different shives (D-1, D-2 and D-3), where the particle size of shiv D-1 are slightly coarser than those of shiv D-2, and shiv D-3 is much finer than the shiv D-1 and D-2. Nguyen [NGU10] fabricated hempcrete samples based on four different shives (T1: 1.25–2.5, T2: 2.5 – 3.15, T3: 3.15 – 5 and T4: > 5mm).

At 28 days, both Arnaud's and Nguyen's results showed that the coarser the particle size of hemp shiv is, the higher the mechanic performances will be.

However, it is difficult to evaluate the influence of shives' particle size distribution on mechanical behaviors of hempcrete in longer time because both Arnaud's and Nguyen's results presented the contradictory mechanical performances at 90 days.

1.5.4.7 Evolution of mechanical properties in function of time
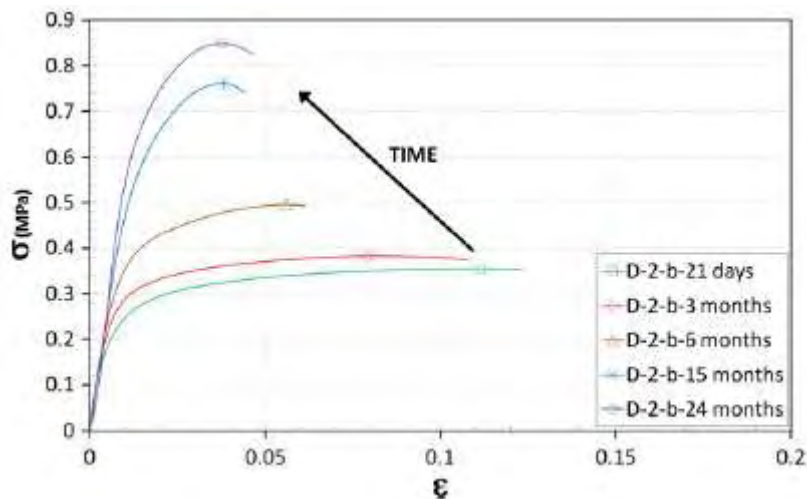
Figure 1.23: Compressive stress vs deformation [ARN12]

Previous studies have shown the mechanical strength evolution of hempcrete in function of variable time (from 1 week to 2 years as presented in Table 1.14). The Figure 1.23 is an example presenting the mechanical strength evolution of hempcrete from 21 days to 24 months.

Figure 1.23 indicates that the mechanical properties of hempcrete increases in function of time until 2 years. The mechanical behavior of hempcrete at the early aging periods (21 days, 3 and 6 months) is linked to the properties of the particles, because the binder has not yet fully formed connected network. In the long term (beyond 6 months), the hardening mechanism of binder plays an important role in the mechanical evolution of composite (the concretes then support increasing stresses (from 0.35 MPa to 0.85 MPa between 21 days and 24 months of setting) and their behavior is less and less ductile (strains go down from 0.11 to 0.04)) [ARN12].

In other study, Magniont [MAG10b, MAG12] presented the evolution of compressive strength of hempcretes conserved by two different conditions after 12 months (Figure 1.21 above). This figure shows the significant increases of compressive strength of hempcretes until 9 months of age (the strengths after 9 months are around 3 times higher than those after 3 months).

1.5.5 *Mass evolution and porosity of hempcrete*

Due to the high water absorption coefficient of the hemp shiv particles, the dosages of mixing water for hempcrete are very high. This induces a long drying time and an important mass loss of the building elements. The kinetics of drying studied in different conditions are presented on Figure 1.24 to Figure 1.26.

The drying kinetics of hempcrete samples presented on Figure 1.24 to Figure 1.26 show that the mass stabilization is reached after around 40 days [NGU10 & NOZ12] or 60 days [CHA08]. After 60 days of drying time, the total mass loss of hempcretes was very different among the studies: approximately 47% for precasted hempcrete formulation and 29% for sprayed hempcrete formulations (Figure 1.24), from 11 to 33% depending on hempcrete formulations (Figure 1.25), and around 39% (Figure 1.26). The Chamoin's and Nguyen's studies [CHA08 & NGU10] illustrated that the total mass loss depends on the mixing water content of the hempcrete mixture (the higher the mixing water content is, the higher the total mass loss of hempcrete after drying time reaches). Indeed, the higher water content of precasted formulations induced its higher mass loss in comparison with the sprayed formulation for Chamoin's results (Figure 1.24); for Nguyen's results, the total mass loss of CP9 sample having maximum water content (43.7 %) is 33% and that of CP1 water content minimum (22.4 %) is 11%; the Nozahic's result was also comparable with Nguyen's results (42.2 % of water content, 39% of mass loss).
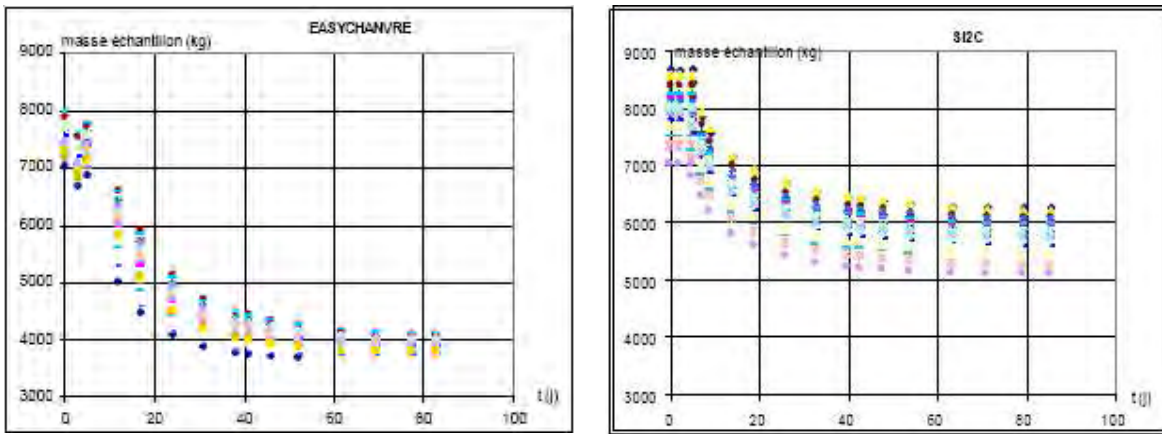
a) Precasted hempcrete - Easychanvre   *b) Sprayed hempcrete – SI2C*

Figure 1.24: The kinetic of mass loss of Easychanvre and SI2C hempcrete samples

at 23°C, 50% HR [CHA08]
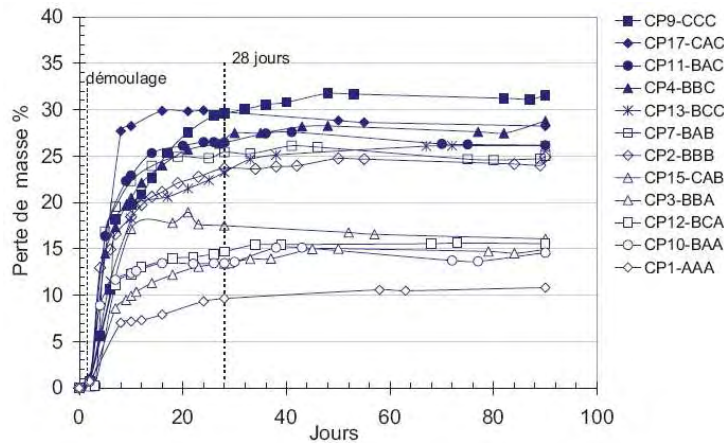
Figure 1.25: The kinetic of mass loss of hempcrete at 20°C, 75% HR [NGU10]
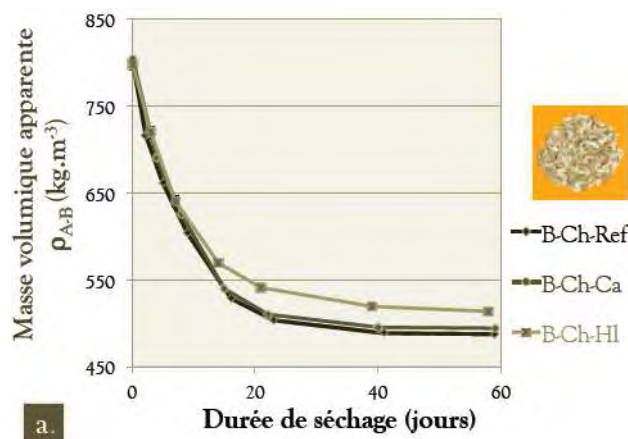
Figure 1.26: The kinetic of mass loss of hempcrete samples

at 20°C, 35% HR [NOZ12]

The porosity measurements and apparent density of hempcrete in literature are presented in Table 1.16 below.

Table 1.16: Porosity of hempcrete in literature

Mixture	Literature	Total porosity (%)	Open porosity (%)	Apparent density (kg/m³)
Hempcrete	[COL04]	76.5 - 78.4		390 - 425
Hempcrete	[COL08]	76.5	70.6	440
Hempcrete	[CER05]	77 - 80	67 - 85	256 - 661
SI2C	[CHA08]	77.43	53.02	290
Easychanvre		79.52	54.71	440
Hempcrete	CEBTP [ARN08]	73.9		620
		67		740
Hempcrete	ENTPE [ARN08]	74 - 78		440
		73 - 76		390
Hempcrete	Gourlay [ARN08]	77 - 85		247 - 386
CHEN10	[MAG10b]		58.5	951
CHEN25			70.5	700
CHEN32			73.5	593
Hempcrete	[NOZ12]	78.4		490
		78.1		491.9
		78		494.5
Hempcrete	[COL13a]	72	68	460
		78	66	430
		79	67	430

Table 1.16 shows that the range of total porosity and apparent density of hempcrete among different studies is very large (total porosity varies from 67 to 85%, and apparent density is respectively from 250 to 951 kg/m³). This is due to the difference of raw material contents. The hempcrete is a porous material obtained from mineral binders, hemp shives and water, thus studying its porous structure allows evaluating the thermal behavior and mechanical strength. The evaporation of this large amount of excess water generates the formation of a significant level of porosity in the dry state. This porosity is added to the initial porosity of hemp shiv particles as well as of the binder (pores of the hydrates).

1.5.6 Thermal conductivity

The thermal conductivity characterizes the ability of a material to transmit heat by conduction. The thermal conductivity of hempcrete depends on various factors such as the nature and dosage of raw materials, the method of the sample manufacture and the water content of the material. In this section, we will investigate the influence of the factors on the thermal conductivity of hempcrete.

1.5.6.1 Synthesis of test parameters and thermal conductivity values

Numerous previous studies measured thermal conductivity of hempcrete based on different methods and mixtures as well as implement methods, the test parameters and thermal conductivity values are synthesized in Table 1.17 and Figure 1.27 respectively.

Table 1.17: Parameters of the thermal conductivity tests

Reference	*Method*	*Sample state*	*Sample Size (cm)*	*T (^{o}C)*	*ΔT (K)*	*Test direction*
Arnaud [ARN09]	-	-	27x27xH5	-	-	//
Bruijn [BRU13]	Hot disk	30°C, 15% RH	Φ5.5xH5			//
		20°C, 65% RH				//
Cerezo [CER05]	Hot box	Dry				//
Collet [COL04]	Hot plate	Dry	Φ10xH5 10x10xH5	23	15	//
Elfordy [ELF08]	Hot plate	-	-	25	10	//
Evrard [EVR08]	Hot plate	Dry; 50, 65 & 80%RH	H3	18 - 34	10	//
Magniont [MAG10b]	Hot plate	Dry, 65&95%RH	15x15xH-var	25	10	//
Nguyen [NGU10]	Hot plate	Dry	6x6xH3	25	10	//, ⊥
Nozahic [NOZ12]	Hot wire	Dry	15x15xH15			//, ⊥
Picandet [PIC11]						//, ⊥
Tran [TRA10a]	-	Variable RH				

H-var: variable height; // & ⊥: parallel & perpendicular direction

Table 1.17 shows that the measurements of thermal conductivity of hempcrete were carried out with the different parameters among authors.

Cerezo's model [CER05]

$y = 0.0002x + 0.0102$
$R^2 = 0.7934$

+ [ARN09]
△ [ASS07]
□ [CER05]
✳ [COL04]
× [MAG10b]
◇ [NGU10]
○ [NOZ12]
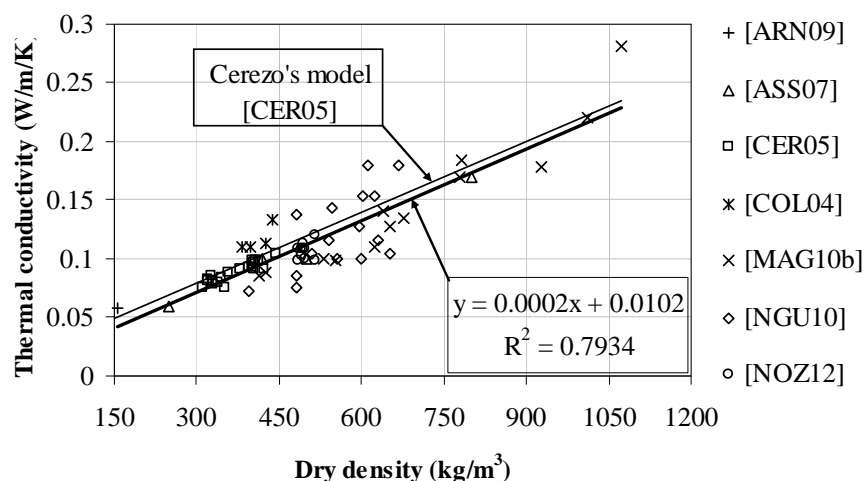
Figure 1.27: Thermal conductivity of hempcrete versus dry density in literature

The Figure 1.27 shows rapport of thermal conductivity and dry density of hempcrete among the studies in the literature. This figure indicates that the thermal conductivity's range of 0.058 to 0.281 W/m/K corresponding the rage of dry density from

155 to 1074 kg/m^3. Thus, the lighter the hempcrete is, the more suitable the thermal conductivity for thermal insulation wall will be. It is interesting to see that the global trend of thermal conductivity of hempcrete is comparable with Cerezo's linear model.

1.5.6.2 Influence of test direction

In order to evaluate the effect of compaction direction on thermal conductivity, several authors [NGU10, NOZ12 & PIC11] measured thermal conductivity of hempcrete according to parallel and perpendicular compacting directions (noted: $\lambda_{//}$ and $\lambda_{\perp}$ respectively). These authors showed that the thermal conductivity values are different between two test directions. The results were synthesized in Table 1.18 below.

Table 1.18: Thermal conductivity of hempcrete

Source	*Test direction*	$\lambda_{\perp}$ *(W/m/K)*	$\lambda_{//}$ *(W/m/K)*	$\lambda_{\perp}/\lambda_{//}$
Nguyen [NGU10]	//		0.066 – 0.120	1.20 – 1.80
	$\perp$	0.104 – 0.170		
Nozahic [NOZ12]	//		0.129 – 0.137	1.15 – 1.33
	$\perp$	0.149 – 0.182		
Picandet [PIC11]	//		0.075 – 0.115	1.30 – 1.60
	$\perp$	0.110 – 0.165		

The results in the Table 1.18 shows the difference between $\lambda_{\perp}$ and $\lambda_{//}$. The thermal conductivities measured according to perpendicular direction were much higher than those measured according to parallel direction ($\lambda_{\perp}/\lambda_{//}$ around 1.15 – 1.8 in function of composition). The authors attributed this difference to the orientation of shiv particles in hempcrete samples which was induced by the initial compaction and the anisotropy of hemp particles.

1.5.6.3 Influence of relative humidity

For the influence of relative humidity on the thermal conductivity of hempcrete, the previous studies measured thermal conductivity of hempcrete at different relative humidity. In literature, the thermal conductivity of hempcrete was measured in the range of relative humidity from 15 to 95% [ARN09, BRU13, EVR08, MAG10b & SAM08]. The measurements confirmed that the thermal conductivity coefficient of hempcretes measured at all relative humidities are higher than that at dry state. Samri [SAM08] attributed this result to the liquid water contained in the hempcrete modifies the thermal conductivity of the hempcrete (the liquid water exhibits a thermal conductivity ($\lambda_{water} = 0.6$ W/(m.K)) 20

times greater than that of dry air (λ_{air} = 0.026 W/(m.K)). However, the influence of each relative humidity on thermal conductivity of hempcrete is very different. Indeed, the measurements at 75 to 95% RH are predominately higher (around 1.32 to 1.74 times), while the measurements at 15 to 65% RH are only slightly higher in comparison with measurements at dry state (around 1.01 to 1.16 times).

1.5.7 Hygroscopic properties

Hempcrete is a highly hygroscopic material. Thus, the use of this material can improve the indoor climate and comfort of occupants because these materials can moderate the indoor humidity variations [ROD05]. The hygroscopic properties of hempcrete are presented by Vapor permeability, Sorption isotherms and Moisture Buffer Value.

1.5.7.1 Sorption isotherms

The equilibrium moisture content plotted versus ambient relative humidity at a given temperature gave the sorption isotherms. Separate sorption isotherms were obtained for specimens initially dry (adsorption isotherm) and specimens initially saturated (desorption isotherm) [COL13a]. Sorption isotherms can be measured by continuous or discontinuous methods. Figure 1.28 below shows the sorption behaviour of a sample.
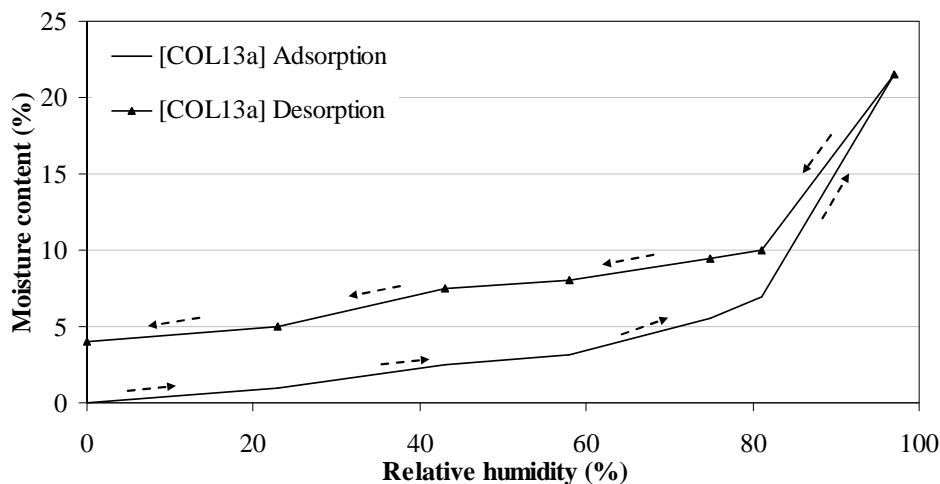
Figure 1.28: Sorption isotherms of hempcrete [COL13a]

The Figure 1.28 shows the absorption and desorption isotherms of hempcrete measured by Collet [COL13a]. For the adsorption isotherm, this figure shows that the moisture content of hempcrete increase gradually in function of relative humidity until the RH = 81% (moisture content is around 7% at RH = 81%), but it increases rapidly with RH > 81% (moisture content is around 22% at RH = 97%).

For the desorption isotherm, it can be seen that the desorption isotherm decreases rapidly with diminution of RH from 97% to 81%, and it gradually decreases with RH < 81% (moisture content is around 10% at RH = 81%). Moreover, the phenomenon of hysteresis between the curves of absorption and desorption isotherms was observed for all ranges of relatively humidity. Collet attributed this phenomenon of hysteresis to the ink-bottle effect and a difference of wet ability in adsorption and desorption. Many previous studies also presented the similar sorption behaviour of hempcrete, there are synthesized in Figure 1.29.
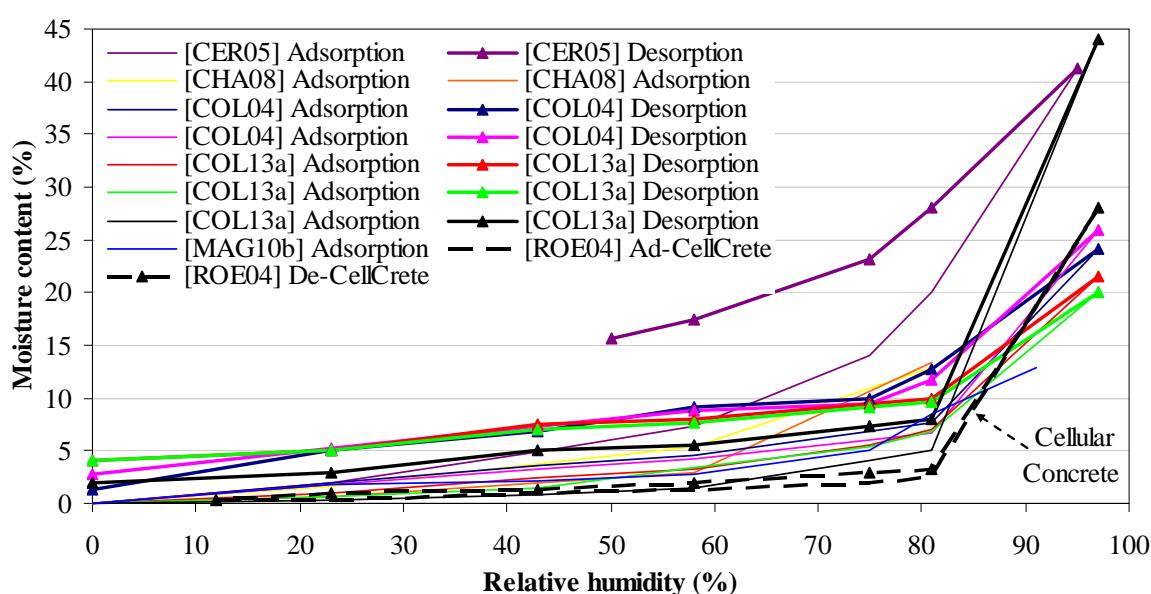
Figure 1.29: Sorption isotherms of materials in literature

Figure 1.29 presents sorption isotherms of hempcretes and cellular concrete. It can be seen that the adsorption - desorption kinetics of both materials was similar each other, which was presented on Figure 1.28 above. However, the measurements of moisture content of hempcretes were very different among studies: the moisture content range is from 5 to 15% for adsorption and from 8 to 28% for desorption at RH = 81%, and from 13 to 44% at highest RH (97%). These differences can be attributed to the different raw material content of each sample measured as well as the implementation methods. Moreover, Collet [COL13a] explained that capillary condensation appears intense in range of high RH for hempcrete samples contained high shiv content, while it starts gradually and occurs on a wide range of RH for hempcrete samples contained low shiv content.

In comparison with other materials, previous studies indicated that the sorption isotherms of hempcrete were similar with those of binder and very low against those of

hemp shiv [CER05 & MAG10b]. Figure 1.29 presents that the sorption isotherm curves of hempcrete were higher than those of cellular concrete curves in range of RH < 81%, while the moisture content of both hempcrete and cellular concrete was comparable each other at highest RH.

1.5.7.2 Water vapor permeability

The water vapour permeability characterizes the ability of a material to transfer moisture under a vapour pressure gradient once the steady state is reached. The commonly called "vapour permeability" includes (i) vapour transfer by diffusion (transport by collision of water molecules with each other), (ii) vapour transfer by effusion (transport by collision of water molecules with walls of pores) and (iii) liquid transfer (connected with capillary condensation) [COL13a].

Water vapour permeability (WVP) is measured according to the cup method (wet cup or dry cup - Figure 1.30) presented in EN ISO 12572-2001 under isothermal conditions ($23^{o}C$) for several sets of relative humidity. Figure 1.31 below synthesized the results of WVP of hempcretes realized by two studies.
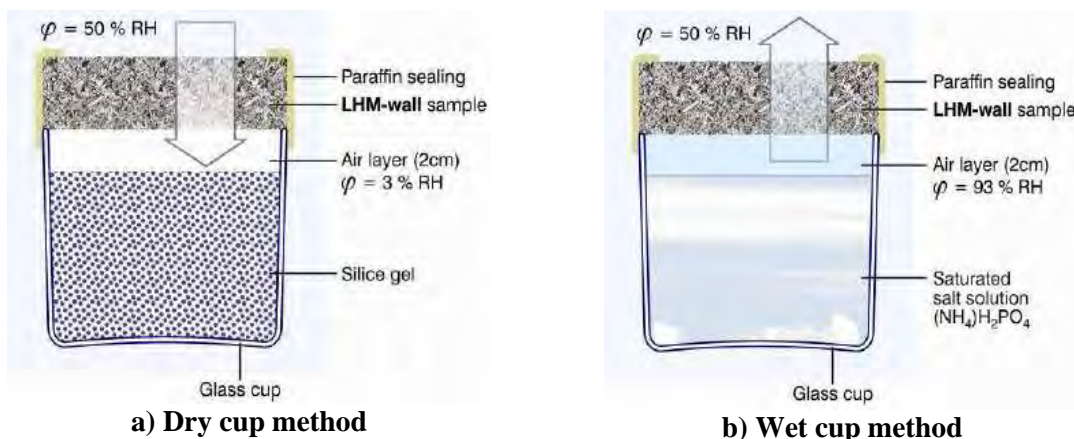
a) Dry cup method   **b) Wet cup method**
Figure 1.30: Measurement of WVP by cup methods [EVR08]

In Figure 1.31, the WVP of all hempcrete samples is little different each other and is respectively higher in comparison with cellular concrete in range of RH < 80%. However, at RH > 80%, WVP of hempcrete among samples is very different each other (from $4.4 * 10^{-11}$ to $1.7 * 10^{-10}$ kg/m/s/Pa), and WVP of cellular concrete is only little higher than the lowest value of hempcrete. Evrard [EVR08] measured WVP of hempcrete by both dry cup and wet cup methods with the sets of RH were respectively 3/50 and 50/93. The results of dry cup and wet cup methods were similar each other ($4.33*10^{-11}$ and

4.39*10^{-11} kg.m^{-1}.s^{-1}.Pa^{-1} respectively). Collet [COL13a] measured WVP on three hempcretes by wet method with several sets of RH for each hempcete. The results showed that the WVP of three hempcretes presented the similar values for the sets of RH < 85%, but the WVP values were very different among three hempcretes for 85/100% RH. Collet [COL13a] attributed this difference to the different raw material content among three hempcretes and the implementation methods.
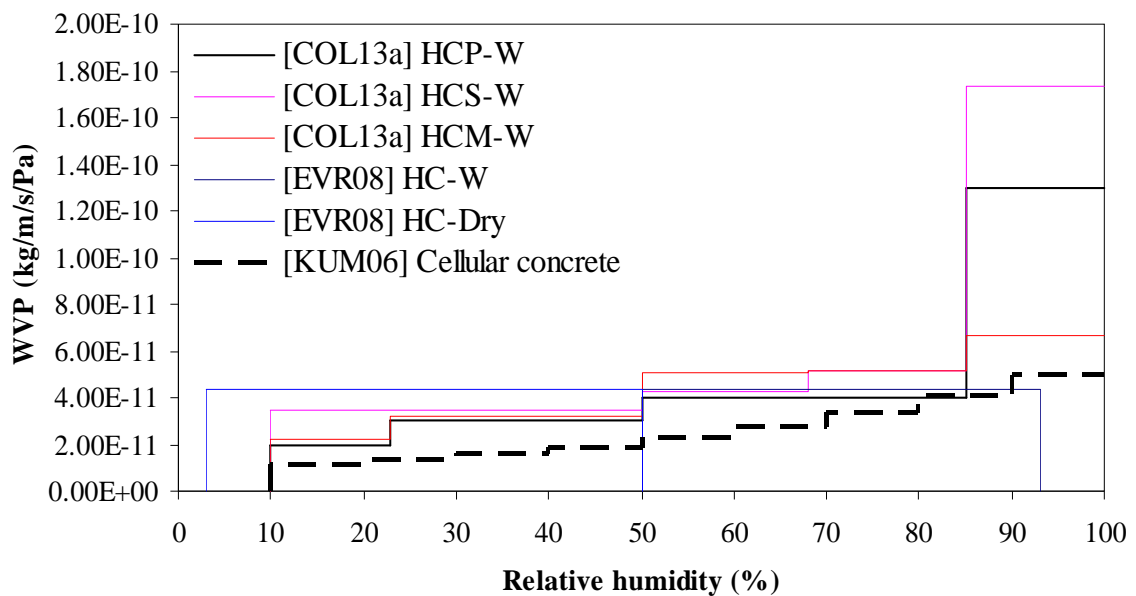
Figure 1.31: Water vapor permeability of hempcrete in literature

1.5.7.3 Moisture Buffer Value

The Moisture Buffer Value (MBV) indicates the amount of moisture uptake or release by a material when it is exposed to repeated daily variations in relative humidity between two given levels. Rode [ROD05] indicated that MBV can be used to appraise the ability of materials used in building to moderate indoor humidity variations.

The experimental determination of MBV is carried out by NORDTEST protocol, where a specimen is subjected to environmental changes that come as a square wave in diurnal cycles at 23°C [ROD05]. This protocol uses climatic exposures which vary in 8 hours + 16 hours cycles: 8 hours of high humidity followed intermittently by 16 hours of low humidity. The low humidity is usually 33% RH, while the high should be 75% RH. However, they may be following alternatives: 33/54%, 54/75%, and 75/93%. Figure 1.32 and Table 1.19 below show the classification and results of MBV in literature.
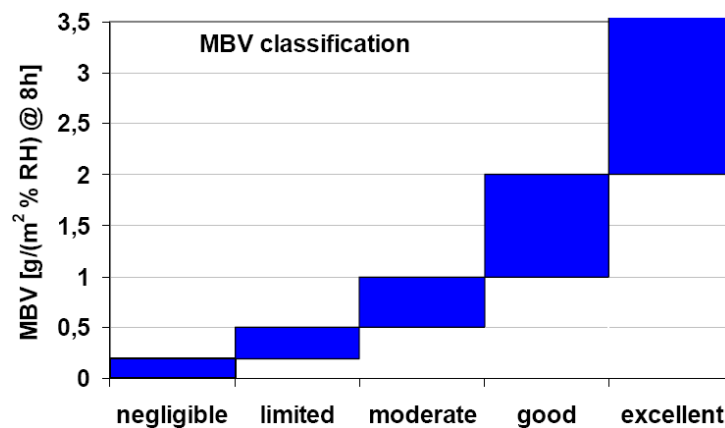
Figure 1.32: Classification of Moisture Buffer Value [NOR05]

The Figure 1.32 illustrates that MBV was classified using five categories. This classification shows that MBV is as high as possible. A previous study [NOR05] also showed that materials like untreated spruce, birch boards and cellular concrete performed as good buffers (0.91-1.22 g/(m^2.%RH)) while materials like brick and cement concrete were able to buffer under the half of the best buffers (0.35-0.69 g/(m^2.%RH), negligeable or limited buffering capacity).

Table 1.19: MBV of hempcrete from the literature

Literature	*Materials*	*RH (%)*		*Temperature*	*Density*	*MBV*
		Low	*High*	*(^{o}C)*	*(Kg/m^3)*	*g/(m^2.%RH)*
[BOU12]	Hempcrete	33	75	23		1.99-2.53
[COL12]	Hempcrete	33	75	23	412-451	2.09-2.21
[COL13]	Hempcrete	33	75	23	473	1.89-2.06
	Hempcrete-plaster (sand-lime)	33	75	23		0.98-1.02
	Hempcrete-plaster (hemp-lime)	33	75	23		1.74-1.88
[COL13a]	Precasted hempcrete	33	75	23	460	1.94
	Sprayed hempcrete	33	75	23	430	2.15
	Moulded hempcrete	33	75	23	430	2.14
[EVR10]	Hempcrete	33	75	23	440	2.11

The results presented in Table 1.19 indicated that the MBV of hempcretes without plaster layer were 1.89 – 2.53 g/(m^2.%RH) which is between good and excellent range, while that of hempcretes with plaster layer were 0.98 – 1.88 depending on the nature of plaster which is good range.

1.5.7.4 Conclusion

Previous paragraphs above presented the hygroscopic properties of hempcrete, which are vapor permeability, sorption isotherms and moisture buffer value. Although the

results of each property are different each other among the different hempcrete samples, they are higher than those of cellular concrete. These results allow concluding that hempcrete possesses a high potential for indoor air humidity control in comparison with conventional materials.

1.5.8   Conclusion

In generally, the previous studies indicated that hempcrete is a potential material for thermal insulation wall thanks to its low environmental impact and thermal conductivity, and regulation of indoor air humidity.

Previous studies also showed the good efficiency of the pretreatment of hemp shives with a substance for reducing water absorption capacity of hemp shives, and therefore tackle well the problems of the interaction between mineral binder and hemp shives. However, the pretreatment methods given spent much time for conservation of treated shives and needed many storages to contain treated aggregates before fabrication of concrete; therefore, they are not suitable for industrial production in large scale.

In our study, we will develop hempcrete from new pozzolanic binder - a friendly-environment material and treated hemp shives. For the pretreatment of hemp shives, we will treat hemp shives using this pozzolanic binder with different methods in order to choose the most suitable method for industrial production. After that, we will study on the mechanical and hygrothermal behaviors in order to compare with the previous studies and on the application for construction.

1.6 *Conclusing remarks*

Previous paragraphs confirmed the need of the sustainable development on a global scale. In the construction area, the development of new materials not only needs to satisfy the mechanical and thermal properties, but also limit negative influence on environment. Thus, in this study, we will develop a new building material, which is hempcrete made of hemp shives and new pozzolanic binder.

For the binder, previous studies indicated that flash metakaolin (MK) can be considered as an eco-material thanks to little CO_2 emission and low energy consumption in the production. However, the mechanical strength of pozzolanic binder made of MK and lime is too low at early age. Thus, we will investigate new pozzolanic binders which contain as much MK as possible to be consistent with the sustainable development in

construction area. On the other hand, organic admixture (GC) and/or mineral admixture (K_2SO_4) will be used to improve strengths at early age and reduce shrinkage of these binders.

For hemp shives, previous works demonstrated that hemp shives are eco-materials, have very low cost, light weight and improve thermal resistance. However, the high water absorption capacity of hemp shives causes negative impact on the interaction between hemp shives and binder leading to reduce the mechanical property of hempcrete. Although the pre-treatment of hemp shives brought the positive effect on the reduction of its water absorption capacity, the pre-treatment methods given were not suitable for the production of hempcrete elements in lage scale due to the complex conservation of treated hemp shives. Thus, we will study on the pre-treatment methods, which not only are suitable for industrial production, but also are as simple as possible for conservation of treated hemp shives and contribute to improve the properties of hempcrete.

Lastly, we will investigate the mechanical and thermal properties of hempcrete using a new pozzolanic binder and untreated and treated hemp shives. The results obtained can allow to choose the most suitable to apply for production of hempcrete elements in construction industry.

Chapter 2:   Methods and Materials

2.1 Introduction

This chapter presents the experimental methods and materials used for this study. Firstly, we will describe the experimental methods applied for characterization of binder, plant aggregates and hempcrete. Secondly, we will present the characterization of the raw materials such as natural hydraulic lime – NHL3.5, slaked lime and flash metakaolin. Moreover, the commercial binder and the admixtures (glycerol carbonate and potassium sulfate) will be characterized. Lastly, bulk density, thermal conductivity, water absorption and particle size distribution of hemp shives will be presented.

Introduction

Ce chapitre présente les méthodes expérimentales et les matériaux utilisés pour cette étude. Premièrement, nous décrirons les méthodes expérimentales appliquées à la caractérisation du liant, des granulats végétaux et du béton de chanvre. Deuxièmement, nous caractériserons les matières premières telles que la chaux hydraulique naturelle - NHL3.5, la chaux éteinte et le métakaolin flash. Le liant commercial et les adjuvants (carbonate de glycérol et sulfate de potassium) seront aussi caractérisés. Enfin, la densité en vrac, la conductivité thermique, l'absorption d'eau et la granulométrie de la chènevotte seront présentées.

2.2 Methods of characterization of binder

2.2.1   Mixing paste

Controls mixer

Procedure of mixing:

- Mixing dry components including powder admixture (if any) with low speed for 30 seconds,

- Adding water which may include liquid admixtures into the bowl, mixing with low speed for 60 seconds,

- Stoping 60 seconds to mix the mixture by hand in order to homogenize and remove the anhydrous parts,

- Mix paste for 30 seconds at high speed and obtain the homogeneous fresh paste for casting molds.

Figure 2.1 Mixer and mixing procedure of the past

In this study, two pozzolanic binders were studied: the first composed of flash metakaolin and natural hydraulic lime - NHL3.5, and the other from flash metakaolin and slaked lime.

Paste is mixed with a Controls mixer conforming to NF-EN 196-1 standard. Mixer and procedure of mixing are shown in Figure 2.1 below.

After mixing, the fresh paste was used to prepare the samples for the different tests which are presented in the next paragraphs.

2.2.2 Microstructural characterization

2.2.2.1 Sample preparation

After mixing, the paste of binder was casted in plastic tubes and closed tight by the plastic caps. The tubes were conserved in the climatic room at 20^oC until the date of the test. At the test date, the binder tubes were immerged in liquid azotes around 15 minutes to stop the hydration reactions and then dried by the method of lyophilization during minimum 24 hours. The dry samples were then powdered and passed through an 80 μm sieve.

2.2.2.2 X-ray diffraction

The X-ray diffraction analyzes (XRD) were performed by the Siemens D5000 diffractometer. This measuring instrument is a system with Co Kα radiation (λ = 1.789 Å) at 40 kV and 30 mA. The 2-Theta values ranged from 4° to 70° and were recorded in 0.04^o steps with a counting time of 10 s per step.

2.2.2.3 Thermogravimetric analyses (TG-DTG)

Thermogravimetric analyses were perform on the dry powdered samples weighing around 1050 to 1550 mg each, using a thermal analyser NETZSCH STA 449 F3 Jupiter® at a heating rate of 10 °C/min up to 1000°C. This test measures the weight loss due to the decomposition of the components in function of temperature.

2.2.3 Shrinkage measurement

Fresh paste was casted into molds of three samples 40 x 40 x 160 mm^3 in two times, it was tamped by the shock table (10 strokes each time). These samples were kept in a room at 20^oC and 100% relative humidity (RH) for 48 hours. After 48 hours, the samples

were demolded and conserved in a climatic room at 20°C and 50%RH: three samples were covered by aluminum paper for measurement of endogenous shrinkage, and three samples without aluminum paper were used to measure total shrinkage.

Total and endogenous shrinkage was measured by a retractometer (Figure 2.2) with an accuracy of 0.001 mm. The first measurements were carried out immediately after demolding. The results are presented as mean values of measurements from 3 different samples. The variations in mass of specimens were also determined immediately after demoulding on a balance accurate to 0.1g. Figure 2.2 below presents apparatus and samples for shrinkage measurement according to the NF EN 196-1 standard.
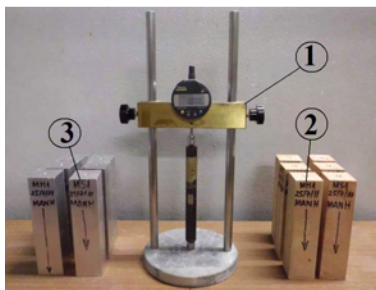
1. Retractometer
2. Samples for total shrinkage measurements
3. Samples for endogenous shrinkage measurements

Figure 2.2: Retractometer and samples for shrinkage measurements

2.2.4 Calorimetric test

This test was carried out to determine the hydration heat of binders. The tests were measured according to NF EN 196–9 standard. This standard describes the semi-adiabatic method or Langavant method. The test was carried out in a climatic room at 20±2 °C.

The measurements were made over 5 days, as indicated in the NF EN 196–9 standard. The variation of the temperature of binder with time was measured immediately after mixing. The hydration heat of the binder was the combination of the accumulated heat in the calorimeter and the heat dispersed in the environment. At time t, the hydration heat Q by gram of binder is obtained by the formula (1.1) below.

$$Q = \frac{c}{m_c} \theta_t + \frac{1}{m_c} \int_0^t \alpha . \theta_t . d_t \qquad (2.1)$$

Where: Q – Hydration heat, J/g

m_c - the binder mass contained in the test sample, g

t - the hydration time, h

c - the total thermal capacity of the calorimeter, J/°C

α - the coefficient of heat loss of the calorimeter, J/h/°C

θ_t - the difference in the temperature of the test calorimeter compared with that of reference calorimeter at time "t", °C.

2.2.5   Mechanical test

2.2.5.1 Sample fabrication

After mixing, the paste of binder was casted in $40 \times 40 \times 160$ mm^3 molds and kept in a room at 20°C and 100% RH for 2 days in endogenous conditions. The samples were then demolded and continuously cured in the same conditions until day 7. Then samples were conserved at 65% RH, 20°C until the mechanical properties were assessed.

2.2.5.2 Compressive tests

Compressive tests were performed by an automatic compressive machine (HOUNSFIELD, H50KS - load cell capacity: 50 kN) with loading speed of 3 mm/minute on specimens with ages from 2 days to 49 days. For each age, 4 samples were tested.

2.2.6   Thermal conductivity

The test was performed on the samples using a hot plate method with a λ-Meter EP 500 (Lambda-Messtechnik, GmbH, Germany). Measurements were made at 25°C with a difference of temperature of 15 K between the two plates. The steady state was assumed to have been reached when the change in conductivity is less than 1% in 90 minutes. In this study, the thermal conductivity of binder was measured for both humid and dry binder samples with a 15x15 cm^2 base and 5 cm in height. Before the test, the samples must reach the stable mass state which the change in mass of the samples was less than 0.1% between two weightings 24 hours apart after conservation at 20°C and 65% RH for humid samples and after drying by oven at temperature of 80°C for dry samples. The measurements were carried out on the samples at the age of 90 days.

2.2.7   Method of standard mortar tests

2.2.7.1 Fresh mortar tests

The mixing of mortar was realized by Controls mixer which mixed automatically, comply with NF EN 196-1 standard.

After mixing, we carried out three tests on fresh mortar: workability, mini-cone and setting time. The workability test measured time of mortar flow, used LCL workability

meter according to NF P18-452 standard. The setting time of mortar was determined by Vicat apparatus conforming to NF EN 480-2 standard.

2.2.7.2 Mechanical properties

The tests were performed by standard test machine - 3R for both bending and compressive tests. Fresh mortar was casted in $40 \times 40 \times 160$ mm^3 molds and kept in a room at 20$^{\text{o}}$C and 100% RH for 2 days in endogenous conditions. The specimens were demoulded after 2 days, then conserved in the same condition until 7-day age, after that they were conserved in climatic room (20$^{\text{o}}$C, 65% RH) until the date of the test. Flexural and compressive strengths of mortars were measured at 2, 7, 28, 49 and 90 days with 2 samples for flexural test and 4 samples for compressive test.

2.3 Methods of characterization of hemp aggregates

Up to now, there is not standardized method to assess the characteristics of these aggregates. In this study, the methods of characterization of hemp shives are based on current work of TC Bio-aggregates based building materials of the RILEM. The sample preparation and the methods are presented in next parts.

2.3.1 Sample preparation

In order to characterize the properties of hemp particles, the size of each sample was chosen depending on the size of the particles, the test method and the test device. Three samples were used for each test.

Hemp shiv was contained in plastic bags. When it was transferred from a factory to a laboratory, the segregation was induced due to vibrations and electrostatics forces, therefore, the fine particles generally move into the bottom of the bags. Thus, when shiv was gradually poured to take samples, coarser particles generally come first, while the finest remain in the bottom and on the walls of the bag. To prevent this kind of segregation when samples were taken, the following procedure will be applied:

- First step: The whole hemp shiv was put on a large slick table, hemp shiv was then homogenized by manual mixing, after that, it was put into a pile.

- Second step: The pile of shiv was manually divided in two similar separate piles.

- Third step: The second step was repeated until obtaining a pile with required quantity to make sample.

Samples were dried in an oven at 60°C until the change in mass of the sample was less than 0.1% between two weightings 24 hours apart. Before the test, the samples were sealed in plastic bags to return to the temperature of the test room.

2.3.2 *Bulk density*

The bulk density of hemp shiv was measured at room temperature (21 ± 2°C). A glass cylinder of 11 cm in diameter and 23.5 cm in height and a balance accurate to 0.01g were used.

The glass cylinder was filled with dry material (to about half the height of cylinder), the level was marked after up-ending the glass cylinder ten times, and the corresponding volume measured with water.

The bulk density is calculated by (2.2) equation below:

$$\gamma = \frac{M_s}{M_w} \cdot \rho_w \tag{2.2}$$

γ: Bulk density (kg/m^3)

M_s: Mass of dry hemp shiv (g)

M_w: Mass of water corresponding to the volume of dry shiv measured (g)

ρ_w: Density of water (1000 kg/m^3)

The bulk density of hemp shiv was the mean value of the measurements made on three different dry samples.

2.3.3 *Thermal conductivity*

The test was performed on dry samples using a hot plate method with a λ-Meter EP 500 (Lambda-Messtechnik, GmbH, Germany). Measurements were made at 25°C with a difference of temperature of 10 K between the two plates. The steady state was assumed to be reached when the change in conductivity was less than 1% in 60 minutes. In order to measure the thermal conductivity of hemp shiv, dry shiv particles were contained in a PVC box with a 15x15 cm^2 base and 5 cm in height. The thermal conductivity of loose hemp shiv was determined by the mean value of the measurements for 03 different dry samples.

2.3.4 Water absorption

The water absorption capacity of hemp shives was determined on three samples. The samples were immersed in water in a synthetic permeable bag and the gain in mass was measured after 1, 15, 240 minutes, and 48 hours. Before each weighting, the material was quickly dried with a salad spinner (in 50 seconds). The aim of this step was to eliminate the water adsorbed at the surface of plant particles or located among them.

This test was carried out for dry, normal and pretreated hemp particles. The quantity of each dry and natural sample is around 25g, and the quantity of pretreated hemp shiv sample is around 60g obtained from around 25g of natural hemp shiv. A balance accurate to 0.01g and a salad spinner (25 cm in diameter and 20 cm in height) were used.

The water absorption capacity of each sample was evaluated by the equation (2.3):

$$A = \frac{M_t - M_0}{M_0} \cdot 100\% \tag{2.3}$$

A: Water absorption capacity (%)

M_0: Mass of sample before immersion (g)

M_t: Mass of sample after each time of the immersion (g)

The water absorption capacity of hemp shiv is the mean value of the measurements made on three different samples.

2.3.5 Particle size distribution

The particle size distribution of the hemp shiv samples was analysed by two methods: mechanical sieving and image analysis. Three samples were analysed for each methods.

The mechanical sieving method used the apparatuses composed of the mechanical sieves, a shaker machine and a balance. A balance accurate to 0.001g and two sets of mechanical sieves with square apertures (from 0.5 to 8 mm) were used. The first set of sieve is 30 cm in diameter and 7 cm in height (used for dry samples weighting around 100 and 200g each), and 20 cm in diameter and 5 cm in height for the other set (for dry samples of around 50g). The shaker machine which can control the vibrational parameters, was used. The different vibrational parameters were applied: three vibrational frequencies (300, 600 and 900Hz), three vibrational times (3, 10 and 30 minutes) with continuous vibrational mode and maximum vibrational amplitude.

The image analysis method used ImageJ software and a colour scanner to analyse images scanned at 600 DPI. In order to obtain the best contrast of images, a black paper was used as a background. Moreover, a transparent plastic plate was put on the surface of scanner before arrangement hemp particles to protect the scanner. This method was carried out on the natural shiv samples weighing around 3 - 6g each. The Figure 2.3 to Figure 2.5 describe the steps of this method.
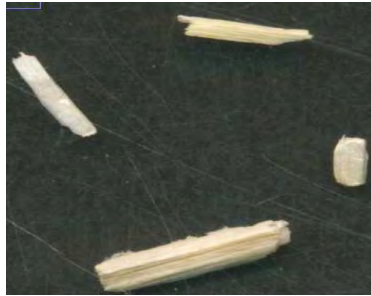
Figure 2.3: TIFF scanned image
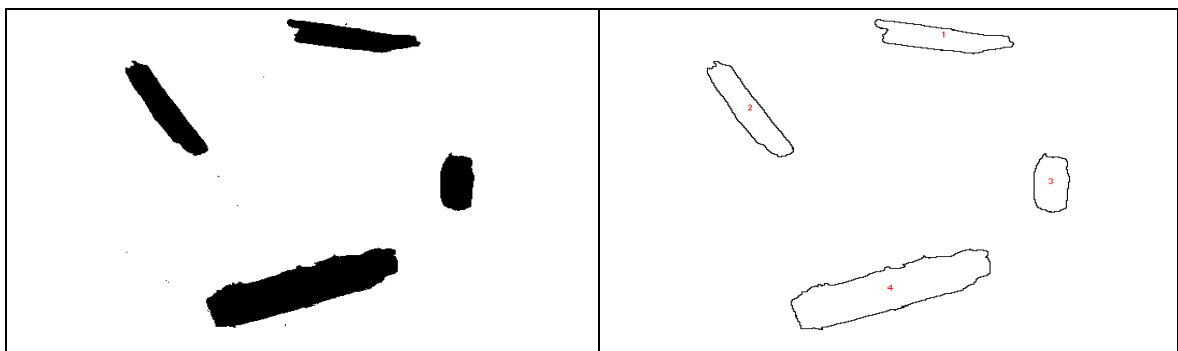
Figure 2.4: Image treatment   **Figure 2.5: Particle analysis**

The process of image analysis was composed of 5 steps. The first step, preparation of hemp shiv samples was realized according to paragraph 2.3.1 without drying. Then colour images of hemp particles were acquired by the scanner in TIFF format at 600 DPI resolution with black background paper (Figure 2.3). Before scanning, the particles were arranged in a manner that they do not touch or overlap one another. The third step was carried out by the ImageJ software. It consisted of several treatments to correct the image brightness and binarization (Figure 2.4). The fourth step used the "Analyze particles" tool of the ImageJ software to determine the hemp particle dimensions and morphological parameters. At the end of this step, each object outline was detected on the binary image (Figure 2.5) and morphological parameters of the hemp particles were saved in an Excel file. The last step used Excel software to draw the grading curves.

2.4 Methods of characterization of hempcrete specimens

2.4.1   Preparation of hempcrete samples

2.4.1.1 Moulds

For the compressive test, the carton moulds of 16 cm in diameter and 32 cm in height were used to fabricate hempcrete samples.

For the thermal conductivity test, three kinds of hard moulds were used to cast samples in order to test it according to parallel and perpendicular directions with the compaction direction: cubic moulds (15 x 15 x 15 cm^3), horizontal parallelepiped moulds which their surfaces of 15 x 15 cm^2 and 5 cm in height, and vertical parallelepiped moulds which their surfaces of 15 x 5 cm^2 and 15 cm in height.

2.4.1.2 Mixing method

In this study, a 50 liter mixer was used to mix hempcrete. Three mixing methods were applied to realise the pre-treatment of hemp shiv and to mix hempcrete with untreated and treated hemp shiv. Mixing methods are presented in Table 2.1 below:

Table 2.1: Process of mixing for hempcrete and hemp shiv pretreatment

Hempcrete with untreated hemp shiv	Hempcrete with treated hemp shiv	Pretreatment of hemp shiv
1. Mix hemp shives for 2 minutes	1. Introduce pretreated shives and binder into mixer, mix for 2 minutes	1. Mix hemp shives for 2 minutes
2. Introduce water to wet hemp shiv, mix for 5 minutes		2. Introduce water to wet hemp shiv, mix for 5 minutes
3. Introduce binder, mix for 2 minutes	2. Introduce water, mix for 5 minutes	
4. Introduce mixing water, mix for 5 minutes	3. Obtain a homogeneous mixture	3. Introduce binder, mix for 2 minutes
5. Obtain a homogeneous mixture		4. Obtain a homogeneous mixture

2.4.1.3 Fabrication and conservation

Samples for compressive test were fabricated in the form of cylinders by Vibrocompression machine. This compaction device is shown in Figure 2.6 below. It consists of a steel cylinder containing a cylindrical cardboard mould of 16 cm in diameter

and 32 cm in height, a piston operated by compressed air that moves down to compress the sample, and an air compression system. Samples were made using a compaction pressure of 0.6 MPa with vibration time of 30 seconds. The hempcrete was put in the mould by one time before compaction.

Figure 2.6: Vibrocompression machine

The samples for thermal conductivity were fabricated in cubic and parallelepiped moulds with the same fresh density as the cylindrical samples. The samples were compacted by vibrational table. Hempcrete was casted in three layers for the samples using cubic and vertical parallelepiped moulds, and in one layer for the samples using horizontal parallelepiped moulds.

Table 2.2: Conservation form of hempcrete at 20oC and 65%RH after 2-day age

Order	Test	2 to 7 days	After 7 days
1	Thermal conductivity	without mould	without mould
2	Compressive test at 7 days	without mould	-
3	Compressive test at 28 days	Conservation in mould without top and bottom	without mould
4	Evolution of hempcrete mass test during 90 days	Conservation in mould without top and bottom	without mould

For the conservation, the samples were conserved in the moulds in reverse position in the humid room at 20^oC and more than 95% RH during 48 hours. After that time, all the samples were conserved in the climatic room at 20^oC and 65% RH until the date of the test. Samples were conserved with or without cardboard moulds depending on different tests, as present in Table 2.2.

2.4.2 Hempcrete tests

2.4.2.1 Mechanical test

The compressive test was realised on the cylindrical samples at 7 and 28 days of age. The device used was the HOUNSFIELD H50KS machine (load cell capacity: 50 kN) with a constant displacement rate of 5 mm/minute.

The young's modulus of hempcrete was determined from the results of compressive test. It was slope of the stress strain curve within elastic region, in which the stress strain curve of hempcrete obeys Hook's Law.

2.4.2.2 Mineralogical analyses

These analyses were performed by X-ray diffraction and thermogravimetric analyses on the powder samples passed through an 80 μm sieve. The preparation of these powder samples was realized by three steps following: the first, the hempcrete specimens were taken at center of the cylindrical samples after the compressive test; the second, these specimens were made dry by oven at $50^{o}C$ until the constant mass (the mass change was less than 0.1% between two times of scaling 24 hours apart); at the last step, these specimens were powered and passed through an 80 μm sieve.

2.4.2.3 Thermal conductivity test

Thermal conductivity test was performed using a hot plate method presented in 2.3.3 section. Measurements were made at 25°C with a difference of temperature of 15 K between the two plates. The steady state was assumed to be reached when the change in conductivity is less than 1% in 90 minutes.

This test was performed on the samples being in both dry and humid state (humid state: $20^{o}C$ and 65% RH). Before the test, the samples must reach the stable mass state which the change in mass was less than 0.1% between two weightings 24 hours.

a) Parallel direction - $\lambda_{//}$ *b) Perpendicular direction - $\lambda_{\perp}$*
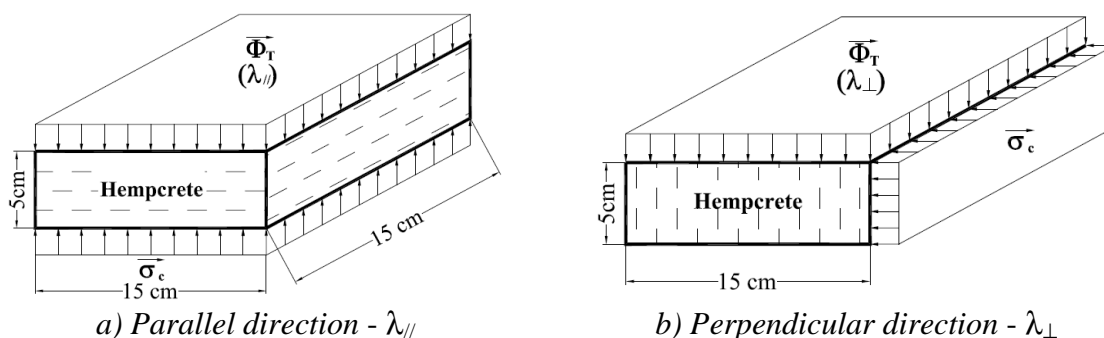
Figure 2.7: Direction of compaction and heat flux

The thermal conductivity of hempcrete was measured according to parallel and perpendicular directions with the compaction direction. Figure 2.7 describes the compaction direction (σ_c) and the heat flux (Φ_T).

In Figure 2.7a, the heat flux is parallel the compaction direction, the thermal conductivity value is noted $\lambda_{//}$. In Figure 2.7b, the heat flux is perpendicular to the compaction direction, the thermal conductivity value is noted $\lambda_{\perp}$.

2.5 Characterization of raw materials used for binder

2.5.1 *Natural hydraulic lime NHL3.5*

In this study, natural hydraulic lime NHL3.5 was used. It is a commercial natural hydraulic lime product. It is known to be an environmental-friendly material in comparison with cement because the calcination temperature of NHL3.5 is much lower than that of cement ($1000^{o}C$ against $1450^{o}C$ for cement) and a part of CO_2 released during production process is captured by carbonation. The chemical and mineralogical compositions of this lime are presented in Table 2.3 and Table 2.4 below.

Table 2.3: Chemical composition of NHL3.5 by producer

Content of Ingredients (% by weight)									
SiO_2	Al_2O_3	CaO	MgO	Fe_2O_3	Na_2O	K_2O	TiO_2	SO_3	LOI
18.20	3.68	56.68	2.10	1.36	0.04	0.85	0.18	1.22	15.04

The Table 2.3 shows that the major chemical components of NHL3.5 are SiO_2 (18.2%) and CaO (56.68%) which are similar with those of some NHL3.5 used in previous studies presented in Table 1.3 in first chapter.

Table 2.4: Mineralogical composition of NHL3.5 by producer

Mineralogical composition (% by weight)						
$Ca(OH)_2$	$CaCO_3$	C_2S	C_3A	$CaSO_4$	Quartz	Gehlenite
31.90	16.92	35.67	6.18	1.63	4.35	3.31

For the mineralogical composition, Table 2.4 indicate that the main ingredients of this lime are $Ca(OH)_2$, $CaCO_3$, and C_2S. Moreover, the X-ray diffraction analysis and thermogravimetric analyses were performed on powder sample of NHL3.5 to confirm the presence of these mineralogical species, these analyses are respectively presented in Figure 2.8 and Figure 2.9 below.

Figure 2.8 shows the mineralogical ingredients of NHL3.5 detected by X-ray diffraction analysis. It indicates the presence of components such as C_2S, C_3A, calcite (Ca), portlandite (P) and quartz (Q), while others (gypsum and gehlenite) indicated in Table 2.4 are not visible due to their small quantity.
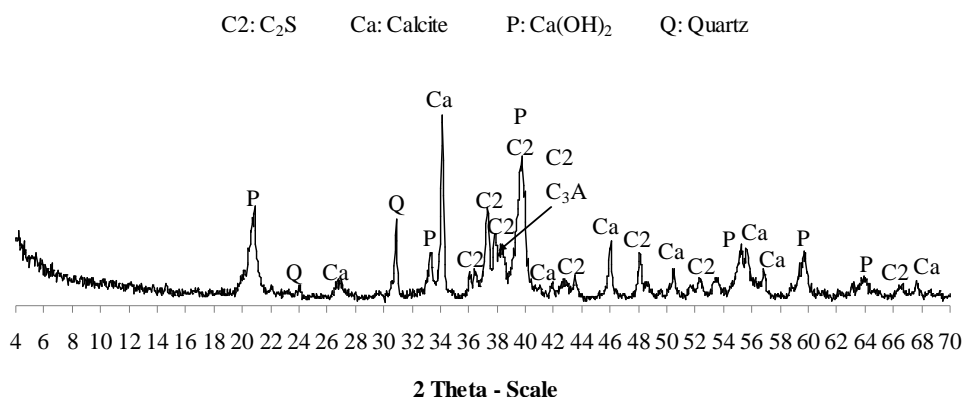
Figure 2.8: X-ray diffraction analysis of NHL3.5
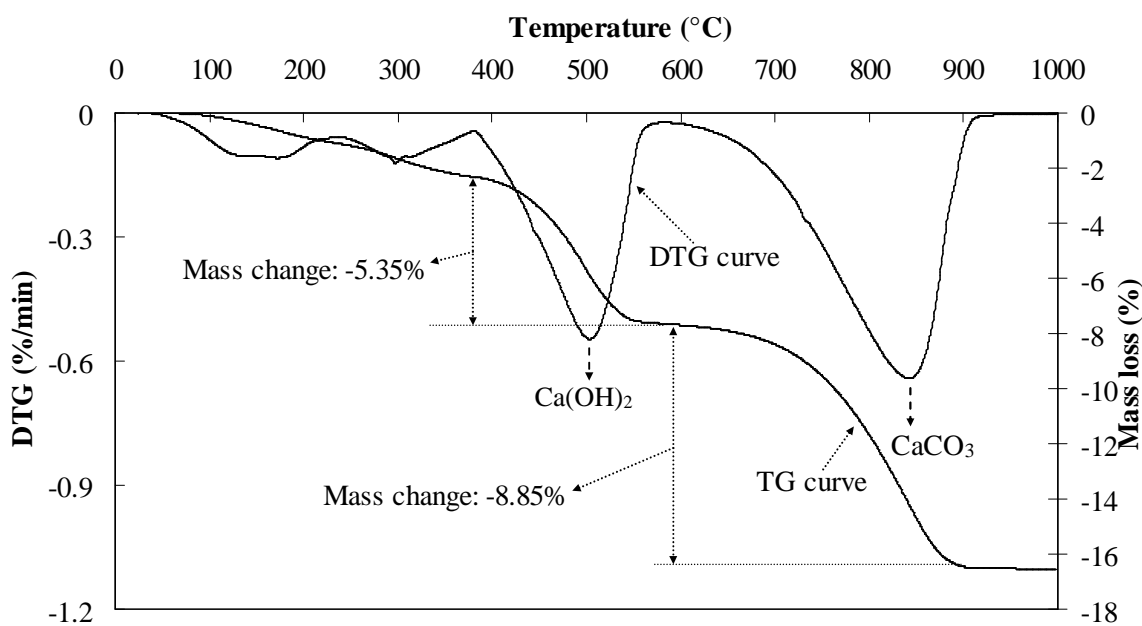
Figure 2.9: Thermogravimetric analyses of NHL3.5 powder

The analysis result in Figure 2.9 gives the mass losses of H_2O and CO_2. This allows to calculate the contents of $Ca(OH)_2$ and $CaCO_3$ ingredients of NHL3.5, calculated as well:

- Content by weight of $Ca(OH)_2$:

$$Ca(OH)_2 \, content = \frac{Mass\,loss\,of\,H_2O}{24.31\%} = \frac{5.35\%}{24.31\%} = 22.01\% \qquad (2.4)$$

Where: 24.31% is H_2O content by weight in one mole of $Ca(OH)_2$.

- Content by weight of $CaCO_3$:

$$CaCO_3 \; content = \frac{Mass \; loss \; of \; CO_2}{43.97\%} = \frac{8.85\%}{43.97\%} = 20.13\% \qquad (2.5)$$

Where: 43.97% is CO_2 content by weight in one mole of $CaCO_3$.

This test shows that the $Ca(OH)_2$ and $CaCO_3$ contents are very different in comparison with those given by producer ($CaCO_3$ content is higher, while $Ca(OH)_2$ content is far less than those respectively given in Table 2.4).

2.5.2 Slaked lime

The slaked lime used in this work is a commercial product. It is considered as a sustainable binder in comparison with cement thanks to its low production energy needs (calcintion temperature of around 1000^oC against 1450^oC for cement) and the equilibrium between CO_2 emission during its production. The major mineralogical ingredient, around 92%, is $Ca(OH)_2$. The chemical ingredients are presented in Table 2.5 below. It can be seen that the CaO component predominates over others.

Table 2.5: Chemical components of slaked lime by producer

Content of Ingredients (% by weight)						
SiO_2	Al_2O_3	CaO	MgO	Fe_2O_3	Mn	LOI
0.60	0.20	70.06	0.70	0.10	0.02	24.60

To determine the mineralogical components of slaked lime, the X-ray diffraction analysis and thermogravimetric analyses were performed on powder samples. The results of these analyses are respectively presented in Figure 2.10 and Figure 2.11 below.
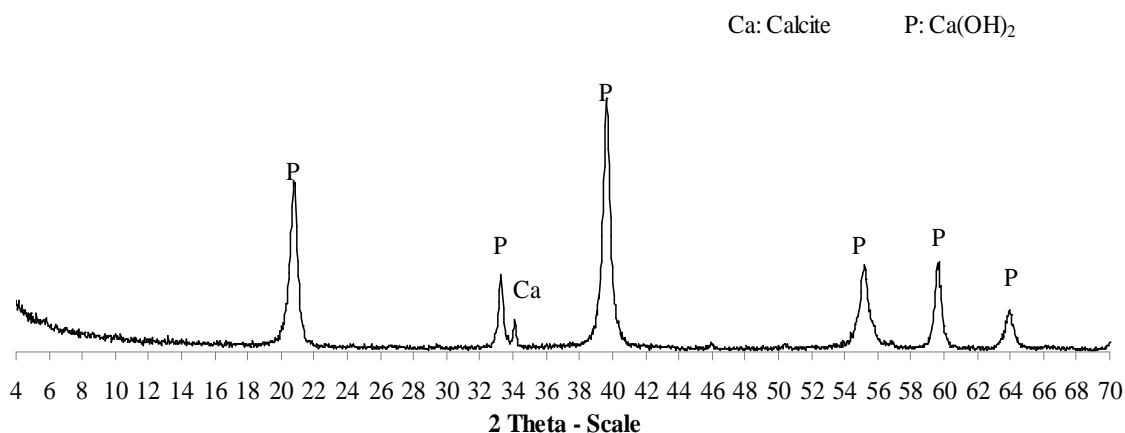
Figure 2.10: X-ray diffraction analysis of Slaked lime

Figure 2.10 shows the result of X-ray diffraction analysis realized on powder sample of slaked lime. It can be seen that the peaks of P predominate, while there is only one small peak of Ca.

The results presented in Figure 2.11 shows the mass losses of H_2O and CO_2 obtained by thermogravimetric analysis of slaked lime. The contents by weight of $Ca(OH)_2$ and $CaCO_3$ were calculated according to (2.4) and (2.5) equation above, which are respectively 90.37% and 4.98%.

Temperature (°C)
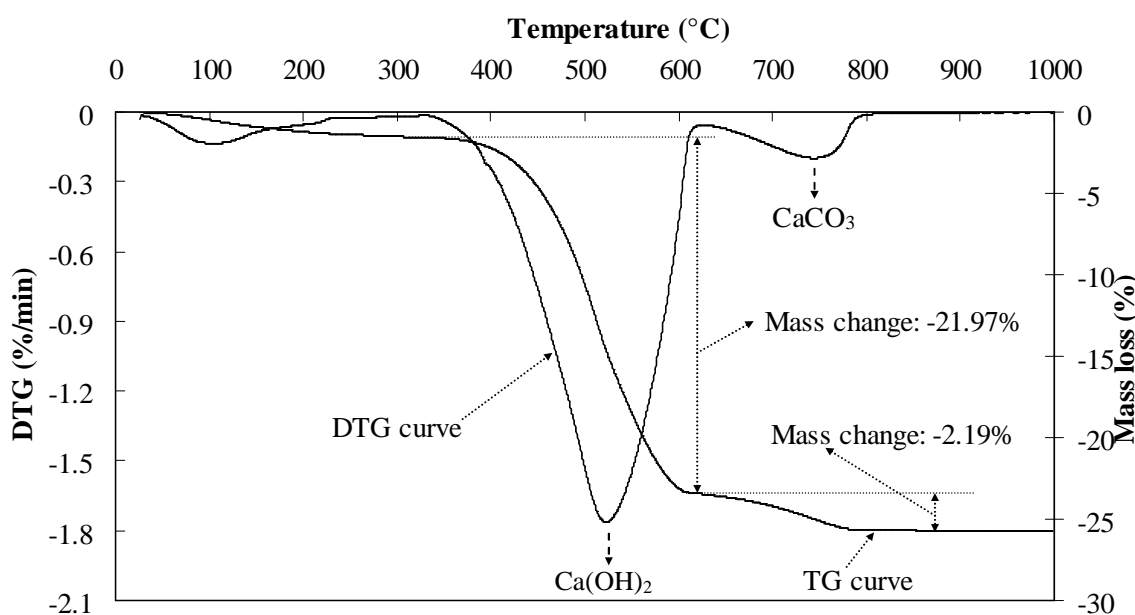
Figure 2.11: Thermogravimetric analysis of Slaked lime powder

2.5.3 Metakaolin

The metakaolin (MK) used in this study is a commercial product from the Argeco Company in Toulouse, France. This MK is a pozzolanic addition, an eco-material produced by flash calcination, a dehydroxylation process of powdered kaolinite clay within several tenths of a second. Its production process consumes far less energy than that of cement (it is 80% less than the energy consumed during cement production, [SAN11 & SAN13]) and emits very little CO_2 [ARG10].

Table 2.6: Chemical compositions of flash metakaolin

Content of Ingredients (% by weight)									
SiO_2	Al_2O_3	CaO	MgO	Fe_2O_3	Na_2O	K_2O	TiO_2	SO_3	LOI
67.10	26.80	1.12	0.11	2.56	0.01	0.12	1.30	<LD	0.84

It is mainly composed of an amorphous silicon-aluminates mineralogical form and quartz (51.4% of amorphous silicon-aluminates and 48.6% quartz [TRI12]). The chemical composition of MK is presented in Table 2.6 below.

Table 2.6 shows that the major chemical constituents of MK are SiO_2 and Al_2O_3 with the whole being around 94%. This table indicates that the content of SiO_2 is very high, this flash metakaolin is therefore impure and has a very high content of quartz, the SiO_2 to Al_2O_3 mass ratio of around 2.5 is more than 2 times higher than that of pure metakaolin (SiO_2/Al_2O_3 = 1.2). However, this table also shows that the chemical composition of this MK is in accordance with NF P 18-513 and ASTM C618 standards.

In order to characterize the mineralogical components of MK, the X-ray diffraction analysis was realized. The result of this analysis is presented in Figure 2.12 below.
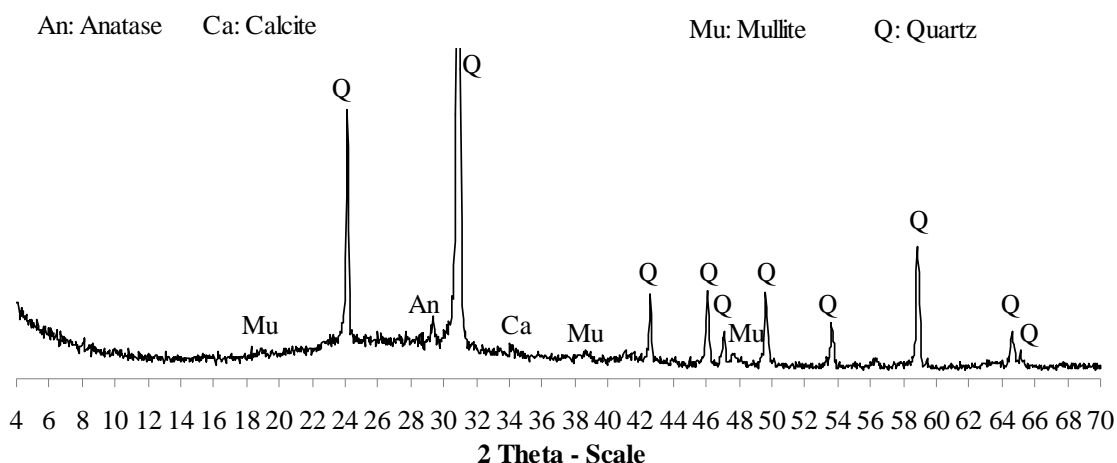
Figure 2.12: X-ray diffraction analysis of flash metakaolin

Figure 2.12 allows to observe the amorphous phase by the area of halo centered at around $2\theta = 27^o$. This amorphous phase composed of very high content of acidic oxides ($Al_2O_3+SiO_2>90\%$) leading MK to react readily and quickly with calcium hydroxide at normal temperature in the presence of water [CAS13 & MAG10b]. This figure also shows the Q peaks with very high intensity which may confirm the impurity of MK as the analysis from chemical components above. Moreover, the small peaks of Anatase (An) and Calcite (Ca) were visible, which were also detected by Magniont's [MAG10b] and Trinh's analyses [TRI12] for this MK. On the other hand, some peaks of Mullite (Mu) were detected. Mullite comes from the structural rearrangement of metakaolin due to the overheating during the calcination. Its presence is undesirable because of its non reactivity with calcium hydroxide.

2.5.4 Commercial binder for hempcrete

In this study, we also used a commercial binder (CB) to compare with our binder in fabrication of hempcrete presenting in fourth chapter. It is mainly composed of natural lime (70%), hydraulic and pozzolanic binder (30%) given by producer.

The analyses of X-ray diffraction and thermogravimetry were performed to characterize the mineralogical components of CB. The result is presented in Figure 2.13.
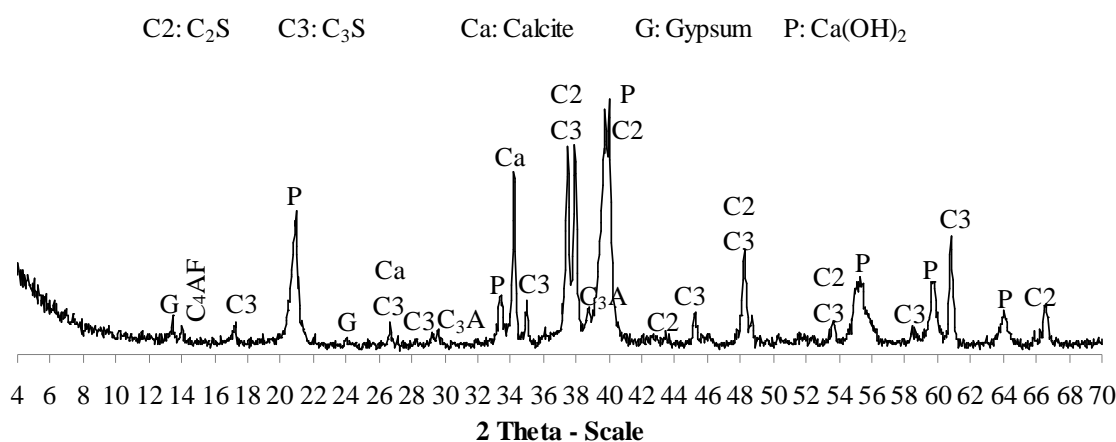
Figure 2.13: X-ray diffraction analysis of CB

Figure 2.13 clearly shows that the main mineralogical components of CB are C_2S, C_3S (two hydraulic components), Calcite and Portlandite. Moreover, the small peaks of gypsum and other hydraulic components (C_3A and C_4AF) are also detected. However, the pozzolanic components were not visible.
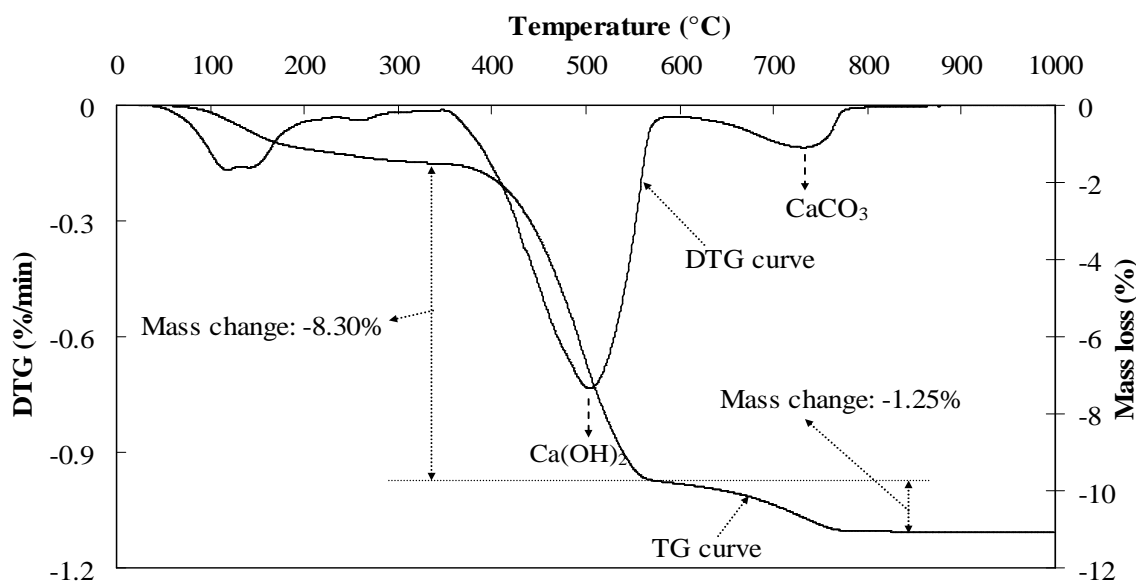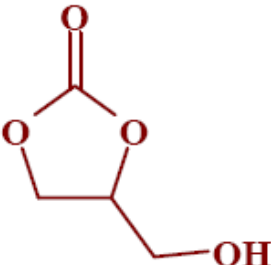
Figure 2.14: Thermogravimetric analysis of CB powder

The results presented in Figure 2.14 shows the mass losses of H_2O and CO_2 obtained by thermogravimetric analysis of CB. The contents by weight of $Ca(OH)_2$ and $CaCO_3$ were calculated according to (2.4) and (2.5) equation above, which are respectively 34.14% and 2.84%.

2.5.5   Admixtures

In this study, the mineral potassium sulfate and/or organic glycerol carbonate admixtures were used to improve the performance of binder at early age.

Glycerol carbonate used is a product from Huntsman, Spain. It is manufactured by using the glycerine co-product of bio-diesel. Thus, it can be used as a "safe" and environmentally friendly solvent. Its structure and typical values are shown in Figure 2.15.

Typical Values

Property	Values
Color (Pt-Co)	75
Glycerine Carbonate, wt%	96
Glycerine, wt%	< 3
Water, wt%	0.1
pH value	4 – 6.5
Density, kg/m^3, 25°C	1400
Viscosity (Kinematic), cSt, 25°C	61

Structure of Glycerine Carbonate

Figure 2.15: JEFFSOL® Glycerol Carbonate, Huntsman [KOB11]

Potassium sulfate (PS) is a chemical activator. It is used in this study because PS not only improves strength but also stabilizes dimension of the paste (see paragraph 1.3.3.2 in first chapter). Potassium sulfate used in this study is a product of VWR BDH Prolabo. Its characteristics are presented in Table 2.7 below.

Table 2.7: Characteristic of Potassium sulfate

Characteristics	Specifications
Assay	Min. 99%
Heavy metal (as Pb)	Max. 20 mg/kg
Cloride (Cl)	Max. 50 mg/kg
Amonium (NH$_4$)	Max. 20 mg/kg
Nitrate (NO$_3$)	Max. 50 mg/kg
Iron	Max. 10 mg/kg
Molecule weight	174.26 g/mol
Density, 20°C	2660 kg/m^3

In addition, superplasticizer (Sika Viscocrete 20 HEVP) was also used to reduce the mixing water content. This leads to reduce the porosity and improves the mechanical performance of binder. Its characteristics are shown in Table 2.8 below.

Table 2.8: Characteristic of Sika Viscocrete 20 HEVP

Characteristics	*Specifications*
Density, 20^oC	1090 kg/m^3
pH value	4.5
Viscosity, 23^oC	145 mPa.s
Cloride (% w/w)	< 0.1 %
Na$_2$O content	< 2 %
Conventional Dry Material (%)	40 %
Dosage (% by weight of binder)	0.2 – 2 %

2.6 Characterization of hemp shiv

2.6.1 Hemp shiv - Agrofibre

In this study, hemp shiv was used as aggregate, the ligneous particles are extracted from hemp stems as a co-product of the process of hemp fibre extraction. The hemp shiv was provided by the Agrofibre company in Cazères (Haute-Garonne, France). Hemp shiv wss obtained through an industrial defibration process by mechanical breaking, after which particles were dusted and calibrated. Hemp shiv particles (Figure 2.16) are beige to white, elongated, plane parallel shapes 1–3 mm thick and 5–25 mm long.

Figure 2.16: Hemp shiv particles

2.6.2 Bulk density and thermal conductivity

This paragraph shows the results of measurement of bulk density and thermal conductivity of hemp shiv. The preparation of hem shiv samples was represented at paragraph 2.3.1. The methods used to measure bulk density and the thermal conductivity, were presented at paragraphs 2.3.2 and 2.3.3 respectively.

The bulk density values of hemp shiv of different origins assessed by various methods can be found in the literature (it varies from 98 to 148 kg/m^3). Table 2.9 presents the result of this study and the results obtained from the literature.

Table 2.9: Bulk density of hemp shiv from this study and literature

Linterature/ This study	*Bulk density (kg/m^3)*
This study	110.9 ± 0.7
Gourlay [ARN08]	110
Arnaud [ARN12]	112, 114, 119
Evrard [EVR08]	100 - 120
Cerezo [CER05]	130
Magniont [MAG10b]	110 - 140
Nozahic [NOZ12]	114.2 ± 2.3
Nguyen [NGU10]	102.83
Paulien [BRU08]	98
Verdier [VER12]	148.3 ± 1.9

Table 2.9 shows that the bulk density of hemp shiv from this study is within range of values found in the literature.

For the thermal conductivity, hemp shiv is expected to be thermally insulating. The results for the thermal conductivity of hemp shiv are presented in Table 2.10 and compared with results obtained from the literature.

Table 2.10: Thermal conductivity of hemp shiv from this study and literature

Linterature/ This study	*Bulk density (kg/m^3)*	*Thermal conductivity (W/(m.K))*
This study	112.0 ± 0.2	0.058 ± 0.0004
Cerezo [CER05]	110	0.048
	155	0.058
Magniont [MAG10b]	134.8	0.055
Nozahic [NOZ12]	114.8	0.057 ± 0.0006
Verdier [VER12]	148.3 ± 1.9	0.056 ± 0.0002

Table 2.10 shows the measurement of this study is similar to the values of thermal conductivity found in the literature and comparable to traditional loose-fill insulation materials.

2.6.3   *Water absorption*

The water absorption capacity of hemp shives was realised according to the method presented at paragraph 2.3.4 with the sampling taken as presented at paragraph 2.3.1. This

test was carried out on dry and normal shiv samples. "Dry" – hemp shiv samples were dried in an oven at 60°C until the change in mass of the sample was less than 0.1% between two weightings 24 hours apart, and "Normal" – hemp shiv samples were directly taken from the plastic bags. The results are presented in Figure 2.17 and Figure 2.18.
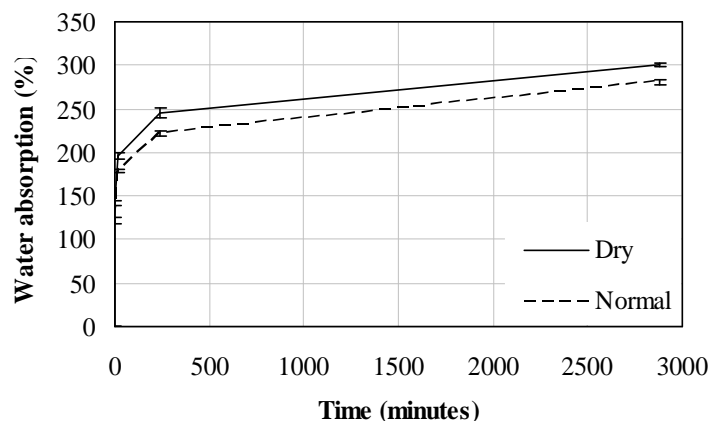
Figure 2.17: Water absorption of hemp shiv during 48 hours

Figure 2.17 shows that the dry and normal shives were found to have absorbed around three times their weight (301% and 281% respectively) after 48 hours. The results also show very fast absorption kinetics during the first minute for dry and natural shives (around 142% and 122% of their weights respectively), the water absorbed representing around 45% of the final value. The water absorption capacity of normal shiv was aroud 20% lower than that of dry shiv due to the fact that normal shiv already contains some water (around 9.74 ± 0.06 %).
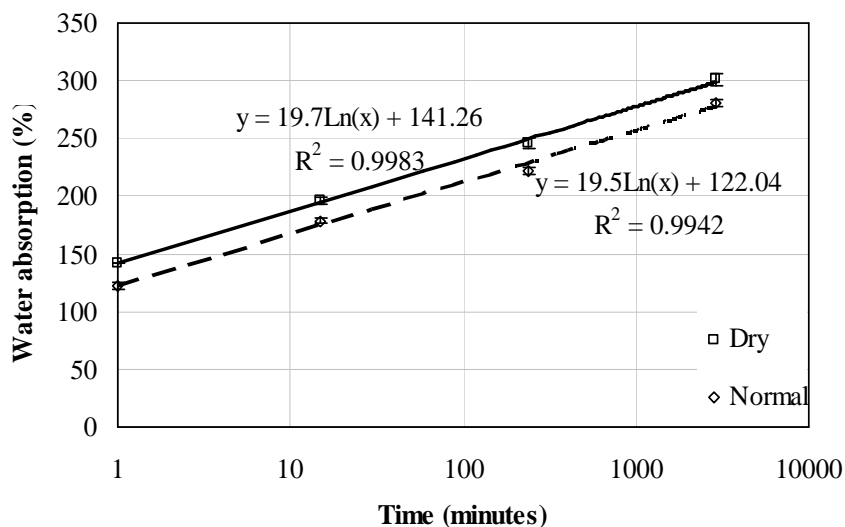
Figure 2.18: Water absorption of hemp shiv according to logarithmic function of time

Figure 2.18 presents the water absorption capacity of hemp shives after first minute to 48 hours in the form of logarithmic function of time as proposed by Nozahic [NOZ12]. We can then distinguish two steps: the initial step corresponds to almost immediate adsorption of water at the surface of the aggregate and the second step is related to the absorption of water into the porosity of the aggregates. The results in Figure 2.18 clearly show that the absorption kinetics of hemp shives in this second step is a logarithmic function of time, with a form as in (2.6).

$$W = A\ln(t) + W_o \tag{2.6}$$

The values of W_0 (141.3% and 122%) correspond to the initial water adsorption of dry and normal hemp shives, respectively, in the first minute. Coefficient A can be regarded as an absorption coefficient.

These results confirm the high water absorption and retention capacity of hemp shiv, attributed to their high porosity and capillary structure in previous studies [ARN12 & NOZ12a]. A previous study has shown that shiv is able to absorb a lot of water (two to three times its dry weight) very quickly (its degree of saturation is over 95% after 10 min of immersion) [ARN12]. Others have found that it can absorb up to four times its mass (406%) of water in 48 hours of immersion [NGU10].

The results obtained in the present study are comparable with those in the literature. Nevertheless, we found that the initial adsorption (W_0) and absorption coefficient of dry shives were significantly lower than Nozahic's result [NOZ12a]. These differences could be due to the variable characteristics of hemp particles (e.g. size, fibre and dust content) but also to different experimental procedures. The size of the sample and the removal of water adsorbed at the surface and between the particles could particularly influence the experimental results.

Hemp shiv's great capacity to absorb water induces competition for water between hemp shives and binder during the fabrication and the hardening process of hempcrete: the hemp particles tend to absorb the water that is needed to hydrate the binder. Moreover, the high water absorption rate of hemp shiv leads to an increase in the amount of mixing water required, so the drying time after demoulding could be very long. Thus, the development of a pretreatment that could reduce the absorption of hemp shiv at the time of mixing would be very interesting in order to avoid the need for excessive amounts of water and to improve the mechanical performance of the concrete.

2.6.4   Particle size distribution (PSD)

In order to study the sizes of hemp shiv particles, the mechanical sieving and image analysis methods were applied. These methods were described in paragraph 2.3.5.

2.6.4.1 Influence of parameters on PSD of hemp shives using mechanical sieving method
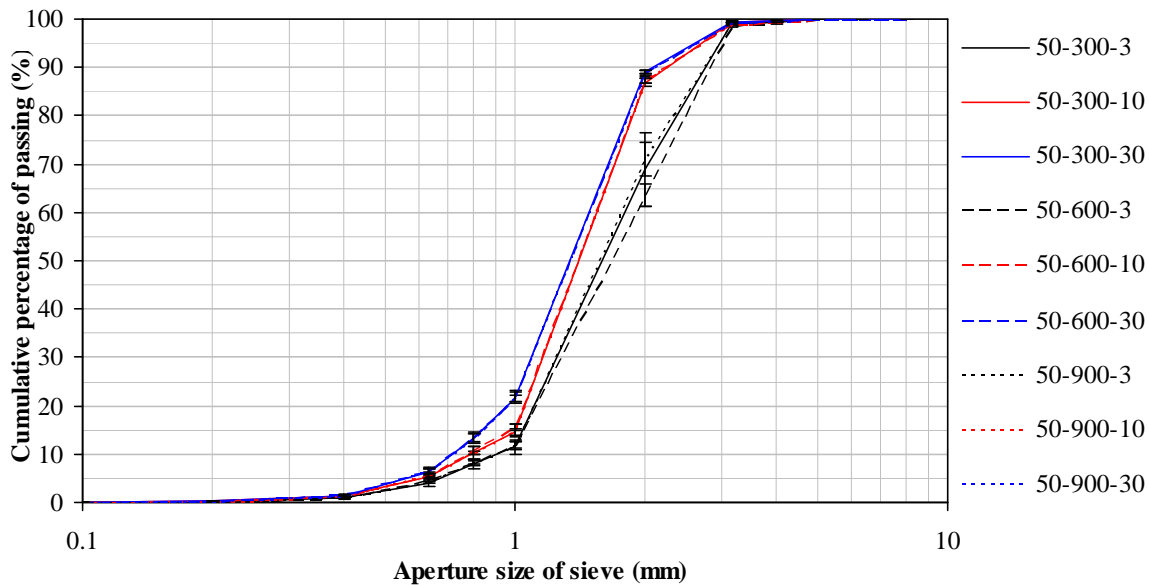
Figure 2.19: Impact of time and frequency of mechanical sieve method
on PSD of hemp shives for 50g samples
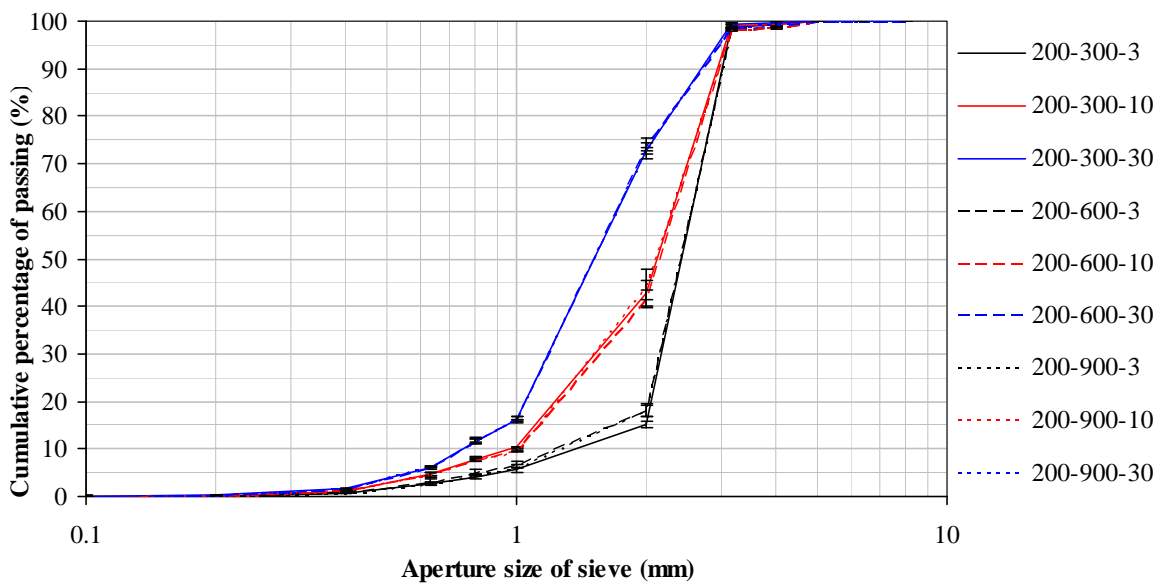
Figure 2.20: Impact of time and frequency of mechanical sieve method
on PSD of hemp shives for 200g samples

For this method, in order to evaluate the influence of the parameters of sieving on the results of particle size distribution of hemp shives, we carried out the measurements on two kinds of dry samples of around 50 and 200g with different parameters. Three samples of each kind were analyzed with continuous vibrational mode and maximum vibrational amplitude. Each sample was sieved for three vibrational times (3, 10 and 30 minutes), and each vibrational time was applied for three vibrational frequency (300, 600 and 900 Hz), and each sample was therefore sieved 9 times. The Figure 2.19, Figure 2.20 and Figure 2.21 below show the results obtained by mechanical sieving method (the notation of sample in these figures present the parameters of seiving, for example, "50-300-3" notation: "50" is 50g of weight, "300" is 300 Hz of vibration frequency and "3" is 3 minutes of vibrational time).

Figure 2.19 and Figure 2.20 present the particle size distribution of two kinds of hemp shiv samples (50 and 200g) with different parameters. These figures show that the grading curves are clearly distinguished by the time of vibration, especially for 200g samples (black curves for 3 minutes, red curves for 10 minutes, and blue curves for 30 minutes). For mechanical sieving, the minimum time of vibration should then be 30 minutes. At the contrary, it could be conclude that vibrational frequency did not influence particle size distribution of hemp shives. Moreover, hemp shiv particles completely passed the 5mm sieve for all samples, and the grading curves under 0.4mm and above 4mm sieves are respectively similar each other for each kind of samples, which did not depend on any parameter.
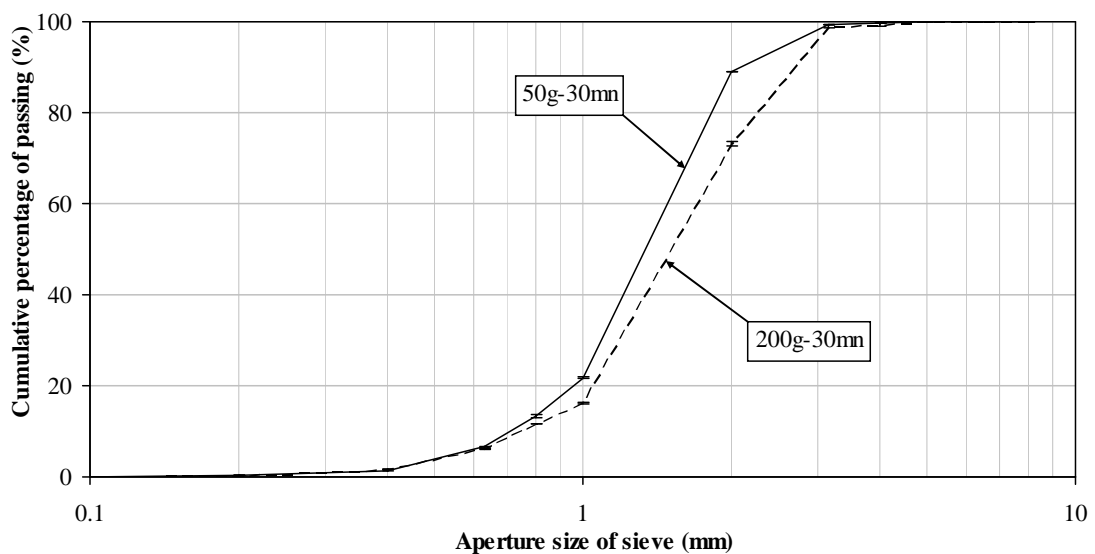
Figure 2.21: Grading curves by mechanical sieve method for both 50 and 200g samples

Figure 2.21 shows the average grading curves according to vibrational time of 30 minutes for each kind of samples. It could be noted that the grading curves are different from their sample weights (50 g and 200 g): the higher quantity of small particles (< 2 mm) passed the sieves for the 50 g sample than for 200 g sample. This can be explained that hemp shiv particles are very light weight; therefore, the greater the weight of shive sample is, the more difficult the hemp particles pass aperture size of sieves (in this case, 200 g of hemp shives are almost a full sieve. That's why in the RILEM protocol, the size of the sample is adapted to the size of the sieve).

2.6.4.2 PSD of hemp shives using mechanical sieving method

Previous paragraph demonstrated that PSD of hemp shives depends on the sample weight, while it was not influenced by vibrational frequency, and the vibrational time should be at least 30 minutes. Moreover, the current work of TC Bio-aggregates based building materials of the RILEM advised that sample weight of hemp shives for PSD should be around 100g. Thus, we decided to choose the parameters to analysis PSD of ISOCANNA hemp shiv which is used to fabricate hempcrete as following: sample weight of around 100 g, vibrational time of 30 minutes, vibrational frequency of 600Hz, continuous vibrational mode and maximum vibrational amplitude. The result was presented in Figure 2.22.
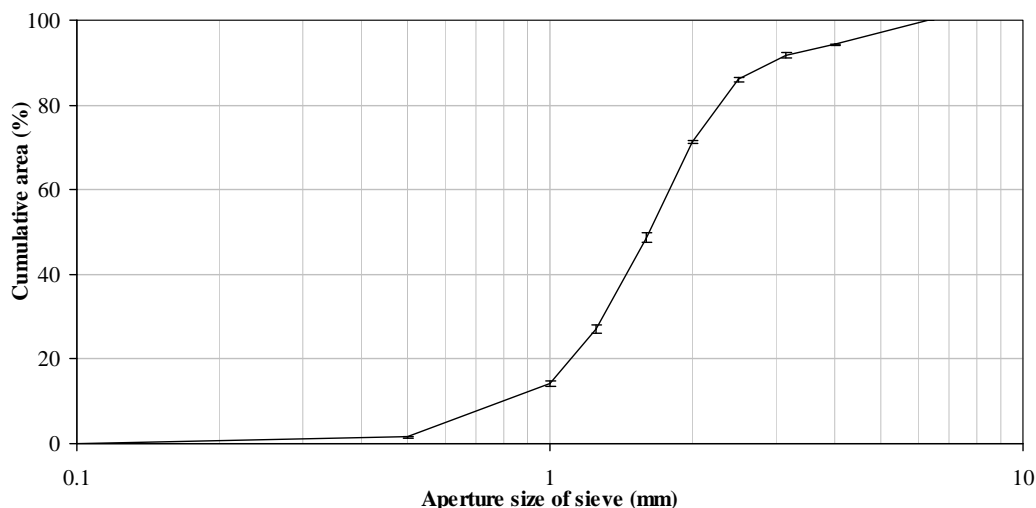
Figure 2.22: Grading curves by mechanical sieve method

Figure 2.22 shows the grading curves of the hemp particles obtained by mechanical sieving. It can be seen that the size of particles varied from 0.5 to 6.3 mm: the cumulative percentage by mass passing the 1-mm sieve was around 15%; for the 4-mm sieve, it

became 94%; and, for the 6.3-mm sieve, 100%. This figure indicates that our hemp shiv's particle size was smaller than that of other studies (see paragraph 1.4.4.1 in first chapter). These differences could be attributed to the different mechanical process of defibration of hemp stem, the different measurement method and the different weight of hemp shiv sample.

2.6.4.3 Image analysis method

It can be seen that PSD of hemp shives obtained by mechanical sieving method was not exact because there were many hemp particles passing through a given sieve that had lengths much larger than the sieve aperture, while this method cannot characterized the width and length of the parallelepiped form of hemp particles. Thus, it is necessary to use an alternative method in order to measure the width and length of the hemp particles exactly. In this study, image analysis method was used to measure PSD of hemp shives using ImageJ software. The advantages of the image analysis method were that it gave us many parameters of the hemp particles (area, perimeter, length, width, etc.) and could therefore show the size distribution results according to two different dimensions.

In this study, the particle size distribution was analysed according to major axis length, the minor axis length and the equivalent diameter as Figure 2.23 below.
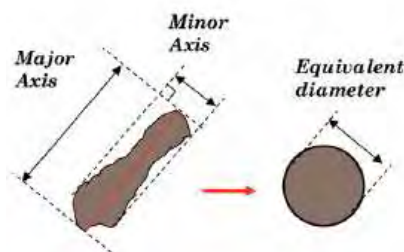
Figure 2.23: Dimensions of hemp shiv particle obtained by Image analysis method

In Figure 2.23, the major axis length was the length of the longest line that could be drawn within the object, the minor axis length was the length of the longest line that could be drawn perpendicular to the major axis and within the object, and the equivalent diameter (ED) was the diameter of a circle having the same area as the object calculated by (2.7) equation, where "A" is the area of the object measured as a polygon [NOZ12].

$$ED = \sqrt{\frac{4.A}{\pi}} \tag{2.7}$$

The result of particle size distribution of hemp shiv by image analysis method is presented in Figure 2.24 below.
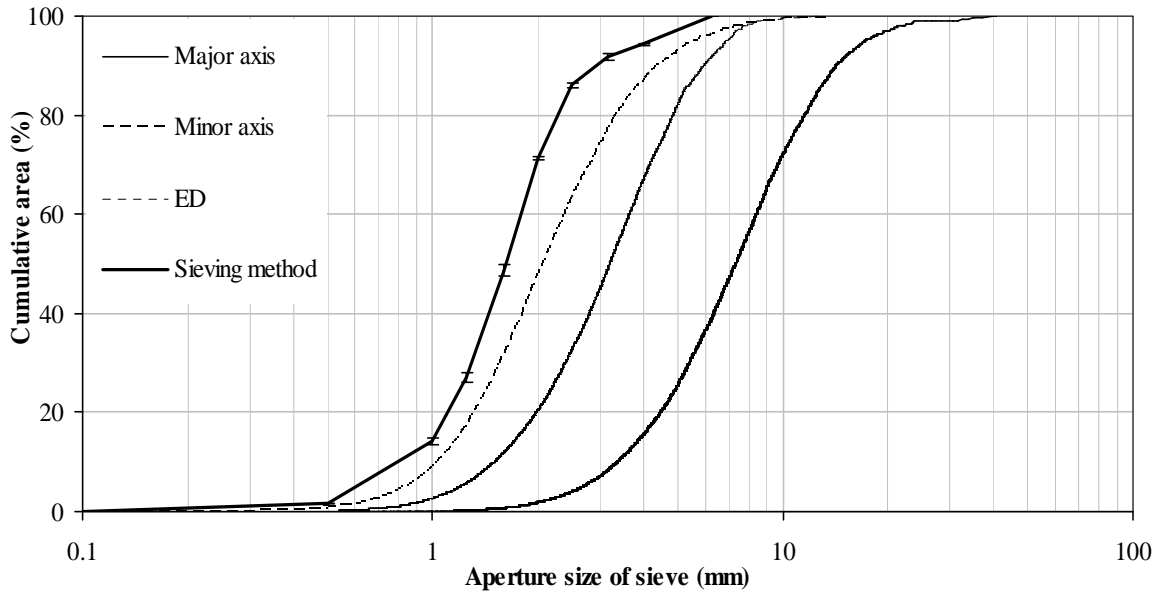
Figure 2.24: Dimensions of hemp shiv particle obtained by Image analysis method

Figure 2.24 shows the curves drawn from particle size distribution of three samples, of 5628, 4356 and 5102 particles (3.56, 3.31 and 3.87g respectively) obtained by image analysis using ImageJ software. This figure indicates that the size distribution of hemp particles according to the minor axis is very close to the distribution obtained by the sieve method. This result is in accordance with the literature [NGU10, NOZ12 & PIC12]. In fact, in previous works, several authors analysed the particle size distribution of hemp shives by image analysis using ImageTool software. Nguyen [NGU10] indicated that his results were quite similar when he analysed different weight samples (2g and 5g) from the same hemp. These results showed that hemp particle size was distributed from 0.35 mm to 8 mm and from 1.25 mm to 20 mm according to the minor and major axes respectively. In another study [NOZ12a], samples of 4g were analysed. The particle size distribution was from 0.35 mm to 6.3 mm, from 1 to 20 mm, and from 1 to 9 mm according to the minor axis, major axis and equivalent diameter respectively. Both studies pointed out that the advantage of this method compared to the mechanical sieve method was its ability to characterize complex particle morphology and heterogeneity.

We remark that quantities of small particles and fibres cannot be detected by this method, as shown by Nozahic[NOZ12a]. This is a drawback of this method.

98

2.7 Conclusion

This chapter presented the methods used in this study, and the characterization of mineral and plant raw materials.

In the first part, the methods were described to characterize the binders, standard mortars, hemp aggregates and hempcrete.

In next part, the chemical and mineralogical characteristics of mineral raw materials (natural hydraulic lime - NHL3.5, slaked lime and flash metakaolin) were characterized. These characteristics allow to optimize the content of these mineral raw materials to formulate two kinds of pozzolanic binders between lime (NHL3.5 or slaked lime) and flash metakaolin, which will be presented in chapter 3.

Moreover, the mineral and organic admixtures (potassium sulphate and glycerol carbonate respectively) as well as the superplasticizer were introduced. These admixtures will be used to improve the properties of new pozzolanic binders. The influence of the admixtures on the properties of binders will be also presented in chapter 3.

Furthermore, a commercial binder (CB) was also characterized. In third chapter, we will compare the mechanical and thermal properties among the CB and two kinds of pozzolanic binders and the properties among the standard mortars using these three binders. In the last chapter, we will compare the hempcrete using CB binder and the hempcrete fabricated by our binder with the same formulation in order to evaluate the mechanical and thermal properties of these two kinds of hempcretes.

In the last part of this chapter, hemp shives was characterized. The great capacity of water absorption of this material requires the pre-treatment before using them as light aggregates in fabrication of hempcrete in order to reach the best properties of hempcrete. This pre-treatment will be presented in the last chapter.

Chapter 3:   Optimization of the pozzolanic binders

3.1 Introduction

This chapter presents the results of development of new pozzolanic binder in order to fabricate hempcrete. In this study, we will develop the new pozzolanic binders from flash metakaolin and lime (natural hydraulic lime NHL3.5 or slaked lime) and some admixtures (superplasticizer, glycerol carbonate and potassium sulphate) to obtain the pozzolanic binder being consist with the strategy of sustainable development in construction area. This chapter will present following results:

- optimization of raw material content to formulate control binder;

- influence of admixtures on the properties of binder;

- thermal conductivity of binder.

Introduction

Ce chapitre présente les résultats des recherches effectuées pour mettre au point de nouveaux liants pouzzolaniques pour la fabrication de béton de chanvre. Dans cette étude, nous développerons de nouveaux liants pouzzolaniques en utilisant du métakaolin flash, de la chaux (chaux hydraulique naturelle NHL3.5 ou chaux éteinte) et des adjuvants (superplastifiant, carbonate de glycérol et sulfate de potassium), en accord avec la stratégie de développement durable dans la construction (pas de ciment portland utilisé). Ce chapitre présentera successivement les résultats suivants:

- *l'optimisation de la teneur en matières premières pour formuler des liants témoins;*

- *l'influence des adjuvants sur les propriétés des liants;*

- *la conductivité thermique des liants optimisés.*

3.2 Optimization of raw material content to formulate control binder

3.2.1 Formulation

We formulated two kinds of pozzolanic binders between MK and limes (NHL3.5 or slaked lime - SL) from theory relation between MK and limes characterized as (1.8) pozzolanic reaction below.

$$AS_2 + 5CH + 5H \rightarrow C_5AS_2H_{10} \qquad (3.1)$$

This reaction (1.8) shows mole relation between MK (AS_2) and calcium hydroxide (CH) as (3.2) equation below.

$$n_{CH} = 5 \times n_{AS_2} \tag{3.2}$$

The number of moles of MK is calculated as (3.3) equation with 51.4% pure MK (as presented in paragraph 2.5.3 in chapter 2):

$$n_{AS_2} = 51.4\% \times \frac{MK\%}{M_{AS_2}} = 51.4\% \times \frac{MK\%}{220} \tag{3.3}$$

For slaked lime (SL), CH content is 90.4% by weight (paragraph 2.5.2 in chapter 2), the number of CH moles of SL therefore is calculated as (3.4) equation:

$$n_{CH}^{SL} = 90.4\% \times \frac{SL\%}{74} \tag{3.4}$$

Thus, the mole relation between MK and SL is presented by (3.5) equation:

$$90.4\% \times \frac{SL\%}{74} = 5 \times 51.4\% \times \frac{MK\%}{220} \qquad Or \qquad \frac{MK\%}{SL\%} = 0.96 \tag{3.5}$$

For NHL3.5 lime, CH content includes 22.01% of disposable CH content in NHL3.5 (paragraph 2.5.1) and CH content formed by hydration reaction of C_2S as (3.6) equation. Thus, the number of CH moles of NHL3.5 is calculated as (3.7) equation:

$$C_2S + H_2O \rightarrow 0.3CH + C-S-H \tag{3.6}$$
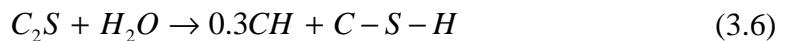
$$n_{CH}^{NHL} = 22.01\% \times \frac{NHL\%}{74} + 0.3 \times \frac{35.67\% \times NHL\%}{172} \tag{3.7}$$

From (3.2) and (3.7) equations, we obtain the relation between MK and NHL3.5 as (3.8) equation below:

$$22.01\% \times \frac{NHL\%}{74} + 0.3 \times \frac{35.67\% \times NHL\%}{172} = 5 \times 51.4\% \times \frac{MK\%}{220}$$
$$Or \qquad \frac{MK\%}{NHL\%} = 0.31 \tag{3.8}$$

On the other hand, the formulations of two pozzolanic binders are presented as (3.9) equation below:

$$MK\% + SL\% = 100\% \qquad and \qquad MK\% + NHL\% = 100\% \tag{3.9}$$

From (3.5), (3.8) and (3.9) equations, we can determine the theoretical content by mass of MK and limes of the two pozzolanic binders in formulation in order to ensure stoichiometric reaction:

- Formulation from MK and SL: 51% SL and 49% MK.
- Formulation from MK and NHL3.5: 76.3% NHL3.5 and 23.7% MK.

In conclusion, from theoretical content by mass of MK and limes presented above and in accordance with results of Magniont's study [MAG10b], we decide to test compressive strength of different formulations between MK and limes with at least 50% by weight to select the formulation of control binder, as Table 3.1 below.

Table 3.1: Proportion of components by weight

Components	*H3M7*	*H4M6*	*H5M5*	*S2M8*	*S3M7*	*S4M6*	*S5M5*
NHL 3.5	30%	40%	50%				
Slaked lime - SL				20%	30%	40%	50%
Flash metakaolin - MK	70%	60%	50%	80%	70%	60%	50%
Water/Binder	0.5	0.5	0.5	0.5	0.5	0.5	0.5

Water/ Binder: mass ratio of water to mixture of lime and MK
H, S and M are respectively notations for NHL3.5, slaked lime and flash metakaolin

3.2.2   Compressive test

The compressive test was performed at 2, 7, 28 and 49 days with 4 samples for each age. This test was carried out according to the method presented in paragraph 2.2.5 in chapter 2. The results of the compressive tests are presented Figure 3.1 and Figure 3.2.

	H5M5	H4M6	H3M7	S5M5	S4M6	S3M7	S2M8
☐ 2 days	2.44	1.88	1.71	0.74	0.96	0.70	0.76
⊠ 7 days	7.06	5.21	3.19	2.75	4.55	4.93	4.37
⊠ 28 days	9.86	7.18	4.50	7.18	11.04	13.50	11.14
▨ 49 days	11.03	8.72	4.08	6.35	11.06	13.61	10.90
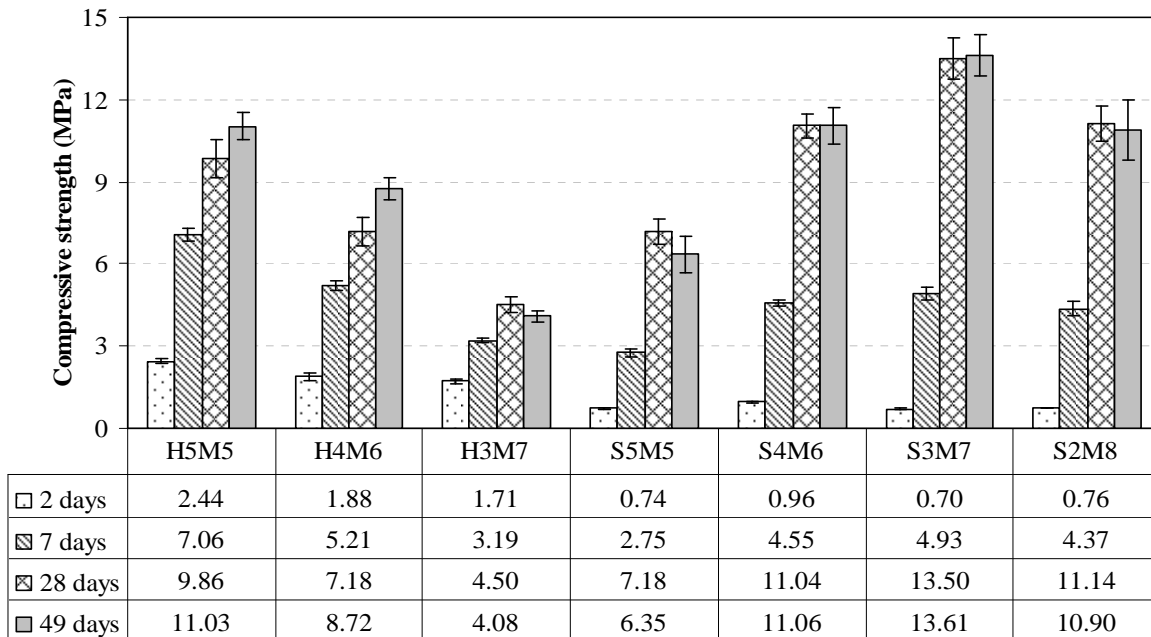
Figure 3.1: Compressive strength of binders in function of age

At 2 days, Figure 3.1 shows that the compressive strength of the mixtures containing NHL3.5 lime predominated (around 2 - 3 times) over the mixtures containing

slaked lime. At 7-day age, the strength of the mixtures containing 40 and 50% NHL3.5 lime (H4M6 and H5M5) was slightly higher than that of the mixtures including slaked lime. This result reveals the role of hydraulic setting in the short term, which confers higher early age strength on the paste. But, for longer ages (28 and 49 days), the compressive strength of the mixtures containing slaked lime was significantly higher than that of the mixtures containing NHL3.5 lime, except S5M5 mixture. These results could be explained by the smaller amount of $Ca(OH)_2$ in NHL3.5 lime after 28-day age, that constitutes a limiting factor for the metakaolin pozzolanic reaction and consequently limits the development of mechanical performance. This phenomenon also explains the low compressive strength obtained with H3M7 mixture, in which the $Ca(OH)_2$ amount is much lower than necessary for the development of pozzolanic reaction with metakaolin.

Figure 3.1 also shows that in seven mixtures, the S3M7 mixture has the highest compressive strength at 28–day age (13.5 MPa) and 49–day age (13.6 MPa) in spite of the lowest strength (0.7 MPa) at 2–day age. This could be explained by a low rate of pozzolanic reaction at early age. However, the MK to lime ration of the highest strength binder differs from the theoretical ratio obtained by molar balance (see paragraph 3.2.1). On the other hand, S5M5 presented the lowest strength (it is around 50% the strength of S3M7) which can be attributed to metakaolin content is lower than the necessary for pozzolanic reaction.
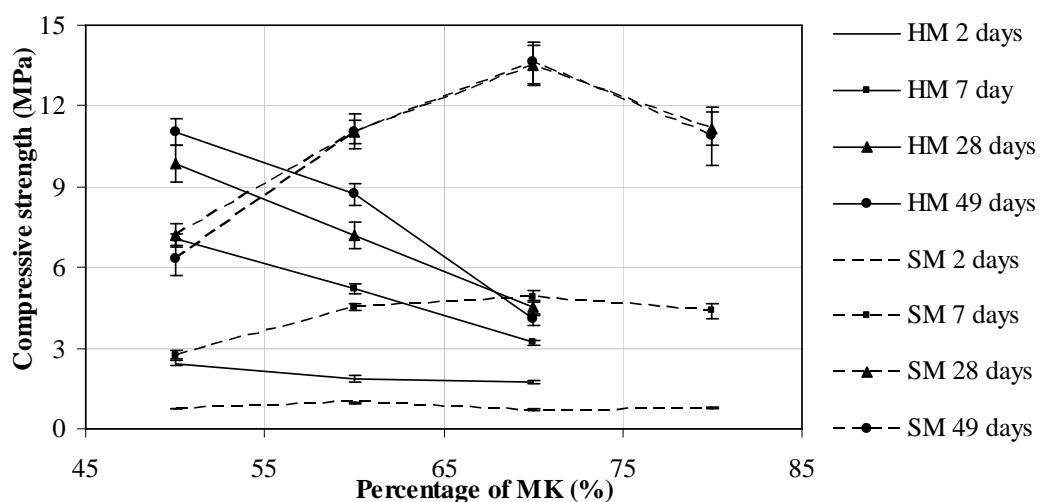
Figure 3.2: Compressive strength of binders in function of metakaolin content

In order to easily evaluate the role of metakaolin in the mechanical performance of binders, Figure 3.2 below presents the relationship between compressive strength and metakaolin content of binders in function of age.

Figure 3.2 evidently shows that for the binders from metakaolin and NHL3.5 lime (HM), the higher the metakaolin content is, the lower the compressive strength will be. For the binders from metakaolin and slaked lime (SM), the compressive strength increases in function of metakaolin content until 70%, but it decreases with metakaolin content of 80% except at 2 days (the strength of all mixtures are similar each other).

In conclusion, this test demonstrates that the H5M5 and S3M7 mixtures have the best mechanical performance. H5M5 mix can be interesting because it allows reaching the highest mechanical strength at early age, nevertheless after 28 days the S3M7 mix is the most efficient. These mixes are also interesting in term of economics and sustainable development in the construction, as the higher the flash metakaolin content in the mixture is, the better the environmental quality will be and the cheaper the cost of the mixture gets.

H5M5 and S3M7 mixtures had then been selected as the control binders, abbreviated HM and SM respectively. In the next parts, we will present other test results of characterization of these two control binders.

3.2.3   Calorimetric test

This test measured the variation of the temperature of HM and SM pastes in 5 days right after mixing. The obtained values of the temperature were used to calculate the hydration heat during hydration of these two binders. The results are presented in Figure 3.3 and Figure 3.4 below.
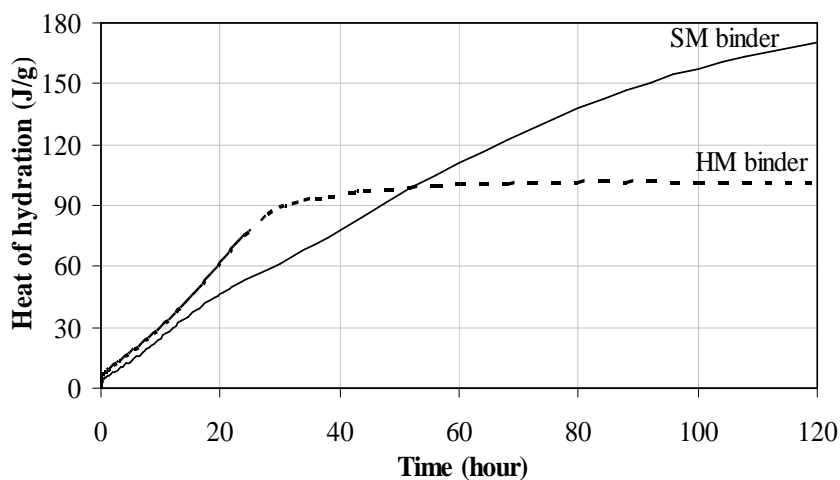
Figure 3.3: The cumulative hydration heat for HM and SM binders
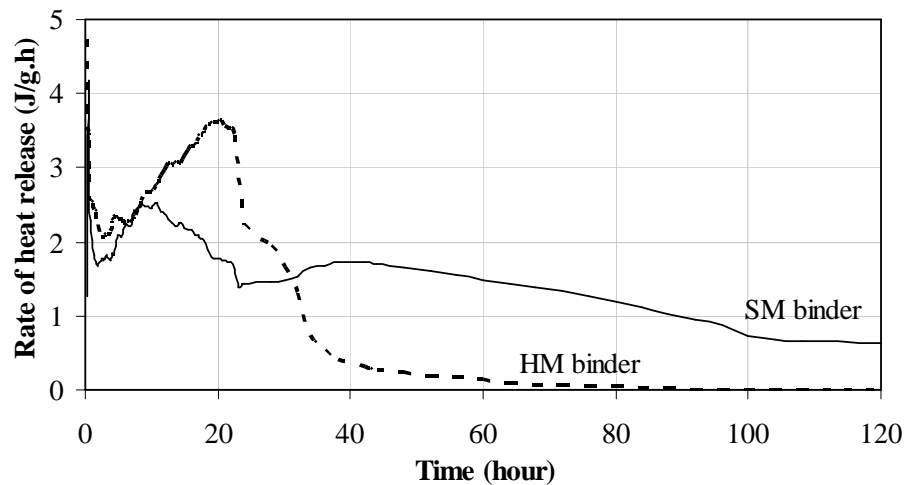
Figure 3.4: Rate of heat release of HM and SM binders

Figure 3.3 shows the evolution of hydration heat of two pastes during 5 days. The heat generation of two pastes was nearly similar to each other during the first 10 hours. After that time, the heat generation of HM paste increased rapidly until the first 28 hours and reached the maximum cumulative hydration heat after 40 hours with a value of around 100 J/g. For the SM paste, the heat generation was slower than that of HM paste after the first 10 hours, and it increased gradually until 5 days with the cumulative value of 170 J/g at 5 days being much higher than that of HM paste.

Figure 3.4 indicates the rate of heat release of these two pastes during 5 days of hydration. For HM paste, the heat release rate increased until the maximum value (around 3.7 J/g/h) after 20 – hour hydration, and then reduced suddenly until 40 hours and reached minimum value after 60 hours. For SM paste, its rate of heat release increased during the first 10 hours of hydration (maximum value is around 2.5 J/g/h), and the reduced gradually until the end of the test.

In conclusion, the results of this test could confirm the role of hydraulic components in NHL3.5 which generated the higher hydration heat of HM paste at early on, and the slow pozzolanic reaction between MK and SL after 28 days. Thus, this phenomenon could explain the difference of compressive strength between HM and SM binders, for which the strength of HM binder is better at early age and of SM binder is higher after 28 days.

3.2.4 Shrinkage measurement

In order to explore the dimensional variations of two pozzolanic binders (HM and SM), endogenous and total shrinkages and the mass loss of the pastes were measured over

the time. This test performed on three samples for each measurement in a controlled room (20°C, 50%RH). Figure 3.5, Figure 3.6 and Figure 3.7 present the measurements.

Figure 3.5 shows the total and endogenous shrinkages of two pastes. It can be seen that after 420 days, the total shrinkage of HM paste was much higher than that of SM paste, while the endogenous shrinkage of SM paste was much higher than that of HM paste. On the other hand, this measurement indicated that the total shrinkage of SM paste was higher during 3 weeks from 7 days to 28 days and lower during the first 7 days and after 28 days than that of HM paste. This figure also shows that the dimensional variations were insignificant after around 160 days for SM binder and 230 days for HM binder and there was not swelling in early age for both pastes.
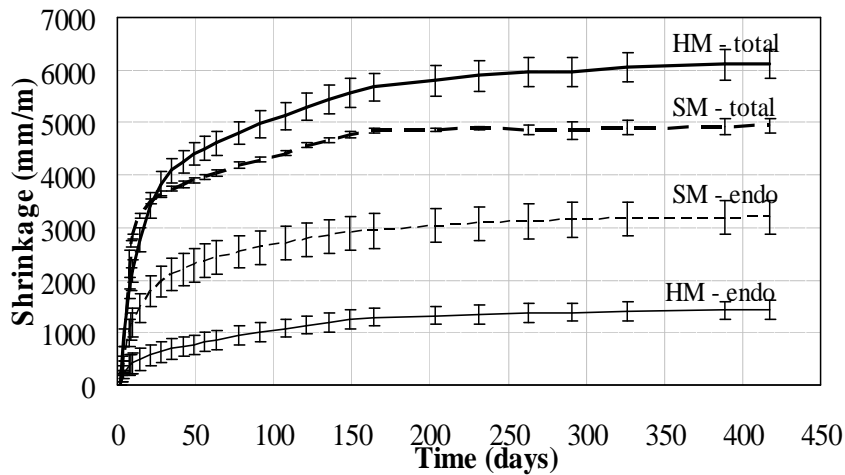
Figure 3.5: Shrinkage of two control binders: HM and SM
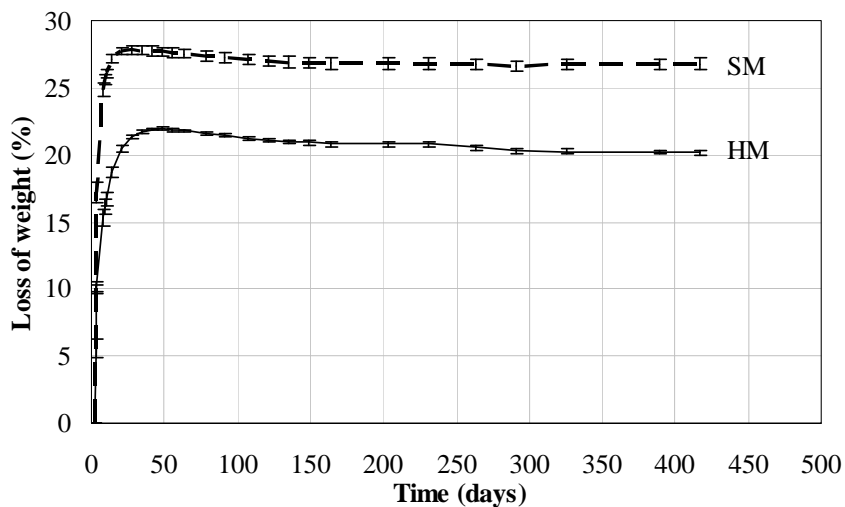
Figure 3.6: Weight loss of two control binders: HM and SM

108
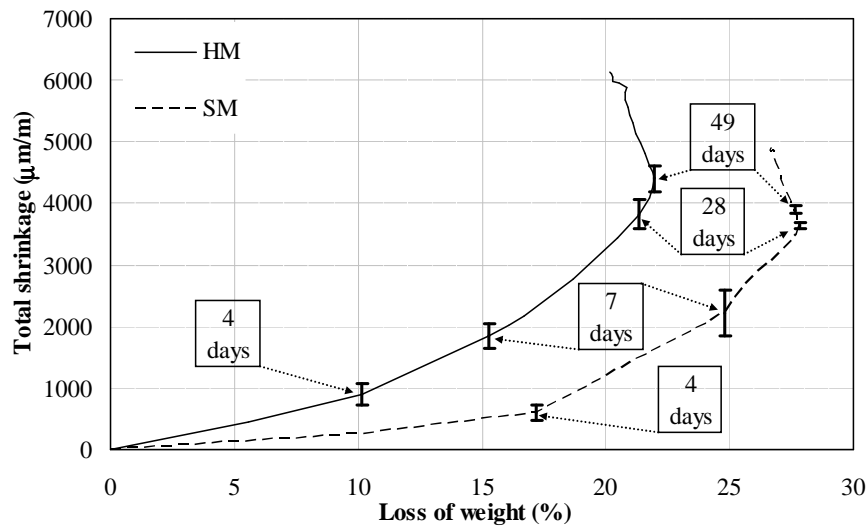
Figure 3.7: Total shrinkage vs weight loss for two control pastes: HM and SM

Figure 3.6 and Figure 3.7 present the weight losses of two binders after 420 days and the relation between total shrinkage and loss of weight for HM and SM binders respectively. It can be seen that the drying kinetics of two binders are significantly different. Indeed, the weight losses of HM and SM binders are respectively 21.9% and 27.8% in spite of the same initial water to binder ratio. The HM paste reached its final mass in 49 days whereas the SM paste only needed 28 days (Figure 3.6 and Figure 3.7). Moreover, the decrease of weight loss of these two binders was observed after reaching their final mass, which was attributed to the carbonation of the pastes (Figure 3.7). These differences between two pastes can be attributed to their different desiccation and hydration mechanisms.

In fact, the higher weight loss of SM binder during first 7 days (24.8%) can be explained by the lower hydration rate of SM binder against that of HM binder at early age (before 2 days, see paragraph 3.2.3).

During following 3 weeks (from 7 to 28 days), SM binder exhibited the higher total shrinkage in comparison with HM binder (see paragraph 3.2.3 and Figure 3.5) that could be explain by its higher hydration rate during this time.

For the longer age, after 28 days, the lower total shrinkage of SM binder against that of HM binder could be in relation with the hydration rate of SM binder was much lower than that of HM binder. This could be explained by the almost complete pozzolanic reaction of SM binder because of the equilibrium between AS_2 and $Ca(OH)_2$ components, while the pozzolanic reaction of HM binder had been occurred because $Ca(OH)_2$ induced

from the hydration of C_2S reacts the residual AS_2. Thus, we can conclude that the difference of hydration rate can explain the difference of total shrinkage between HM and SM binders: the higher the hydration rate of the binder is, the higher the total shrinkage of binder will be.

For the difference of endogenous shrinkage between HM and SM binders, it can be attributed to the difference of volume between the reaction products and the reactants [NEV11 & TAZ95]. Indeed, the different chemical components and hydration mechanism between HM and SM binders can form different hydration products, and consequently different volume of reaction products. This can be confirmed by the analyses of the mineralogical characteristics of each binder in next part.

3.2.5 *X-ray diffraction and thermogravimetric analyses*

In order to study the mineralogical characteristics of two control binders (HM and SM) during their hydration processes, X-ray diffraction (XRD) and thermogravimetric (TGA) analyses were realized. These analyses were carried out on the dry powder samples passing through a 80 µm sieve of the two control binders at 2, 7, 28 and 49 days.

For the TGA analyses, the Table 3.2 presents temperatures ranges of mineral decomposition which is synthesised from literature [AGG11, BAK06, FRI02 & SEP10] and used in this study.

Table 3.2: Temperature ranges of mineral decomposition from literature

Temperature (^oC)	Nature of reaction	Type of reaction
< 100	Evaporation of free water	endo
70-140	Deshydration of ettringite	endo
105-250	Deshydration of C-S-H	endo
160-265	Deshydration of straetlingite (C_2ASH_8),	endo
210-265	Deshydration of C_4AH_{13}, hemicarboaluminate, monocarboluminate, monosulfualuminate	endo
300-360	Deshydration of hydrogarnets	endo
380-525	Deshydration of portlandite ($Ca(OH)_2$)	endo
600-800	Decarbonation of calcite $CaCO_3$	endo

endo : endothermy

3.2.5.1 Analyses of HM binder

Figure 3.8 shows the mineralogical characteristics determined by XRD for control binder from 50% MK and 50% NHL3.5 by weight in function of the age.
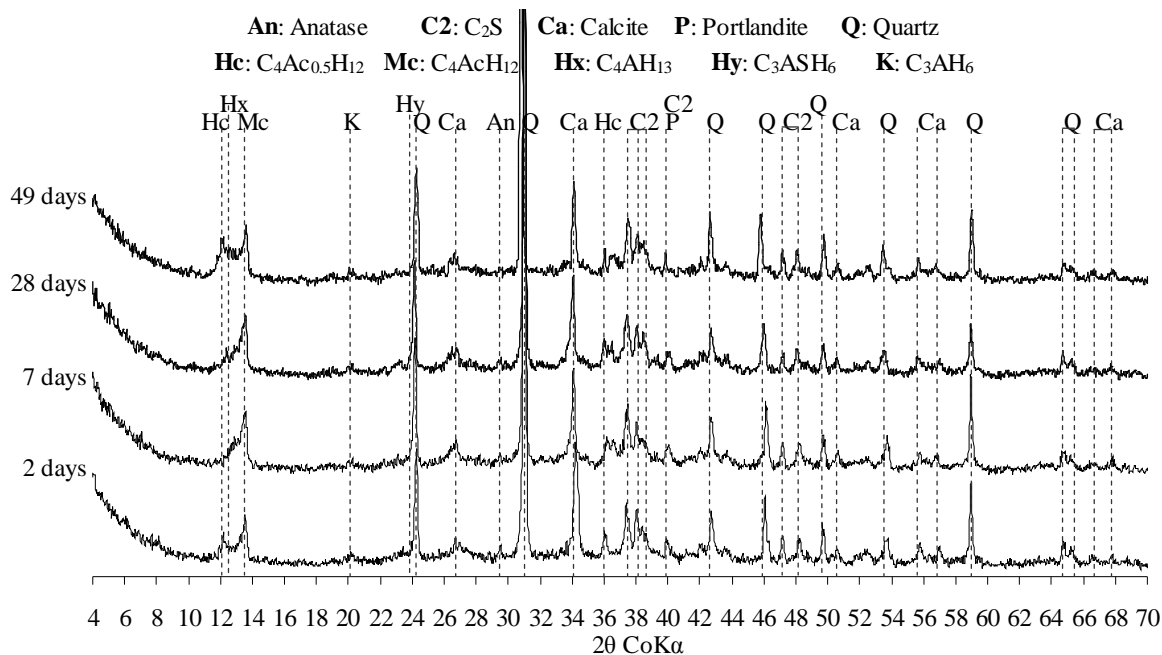
Figure 3.8: XRD analysis of HM reference binder

It can be seen that the consumption of portlandite (P) initially presented in NHL3.5 by pozzolanic reaction was almost complete right after 2 days (it only present small peak at around $2\theta = 39.9^{o}$). This observation could confirm the limiting role of portlandite, contained in too low quantity in NHL3.5, on the pozzolanic reaction of metakaolin.

For the other hydration products, one calcium aluminate phase (Hx - C_4AH_{13}), two carboaluminate phases (calcium hemicarboaluminate, Hc - $Ca_4Al_2O_7(CO_2)_{0.5}(H_2O)_{12}$ – $C_4Ac_{0.5}H_{12}$ and calcium monocarboaluminate, Mc - $Ca_4Al_2O_7CO_2(H_2O)_{11}$ - C_4AcH_{11}) and one hydrogarnet phase (katoite, K – C_3AH_6) occurred right at 2-day age, other hydrogarnet phase (Hy – C_3ASH_6) was detected after 7 days. In a previous study, Magniont [MAG10b] had synthesized the analyses in literature and demonstrated by her study that Hx is the hydration product of reaction between MK and lime at ambient temperature, and the formation of Hc and Mc is attributed to the presence of CO_2 or $CaCO_3$ in the paste. This confirmed our results for the formation of Hc and Mc because the HM binder contained the large amount of $CaCO_3$ in NHL3.5 component (around 20%). For the hydrogarnet phases, the small peaks of K – C_3AH_6 and Hy – C_3ASH_6 were detected at $2\theta = 20.2^{o}$ and 23.9^{o} respectively. Sepulcre-Aguilar [SEP10] attributed the formation of hydrogarnet phases at temperature of $20^{o}C$ to the presence of very high content of SiO_2 (in our case, MK contains very high SiO_2 content – 67.1%, Table 2.6 in chapter 2).

For other components, the quartz (Q) and anatase (An) from MK and some inert or anhydrous phases from NHL3.5 such as the peaks of calcite (Ca) and C_2S (C2) were still present. The presence of C_2S after 49 days can explain the continuous evolution of mechanical strength, and consequently the performance of that mix will potentially continue to increase thanks to pozzolanic reaction of MK with $Ca(OH)_2$ resulting from C_2S hydration.

However, the XRD test did not identify the amorphous hydrates like C-S-H due to very low degree of crystallization. Thus, it is necessary to carry out the analyses of thermogravimetry on the similar powder samples.

The DTG curves of HM binder at 2, 7, 28 and 49 days are shown in the Figure 3.9 below.

Ca: $CaCO_3$ **Hx**: C_4AH_{13} **Hc**: $C_4Ac_{0.5}H_{12}$ **Mc**: C_4AcH_{12} **K**: C_3AH_6 **Hy**: C_3ASH_6
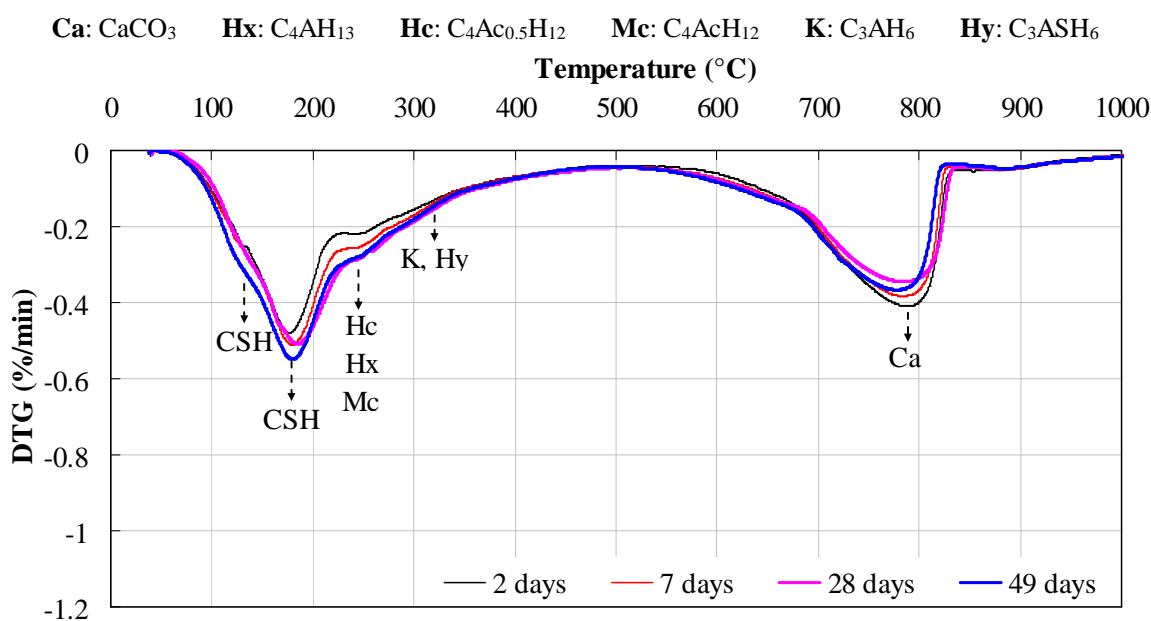
Figure 3.9: DTG curves of HM binder in function of age

This Figure 3.9 and Table 3.2 can permit to identify the major mineralogical decompositions during the test, characterized as follows:

- The peak of P was not visible (around 475°C) on the all DTG curves confirmed the observations on the XRD analyses (Figure 3.8) and the lack of calcium hydroxide for the pozzolanic reation of MK.

- The peaks at around 780°C concerned departing of CO_2 linked with decarbonation of $CaCO_3$ of the NHL3.5, which confirmed the XRD results (Figure 3.8).

- For the hydration products, the peaks at around 130°C and 180°C can imply the decomposition of C-S-H, which are principal hydration products formed from reaction of C_2S and also metakaolin with lime and water [MUR83]. They were not observed by the XRD analyses (Figure 3.8) due to very low degree of crystal [FRI03]. The peaks at around 240°C could be attributed to decomposition of Hc, Hx and Mc [MAG10b, MUR83, SEP10 and TRI12]. The decomposition of hydrogarnets may be the small peaks at around 320°C, [MAG10b & SEP10].

We remarked that the evolution of the curves in function of time is weak. This can be explained by the heat generation of HM binder: it generated much little heat after 2 days (Figure 3.3 and Figure 3.4), which corresponded with the insignificant difference of hydrated phase volume among 2-day age and other ages.

3.2.5.2 Analyses of SM binder

Figure 3.10 presents the mineralogical analysis performed by XRD for SM control binder from 70% MK and 30% SL by weight in function of the age.
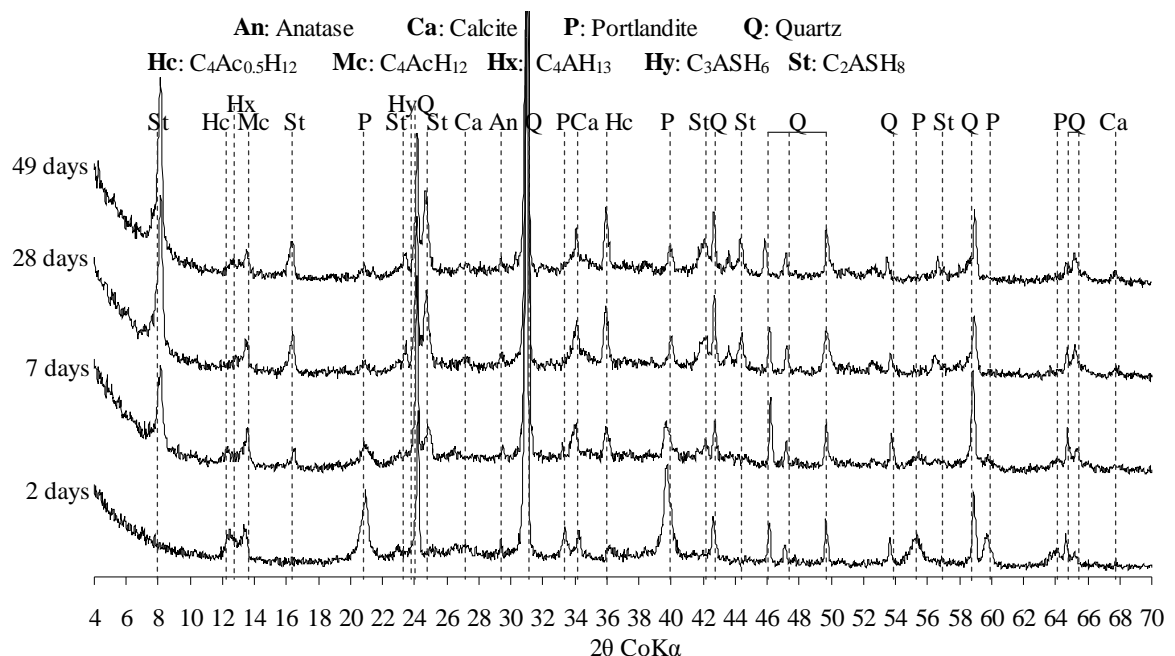
Figure 3.10: XRD analysis of SM reference binder

This figure allows observing the hydration products: Hx, Hc, and Mc were visible at 2-day age, and small peak of Hy was detected after 7 days, which are similar to the observation in HM binder above, while K was not visible.

113

In opposition to the XRD analysis of HM binder, it is evidently to see that the portlandite was not completely consumed by pozzolanic reaction of metakaolin until 49-day age. This figure shows that the residual portlandite was a very high intensity after 2-day age, and significantly reduced after 7-day age, and was only small peaks after 28 days. This observation could confirm that the high content of portlandite in slaked lime is enough for the pozzolanic reaction of metakaolin. Furthermore, it is clearly to see the appearance of straetlingite (St - C_2ASH_8) with a very high intensity from 7-day age, which was not detected on XRD diagrams of HM binder. This figure also showed the rapid evolution of intensity of straetlingite paralleling level of portlandite consumption during hydration time, which can confirm the rapid evolution of straetlingite quantity in function of hydration time. This can explain the rapid increase of the compressive strength of SM mixture from 7 days (see Figure 3.1) which is in agreement with Seppulcre-Aguilar's study [SEP10].

For other components, the peaks of quartz and anatase from MK, and a small peak of calcite from SL were also observed as similar as the analysis of HM control binder.

Figure 3.11 presents the analyses of thermogravimetry of SM binder at 2, 7, 28 and 49 days of age.
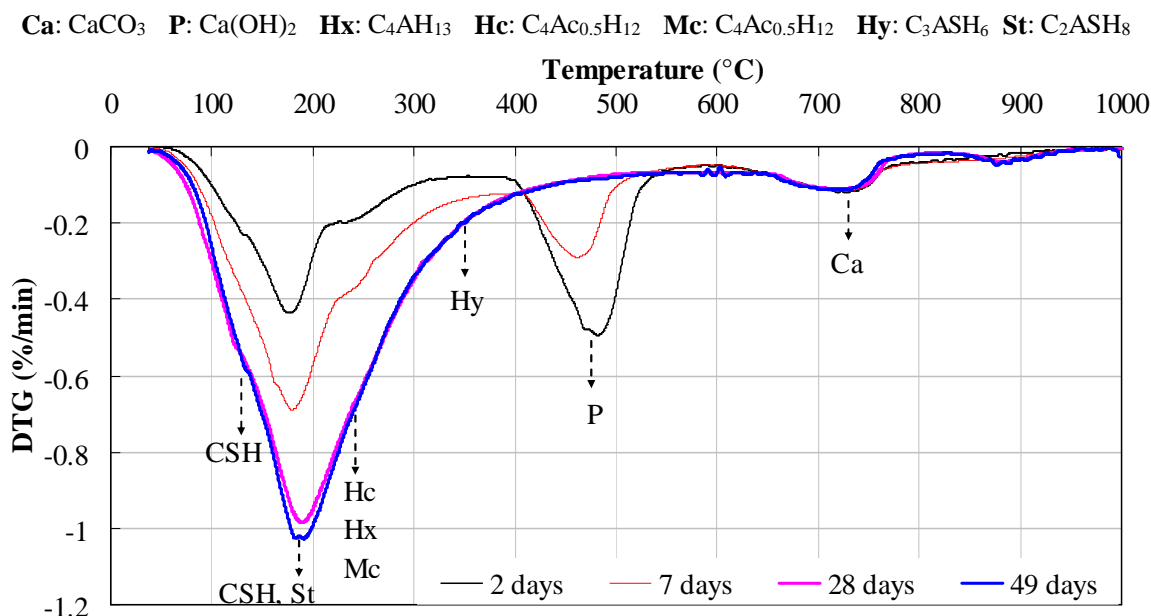
Figure 3.11: DTG curves of SM binder in function of age

This figure and Table 3.2 could permit us to distinguish the major mineralogical decompositions during the test, characterized as well:

- The peaks linked to decomposition of P were only visible on the DTG curves at 2 and 7 days around 475°C confirmed the observations on the XRD analyses (Figure 3.10) about the consumption of portlandite over time by pozzolanic reaction of metakaolin.

- The peaks at around 740°C concerned departing CO_2 because of decarbonation of $CaCO_3$ of the SL, which confirmed the XRD results (Figure 3.10). Moreover, this figure showed the much lower amount of $CaCO_3$ contained in SM binder in comparison with HM binder (Table 3.3).

- For the decomposition of hydration products, we also observed the peak of C-S-H at around 130°C, the peaks of C-S-H and straetlingite at around 180°C, and the peaks concerned the decomposition of Hc, Hx and Mc at around 240°C as the analyses for HM binder. Moreover, the DTG curves can also indicate the important evolution of quantity of hydrate phases in function of time.

Furthermore, Figure 3.11 shows the large evolution of the curves in function of time until 28 days, the insignificant evolution after 28 days. On one hand, this can be attributed to the heat generation of SM binder gradually increases until 5 days, and may continuously generate after 7 days (Figure 3.3 and Figure 3.4), which linked to the significant evolution of hydrated phase volume from 2-day age to 28-day age. On the other hand, intensity of Straetlingite observed at 28 and 49-day age of SM binder was similar to each other and much higher that observed at 7 days (Figure 3.10), which could also link to the much higher quantity of Straetlingite at 28 and 49 days against at 7 days. Consequently, we could attribute the large evolution of the DTG curves of SM binder over time to the quantity evolution of Straetlingite.

3.2.5.3 Relation between hydrated phases and compressive strength

The previous paragraphs (3.2.5.1 and 3.2.5.2) analyzed the mineralogical characteristics of HM and SM binders. Although TGA analyses cannot clearly distinguish among hydrated phases (C-S-H, St, Hx, Hc and Mc), they can allow to distinguish between hydrated phases and other phases (portlandite and calcite). In this part, we thus investigate the relation between total quantity of hydrated phases and the compressive strength for each binder. The total quantity of hydrated phases, $Ca(OH)_2$ and $CaCO_3$ was calculated according to the temperature interval of 80 - 380°C, 380 – 550°C and 550 – 900°C respectively. These results of HM and SM binders are presented in Table 3.3.

Table 3.3: Percentage by weight of hydrated phases – H%,

Ca(OH)$_2$ – P% and CaCO$_3$ – Ca% of both HM and SM binders

Binder	2 days			7 days			28 days			49 days		
	H%	P%	Ca%	H%	P%	Ca%	H%	P%	Ca%	H%	P%	Ca%
HM	23.2	-	15.0	25.5	-	14.9	26.4	-	14.8	27.7	-	14.4
SM	17.7	19.3	4.9	34.9	11.9	4.5	61.7	-	4.2	63.3	-	3.4

The residual portlandite quantity in this table can confirm the lack of portlandite in HM binder as well as the much high amount of portlandite contained in SM binder leading the complete pozzolanic reaction and appearance of straetligite for SM binder. Thus, the evolution of total hydrated phases of SM binder is higher than that of HM binder, which can confirm the much higher compressive strength of SM binder in comparison with that of HM binder after 28 days as well as the higher endogenous shrinkage for SM binder against for HM binder (paragraph 3.2.4). Moreover, the little consumption of CaCO$_3$ in function of time can be attributed to the formation of Hc and Mc phases which were detected by XRD analysis.

Figure 3.12 presents the relation between compressive strength and quantity of total hydration products for each binder.
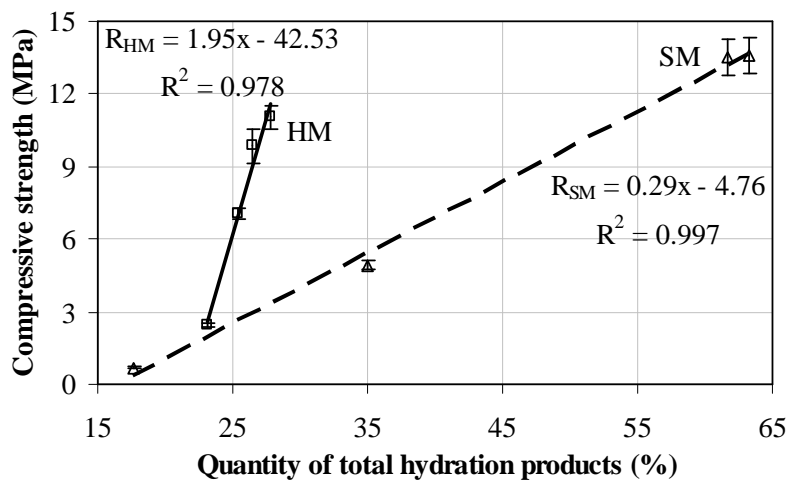
Figure 3.12: Compressive strength and quantity of total hydration products

This figure shows two linear relations with the fairly high regression coefficients. For each binder, the higher the quantity of total hydration products is, the better the compressive strength will be. This confirmed that the quantity evolution of total hydration products in function of time could explain the evolution of binder compressive strength.

This figure also shows the different evolution of the quantity of total hydrated

116

phases between HM and SM binders. We attributed this difference to quantity of Straetlingite: it was not visible on XRD diagram of HM binder, while its quantity of SM binder was very high (Figure 3.8 and Figure 3.10).

3.2.6   Conclusion

XRD analyses could confirm the different role of portlandite in two kinds of limes, the appearance of calcium aluminate, carboaluminate and hydrogarnet phases in both HM and SM binders as hydration products presented in literature. Moreover, straetlingite was detected on XRD diagram of SM binder, while it was not visible on analysis of HM binder.

The thermogravimetric analyses complete the observations from XRD analyses through the observation of amorphous phases such as C-S-H. DTG-TG test clearly linked the evolution of the compressive strength of the binders in function of time with the evolution of the different mineralogical phases. Furthermore, the much higher amount of portlandite contained in SM binder in comparison with HM binders directly linked to complete pozzolanic reaction of MK for SM binder against HM binder, which confirmed the much higher compressive strength of SM binder after 28 days in comparison with that of HM binder.

The experimental results permitted us to select the compositions for two control binders from two kinds of limes and flash metakaolin (HM and SM). However, the mechanical performance of both binders was still very low to use in the construction industry, especially at early age. Thus, it is necessary to improve the mechanical performance and reduce the shrinkage of these binders especially at early age in order to effectively use for the construction industry.

3.3 Influence of admixtures on the properties of binder

3.3.1   Formulation

In the previous parts, we optimized the components of two pozzolanic binders from NHL3.5, slaked lime and flash metakaolin. In a previous study, Magniont [MAG10b] showed the positive effect of glycerol carbonate for the pozzolanic binder (it not only improve the mechanical performance at short term, but also reduce the shrinkage of binder). On the other hand, the presence of a chemical activator of K_2SO_4 enhances not only the mechanical strength but also stabilize dimension of paste [MAA10].

Thus, in this study, we investigated two pozzolanic binders with two admixtures

(glycerol carbonate or/ and K_2SO_4). Moreover, the superplasticizer (SP) was also used to reduce water and improve the mechanical strength of the binders. The components of the binders are presented in Table 3.4 and Table 3.5.

In Table 3.4 and Table 3.5, contents of the admixtures (SP, GC and K_2SO_4) were calculated according to the total weight of lime (NHL3.5 or SL) and MK (HM and SM are two control binders). Furthermore, a commercial binder (CB) was also used with the same water to binder ratio (0.4) and superplasticizer (0.8% by mass of CB).

Table 3.4: The components of NHL3.5-MK binders

Components	Content (% by weight)				
	HM	H	HC	HP	HCP
Natural hydraulic lime - NHL 3.5	50	50	50	50	50
Flash metakaolin - MK	50	50	50	50	50
Superplasticizer – SP[*]	-	0.8	0.8	0.8	0.8
Glycerol carbonate - GC[*]	-	-	0.5	-	0.5
K_2SO_4 - PS[*]	-	-	-	3	3
Water/ Binder (NHL3.5+MK)	0.5	0.4	0.4	0.4	0.4

The contents by weight of SP, GC and PS were these substances to (NHL3.5+MK) ratios

Table 3.5: The components of SL-MK binders

Components	Content (% by weight)				
	SM	S	SC	SP	SCP
Slaked lime - SL	30	30	30	30	30
Flash metakaolin - MK	70	70	70	70	70
Superplasticizer - SP[*]	-	1.6	1.6	1.6	1.6
Glycerol carbonate - GC[*]	-	-	0.5	-	0.5
K_2SO_4 - PS[*]	-	-	-	3	3
Water/ Binder (SL+MK)	0.5	0.4	0.4	0.4	0.4

The contents by weight of SP, GC and PS were these substances to (SL+MK) ratios

The fabrication and conservation of the samples were described in the paragraph 2.2.5.1 of second chapter.

3.3.2 Compressive test

As the same control binders, this test was performed at 2 days, 7 days, 28 days and 49 days with 4 samples for each age.

	HM	H	HC	HP	HCP	CB
▫ 2 days	2.44	5.47	2.70	17.53	17.68	15.76
▨ 7 days	7.06	13.07	11.34	18.93	19.48	16.67
▧ 28 days	9.86	17.85	16.16	20.69	21.16	22.92
▪ 49 days	11.03	18.69	15.35	23.07	23.98	29.11
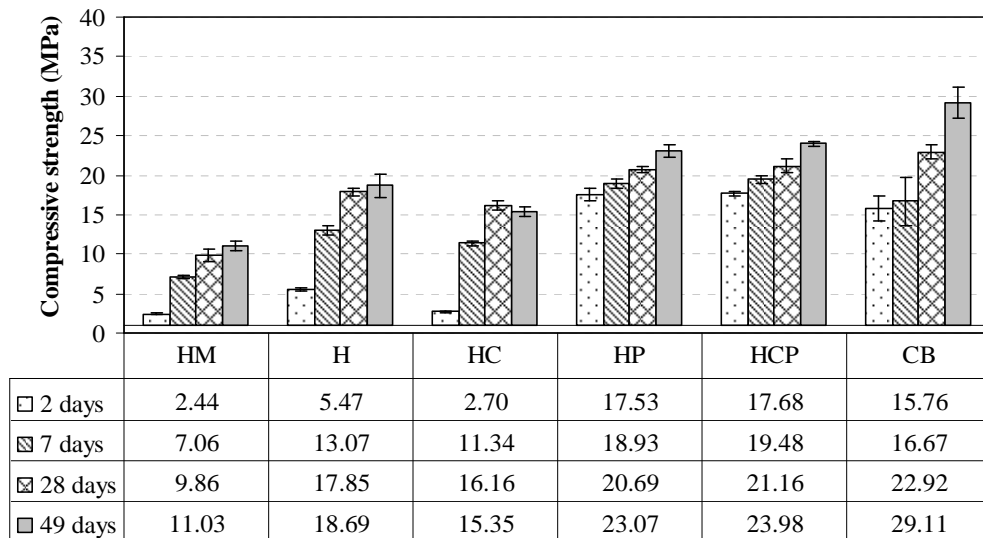
Figure 3.13: Compressive strength of NHL3.5-MK binders

	SM	S	SC	SP	SCP	CB
▫ 2 days	0.70	3.69	5.37	19.11	19.49	15.76
▨ 7 days	4.93	15.42	12.17	22.55	23.06	16.67
▧ 28 days	13.50	23.67	19.32	25.61	28.59	22.92
▪ 49 days	13.61	31.88	20.57	34.54	36.25	29.11
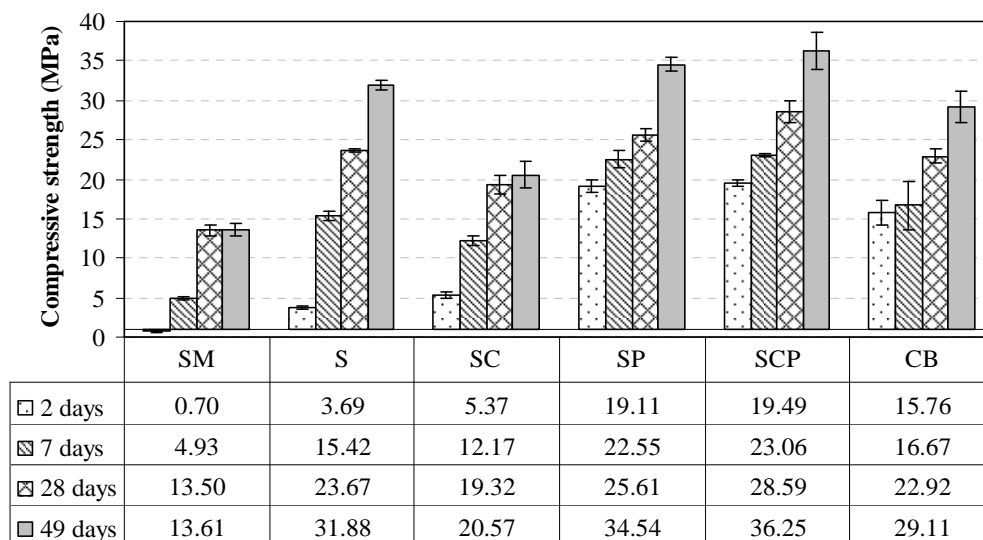
Figure 3.14: Compressive strength of SL-MK binders

In generally, Figure 3.13 and Figure 3.14 indicate that the compressive strengths of binders contained the admixtures were much higher than those of the control binders right at early age. These figures also indicate that the influence of the different admixtures on the mechanical performance of the binders was different.

For H and S formulations, the superplasticizer increased compressive strength in early age and in long term, this phenomenon is directly linked to the reduction of water on binder ratio i.e. porosity. Indeed, the compressive strengths of H binder were around 2 times higher than those of HM – control binder among 2 days and 49 days respectively; while, those of S binder were around 5 and 2.3 times higher than those of SM – control binder at 2 days and 49 days respectively.

As far as influence of GC is concerned (HC and SC binders), the addition of GC did not have a positive effect on the mechanical performances of the binders except for SC binder at 2 days. This observation differs from results obtained by Magniont [MAG10b] with a mix of MK and natural hydraulic lime - NHL5.

In regard to influence of potassium sulfate (HP and SP binders), it clearly leads to a significant improvement of compressive strengths of HP and SP binders in comparison with the H and S binders respectively, especially at early age. Indeed, the compressive strengths of HP and SP binders were more than three and five times higher than those of H and S binders, respectively, at 2 days of age and around 1.5 times at 7 days. At 2 days, HP and SP binders reached the much high resistance, 17.5 MPa and 19.1 Mpa respectively and gained 76% and 55% compressive strength of HP and SP binders at 49 days respectively. This is consistent with the literature [MAA10, SHI00 & WIL98] which could confirm the important role of K_2SO_4 in improvement of strength of pozzolanic binder thanks to the formation of ettringite - $Ca_6Al_2(SO_4)_3(OH)_{12}.26H_2O$ right at early time.

On the other hand, the incorporation of both GC and PS in the binder (HCP and SCP formulations) gave the best compressive strength. We can remark the positive effect of GC on the mechanical performance of binder when it was used with K_2SO_4. The strengths of HCP and SCP binders are slightly higher than those of HP and SP binders respectively in all the ages. At 2 days, the compressive strength of HCP and SCP binders was very high (17.7 and 19.5 MPa respectively), which is comparable with that of Portland cement paste (around 20.2 - 21.4 MPa, [TRI12]).

In comparison between NHL3.5-MK and SL-MK binders, it can be seen that the compressive strength of the SL-MK binders is generally higher than that of the NHL3.5-MK binders, except SM binder at 2 and 7 days of age and S binder at 2 days of age. The strengths of SL-MK binders were around 1.5 times higher than those of NHL3.5-MK binders at 49 days respectively. This result confirmed the role of hydraulic setting in the short term, which confers higher early age strength on the paste. But, for longer ages, the smaller amount of $Ca(OH)_2$ in NHL3.5 constitutes a limiting factor for the metakaolin pozzolanic reaction and consequently limits the development of mechanical performance.

In comparison with a commercial binder (CB), we remarked that the strengths of SP and SCP binders were around 1.2 times higher than those of CB binder, while the strengths of HP and HCP binders were slightly higher at 2 and 7 days, and lower at 28 and 49 days than those of CB binder.

In conclusion, the compressive test demonstrated that the K_2SO_4 increased significantly the strength of binder especially at early age, while GC only had positive effect when it was combined with K_2SO_4 in the binder. The combination both GC and K_2SO_4 in the binder brought the highest strength of binder. Furthermore, it is interesting to see that the strength SP and SCP binders were higher in comparison with that of the commercial binder. In the next parts, we will present the results of other tests to confirm the applicable capacity of new pozzolanic binders in the construction industry.

3.3.3 Calorimetric test

In previous paragraph (3.2.3), we showed the results of this test for two control binders (HM and SM). In this part, we will present the calorimetric results of the binders containing different admixtures in comparison with those of two control binders.

3.3.3.1 NHL3.5-MK binders

The cumulative hydration heat and rate of heat release of NHL3.5-MK pastes are presented in Figure 3.15 and Figure 3.16.

The cumulative heat of the binders from NHL3.5 and MK in Figure 3.15 showed that the total heat generation of all binders was similar to control binder - HM (around 100 J/g) except HP binder (it was a little lower than others), but the heat generation evolution of the pastes is very different each other. The heat generation of H binder is similar to that of control binder (HM), that of HP and HCP binders is fastest, while that of HC binder is lowest (it reaches stable value around 30 hours of hydration for HM and H binders, around 8 hours for HP and HCP binders and around 50 hours for HC binder). The maximum heat generation takes place at around 22 h for MH and H binder, 30 h for HC binder and 6 h for HP and HCP binders (Figure 3.16). The heat of all binders did not almost generate after 70 hours.

These results indicate that GC retarded significantly the initial hydration of the binder, while the incorporation of K_2SO_4 in binder considerably accelerated that of binder. These results could explain the reduction of the compressive strength due to GC at early age and confirm the significant improvement of compressive strength in the binders containing K_2SO_4 thanks to formation of ettringite, especially at early age (Figure 3.13).
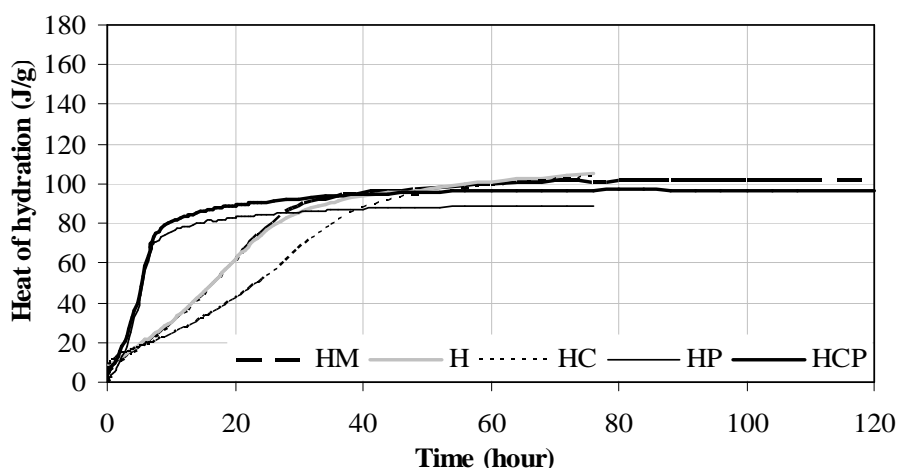
Figure 3.15: Hydration heat of NHL3.5-MK binders
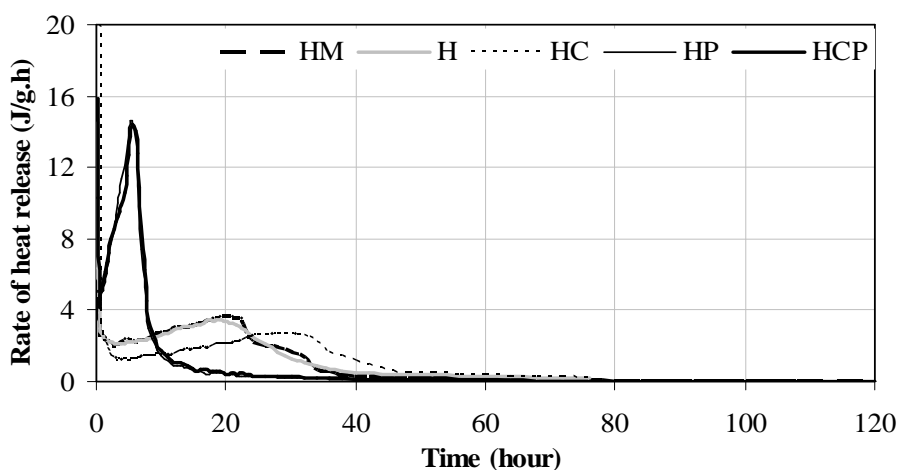
Figure 3.16: Rate of heat release of NHL3.5-MK binders

3.3.3.2 SL-MK binders

For SL-MK binders, their cumulative hydration heat and rate of heat release are shown in Figure 3.17 and Figure 3.18.

The results in Figure 3.17 and Figure 3.18 evidently confirmed the different influence of K_2SO_4 and GC in the initial hydration of the binders. Indeed, the heat hydration evolution is the fastest in the binders containing K_2SO_4 (SP and SCP) with maximum heat release at around 6 h, and is the lowest in the binder containing GC (SC).

It can be seen that SL-MK binders produced the much higher hydration heat than NHL3.5-MK binders did respectively (Figure 3.15 and Figure 3.17). This can explain for the larger amount of $Ca(OH)_2$ in SL constitutes is enough for the metakaolin pozzolanic reaction and consequently enlarges the development of mechanical performance for the

long time. However, for the binders without K_2SO_4, the evolution of hydration heat of the binders containing slaked lime (SM, S and SC) is weaker than that of the binders containing NHL3.5 lime (HM, H and HC). This can be explained by the presence of C_2S in NHL3.5-MK binders which gives a hydraulic reaction more quickly.
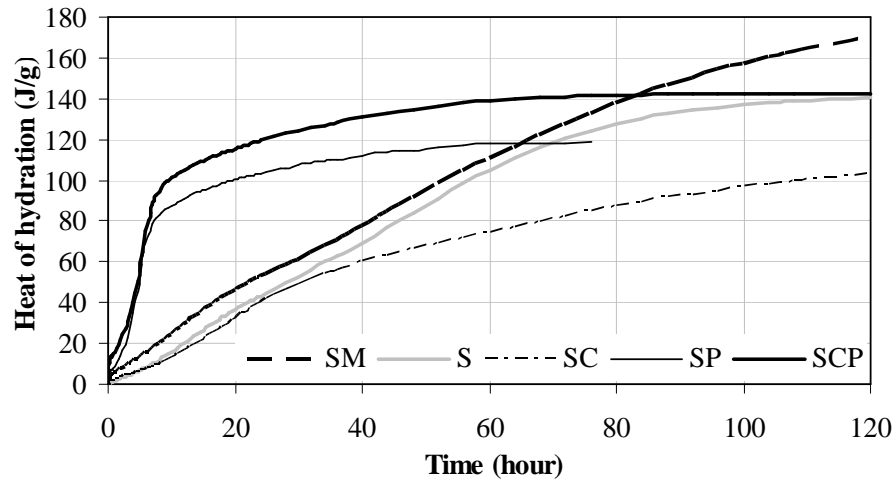
Figure 3.17: Hydration heat of SL-MK binders
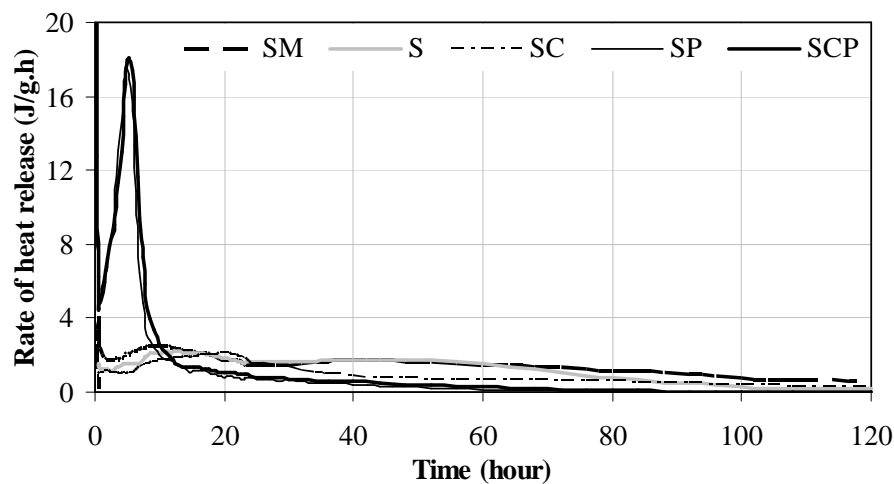
Figure 3.18: Rate of heat release of SL-MK binders

3.3.3.3 Conclusion

The results of calorimetric experiment with respect to NHL3.5-MK and SL-MK binders illustrate the positive effect of K_2SO_4 and negative effect of glycerol carbonate on the hydration of the pastes. This can explain the distinct strength-enhancing effect on binders thanks to K_2SO_4, especially at early age and the reduction of compressive strength of the binders due to glycerol carbonate.

3.3.4   Shrinkage measurement

In order to assess the influence of glycerol carbonate and/or K_2SO_4 on the shrinkage reducing effect, the total and endogenous shrinkages and the mass losses of the different pastes were measured.

3.3.4.1 NHL3.5-MK binders

The measurements of the NHL3.5-MK pastes were realized around 420 days, which are shown in Figure 3.19.

a)

b)
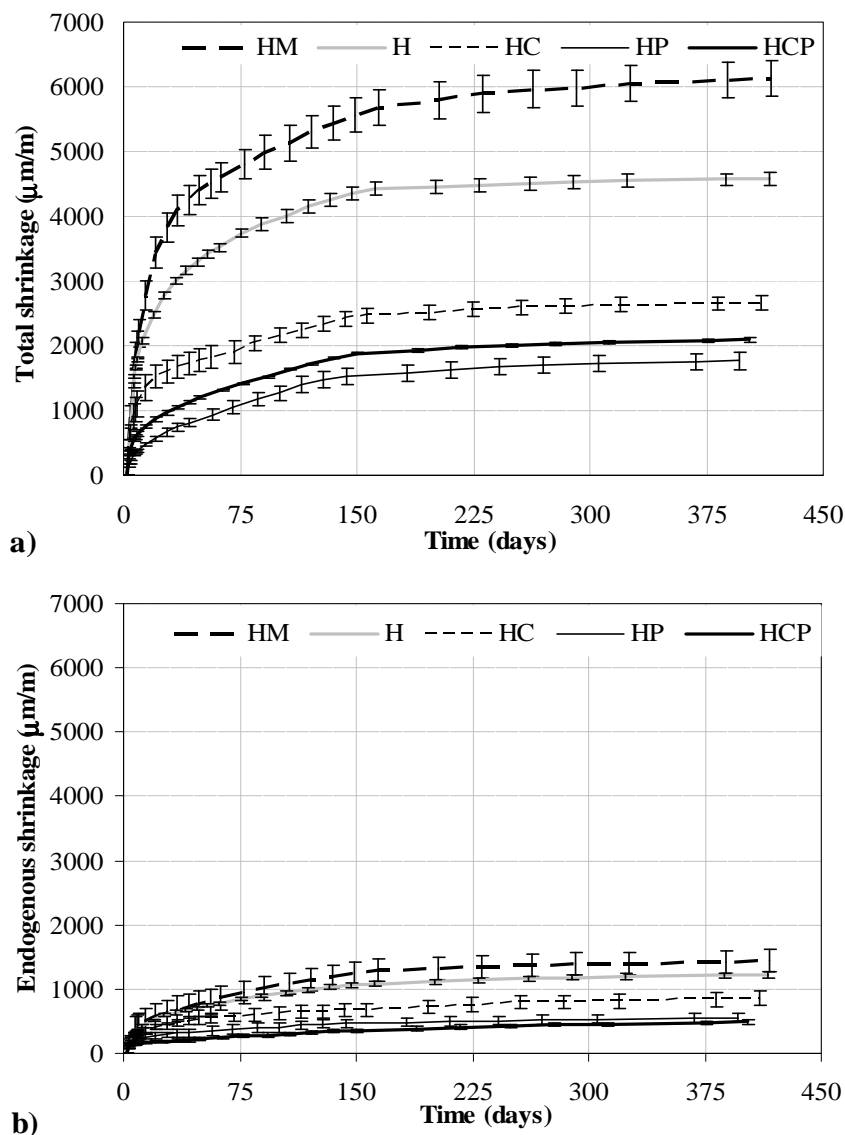
Figure 3.19: Total (a) and Endogenous (b) shrinkages of NHL3.5-MK binders

The results of shrinkage measurements in Figure 3.19 show that the admixtures reduced significantly both total and endogenous shrinkages of the pastes. The results

indicated that the dimensional variations were insignificant after around 230 days for HM – control binder and 160 days for other binders and there was not swelling in early age for all pastes.

As regard to influence of glycerol carbonate, this figure confirmed the considerable shrinkage reducing effect of glycerol carbonate, which is consistent with a previous study [MAG10b]. In this study, glycerol carbonate reduced 57% total shrinkage and 41% endogenous shrinkage of HC binder in comparison with control binder.

For the influence of K_2SO_4 on the shrinkage, the measurements illustrated the best shrinkage-reducing effect of incorporated into HP binder (it showed 71% total shrinkage and 61% endogenous shrinkage reduction against control binder). This can be attributed to the formation of ettringite in the binders containing K_2SO_4 because of the swelling of ettringite at early age. This result is consistent with the result of Martinez-Aguilar et al [MAA10] about the dimensional stability of the binder containing K_2SO_4.

Figure 3.20 and Figure 3.21 show the mass loss measurements and the relation between total shrinkage and loss of weight for NHL3.5-MK binders respectively (the mass loss is measured in the same time with the total shrinkage measurement).

Figure 3.20: Weight loss of NHL3.5-MK binders

Figure 3.21: Total shrinkage vs weight loss of NHL3.5-MK binders

These figures indicate that the weight losses of the binders are insignificantly different. Indeed, the final weight loss of HM binder was highest (21.9%), that of HC binder was 21.1%, and that of other binders were similar to each other (19 – 19.5%). However, the drying kinetics of different binders is considerably different. HM, H and HC pastes reached their final masses at 49, 201 and 35 days respectively whereas the HP and HCP pastes needed more than 180 days (Figure 3.21). These differences can be attributed to the different influences of the admixtures on the desiccation and hydration mechanisms among the pastes.

These figures confirmed that the mass loss of HM paste is the highest due to the highest water to binder ratio (W/B = 0.5 for HM and 0.4 for other binders). Thus, in order to evaluate influence of the admixtures on the shrinkage measurements, we compared the measurements of the binders containing glycerol carbonate and/ or K_2SO_4 with those of H binder (they were same water to binder ratio, W/B = 0.4).

For the influence of glycerol carbonate, HC binder presented the higher mass loss than H binder because glycerol carbonate is hydrophobia and accelerates water evaporation from big pores at early age [MAG10a]. In Figure 3.21, we observed that glycerol carbonate significantly increased of drying kinetics and reduced the total shrinkage of HC binder, which is consistent with Magniont's result [MAG10a].

In regard to influence of K_2SO_4, it encouraged the formation of ettringite early on [SHI00], and the large water amount of the pastes was therefore fixed for this reaction leading to limit the mass loss of the pastes. Moreover, the formation of ettringite increased

the solid volume [SHI00] which reduced the big pore volume, and consequently limit the water evaporation leading to retard drying kinetics of HP and HCP pastes (Figure 3.21). The best shrinkage-reducing effect was observed on HP and HCP binders because of the swelling of ettringite formed right at early age in the presence of K_2SO_4.

Moreover, Figure 3.21 allows to observe the carbonation of all binders. The soonest carbonation of HC binder (after 35 days) was attributed to the carbonate ions originated from the hydrolysis reaction of glycerol carbonate in alkaline environment reacted calcium ions from dissolution of $Ca(OH)_2$ of NHL3.5. The carbonation of HM binder was earlier than other pastes, which can be explained by the higher big pore volume of HM paste due to the higher water to binder ratio against others; therefore, CO_2 from air can easily penetrate through big pores to react $Ca(OH)_2$. The carbonation of H, HP and HCP pastes was much later than HC and HM binders, which can be attributed to reduction of big pore volume thanks to superplasticizer for H binder and to the increase of the solid volume because of ettringite for HP and HCP binders, and consequently limited the penetration of CO_2 into these pastes.

3.3.4.2 SL-MK binders

The influence of glycerol carbonate and/or K_2SO_4 on the shrinkage reducing effect of the SL-MK pastes is presented in Figure 3.22.

a)

127

b)
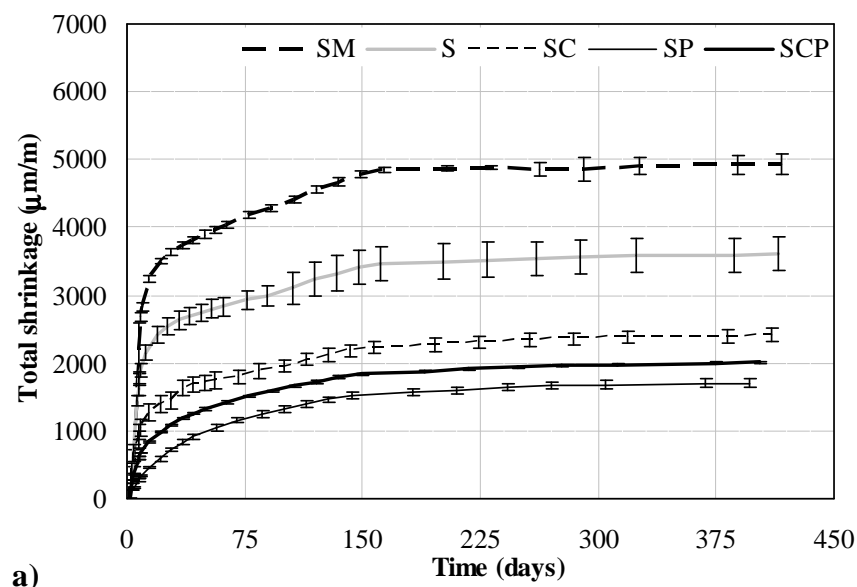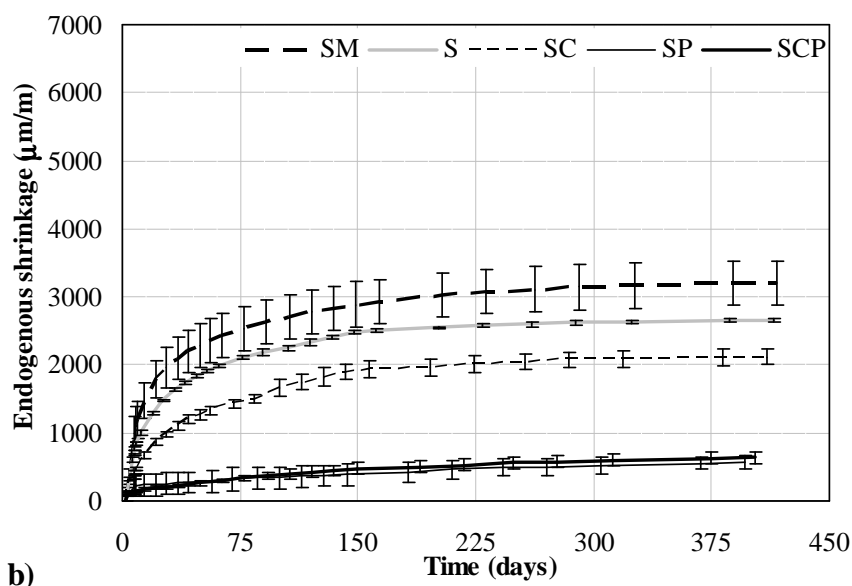
Figure 3.22: Total (a) and Endogenous (b) shrinkages of SL-MK binders

These measurements confirm that both glycerol carbonate and K_2SO_4 reduced significantly shrinkages of SL-MK pastes as similar to observation in NHL3.5-MK binders. The shrinkage-reducing effect of K_2SO_4 on the paste was the highest. It reduced 65% total shrinkage and 82% endogenous shrinkage of SP paste against those of control paste – SM. The combination of both GC and K_2SO_4 also brought effects on the shrinkage-reducing of the SCP binder (this effect was only a little lower than that of SP binder).
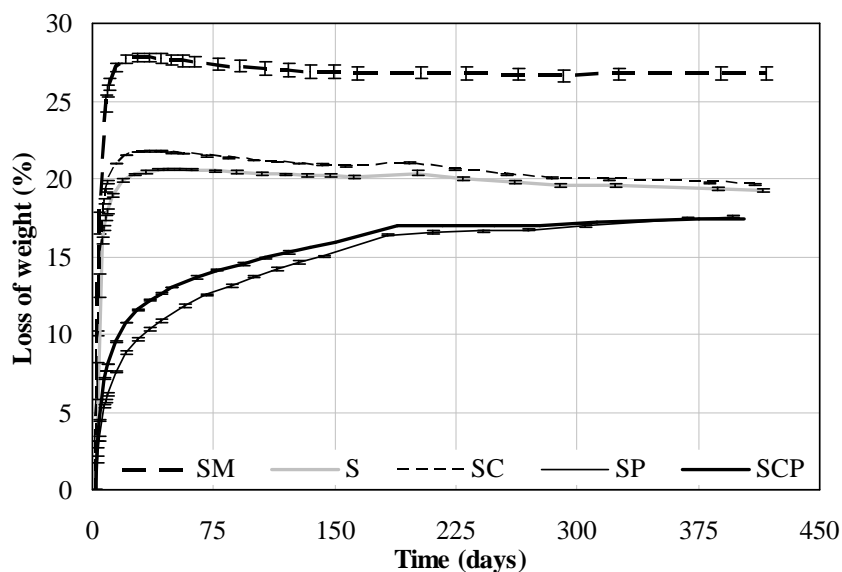
Figure 3.23: Weight loss of SL-MK binders
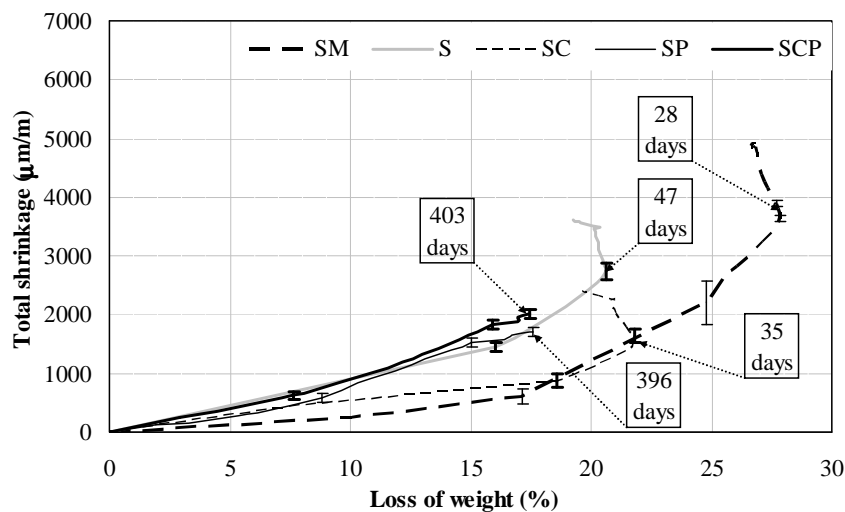
Figure 3.24: Total shrinkage vs weight loss of SL-MK binders

Figure 3.23 and Figure 3.24 show the mass loss measurements and relation between total shrinkage and weight loss of SL-MK binders (the mass loss was measured in the same time with the total shrinkage measurement).
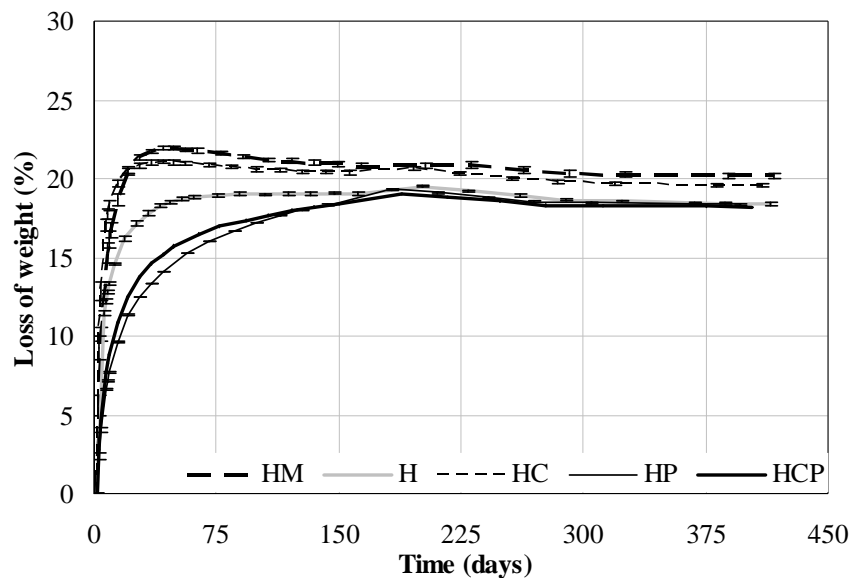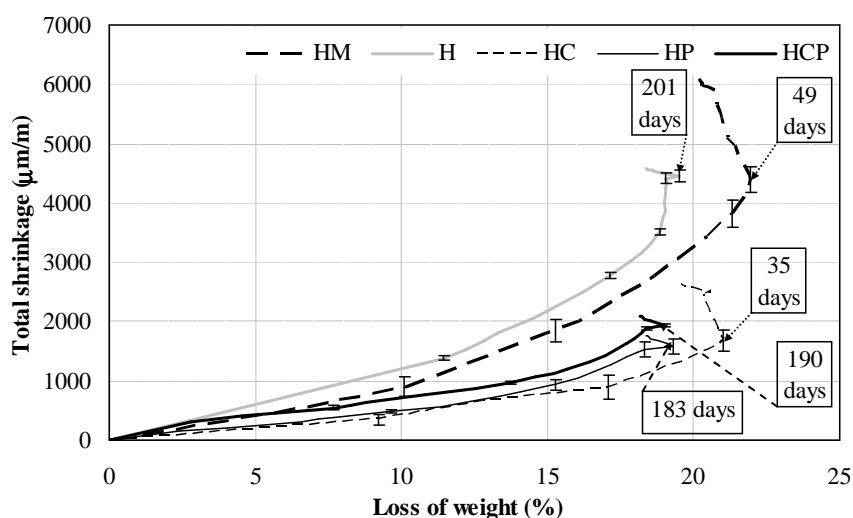
It can be seen that the weight losses of the binders are significantly different. Indeed, the final weight losses of SM binder was the highest (27.8%), while that of S and SC binders were 20.6 and 21.8% respectively, and that of two other binders were 17.5%. As similar as the weight loss measurements of NHL3.5-MK pastes, these results confirmed the highest mass loss of SM binder due to the highest water to binder ratio. We also observed the influence of glycerol carbonate on drying kinetics increased and the total shrinkage of SC binder as similar to observation on HC binder above. K_2SO_4 also reduced the most significantly of mass loss and shrinkages of SP and SCP binders.

For the carbonation of SL-MK binders, Figure 3.24 shows that the soonest carbonation was observed on SM paste, which could be attributed to the pozzolanic reaction could be weaker than carbonation reaction after 28 days. This could be explained that the high water to binder ratio of SM binder encouraged the pozzolanic reaction during 28 days because the compressive strength of SM binder insignificantly increased after 28 days (Figure 3.14). The carbonation of SC binder was earlier than that of S binder, which could confirm the role of glycerol carbonate as similar to observation on HC binder above and in literature [MAG10a]. However, the carbonation was not observed on SP and SCP binders (Figure 3.24), which could be attributed to the formation of ettringite because of the presence of K_2SO_4. Indeed, at early age, the pozzolanic reaction between slaked lime

and metakaolin was stronger than carbonation reaction, and in long time, the increase of the solid volume thanks to formation of ettringite at early age was enough to prevent CO_2 penetration for carbonation and the hydrates formed are less sensitive to carbonation.

3.3.4.3 Conclusion

The measurements of shrinkage for NHL3.5-MK and SL-MK binders confirmed the good shrinkage-reducing effect of glycerol carbonate as previous study; the highest effect of K_2SO_4 on the shrinkage-reducing of the paste thanks to the ettringite formation at early age, and on the reduction of mass loss of the paste. The combination both glycerol carbonate and K_2SO_4 in the binders also reduced significantly all the shrinkages of the binders (it was only a little lower than that of the binder containing K_2SO_4 in both endogenous and total shrinkage).

3.3.5   Monitoring of hydration by X-ray diffraction and thermogravimetric analyses

In order to understand clearly the influence of admixtures on behaviors of these binders, the X-ray diffraction (XRD) and thermogravimetric (TGA) analyses were studied.

3.3.5.1 Analyses of NHL3.5-MK binders

a.   H binder

XRD and TGA analyses of H binder are presented in Figure 3.25 and Figure 3.26. This binder contained superplasticizer admixture aiming to reduce water content of the paste (W/B ratio is 0.5 for HM control binder, and is 0.4 for H binder).
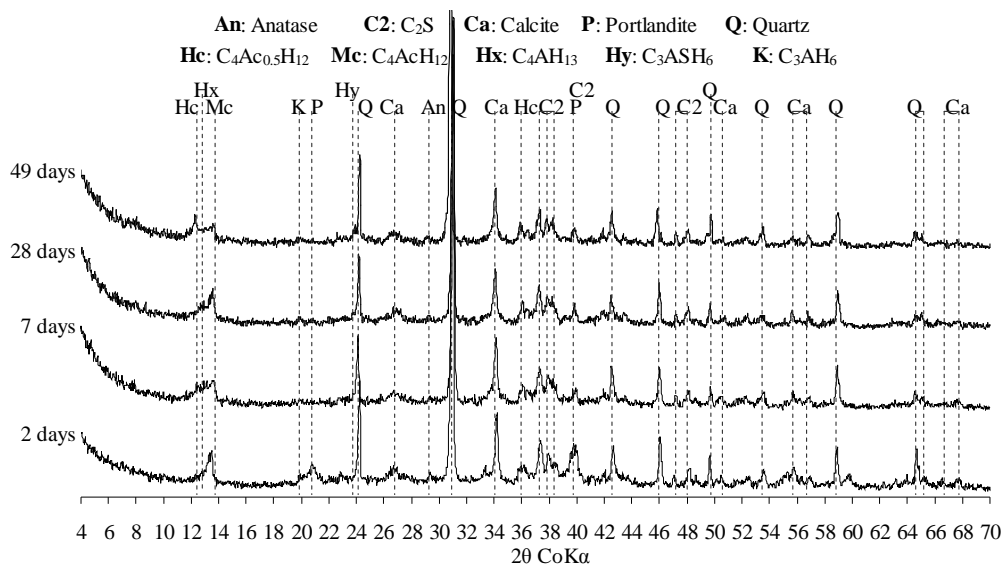
Figure 3.25: XRD analyses of H binder

Ca: $CaCO_3$ P: $Ca(OH)_2$ **Hx**: C_4AH_{13} **Hc**: $C_4Ac_{0.5}H_{12}$ **Mc**: C_4AcH_{12} **K**: C_3AH_6 **Hy**: C_3ASH_6
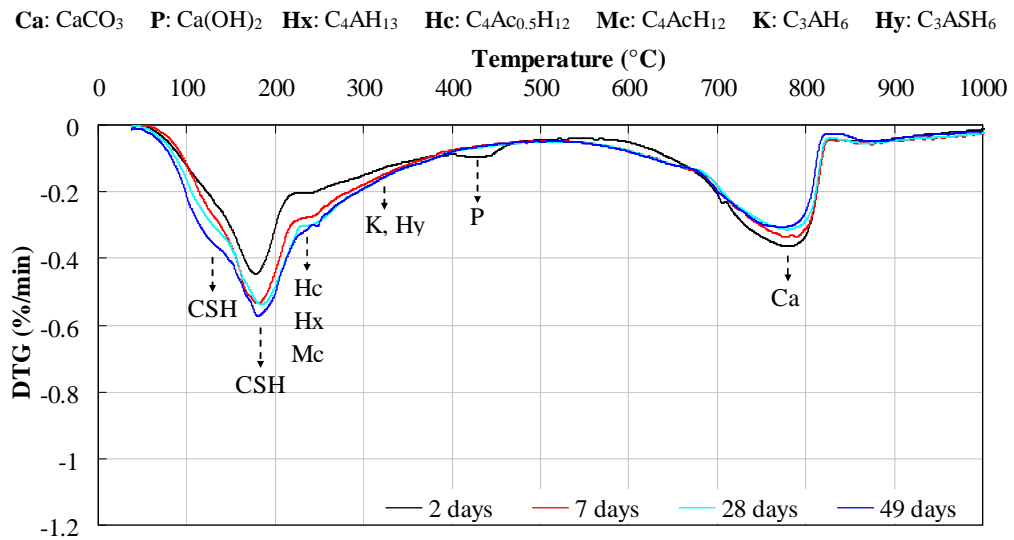
Figure 3.26: Thermogravimetric analyses of H binder

The results of XRD analyses in Figure 3.25 allowed to determine the mineralogical characteristics of H binder as follows:

- Consumption of portlandite: the peaks of portlandite were only detected at 2 days, which is different from HM-control binder. This can be attributed to the lower water content of H binder against that of control binder that would limit the pozzolanic reaction.

- Hydration products were determined as similar to control binder (HM): calcium aluminate phase (Hx-C_4AH_{13}), two carboaluminate phases (Hc - $C_4Ac_{0.5}H_{12}$ and Mc - C_4AcH_{11}) and katoite (K- C_3AH_6) were visible right at 2 days, and small peak of other hydrogarnet (C_3ASH_6) presented after 7 days.

- Inert and anhydrous components: anatase, calcite, quartz and C_2S were still present up to 49 days, which is the same in control binder.

Table 3.6: Percentage by weight of hydrated phases – H%,

$Ca(OH)_2$ – P% and $CaCO_3$ – Ca% of H binder

2 days			*7 days*			*28 days*			*49 days*		
H%	*P%*	*Ca%*	*H%*	*P%*	*Ca%*	*H%*	*P%*	*Ca%*	*H%*	*P%*	*Ca%*
21.0	3.5	12.7	29.1	-	12.8	30.3	-	13.1	31.9	-	12.1

For the TGA analyses, the results in Figure 3.26 confirmed the presences of portlandite at 2 days, hydration products and calcite which observed by XRD analyses. Moreover, TGA curves showed a little increase of C-S-H gel over the age, which was not

detected by XRD tests due to low crystallization degree. The evolution of quantity of total hydration products, residual $Ca(OH)_2$ and $CaCO_3$ for H binder are presented in Table 3.6.

b. HC binder
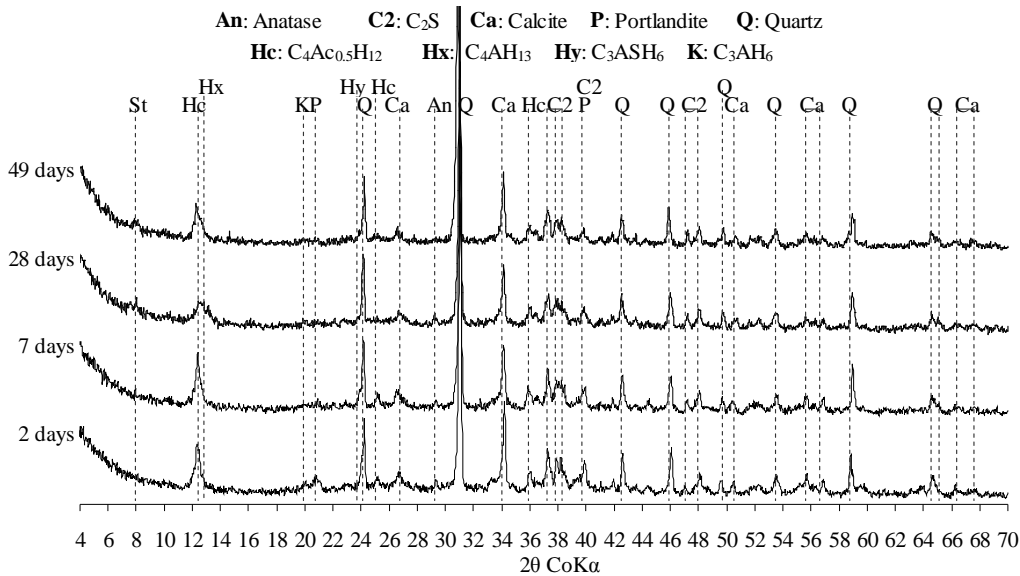
Figure 3.27: XRD analyses of HC binder
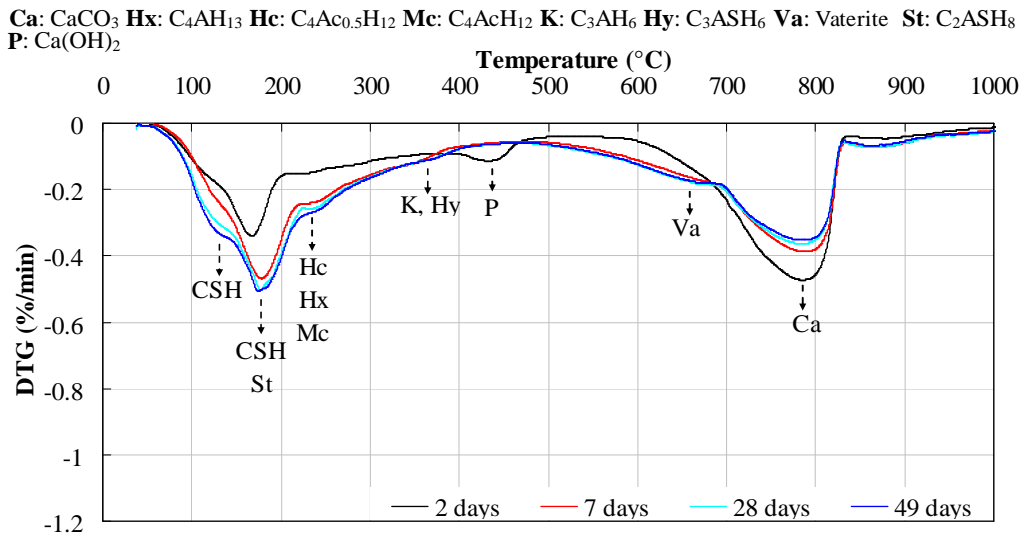
Figure 3.28: Thermogravimetric analyses of HC binder

This binder uses superplasticizer and glycerol carbonate admixtures. Their results of XRD and TGA analyses are shown in Figure 3.27 and Figure 3.28. These figures permit to characterize the mineralogical components of HC binder as follows:

- The portlandite was only visible at 2 days.

- Hydration products: the difference in HC binder is that a small peak of

straetlingite (St – C_2ASH_8) presented at 28 and 49 days, which was not observed on XRD diagrams of HM and H binders. $C_4Ac_{0.5}H_{12}$ - Hc were detected with the much higher intensity in comparison with HM and H binders, while C_4AcH_{11} - Mc was not occurred (this is consistent with Magniont's observation [MAG10b]). Moreover, vaterite – another form of calcite was attributed to decomposition at around 660^oC (it was not detected by XRD analyses). The formation of vaterite can be attributed to the hydrolysis of glycerol carbonate in high alkaline environment formed glycerol and CO_2, then carbonate ions react with calcium ions leading to precipitation of $CaCO_3$ [MAG10a]. This carbonate formation could explain the formation of calcium hemicarboaluminate observed also in XRD diagram (Figure 3.27).

- Inert and anhydrous components: they were observed as similar with H binder.

The total quantity of hydration products, residual $Ca(OH)_2$ and $CaCO_3$ for HC binder are summarized in Table 3.7.

Table 3.7: Percentage by weight of hydrated phases – H%,

$Ca(OH)_2$ – P% and $CaCO_3$ – Ca% of HC binder

2 days			7 days			28 days			49 days		
H%	P%	Ca%	H%	P%	Ca%	H%	P%	Ca%	H%	P%	Ca%
16.5	4.7	15.1	24.9	-	16.4	27.1	-	16.4	28.4	-	15.7

c. *HP binder*
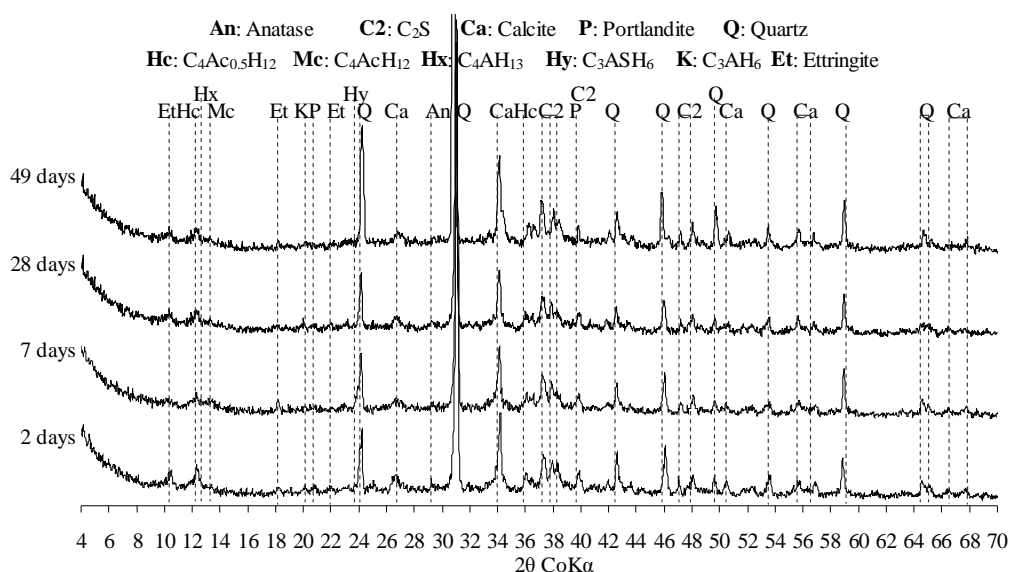
Figure 3.29: XRD analyses of HP binder

133

Ca: $CaCO_3$ **P**: $Ca(OH)_2$ **Hx**: C_4AH_{13} **Hc**: $C_4Ac_{0.5}H_{12}$ **Mc**: C_4AcH_{12} **K**: C_3AH_6 **Hy**: C_3ASH_6 **Et**: Ettringite
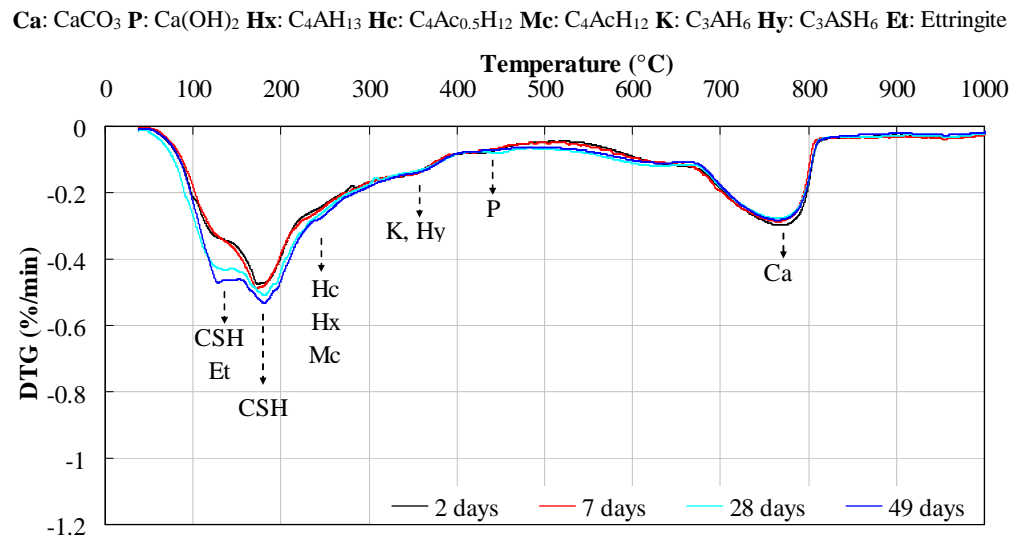
Figure 3.30: Thermogravimetric analyses of HP binder

HP binder contains superplasticizer and K_2SO_4 admixtures. The results of XRD and TGA analyses are presented in Figure 3.29 and Figure 3.30.

These figures present mineralogical determination of HP binder as follows:

- Portlandite consumption: it was not completely consumed by MK pozzolanic reaction up to 49 days (the P peaks is very small). This can be attributed to K_2SO_4 which increases the alkalinity of solution and thus decreases the solubility of $Ca(OH)_2$. This phenomenon could be explained by Shi et al [SHI00] for pozzolanic reaction in presence of Na_2SO_4.

- Hydration products: the difference in HP binder is the presence of ettringite $(Ca_6Al_2(SO_4)_3(OH)_{12}.26H_2O)$ right at 2 days. This confirmed the role of sulfate ion which encourages formation of ettringite and so significantly enhances the strength of the paste at early age [MAA10, SHI00 & WIL98]. Thus, compressive strength of HP binder is very high right at 2 days.

- Inert and anhydrous components: they were observed as similar with HM, H and HC binders.

The total quantity of hydration products, residual $Ca(OH)_2$ and $CaCO_3$ for HP binder are presented inTable 3.8.

Table 3.8: Percentage by weight of hydrated phases – H%,

Ca(OH)₂ – P% and CaCO₃ – Ca% of HP binder

2 days			7 days			28 days			49 days		
H%	*P%*	*Ca%*	*H%*	*P%*	*Ca%*	*H%*	*P%*	*Ca%*	*H%*	*P%*	*Ca%*
27.4	2.7	11.1	27.5	2.3	11.2	31.1	2.0	11.4	31.8	1.7	11.1

d. *HCP binder*
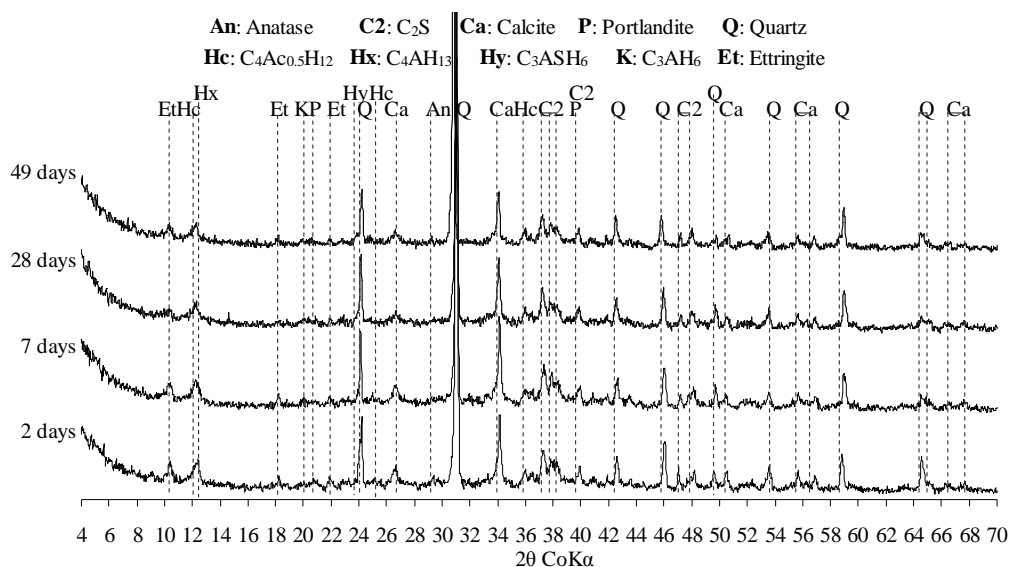
Figure 3.31: XRD analyses of HCP binder

Figure 3.32: Thermogravimetric analyses of HCP binder

This binder contains superplasticizer, glycerol carbonate and K_2SO_4. XRD and TGA analyses are exhibited in Figure 3.31 and Figure 3.32. These figures allow determining the mineralogical characteristics of HCP binders as follows:

135

- Portlandite consumption: the small portlandite peaks were still present up to 7 days. This can confirm the influence of K_2SO_4 on reduction of solubility of $Ca(OH)_2$ as similar to HP binder.

- Hydration products: ettringite was detected because of presence of K_2SO_4; the formation of vaterite and the very high intensity of $C_4Ac_{0.5}H_{12}$ as well as lack of C_4AcH_{11} explained by the presence of glycerol carbonate. Other components were present as similar to other binders.

- Inert and anhydrous components were also observed as similar to other binders.

The total quantity of hydration products, residual $Ca(OH)_2$ and $CaCO_3$ for HCP binder are presented in Table 3.9.

Table 3.9: Percentage by weight of hydrated phases – H%, Ca(OH)$_2$ – P% and CaCO$_3$ – Ca% of HCP binder

2 days			7 days			28 days			49 days		
H%	*P%*	*Ca%*	*H%*	*P%*	*Ca%*	*H%*	*P%*	*Ca%*	*H%*	*P%*	*Ca%*
24.7	1.8	15.2	26.6	1.5	14.2	30.0	-	13.5	33.0	-	13.2

e. Comparison of mineralogical characteristics among the NHL3.5-MK binders

In order to easily compare the mineralogical characteristics among these binders, we present the TGA curves of all binders for 2 and 49 days (Figure 3.33 and Figure 3.34 respectively).

Ca: $CaCO_3$ **Hx**: C_4AH_{13} **Hc**: $C_4Ac_{0.5}H_{12}$ **Mc**: C_4AcH_{12} **K**: C_3AH_6 **Hy**: C_3ASH_6 **Va**: Vaterite **Et**: Ettringite
P: $Ca(OH)_2$

Figure 3.33: Thermogravimetric analyses of NHL3.5-MK binders at 2 days

Ca: CaCO$_3$ **Hx**: C$_4$AH$_{13}$ **Hc**: C$_4$Ac$_{0.5}$H$_{12}$ **Mc**: C$_4$AcH$_{12}$ **K**: C$_3$AH$_6$ **Hy**: C$_3$ASH$_6$ **Va**: Vaterite **Et**: Ettringite
St: Straetlingite

Figure 3.34: Thermogravimetric analyses of NHL3.5-MK binders at 49 days

The analyses of all the binders at 2 and 49 days could confirm the different influence of different admixtures on the mineralogical characteristics.

For the influence of glycerol carbonate, the smallest C-S-H peak on the curve of HC binder at 2 days could confirm that glycerole carbonate retarded the the pozzolanic reaction at early age (see paragraph 3.3.3.1). Moreover, the biggest peak of CaCO$_3$ on the curve of HC binder could explain the role of glycerol carbonate in the formation of calcite.

In regard to influence of K$_2$SO$_4$, it can be seen that the ettringite peak was difference among the cuves of the binders containing K$_2$SO$_4$ and those of other binders right at early age, which confirmed the important role of K$_2$SO$_4$ in the ettringite formation of HP and HCP binders.

Moreover, the association of both glycerol carbonate and K$_2$SO$_4$ slightly increased the C-S-H gel in HCP binder against in HP binder (it contained K$_2$SO$_4$ and without glycerol carbonate).. In fact, Magniont's result [MAG10a] showed that glycerol carbonate slightly increase pH of the paste after 10 hours. This pH increase could explain the increase of the C-S-H gel in HCP binder [ESC12].

In conclusion, the presence of glycerol carbonate retarded the pozzolanic reaction at early age, which can explain the lower compressive strength of HC binder in comparison with that of other binders. The ettringite formation right at 2 days can explain the much higher compressive strength of the binders containing K$_2$SO$_4$ (HP and HCP binders) against that of other binders. Moreover, the use of glycerol carbonate with K$_2$SO$_4$ brought

the positive effect in the slight increase of C-S-H gel found in HCP binder, which can explain the highest compressive strength of HCP.

3.3.5.2 Analyses of SL-MK binders

a. *S binder*

The XRD and TGA analyses of S binder are shown in Figure 3.35 and Figure 3.36.
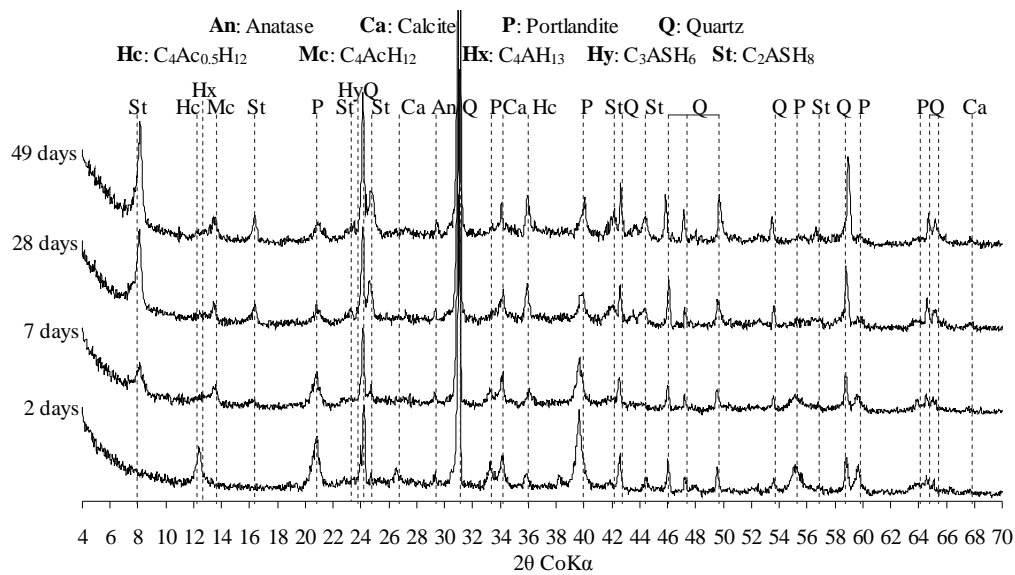
Figure 3.35: XRD analyses of S binder
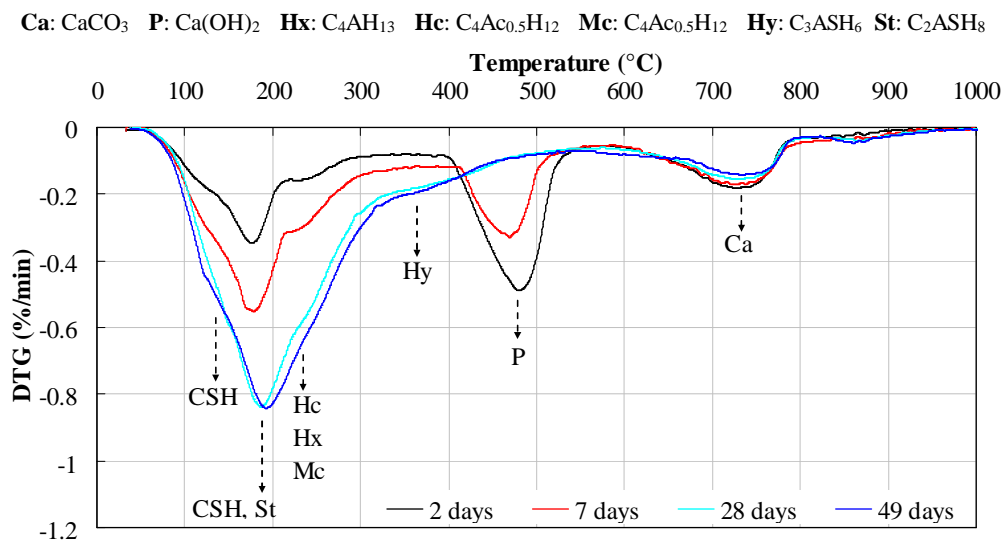
Figure 3.36: Thermogravimetric analyses of S binder

Figure 3.35 and Figure 3.36 shows the mineralogical characteristics of S binder, this binder contains superplasticizer aiming to reduce water content (W/B ratios are 0.5 for SM – control binder and 0.4 for S binder). The results are characterized as follows:

138

- Portlandite consumption was the same with SM – control binder: it was completely consumed by MK pozzolanic reaction before 28 days.

- Hydration products were observed as similar to control binder (SM).

- Inert and anhydrous components were also detected as the same as SM binder.

The total quantity of hydration products, residual $Ca(OH)_2$ and $CaCO_3$ for S binder are summarized in Table 3.10.

Table 3.10: Percentage by weight of hydrated phases – H%,

$Ca(OH)_2$ – P% and $CaCO_3$ – Ca% of S binder

2 days			*7 days*			*28 days*			*49 days*		
H%	*P%*	*Ca%*	*H%*	*P%*	*Ca%*	*H%*	*P%*	*Ca%*	*H%*	*P%*	*Ca%*
16.1	18.8	6.2	27.0	13.3	6.4	51.0	-	6.1	55.4	-	5.8

b. SC binder

This binder used superplasticizer and glycerol carbonate admixtures. XRD and TGA analyses are shown in Figure 3.37 and Figure 3.38.
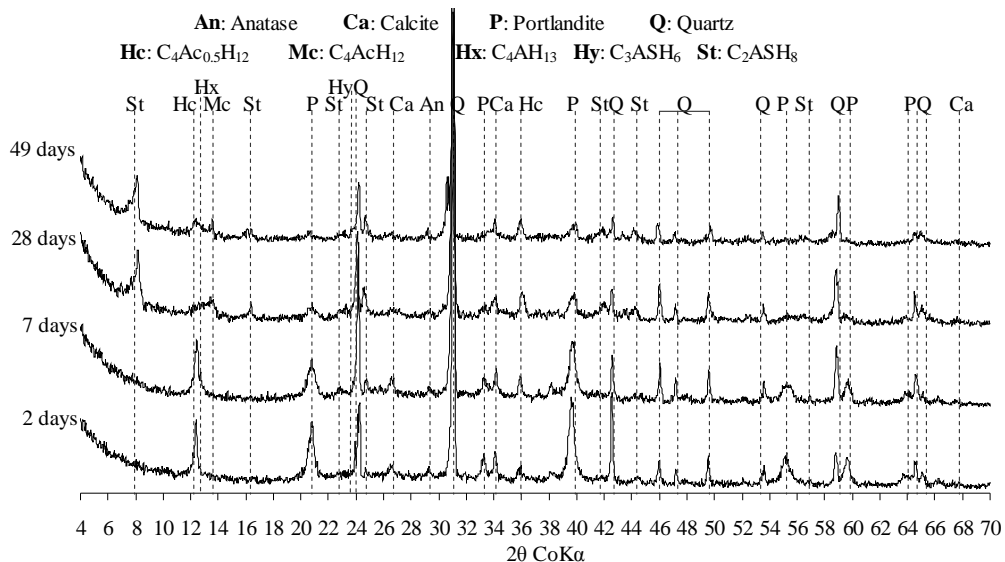
Figure 3.37: XRD analyses of SC binder

Ca: $CaCO_3$ **P**: $Ca(OH)_2$ **Hx**: C_4AH_{13} **Hc**: $C_4Ac_{0.5}H_{12}$ **Mc**: $C_4Ac_{0.5}H_{12}$ **Hy**: C_3ASH_6 **Va**: Vaterite **St**: C_2ASH_8
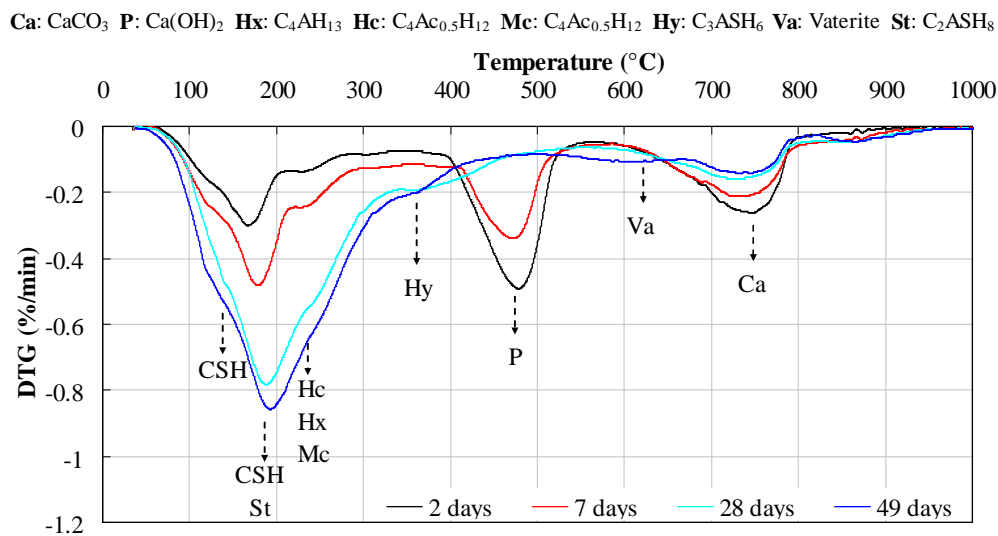
Figure 3.38: Thermogravimetric analyses of SC binder

Figure 3.37 and Figure 3.38 permit to determine the mineralogical components of SC binder as follows:

- Portlandite was also completely consumed before 28 days like SM and S binders.

- Hydration products: the differences of SC binder against SM and S binder are the appearance of $C_4Ac_{0.5}H_{12}$ in XRD diagram with very high intensity at 2 and 7 days and its disappearance after 28 days, while C_2ASH_8 was observed from 28 days. This can be attributed that a part of C_2ASH_8 could be formed by reaction between metakaolin and $C_4Ac_{0.5}H_{12}$. These differences, together with the presence of vaterite peaks in DTG curves, can confirm the influence of glycerol carbonate on the mineralogical characteristics of SC binder.

- Inert and anhydrous components were observed as similar to SM and S binder.
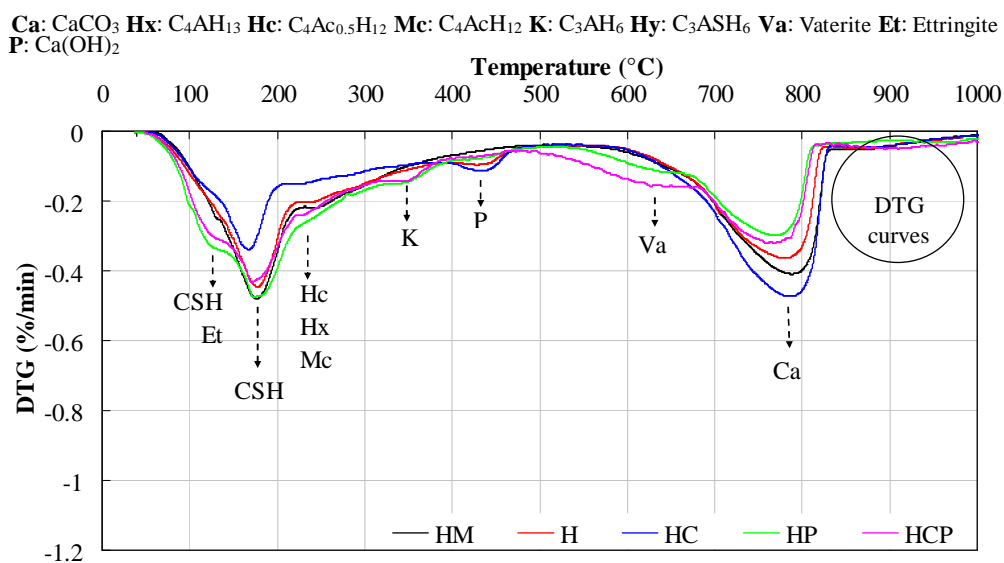
The total quantity of hydration products, residual $Ca(OH)_2$ and $CaCO_3$ for SC binder are presented in Table 3.11.

Table 3.11: Percentage by weight of hydrated phases – H%,

$Ca(OH)_2$ – P% and $CaCO_3$ – Ca% of SC binder

2 days			7 days			28 days			49 days		
H%	P%	Ca%	H%	P%	Ca%	H%	P%	Ca%	H%	P%	Ca%
13.1	17.0	8.3	21.9	14.4	8.0	49.3	-	7.0	48.5	-	8.1

c. SP binder

The analyses of XRD and TGA are presented in Figure 3.39 and Figure 3.40. SP binder used superplasticizer and K_2SO_4.

Figure 3.39 and Figure 3.40 below characterize the mineralogical components as follows:

- Portlandite was not completely consumed by MK pozzolanic reaction up to 49 days which confirm the reduction of $Ca(OH)_2$ solubility due to the presence of K_2SO_4. This phenomenon was also observed in HP binder.

- Hydration products: the presence of ettringite confirmed the role of K_2SO_4. The straetlingite was not visible on the XRD diaram (Figure 3.39), which attributed to the reduction of $Ca(OH)_2$ solubility due to the presence of K_2SO_4.

- Inert and anhydrous components were also observed as SM, S and SC binders.

The total quantity of hydration products, residual $Ca(OH)_2$ and $CaCO_3$ for SP binder are presented in Table 3.12.

Table 3.12: Percentage by weight of hydrated phases – H%,

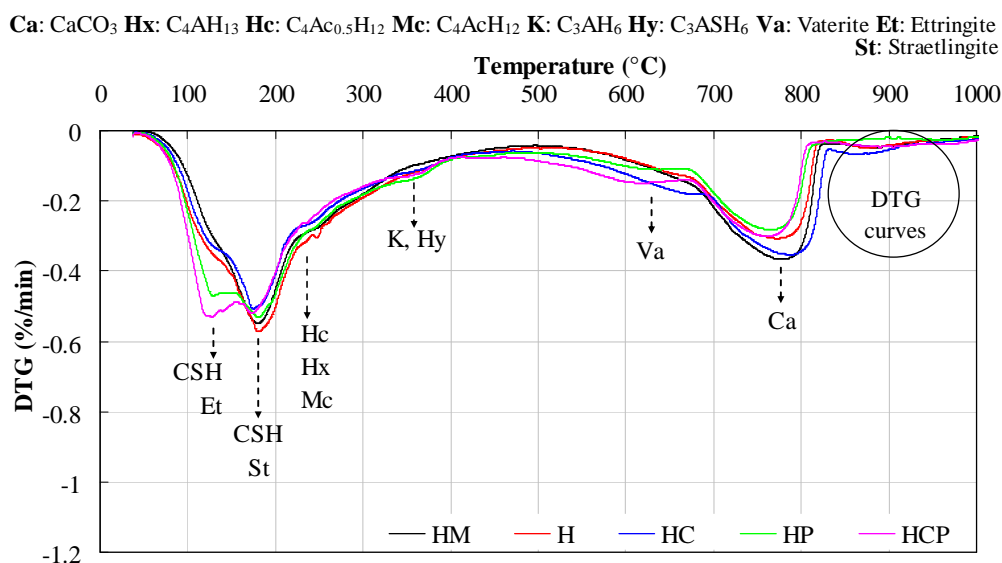***$Ca(OH)_2$ – P% and $CaCO_3$ – Ca% of SP binder***

2 days			7 days			28 days			49 days		
H%	*P%*	*Ca%*	*H%*	*P%*	*Ca%*	*H%*	*P%*	*Ca%*	*H%*	*P%*	*Ca%*
28.6	11.5	6.4	34.4	9.1	6.3	36.5	7.5	6.1	42.4	5.7	7.1
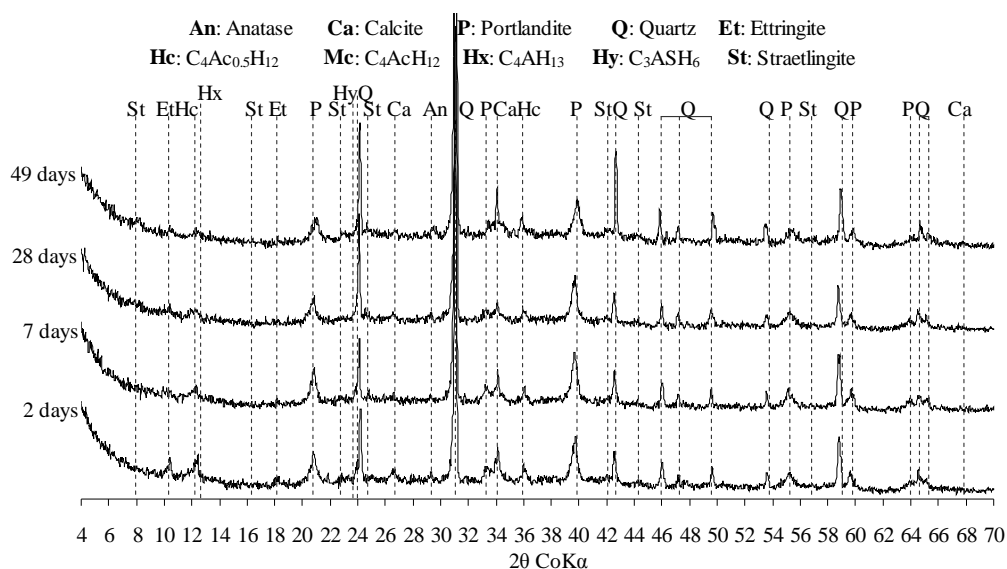
Figure 3.39: XRD analyses of SP binder

Ca: CaCO$_3$ **P**: Ca(OH)$_2$ **Hx**: C$_4$AH$_{13}$ **Hc**: C$_4$Ac$_{0.5}$H$_{12}$ **Mc**: C$_4$Ac$_{0.5}$H$_{12}$ **Hy**: C$_3$ASH$_6$ **Et**: Ettringite **St**: C$_2$ASH$_8$
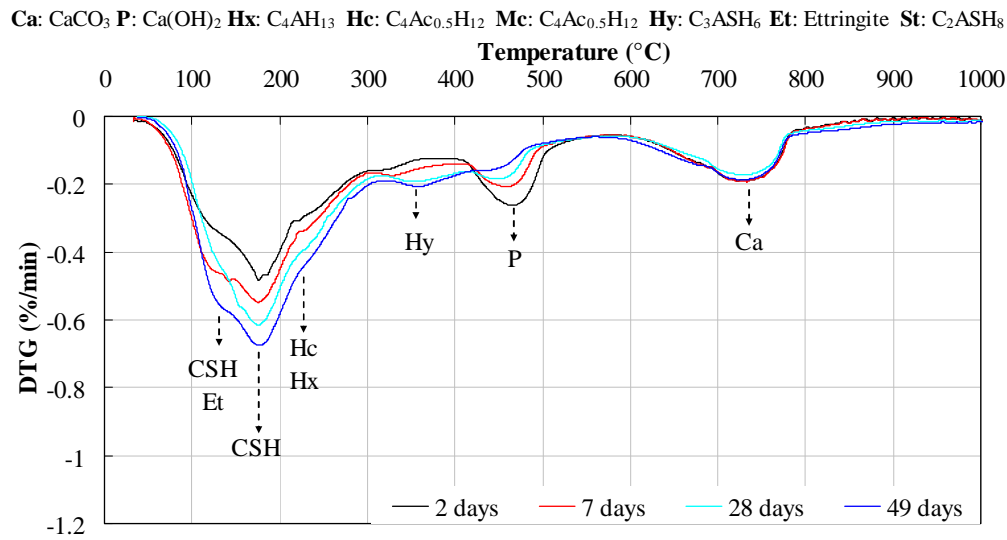
Figure 3.40: Thermogravimetric analyses of SP binder

d. SCP binder

This binder contained superplasticizer and both glycerol carbonate and K$_2$SO$_4$. The XRD and TGA analyses are presented in Figure 3.41 and Figure 3.42.
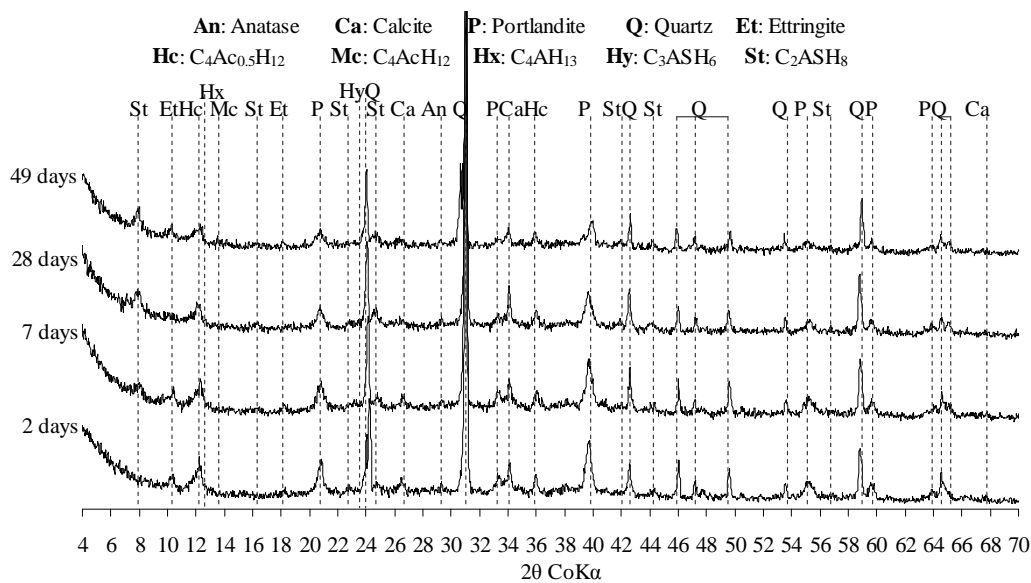
Figure 3.41: XRD analyses of SCP binder

These figures below present the mineralogical characteristics of CSP binder in function of time, characterized as follows:

- Portlandite was not completely consumed by pozzolanic reaction up to 49 days as similar to SP binder.

- Hydration products: the presence of ettringite confirmed the important role of

142

K$_2$SO$_4$; the formation of vaterite and the very high intensity of calcium hemicarboaluminate confirmed the chemical reaction of glycerol carbonate with the binder. We also remarked the reduction of straetlingite by decrease of its intensity in comparison with that of SM and S binders.

- Inert and anhydrous components were also visible as the same other binder.

Ca: CaCO$_3$ **P**: Ca(OH)$_2$ **Hx**: C$_4$AH$_{13}$ **Hc**: C$_4$Ac$_{0.5}$H$_{12}$ **Mc**: C$_4$Ac$_{0.5}$H$_{12}$ **Hy**: C$_3$ASH$_6$ **Va**: Vaterite **St**: C$_2$ASH$_8$
Et: Ettringite
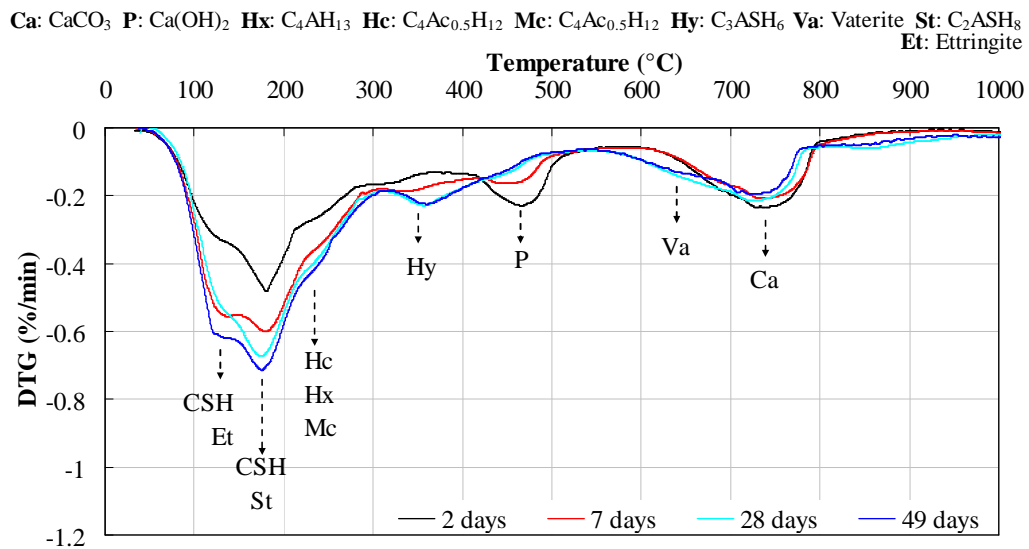
Figure 3.42: Thermogravimetric analyses of SCP binder

The total quantity of hydration products, residual Ca(OH)$_2$ and CaCO$_3$ for SCP binder are presented in Table 3.13.

Table 3.13: Percentage by weight of hydrated phases – H%,

Ca(OH)$_2$ – P% and CaCO$_3$ – Ca% of SC binder

2 days			7 days			28 days			49 days		
H%	P%	Ca%	H%	P%	Ca%	H%	P%	Ca%	H%	P%	Ca%
27.9	10.5	7.7	37.9	7.1	7.4	40.3	4.8	9.3	44.1	4.7	8.3

e. Comparison of mineralogical characteristics among the SL-MK binders

As similar to the NHL3.5-MK binders, we present the TGA curves of all SL-MK binders in the Figure 3.43 and Figure 3.44 at 2 days and 49 days respectively to compare the mineralogical characteristics among these binders.

As similar to the NHL3.5-MK binders, these figures also confirm the different influence of the admixtures on the mineralogical characteristics of the SL-MK binders. The glycerole carbonate retarded the the pozzolanic reaction, and increased the formation of

calcite. The K_2SO_4 encouraged the hydration reaction as well as the formation of ettringite right at 2 days.

Ca: $CaCO_3$ **P**: $Ca(OH)_2$ **Hx**: C_4AH_{13} **Hc**: $C_4Ac_{0.5}H_{12}$ **Mc**: $C_4Ac_{0.5}H_{12}$ **Hy**: C_3ASH_6 **Va**: Vaterite **Et**: Ettringite
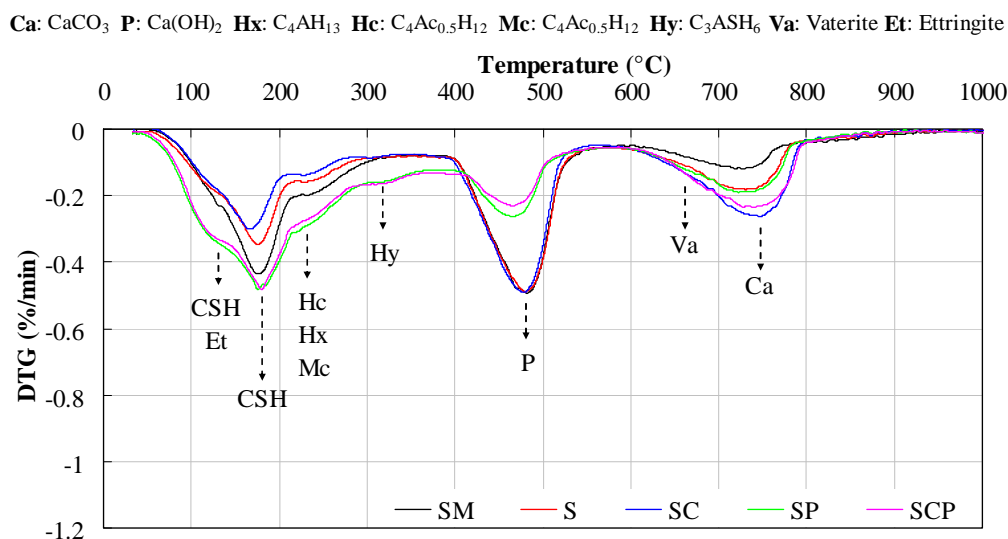
Figure 3.43: Thermogravimetric analyses of SL-MK binders at 2 days

Ca: $CaCO_3$ **P**: $Ca(OH)_2$ **Hx**: C_4AH_{13} **Hc**: $C_4Ac_{0.5}H_{12}$ **Mc**: $C_4Ac_{0.5}H_{12}$ **Hy**: C_3ASH_6 **Va**: Vaterite **St**: C_2ASH_8
Et: Ettringite
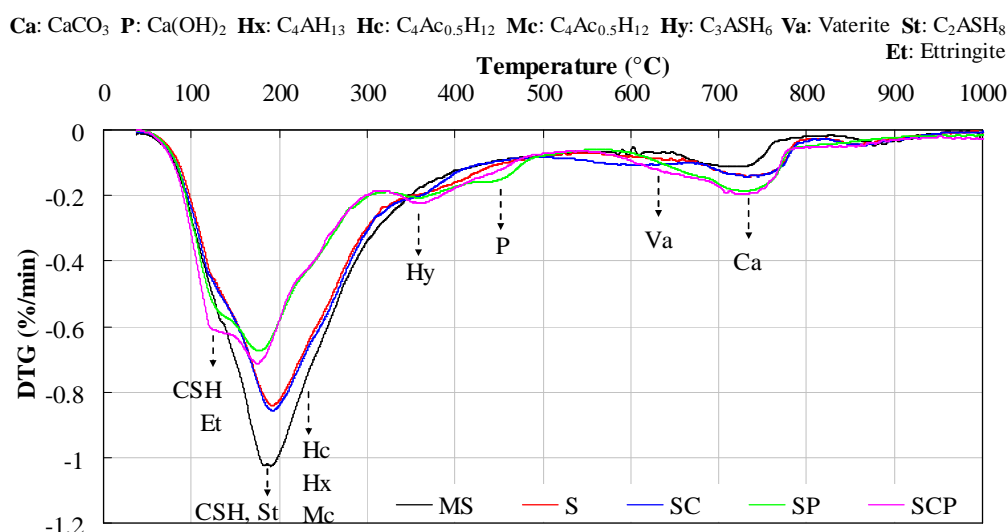
Figure 3.44: Thermogravimetric analyses of SL-MK binders at 49 days

At longer age (49 days), the curves on Figure 3.44 showed that in temperature interval from 80 to 350°C, the area of the peaks of SP and SCP binders is much smaller than that of other binders. This difference can be attributed to the difference of straetlingite quantity. Moreover, the ettringite was only observed on the curves of SP and SCP binders at the peaks around 130°C. Thus, this result can confirm that the presence of K_2SO_4 contributes to form ettringite, but limit the formation of straetlingite in the pozzolanic reaction. On the other hand, this result can also confirm the role of glycerol carbonate in the formation of calcium carbonate.

3.3.5.3 Conclusion

The XRD and TGA analyses confirmed the different mineralogical characteristics between the NHL3.5-MK binders and SL-MK binders and the difference among the binders because of the influence of different admixtures.

For the influence of glycerol carbonate, it retarded the pozzolanic reaction that can explain the lower compressive strength of HC and SC binder in comparison with H and S binders respectively. On the other hand, glycerol carbonate increased the formation of calcium hemicarboaluminate and contributed to form vaterite by consumption of portlandite. However, we remarked that both calcium hemicarboaluminate and vaterite cannot contribute to the development of strength of HC and SC binders.

For the influence of K_2SO_4, it encourages the hydration reaction and formation of ettringite leading to increase compressive strength of binders. Thus, this study confirmed the important role of sulfate ion in improvement of compressive strength of pozzolanic binder, which is consistent with the studies in literature [MAA10, SHI00 & WIL98]. On the other hand, the results showed that the presence of K_2SO_4 decreases the solubility of portlandite, and therefore limits the formation of straetlingite. Although K_2SO_4 decrease straetlingite quantity of the binders, the compressive strength of the binders containing K_2SO_4 is much higher than that of other binders, which can demonstrate the much more important role of ettringite against that of straetlingite in the compressive strength improvement of the binders.

3.3.6   *Relation between hydration products and strength or endogenous shrinkage*

3.3.6.1 Relation between hydration products and strength

In order to investigate this relation among the binders, the relationship between the compressive strength and the quantity of total hydration products for each binder is studied. These relations are presented in Figure 3.45 and Figure 3.46.

Figure 3.45 and Figure 3.46 show the linear relationship between the compressive strength and quantity of total hydration products for each binder. It can be seen that the evolution of quantity of total hydration products over time can explain the evolution of the compressive strength for each binder: the higher the quantity of total hydration products is, the greater the compressive strength will be.
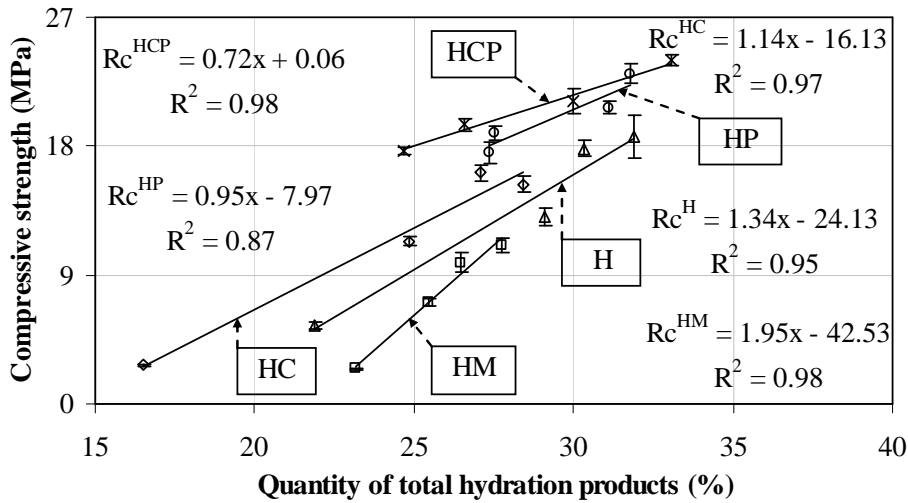
Figure 3.45: Compressive strength vs total quantity of hydration products for NHL3.5-MK binders
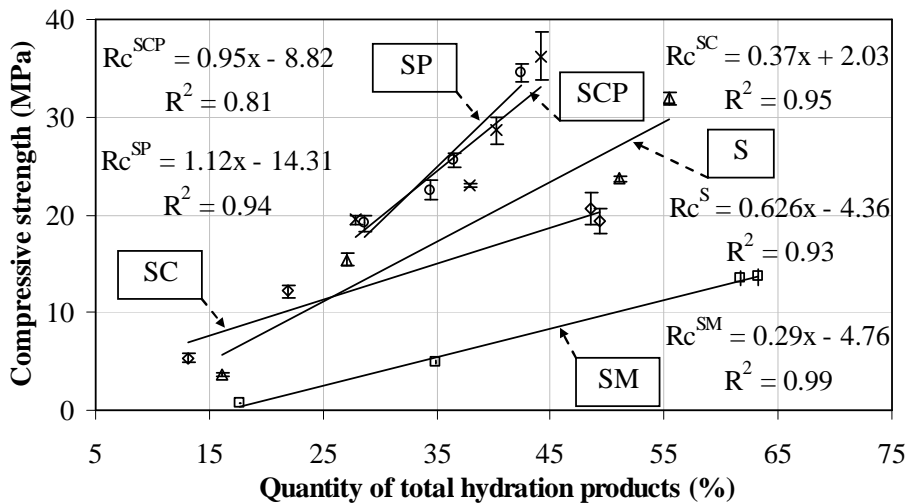
Figure 3.46: Compressive strength vs total quantity of hydration products for SL-MK binders

However, the quantity of total hydration products cannot evaluate the evolution of the compressive strength among the different binders. Previous paragraph (3.3.5) demonstrated that glycerol carbonate decreases the compressive strength of binder because it retards the hydration reaction, while K_2SO_4 significantly increases the compressive strength of binder thanks to the encouragement of hydration reaction and ettringite formation in its presence. Moreover, superplasticizer also increases the compressive strength of binder because of reduction of pore volume. Thus, we can conclude that the nature of hydration products is responsible for the compressive strength of binder (in this

146

case: ettringite brings the much more positive effect on improvement of the compressive strength in comparison with straetlingite).

3.3.6.2 Relation between hydration products and endogenous shrinkage

In order to study this relation, the relationship between quantity of total hydration products and endogenous shrinkage for the NHL3.5-MK binders and SL-MK binders is considered. Figure 3.47 below presents the endogenous shrinkage of NHL3.5-MK binders and SL-MK binders corresponding with their quantity of total hydration products respectively from 7 to 49 days.

a) NHL3.5-MK binders   b) SL-MK binders
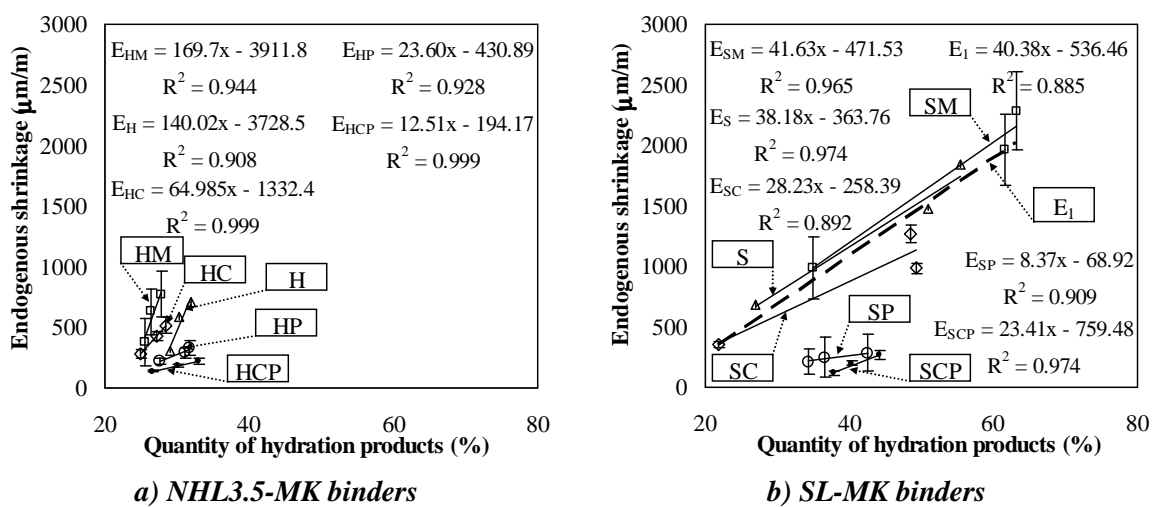
Figure 3.47: Endogenous shrinkage vs quantity of total hydration products from 7 to 49 days

Figure 3.47 presents the linear relations between endogenous shrinkage and quantity of total hydration products of each binder from 7 to 49 days: the higher the quantity of total hydration products is, the higher the endogenous shrinkage will be.

For the role of glycerol carbonate, this figure confirms significant decrease of endogenous shrinkage of binders containing glycerol carbonate for both kinds of pozzolanic binders as shown in literature [MAG10a].

In regard to the role of K_2SO_4, this figure also confirms the best shrinkage reducing effect of K_2SO_4 for both kinds of pozzolanic binders. This can be attributed to increasing the solid volume of the paste because of ettringite formation in the presence of K_2SO_4 [SHI00]. Moreover, this figure also indicates the endogenous shrinkage of the binders containing K_2SO_4 (HP, HCP, SP and SCP) is insignificantly different, which can confirm the important role of ettringite for endogenous shrinkage evolution of binders.

147

For the binders without K_2SO_4, Figure 3.47b presents a linear relation (E_1) between endogenous shrinkage and quantity of total hydration products among all SL-MK binders without K_2SO_4. Moreover, the evolution of E_1 relation was much larger than that of the relation of SP and SCP binders. Thus, these observation can link to the endogenous shrinkage increase of binders due to straetlingite because the straetlingite quantity of S binder is less than that of SM binder and higher than that SC binder, while that is absent in SP binder and insignificant in SCP binder (see XRD diagram in paragraph 3.3.5.2). This can also explain the endogenous shrinkage and quantity of total hydration products of SL-MK binders were respectively higher than those of NHL3.5-MK binders.

3.3.6.3 Conclusion

This part confirmed the linear relation between quantity of total hydration products and the evolution of compressive strength for each binder, and the nature of hydration products is responsible for the difference of the compressive strength among the different binders.

For the endogenous shrinkage, these results can confirm the evolution of endogenous shrinkage of each binder in function of quantity of total hydration products and the predominant endogenous shrinkage reducing effect of K2SO4 over glycerol carbonate. On the other hand, this study indicated that straetlingite increases endogenous shrinkage, while ettringite significantly reduces endogenous shrinkage.

3.3.7   Conclusion

This part evidently allows evaluating the different influence of two admixtures (glycerol carbonate and K_2SO_4) on the development of compressive strength and the dimensional variation of two kinds of pozzolanic binders (NHL3.5-MK and SL-MK binders).

For the influence of glycerol carbonate, this study indicated that glycerol carbonate reduces the compressive strength of the binders because it retards the hydration of the binders (HC and SC binders), which opposites to the result in literature [MAG10b]. However, glycerol carbonate brought the good effect in shrinkage reducing of binders.

For the influence of K_2SO_4, our results confirmed that K_2SO_4 encourages formation ettringite leading to significantly improve the compressive strength of binders, especially at

early age, which confirmed the important role of sulfate ion in improvement of compressive strength of binder [MAA10, SHI00 & WIL98]. Moreover, the shrinkage reducing effect of the binders containing K_2SO_4 is much more important than that of the binders containing glycerol carbonate.

Furthermore, the incorporation both glycerol carbonate and K_2SO_4 in binder not only brings the best compressive strength, but also significantly limits the dimensional variation of the binders.

3.4 Thermal conductivity of binders

The thermal conductivity values of three binders (commercial binder – CB, HCP and SCP binders with the same water to binder ratio – W/B = 0.4) are shown in Table 3.14.

Table 3.14: Thermal conductivity of binders

Binders	Humid state (65%RH)			Dry state	
	Density (kg/m^3)	Water Content (%)	λ (W/m/K)	Density (kg/m^3)	λ (W/m/K)
CB	1462	11.94	0.432	1303 ± 1.7	0.352 ± 0.035
HCP	1412	8.24	0.233	1303 ± 3.4	0.223 ± 0.003
SCP	1496	16.14	0.326	1290 ± 2.2	0.267 ± 0.010

Table 3.14 shows the values of thermal conductivity of our binders (HCP and SCP) and a commercial binder (CB). It can be seen that the thermal conductivity of our binders was much lower than that of the commercial binder in both humid and dry state. In comparison with the measurements in literature, the thermal conductivity values of our pozzolanic binders were also much lower than those of lime binders and Portland cement paste. Indeed, the dry thermal conductivity values of three of lime binders (NHL2, NHL3.5Z and Tradical PF70) were 0.363, 0.37 and 0.373 W/m/K respectively with the dry density of around 1200 kg/m^3 [NGU10]; dry thermal conductivity of Portland cement paste was from 0.7 to 1.186 W/m/K with the dry density of 2010 – 2014 kg/m^3 [BEN08 & DEM03].

In conclusion, the thermal conductivity of pozzolanic binders (HCP and SCP) was fairly low in comparison with lime binders and Portland cement paste. Thus, they can apply for fabrication of insulating building materials, especially plant concrete because they can contribute to reduce thermal conductivity of the materials.

3.5 Properties of standard mortar

In order to evaluate the application of pozzolanic binders, some properties of fresh and harden mortar are tested. In this study, three tests of workability, mini-cone and setting time were performed on fresh mortar, and the mechanical properties were carried out on harden mortar in function of time.

3.5.1.1 Mortar constituents

In this study, mortar formulations was conformed to NF EN 196-1 standard. The mortar components of each batch are presented in Table 3.15.

Table 3.15: Formulation of a mortar batch

Components	HCP mortar	SCP mortar	CB mortar
CB (g)			450.0
NHL3.5 (g)	225.0		
Slaked lime (g)		135.0	
Flash metakaolin (g)	225.0	315.0	
Glycerol carbonate (g)	2.3	2.3	
K_2SO_4 (g)	13.5	13.5	
Superplasticizer (g)	3.6	7.2	3.2
Standard sand (g)	1350	1350	1350
Water (g)	225	225	225

These three mortars were formulated from two pozzolanic binders (HCP and SCP) and a commercial binder (CB) and CEN standard sand (this sand was pre-packed in bags with a content of 1350 ± 5 g). The mixing of mortar was realized by automatic Controls mixer whose mixing method complies with the NF EN 196-1 standard.

3.5.1.2 Tests on fresh mortar

The results of the tests realised on three fresh mortars are presented in Table 3.16.

Table 3.16: Results of tests realised on fresh mortars

Mortar	Workability (s)	Mini-cone test		Setting time	
		Diameter	Slump	Initial	Final
CB	2	24.1 cm		3h 10min	3h 30min
HCP	4		2 cm	2h 10min	3h 10min
SCP	3		8.5 cm	3h 10min	3h 30min

Table 3.16 shows the results of workability, mini-cone test and setting time of three kinds of mortar. This table indicates that three mortars showed good workability which can

compare to workability of Portland cement mortars (5s) in the previous studies [CAS13 & COU03]. For the mini-cone test, our results in this table illustrate that only CB mortar presented slump flow with diameter of 24.1 cm, while HCP and SCP mortars exhibited the slump values of 2 and 8.5 cm respectively which were comparable with slump value of cement mortar (3.8 cm) in literature [CAS13]. These small slumps of HCP and SCP mortars can be attributed to the rapid reaction of glycerol carbonate with lime [MAG10b].

For the setting time, Table 3.16 shows that the initial setting time of HCP mortar was much faster than that of two other mortars and similar with the initial setting time of Portland cement mortar, around from 1h45min to 2h20min [APP03 & SID12]. We remarked that the initial and final setting time of CB and SCP mortar were insignificantly different. The final setting time of three mortars was similar each other and in range of final setting time of cement mortar in previous studies, around from 2h49min to 5h40min [APP03 & SID12].

3.5.1.3 Mechanical properties

The flexural and compressive strengths of three mortars are presented in Figure 3.48 and Figure 3.49.

	CB	HCP	SCP
⊡ 2 days	1.97	3.89	3.96
⊠ 7 days	2.28	4.46	4.79
⊠ 28 days	3.65	4.70	5.48
⊞ 49 days	3.84	5.36	6.07
◪ 90 days	4.84	5.50	5.77
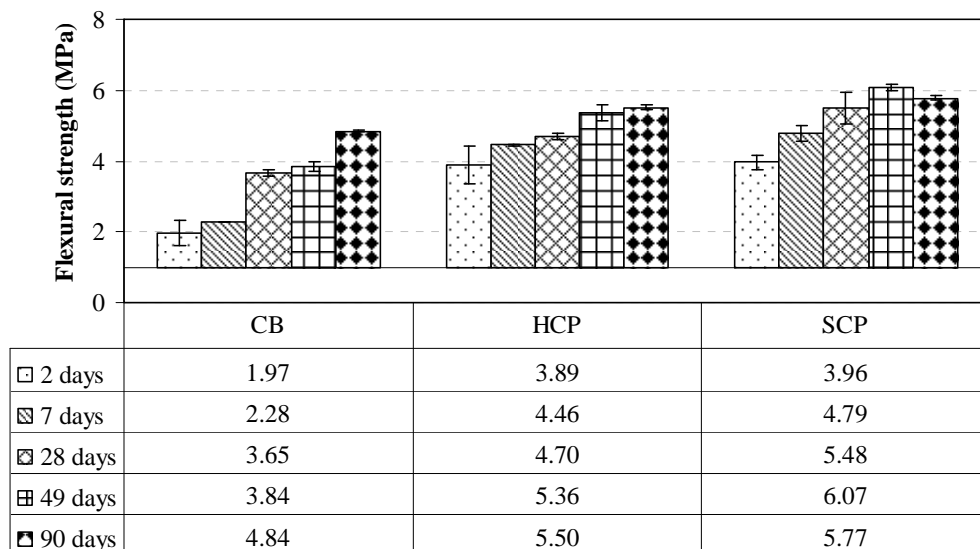
Figure 3.48: Flexural strength of mortars

Figure 3.48 shows flexural strengths of three mortars. It can be seen that strengths of HCP and SCP mortars were higher than those of CB mortar, especially at early age (at 2 and 7 days, strengths of HCP and SCP mortars were double CB mortar's strengths). It is

obvious to see that SCP mortar possessed the highest strength in all the test dates. Its strength increased gradually until 49-day age, but the strength at 90 days decreased slightly in comparison with that at 49 days, while strengths of two other mortars increased until 90-day age. The decrease of flexural strength of SCP mortar at 90 days can be attributed to the development of micro cracks and carbonation.

	CB	HCP	SCP
⊡ 2 days	9.24	14.13	14.80
⊠ 7 days	12.66	17.49	23.35
⊠ 28 days	16.91	20.28	30.40
☐ 49 days	16.97	21.95	32.19
◪ 90 days	18.04	21.80	30.41
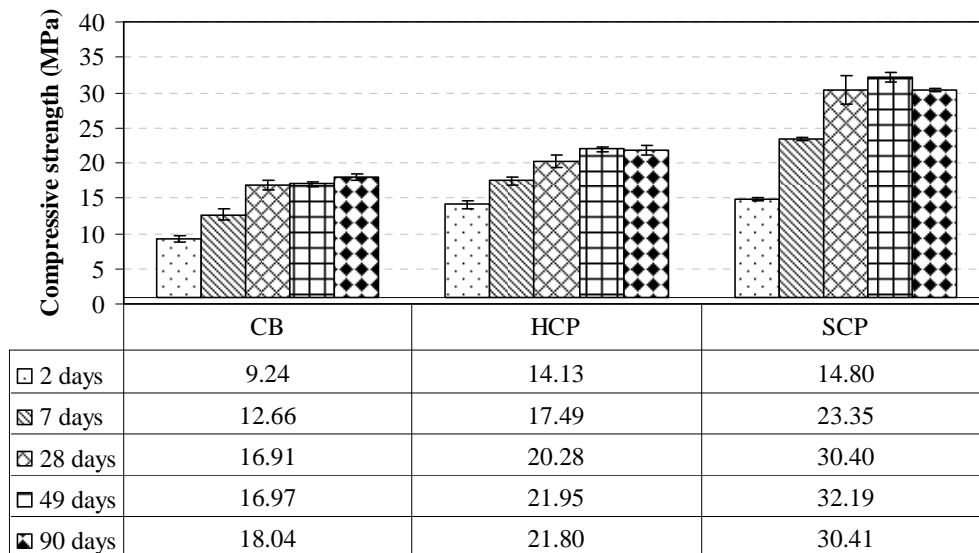
Figure 3.49: Compressive strength of mortars

Figure 3.49 presents the compressive strengths of three mortars. As similar as the flexural strength, SCP mortar exhibited the highest compressive strength in all test dates. At 2 days, it was slightly higher than that of HCP mortar and 1.5 times higher than that of CB mortar. At 7, 28 and 49 days, its strengths were around 1.5 and 2 times higher than those of HCP and CB mortars respectively. At 90 days, the strengths of HCP and SCP mortars reduced slightly, while CB's strength increased slightly in comparison with those at 49 days. We attributed the reduction of the strength of HCP and SCP mortars to the development of micro cracks and carbonation.

3.5.1.4 Conclusion

The results of mortar tests indicated that two mortars using HCP and SCP binders presented the fresh properties as comparable as commercial binder and Portland cement mortars. Moreover, the mechanical properties of HCP and SCP mortars were much higher than those of CB mortar, especially at early age. Thus, HCP and SCP binders can be applied for construction.

3.6 Conclusion

In this chapter, we presented the results of optimization of raw material contents for two pozzolanic binders (from NHL3.5 or slaked lime and flash metakaolin) and the influence of glycerol carbonate and K_2SO_4 admixtures on the properties of the pozzolanic binders.

In the first part, we selected two control pozzolanic binders with following weight ratios: the first (HM) included 50% NHL3.5 and 50% flash metakaolin, the second (SM) included 30% slaked lime and 70% flash metakaolin. HM binder reaches the highest mechanical strength at early age. Nevertheless, the SM binder is the most efficient after 28 days. Moreover, both HM and SM binders are very interesting in the areas of the economics and the sustainable development in the construction thanks to using very high content of flash metakaolin.

In the other parts, we studied the influence of glycerol carbonate and K_2SO_4 admixtures on the properties of the pozzolanic binders.

For the mechanical properties, glycerol carbonate decreased the compressive strength, while K_2SO_4 improved significantly strength of the binders especially at early age. The combination of glycerol carbonate and K_2SO_4 in the binders also slightly increased strength in comparison with the binders using only K_2SO_4 admixture. This study showed that the compressive strength of SCP and SP binders was 1.5 and 1.2 times higher than that of HCP and commercial binder (CB) respectively at 49 days. Especially, the 2-day strength of HP, HCP, SP and SCP binders was comparable with that of Portland cement paste.

As regard to dimensional variation, the shrinkage measurements of the pastes confirmed significant shrinkage-reducing effect of incorporation of glycerol carbonate, and the binders containing K_2SO_4 (SP and HP) exhibited the best effect of shrinkage reduction. This study also showed that the shrinkage-reducing effect of the binders containing both glycerol carbonate and K_2SO_4 (SCP and HCP) was similar with that of the binders containing K_2SO_4 admixture (SP and HP) respectively.

Moreover, the thermal conductivity measurements of the binders showed the lower values for HCP and SCP binders than those for lime binders and Portland cement paste. This illustrated that they can be applied for fabrication of insulating building materials

especially for plant concrete.

On the other hand, standard mortars using HCP and SCP binders were tested to compare with the mortar using a commercial binder (CB). For fresh mortar, three mortars presented good fresh properties, which can compare with those of Portland cement mortar. For the mechanical properties, HCP and SCP mortars presented the better flexural and compressive strength than CB mortar did, where SCP mortar showed the best mechanical performance.

In conclusion, our results showed that both HCP and SCP binders are the best mechanical performance for the NHL3.5-MK and the SL-MK binders respectively. Moreover, these two binders present the significant limitation of shrinkage, the low conductivity, and the suitability for economic criterion and sustainable development in construction area. Thus, these two binders can be used for fabrication of hempcrete, which will be present in the next chapter.

Chapter 4:   Development and characterization of pozzolanic hempcrete

4.1 Introduction

The third chapter indicated that both HCP and SCP binders can be used to fabricate hempcrete using hemp shives as aggregates. In fact, thanks to the use of a very high flash metakaolin content (70%), the SCP binder not only has higher mechanical performance, but can also be a better eco-material in comparison with HCP binder. Thus, we chose SCP binder to develop the new composite with plant aggregates – hemp shiv, called hempcrete. In this chapter, we will present the properties of this hempcrete using untreated and treated hemp shives.

Introduction

Le troisième chapitre a montré que les deux liants HCP et SCP peuvent être utilisés pour fabriquer du béton de chanvre. Cependant, grâce à l'utilisation d'une très forte teneur en métakaolin flash (70%), le liant SCP a non seulement des performances mécaniques plus élevées, mais peut être également un meilleur éco-matériau en comparaison avec le liant HCP. Ainsi, nous choisissons le liant SCP pour développer le nouveau composite utilisant la chènevotte, appelé le béton de chanvre. Dans ce chapitre, nous présenterons différentes propriétés du béton de chanvre utilisant de la chènevotte traitée et non traitée.

4.2 Treatment of hemp shives by pozzolanic binder

The first chapter showed some treatment methods of the plant aggregates by different substances and the different benefits of the use of treated aggregates. However, these treatment methods need many storages to contain treated aggregates before fabricating concrete due to the conservation of treated aggregates in long time (up to 28 days – paragraph 1.5.3.2); therefore, it is not suitable to the production of concrete on the large scale. Thus, our study intends to treat hemp aggregates with the pozzolanic binder used to fabricate the hempcrete and to conserve the treated aggregates for a short time (up to 2 days).

4.2.1   Treatment description

To make hempcrete samples, hemp shives were pretreated 2 days before being used. The pretreatment employed the binder concerned in the fabrication of the hempcrete. The formulation of the pretreatment of hemp shives is presented in Table 4.1.

Table 4.1: Pretreatment of hemp aggregates for 1 m³of hempcrete

Mixture	Hemp shiv (kg/m³)	Binder (kg/m³)						Water (kg/m³)	W/B	S/B
		CB	MK	SL	GC	K₂SO₄	SP			
SP1, SP3, SP4	161.90	-	74.80	32.06	0.53	3.21	1.71	106.85	1	1.5
SP2	161.90	-	74.80	32.06	1.78	3.21	-	106.85	1	1.5
CP	161.90	109.02	-	-	-	-	-	109.02	1	1.5

- CB: Commercial binder; MK: Metakaolin; SL: Slaked lime; GC: Glycerol carbonate; SP: Superplasticizer; W/B: water to binder ratio; S/B: hemp shives to binder ratio
- W/B and S/B were calculated according to weight of CB for CP mixture, and of total mix of MK and SL for other mixtures(from SP1 to SP4).

The pretreatment process consisted of putting the hemp shives into a mixer and mixing for 2 minutes, then gradually introducing the water and mixing for 5 minutes to wet the hemp particles, before adding the binder and mixing the whole for a further 2 minutes (Table 2.1 in chapter 2).

In the conservation process, the treated hemp shives were conserved for 2 days according to two modes: keeping them in tight plastic bags (mode 1) or putting them on the waterproof floor of indoor room in 5 cm thickness (mode 2). In Table 4.1, the treated hemp shives for the SP1 and SP2, and CP mixtures were conserved according to mode 1 (called treated-1), and for SP3 and SP4 mixtures were conserved according to mode 2 (called treated-2, Figure 4.1).

Figure 4.1: Conservation of treated hemp shives in mode 2 (SP3 and SP4)

4.2.2 Water absorption capacity of treated hemp shives

The water absorption capacity of treated hemp shives was determined on three samples weighing around 50g each for every Treated–2 sample obtained from around 25g of untreated hemp shiv after 2 days of conservation. The method of measurement was presented at paragraph 2.3.4 in the second chapter. The water absorption capacity of the

treated sample was compared with that of the untreated hemp shiv sample – noted "Normal" (it was described in paragraph 2.6.3 in chapter 2). In order to compare the water absorption capacity between treated and untreated hemp shives, the water absorption capacity of treated hemp shives was relatively calculated according to the initial mass of untreated hemp shives; therefore, M_t and M_o in equation (2.3) in chapter 2 were canculated by equations (4.1) and (4.2).

$$M_t = M_{t1} - M_p \qquad\qquad (4.1)$$

$$M_0 = M_{01} - M_p \qquad\qquad (4.2)$$

M_{t1}: Mass of treated hemp shive after each time of the immersion containing enclosed paste mass(g)

M_p: Mass of enclosed paste used to treat hemp shives (g)

M_{01}: Mass of untreated sample before immersion (g)

We note that our calculation of water absorption of treated hemp shives considered the enclosed paste did not absorb water during the test.

The results are shown in Figure 4.2 and Figure 4.3 below.
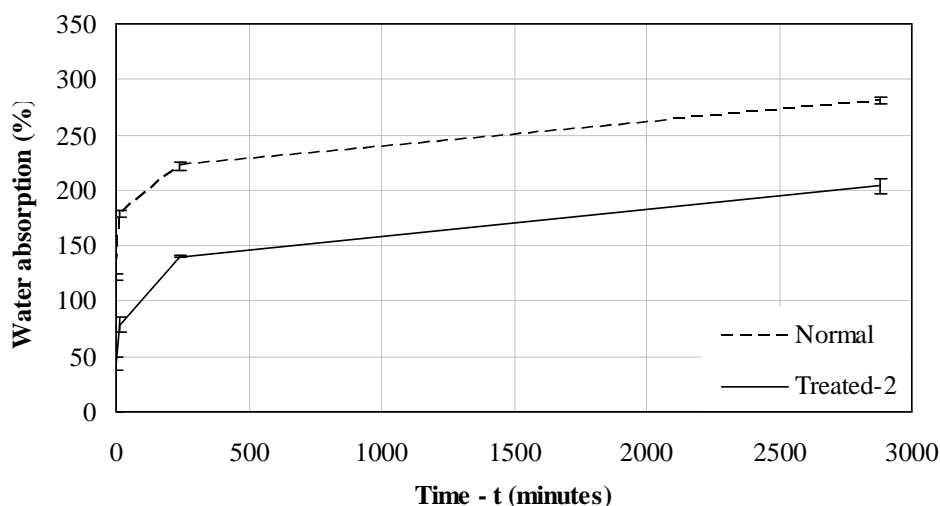
Figure 4.2: Water absorption capacity of treated hemp shives during 48 hours

Figure 4.2 shows the water absorption capacity of treated hemp shives in comparison with the normal hemp shives. After 48 hours, the water absorption of treated hemp shives was notably lower in comparison with that of non-pretreated shives. Indeed, it absorbed around 204% in mass, which reduced 27% in comparison with the non-pretreated

shives. During the first minute, the pretreated shives absorbed only 44% in mass (around 20% of the final value), which decreased 65% in comparison with the untreated hemp shives.

As the results of water absorption of non-treated shives in second chapter, the water absorption of treated shives also conforms to logarithmic function of time (Figure 4.3). The absorption coefficient of Treated-2 shives is slightly higher in comparison with that of normal shives. This is attributed to the water adsorption of harder binder-coated surface of the hemp particles. Nevertheless, the initial water adsorption of treated-2 hemp shives is much less than that of untreated hemp shives. This demonstrates that harder binder-coated surface of the hemp particles significantly reduced the initial water adsorption of hemp shives, and therefore limited their water absorption capacity.

Figure with legend:
- - - - Log. (Normal)
——— Log. (Treated-2)

$W_N = 19.52 Ln(t) + 122.04$
$R^2 = 0.99$

$W_T = 20.29 Ln(t) + 34.46$
$R^2 = 0.98$

Y-axis: **Water absorption-W (%)**, X-axis: **Time - t (minutes)**
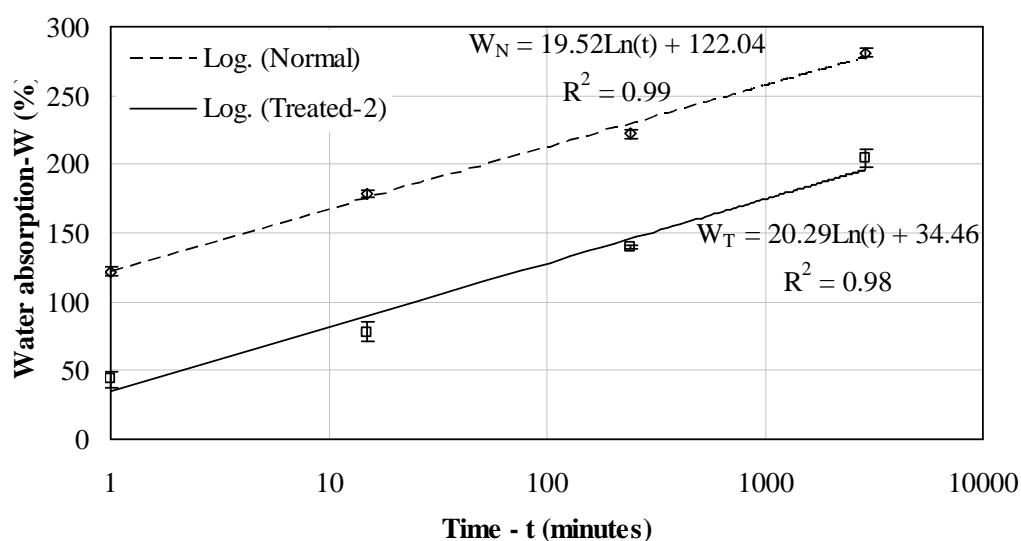
Figure 4.3: Water absorption of treated shives according to logarithmic function of time

In comparison with other studies, we found in Nozahic's study [NOZ12] that the shives treated by linseed oil presented a water absorption reduction of 40%, while the water absorption of hemp shives treated by $Ca(OH)_2$ solution did not reduce in comparison with the non-treated shives. For other plant aggregates, Khazma et al [KHA08] indicated that the significant decrease of water absorption of treated flax particles was 70% in comparison with that of the non-treated flax particles (Khazma et al treated flax particles by mixture of cement and sucrose and conserved in humid room in 28 days before the test). Monreal et al [MON08 & MON11] measured the water absorption of two kinds of treated beet pulps (with cement and linseed oil) after 21 days conservation. The results showed

that the water absorption of both kinds of treated beet pulps reduced 25% and 35% respectively in comparison with untreated beet pulp.

In conclusion, our results confirmed that the pretreatment of hemp shives significantly reduces water absorption capacity of hemp shives. Our results are similar with those of other studies, and our methods of pretreatment were also simpler than that of previous studies. This may be promising for the improvement of hempcrete properties using treated hemp shives. We will present the effect of treated shives on the mechanical and thermal properties of hempcrete in the next parts.

4.3 Formulation of hempcrete

In this study, we used the formulation of hempcrete with the same hemp shives to binder ratio as that of French Building Confederation [ASS07] for the "wall" formulation. Moreover, we used the commercial binder (CB) with the same formulation as that of hempcrete using pozzolanic binder in order to compare the properties of the two kinds of hempcretes.

The formulations of hempcretes are presented in Table 4.2 below.

Table 4.2: The quantity of components for 1 m^3 hempcrete

Mixture	Binder (kg)		Hemp shiv (kg)	Water (kg)	S/B	W/B	ρ_f (kg/m^3)
	CB	PB					
S1		283.39	122.56	188.75	0.43	0.67	594.7
S2, SP1, SP2, SP4		374.35	161.90	302.75	0.43	0.81	839.0
SP3		417.99	179.73	241.27	0.43	0.58	839.0
C, CP	374.35		161.90	302.75	0.43	0.81	839.0

CB and PB: Commercial and pozzolanic binder respectively
S/B and W/B: hemp shiv and water to binder ratios
ρ_f: fresh density of hempcrete

In Table 4.2, the S1, S2, and C mixtures are the hempcretes using untreated hemp shives, and the other mixtures are the hempcretes using treated hemp shives. The C and CP mixtures used commercial binder, and other mixtures used pozzolanic binder. Table 4.2 shows the total quantity of binder, hemp shives and water for 1 m^3 of each mixture, which included the quantity of materials used to treated hemp shives for the mixtures made of treated hemp shives.

In order to choose the suitable water to binder ratio and fresh density, S1 and S2 mixtures were fabricated with different W/B ratio and maximum fresh density for each.

We observed appearance of dry binder on surface of S1 after the compressive test, while did not for S2 mixtures. Thus, we chose the W/B ratio and fresh density of S2 mixture to apply for other mixtures.

For the hempcretes made of pozzolanic binder and treated hemp shives, all these hempcretes were fabricated with the same fresh density. SP1, SP3 and SP4 hempcretes used the same quantity of dry binder (metakaolin and slaked lime) and admixtures for both hemp shiv pretreatment and mixing hempcrete. Difference of the SP2 hempcrete against other hempcretes is the use of admixtures: all quantity of glycerol carbonate was used for pre-treatment of hemp shives (without superplasticizer Table 4.1), and all quantity of superplasticizer was used for the final mixing hempcrete (without glycerol carbonate). The amount of water evaporated during the time of conservation of treated hemp shives was added to he SP4 mixture, while it was not added to SP3. We will present the properties of these mixtures in the next paragraphs.

4.4 Evolution of hempcrete mass

The variation of hempcrete mass was regularly measured after 7 days each during 90 days. All hempcrete samples measured had the same fresh density and were conserved in the climatic room at $20^{\circ}C$ and 65% RH after 2 days until 90 days (the cylindrical samples were conserved without tops and bottoms of the moulds after 2-day until 7-day age, and then without cardboard moulds after 7 days, RILEM recommendation).

The mass loss of hempcrete samples was determined by equation (2.6) below.

$$\Delta m = \frac{m_0 - m_t}{m_0}.100\% \qquad\qquad (4.3)$$

Δm: Relative mass variation of sample at the time measured (%)

m_0: Mass of fresh hempcrete sample (kg)

m_t: Mass of hempcrete sample at the time measured (kg)

The mass of each hempcrete mixture was the mean value of the measurements made on three different samples. Figure 4.4 shows the evolution of apparent density and weight loss of seven mixtures of hempcretes during 90 days.

Figure 4.4 allows to conclude that the mass stabilization is reached after 60 days, which consists with observations realized in a previous study [CHA08]. The mass

variations are the most intense during the second week of drying time, which is the first week after remove all cardboard moulds and these variations were insignificant after day 40th.
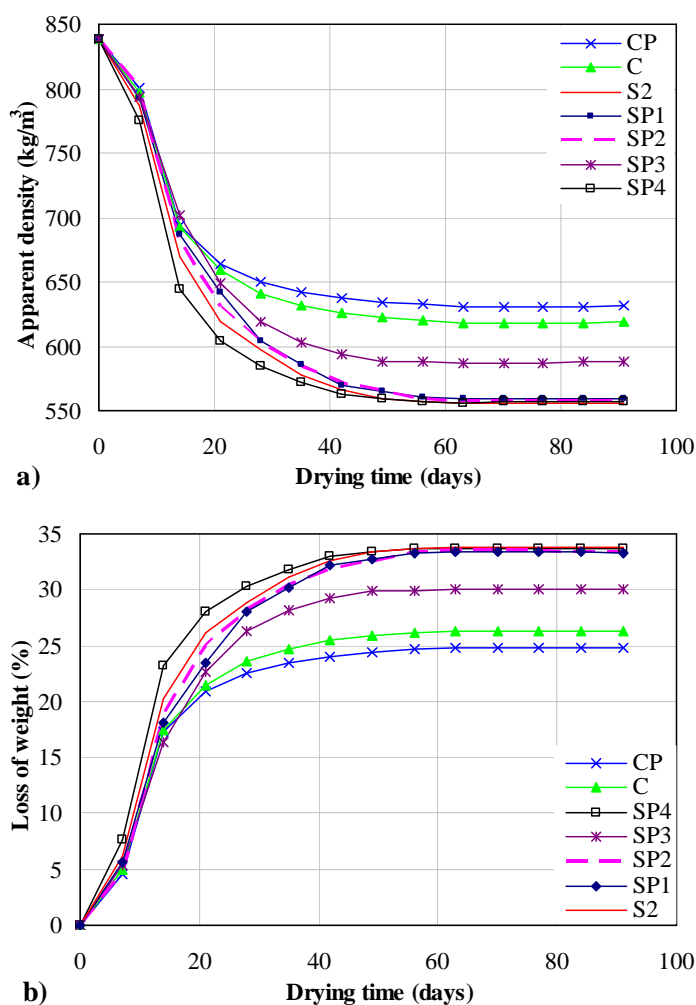
Figure 4.4: Apparent density change of hempcretes during 90 days

This figure also shows that the mass evolutions of hempcrete mixtures are different in spite of the same fresh density. After 90-day age, the apparent density of the samples reached from 556 to 588 kg/m^{3} for the pozzolanic hempcrete samples, and from 619 to 632 kg/m^{3} for the CB hempcrete samples (Figure 4.4a). The mass losses were respectively from 30% for SP3 micture to 33.3 - 33.7% for SP1, SP2 and SP4 mixtures, and 24.8% for CP mixture and 26.3% for C mixture (Figure 4.4b).

For the pozzolanic hempcrete samples, the final mass losses of the mixtures were similar to each other after 60 days, except the SP3 mixture. This result explained that the mass loss of hempcrete samples depends on their water content of the mixture, which consists with the studies in literature presented in paragraph 1.4.4 in first chapter. Indeed,

the mass evolution of S2, SP1, SP2 and SP4 mixtures was similar to each other and much higher than that of the SP3 mixture (the water content of SP3 mixture is much less than that of others - Table 4.2). For the influence of hemp shiv treatment, we found that this influence is insignificant because the final mass loss of hempcrete with untreated shiv (S2 samples) was only 2% higher than that of hempcrete with treated shives (SP1, SP2 and SP4 samples), in which the drying kinetics of SP4 is different from others because we added some water at mixing time to supplement the water amount evaporated during the conservation process of treated hemp shives.

For the CB hempcrete samples, the mass loss of hempcrete with untreated hemp shiv (C) was only slightly higher (around 1.5%) than that of hempcrete with treated hemp shiv (CP) after 28 days. This confirms that the influence of treatment of shiv on the mass variation of hempcrete is inconsiderable. However, our results remark that the mass loss of CB hempcrete samples reduced considerably in comparison with that of pozzolanic hempcrete samples after 14 days (24.8% and 26.3% for CB mixtures versus 30% and 33.7% for the pozzolanic mixtures). This can be attributed to the hydraulic components in commercial binder fix more rapidly water for their hydration in comparison with the pozzolanic binder in the hempcrete mixture.

In conclusion, the results of the evolution of hempcrete mass confirmed that the mass loss of hempcrete depended on the mixing water content of the mixture and on the binder nature.

4.5 Mechanical properties

To characterize the mechanical behaviour of hempcrete mixture, the compressive test was realized with a constant displacement of 5 mm/minute. In this study, we used two kinds of hemp shives: untreated hemp shiv and treated hemp shiv. The mixtures using untreated hemp shiv – are called "untreated hempcrete" such as S1, S2, and C mixtures, and the mixtures using treated hemp shiv – are called SP1, SP2, SP3, SP4 and CP mixtures).

4.5.1   *Mechanical behaviour of pozzolanic hempcretes*

4.5.1.1 Mechanical behaviour of untreated hempcretes

In order to characterize the mechanical behaviour of untreated hempcretes, the compressive test was realized on the samples of S1 and S2 hempcretes at 28 days (S1 and

S2 have different mixing water contents and fresh densities). The mechanical behaviour of the hempcretes is presented in Figure 4.5 to Figure 4.8, and Table 4.3 below.
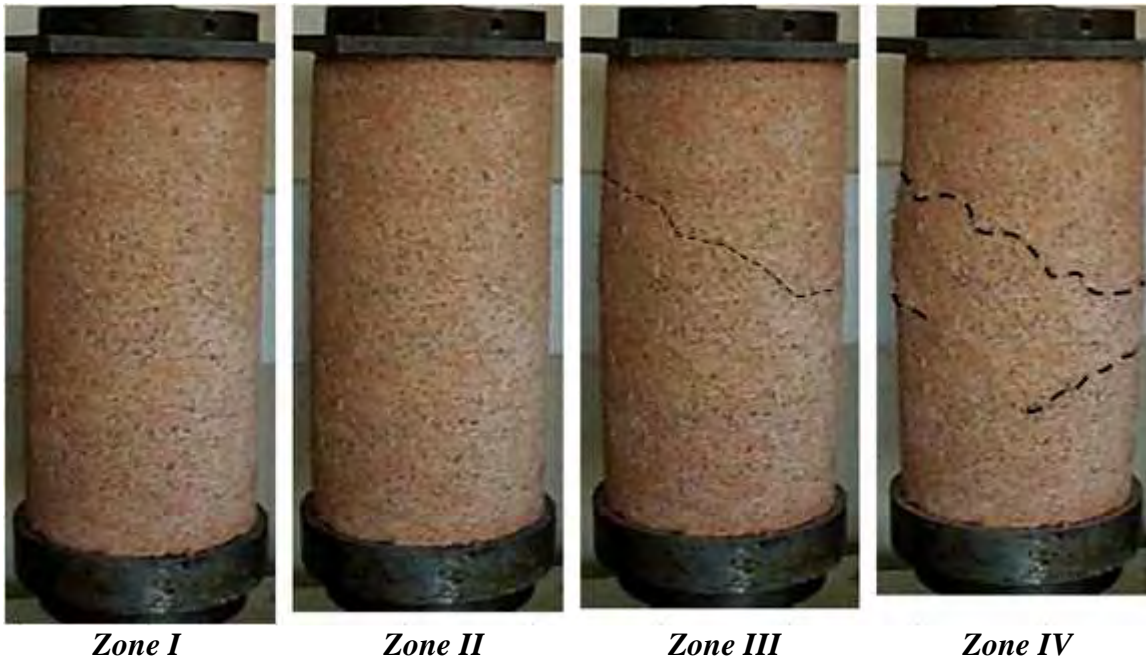
Zone I   *Zone II*   *Zone III*   *Zone IV*
Figure 4.5: Destructural stages of hempcrete at 28 days

Figure 4.5 shows the destructural stages of a hempcrete sample during the compressive test at 28 days. This observation indicated that in zone I, hempcrete sample presented a homogeneous material without fissure. In zone II, although it is very difficult to observe the fissure at the surface level of the samples, the horizontal deformation can be visible at the end of this phase. In zone III, the horizontal deformation of sample clearly increased, the small fissures was observed at the end of this phase, but the samples were not completely ruptured. In zone IV, the samples were totally ruptured.

Figure 4.6 presents the typical relation between compressive strength and deformation of S1 hempcrete at 28 days. This figure indicates that the S1 mixture is a very ductile material as its relative deformation is very large: strain to failure is more than 20%.

We can separate the mechanical behaviour of the hempcrete sample into four zones (I to IV), characterized as follows:

- Zone I, the mechanical behavior of hempcrete presented as a linear elastic material, which performed as a homogeneous material. In this phase, the stress-strain curve is a linear line with the smallest deformation zone (form 0 to 1%). This result was in accordance with the results in literature [CER05 & NGU10].

- Zone II, the behavior showed as an elastic-plastic material, which was found in Nguyen's study [NGU10] and similar to the beginning of pre-peak phase in Cerezo's study [CER05]. Figure 4.6 indicated that the relation between the compressive strength and the deformation of hempcrete sample was a continuous flexural curve. This phase exhibited larger deformation zone and slower increase of strength in comparison with those of zone I. This phenomenon can be attributed to the fact that the matrix and/or the interface between the hemp particles and the binder were progressively ruptured.

- Zone III exhibited a constantly and slightly increasing stress with the recorded deformation, end point of this phase is the peak of stress, which consisted with Nguyen's study [NGU10], but it was not observed in Cerezo's study [CER05]. In this phase, the stress increased the most slightly with the largest deformation interval. At the end of this phase, the stress curve was horizontal before going down, this is called stress plateau with the maximum stress value. This behavior can be attributed to the distribution of the stress into the hemp particles and the complete destruction of matrix; moreover, the stress during fabrication of hempcrete could also contribute to strength of hempcrete in this phase [NGU10].

- Zone IV presented the complete destructive phase of hempcrete (the strength decreased after reaching the maximum value).
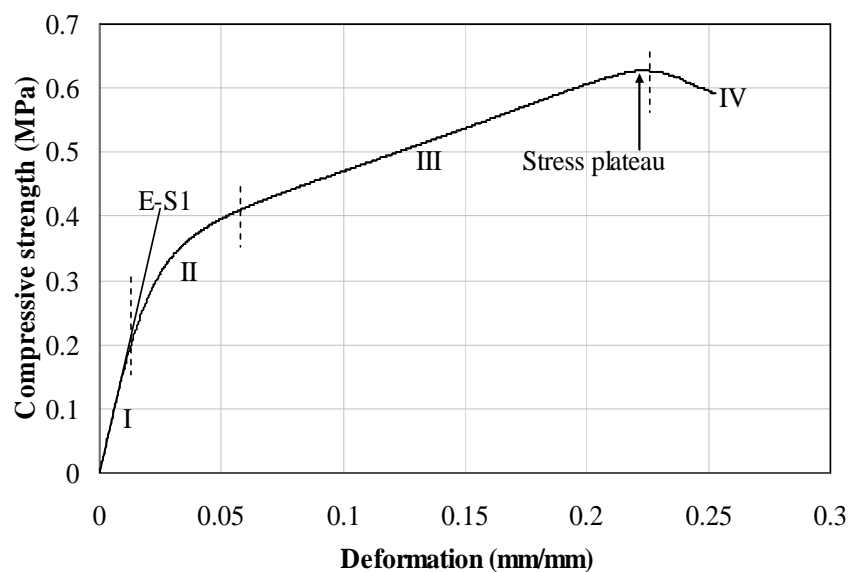
Figure 4.6: Compressive strength of S1 hempcrete at 28 days

165
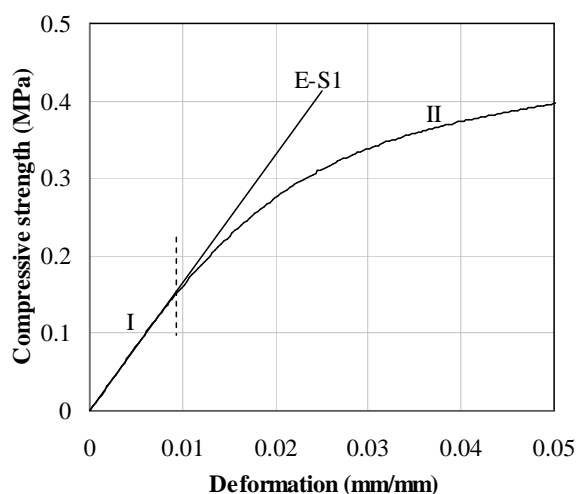
Figure 4.7: Elastic modulus vs deformation of S1 hempcrete at 28 days

Figure 4.7 presents the method calculating elastic modulus of S1 hempcrete samples at 28-day age. The E-S1 line exhibited the linear relation of the stress strain curve in zone I from the origin point of coordinate, which mean that zone I of the stress strain curve of S1 hempcrete obeys Hooke's Law. Thus, elastic modulus of S1 hempcrete was determined by ratio of stress to strain in elastic region of the stress strain curve.
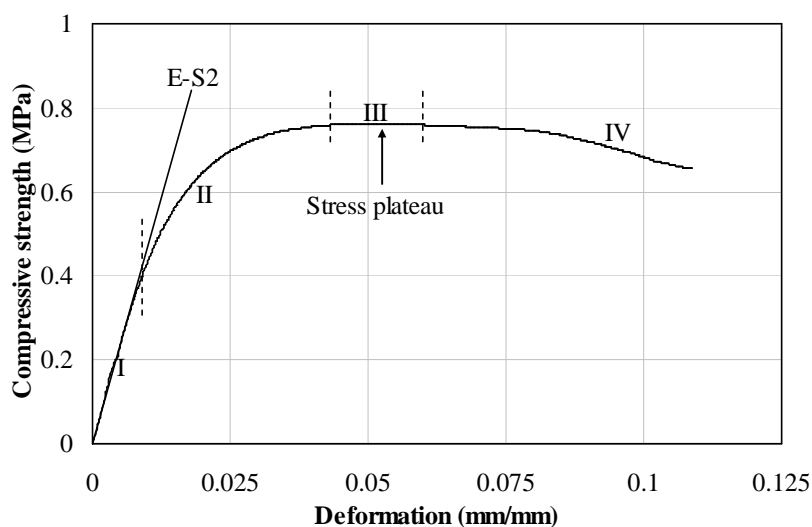
Figure 4.8: Compressive strength of S2 hempcrete at 28 days

Figure 4.8 clearly shows that the mechanical performance of S2 hempcretes presented four zones, where zone I and zone IV were the same as the behaviour of S1 hempcrete, but zone II and zone III were slightly different. Zones II and III were characterized as follows:

- Zone II, it was similar to S1 hempcrete, but the compressive strength of hempcrete

reached maximum value at the end point of this phase.

- Zone III, the mechanical behavior of S2 hempcrete was the stress plateau state which exhibited as the same as the last stage of zone III of S1 hempcrete.

The maximum compressive and modulus values of untreated hempcrete were presented in Table 4.3 below.

Table 4.3: Compressive strength and modulus of S2 hempcretes at 28 days

Mixture	ρ_f *(kg/m³)*	ρ_{28} *(kg/m³)*	ρ_{90} *(kg/m³)*	σ_{max} *(MPa)*	*E (MPa)*	$\varepsilon_{\sigma max}$
S1	594.7	448.3	439.7	0.65 ± 0.06	14.09 ± 2.32	$0.22 - 0.26$
S2	839.0	597.2	556.0	0.77 ± 0.01	46.79 ± 0.11	$0.04 - 0.07$

ρ_f, ρ_{28} and ρ_{90}: fresh density, 28-day density and 90-day density; σ_{max}: maximum compressive strength; $\varepsilon_{\sigma max}$: the value of deformation corresponding with σ_{max}

Table 4.3 shows that although the maximum strength of S1 hempcrete at 28 days (0.65±0.06 MPa) was more than 3 times higher in comparison with the value according to the recommendation of French Buiding Confederation (FBC) for hempcrete (> 0.2 MPa) [ASS07], its modulus value was around 1 MPa lower than that in FBC (14.1 ± 2.3 MPa versus 15 MPa in FBC). These results and the observation of samples after rupture (certain dry binder content) showed that the water content used for S1 mixture was not enough for the hydration of pozzolanic binder in hempcrete, which leads to much low modulus. Thus, we decided to use higher mixing water content for S2 hempcrete, which was presented in the following part.

For S2 hempcrete, Table 4.3 indicates that although the compressive strength of S2 mixture was similar with that of S1 mixture and comparable with results in literature with the same dry density (Figure 1.16 in chapter1), its modulus was much higher than that of S1 hempcrete and in range found in literature (Table 1.15 in chapter 1). The deformation value of S2 hempcrete corresponding to the maximum compressive strength was very small, which illustrates that this S2 hempcrete is more fragile. Moreover, the observation of S2 hempcrete samples after rupture showed that there is not dry binder content, which can confirm enough water for hydration of binder in S2 hempcrete. Thus, the good mechanical performance of S2 hempcerete can be attributed to the fact that the binder forms better connected network in S2 hempcrete than in S1 hempcrete because mixing water was enough for the hydration of binder.

4.5.1.2 Mechanical behavior of treated hempcretes

In order to evaluate the influence of the treatment of hemp shives on the mechanical behavior of hempcrete, compressive tests were performed on different mixtures using treated hemp shives with the same fresh density of S2 hempcrete at 28 days. These results were compared to the results obtained with untreated hemp shives. The results are shown in Figure 4.9 to Figure 4.11, and Table 4.4 below.
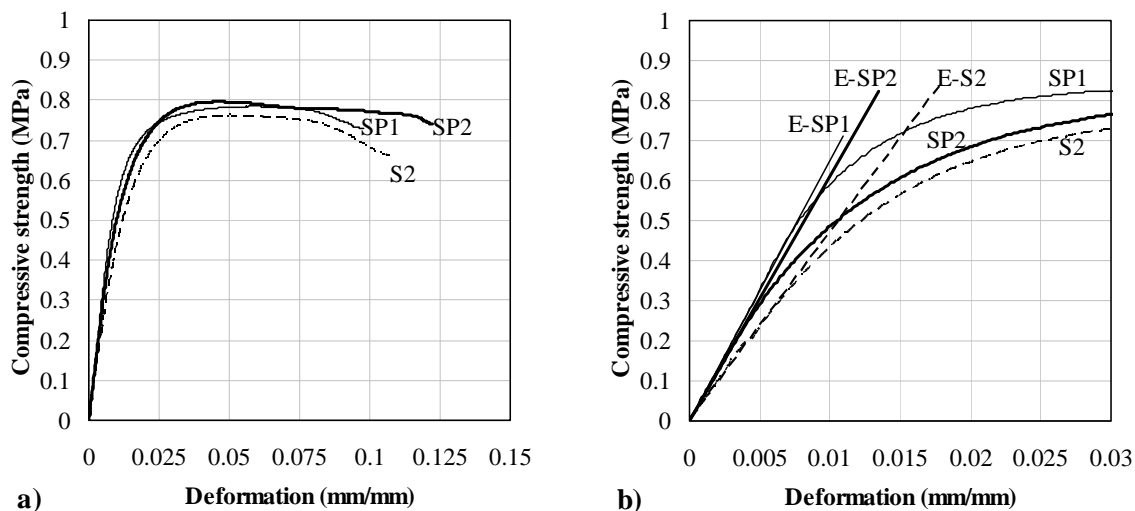
Figure 4.9: Mechanic behaviors of treated hempcretes – SP1, SP2 at 28 days

The results in Figure 4.9a show that SP1 and SP2 samples exhibited four zones of mechanical behaviour the same as S2 mix presented in paragraph 4.5.1.1. The difference between SP1 and SP2 mixtures were presented in paragraphs 4.2 and 4.3 above. Although there are different amounts of admixture ingredients between SP1 and SP2 mixtures, the mechanical behaviours of these two mixtures were insignificantly different.

In comparison with the untreated hempcrete (S2), we remarked that although the maximum compressive strength of treated hempcretes was slightly higher (around 3%), the moduli were much higher than those of untreated hempcrete (Figure 4.9b, Table 4.4). This shows an insignificant efficiency of treated hemp shives on the mechanical performance at 28 days. However, this conservation method of treated hemp shives before mixing was not convenient for the hempcrete production in the large scale because the treated hemp shives were conserved in tight plastic bags. Thus, the conservation of treated hemp shives in the storage house would be more suitable with industrial production (SP3 and SP4 treated shives, paragraph 4.2.1). We will present the mechanical behaviour of these treated hempcretes in Figure 4.10, Figure 4.11 and Table 4.4 below.

168
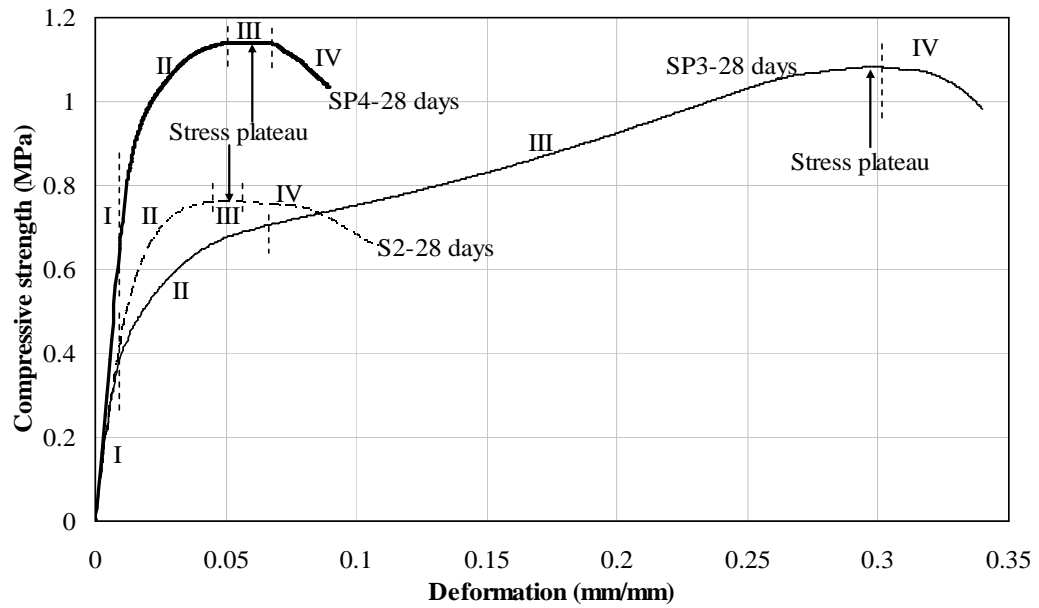
Figure 4.10: Compressive strength of treated hempcretes – SP3, SP4 at 28 days
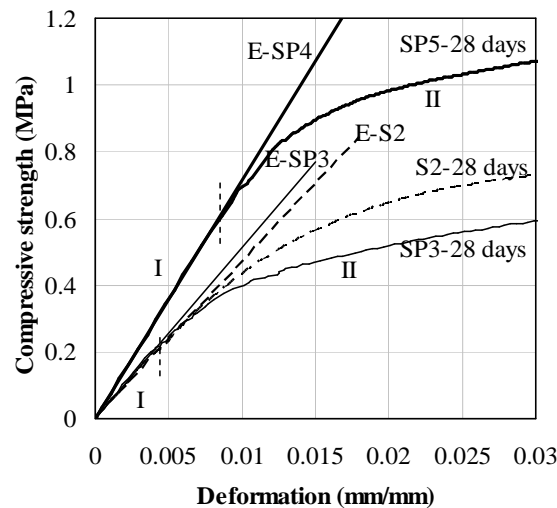
Figure 4.11: Elastic modulus of treated hempcretes – SP3, SP4 at 28 days

Table 4.4: Compressive strength and elastic modulus of treated hempcretes at 28 days

Mixture	$\rho_f (kg/m^3)$	$\rho_{28} (kg/m^3)$	$\rho_{90} (kg/m^3)$	σ_{max} *(MPa)*	*E (MPa)*	$\varepsilon_{\sigma max}$
S2	839.0	597.2	556.0	0.77 ± 0.01	46.79 ± 0.11	0.04 – 0.07
SP1	839.0	604.5	560.0	0.79 ± 0.05	64.91 ± 0.15	0.04 – 0.07
SP2	839.0	603.4	559.0	0.80 ± 0.03	59.74 ± 2.19	0.04 – 0.06
SP3	839.0	619.3	588.0	1.08	51.41	0.29 – 0.30
SP4	839.0	585.2	557.2	1.14	71.69	0.05 – 0.06

The SP3 and SP4 mixtures used the same treated hemp shives, which were conserved in the laboratory as presented in paragraph 4.2.1 above. The mixing water content of SP4 mixture is higher than that of SP3 mixture (the higher mixing water content

169

of SP4 mixture against SP3 mixture equalled the amount of water evaporated during the time of conservation of treated shives). The SP3 and SP4 mixtures were fabricated with the same fresh density.

The results in Figure 4.10 indicate the mechanical performance difference between SP3 and SP4 mixtures. SP3 mixture exhibited four zones of mechanical behaviour as S1 mixture, while SP4 mixture showed the behaviour zones being the same as the behaviour of S2 mixtures as presented in paragraph 4.5.1.1. It can be seen that although the maximum compressive strength of SP3 and SP4 mixtures were similar to each other, the deformation zone of SP3 mixture was much larger than that of SP4 mixture, and the modulus of SP4 mixture was therefore much higher than that of SP3 mixture (Figure 4.11 and Table 4.4).

Table 4.4 shows that the modulus of SP4 mixture was around 1.5 times higher than that of SP3 mixture. We attributed the higher modulus to the higher mixing water content of SP4 mixture, that leads to a better cohesion between binder and hemp shives. At the contrary, in SP3 mix, an incomplete hydration of binder occurred due to a lack of water. This confirmed by the detection of anhydrous binder content in ruptured SP3 sample (like S1 samples), while it was not visible in SP4 sample.

In comparison with untreated hempcrete (S2), it can be seen that the mechanical compressive properties of both SP3 and SP4 mixtures were higher than those of S2 mixture, especially those of SP4 hempcrete (they were the highest and 1.5 times higher than those of S2 hempcrete). This demonstrated a significant efficiency of SP3 and SP4 treated hemp shives on the mechanical performance at 28 days.

In comparison with SP1 and SP2 hempcretes, the compressive strengths of SP3 and SP4 mixtures were 1.5 times higher than those of SP1 and SP2 mixtures. On the other hand, the modulus of SP3 mix was significantly lower (around 10 to 20%), while the modulus of SP4 mix was 10 to 20% higher than that of SP1 and SP2 mixes. Moreover, the conservation method of SP3 and SP4 treated hemp shives before mixing was much simpler in comparison with that of SP1 and SP2 treated hemp shives; therefore, it is very convenient for the hempcrete production in the large scale.

4.5.1.3 Conclusion

The results of the mechanical behaviours of pozzolanic hempcretes demonstrated that SP4 hempcrete has the best mechanical properties among all of hempcretes in this

study. Moreover, SP4 hempcrete also has a simpler method of hemp shiv pre-treatment than previous studies. Thus, we can conclude that SP4 hempcrete formulation can be applied for industrial production.

4.5.2 *Mechanical behaviour of CB hempcrete*

CB hempcrete is fabricated by a commercial binder and hemp shives. In this part, we will present the mechanical performances of untreated and treated CB hempcretes (C and CP) with the same formulation and fresh density as S2 and SP2 mixtures (Table 4.2). The mechanical behaviours of CB hempcretes are presented in Figure 4.12 and Figure 4.13 below.
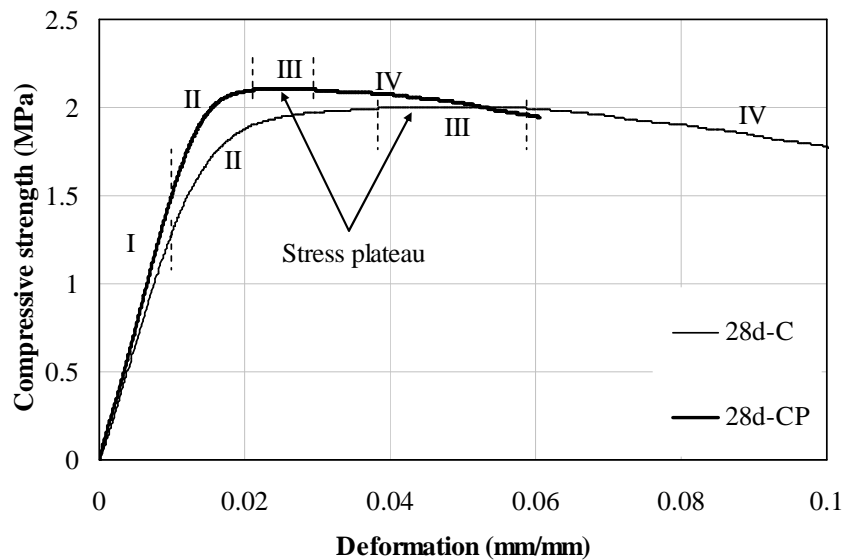
Figure 4.12: Compressive strength of CB hempcretes at 28 days
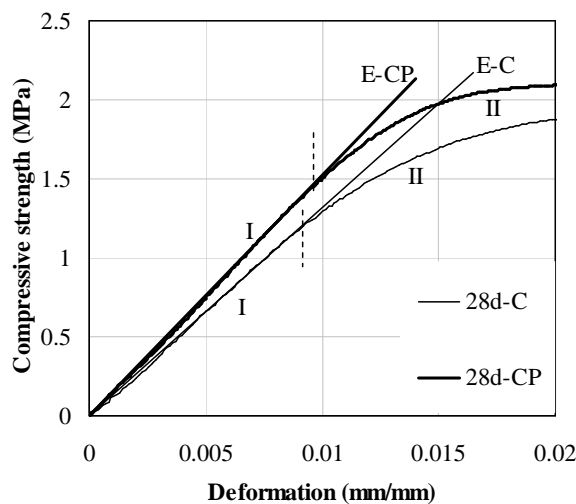
Figure 4.13: Elastic modulus of CB hempcretes at 28 days

Figure 4.12 and Figure 4.13 show that the mechanical behaviours of both untreated CB hempcrete (C) and treated CB hempcrete (CP) presented four zones as S2 hempcrete shown in 4.5.1.1 above. The maximum compressive strength and modulus of C and CP mixtures are shown in Table 4.5 below.

Table 4.5: Compressive strength and elastic modulus of B2 and BP at 28 days

Mixture	$\rho_f (kg/m^3)$	$\rho_{28} (kg/m^3)$	$\rho_{90} (kg/m^3)$	σ_{max} (MPa)	*E (MPa)*	$\varepsilon_{\sigma max}$
C	839.0	641.4	619.0	1.99 ± 0.03	115.76 ± 14.50	$0.04 - 0.06$
CP	839.0	650.2	631.7	2.14 ± 0.03	156.98 ± 17.08	$0.02 - 0.03$

The results in Table 4.5 confirm that the mechanical properties of CP hempcrete were better than those of C hempcrete, especially the modulus. Indeed, the maximum compressive strength and the modulus of CP hempcrete were respectively around 1.1 and 1.5 times higher than those of C hempcrete.

4.5.3 *Comparison of mechanical properties among hempcretes*

In order to easily compare the mechanical properties among the hempcrete mixtures in this study, Figure 4.14 and Figure 4.15 synthesize the maximum compressive strength and elastic modulus values of all hempcrete mixtures at 28 days.
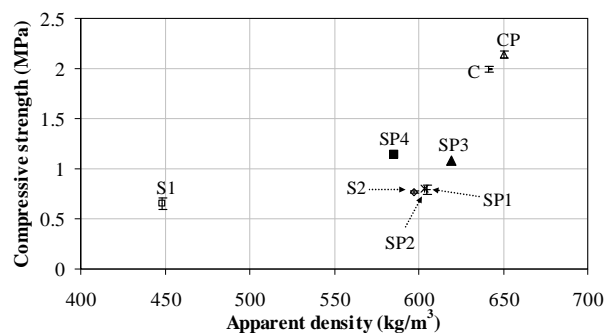
Figure 4.14: Compressive strength vs apparent density at 28 days
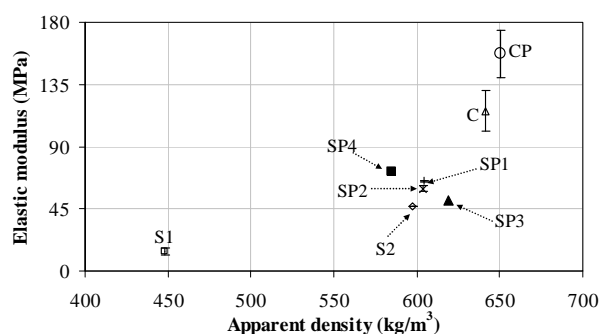
Figure 4.15: Elastic modulus vs apparent density at 28 days

172

Figure 4.14 and Figure 4.15 indicate that the mechanical properties of SP4 mixture, a treated hempcrete, used treated hemp shives conserved in normal room presented the best mechanical properties in comparison with other hempcrete mixtures using pozzolanic binder. Moreover, the pre-treatment and conservation methods of hemp shives used for SP4 hempcrete are very simple and easily applicable to produce in large scale in construction industry.

Figure 4.14 and Figure 4.15 also show that the mechanical properties of CB hempcretes were much higher than those of pozzolanic hempcretes. Indeed, both compressive strength and modulus of C and CP hempcretes were around three times higher than those of S2 and SP1 hempcretes respectively. This demonstrates the better hydration of this commercial binder when it is mixed with hemp shives in comparison with the pozzolanic binder developed in this study. The results of chapter 3 showed that the compressive strength of this pozzolanic binder is around 1.25 times higher than that of commercial binder. Thus, the better mechanical properties of CB hempcretes against pozzolanic hempcretes can reveal a problem of chemical interaction between soluble products extracted from the hemp shives and mineral particles of our pozzolanic binder. In the next part, we aim to confirm this hypothesis through mineralogical analyses of hempcretes.

In comparison with the previous studies in literature, Figure 4.16 below shows the the relation between compressive strength and dry density of hempcrete in literature and the results of pozzolanic and CB hempcretes at 28 days (noted POZ-28d and CB-28d respectively).
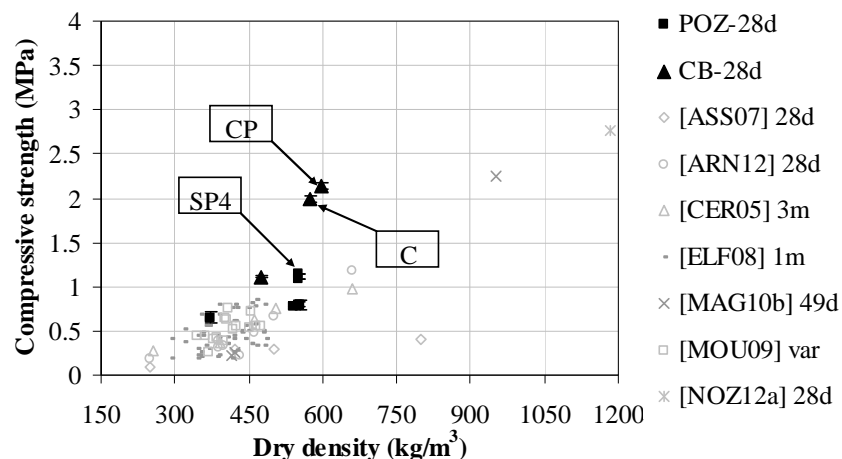
Figure 4.16: Relation between compressive strength and dry density

Figure 4.16 shows that the compressive strength values of our pozzolanic hempcretes were fairly high in comparison with results of previous studies with the similar dry density. For CB hempcretes, we remarked that our results were comparable with Nguyen's results [NGU10] with the same dry density in spite of much less initial compaction, and much higher than the results of other authors with the same dry density. This can confirm the large influence of binder nature on the interaction between binder and hemp shives.

4.5.4 Conclusion

In generally, the mechanical properties of hempcretes using our pozzolanic binder were fairly good and comparable with previous study, especially the hempcrete treated mixed with treated hemp shives which improved significantly the modulus of hempcrete. SP4 mixture was not only the best mechanical properties, but also applicable to produce in large scale because its hemp shives can be simply treated and conserved.

Nevertheless, these mechanical performances were lower than those obtained with a commercial binder in the same conditions. As we showed in chapter 3 that the intrinsic mechanical properties of our pozzolanic binder were higher than those of the commercial binder, we can conclude that hemp particles cause a negative influence on the development of the pozzolanic reaction. Mineralogical analyses of hempcretes were then realised to confirm this hypothesis, their results will be presented in the next part.

4.6 Mineralogical analyses

In order to understand the differences of mechanical performances observed among hempcretes, especially between our pozzolanic hempcretes and hempcretes using a commercial binder, X-ray diffraction (XRD) and thermogravimetric (TGA) analyses were realized. These tests were carried out on the dry powder samples passing through a 80 µm sieve of hempcretes at 28 days. The results of XRD and TGA analyses of hempcretes are presented in Figure 4.17 and Figure 4.18 respectively.

Figure 4.17 shows the XRD diagrams of pozzolanic binder (SCP), commercial binder (CB) and all hempcretes using these two binders at 28 days.

For pozzolanic hempcretes, it can be seen that the diagrams of untreated hempcrete (S2) and treated hempcretes (SP1, SP2, SP3 and SP4) at 28 days are similar to each other.

This figure indicates that the residual portlandite of all hempcrete mixtures were much higher than that of the pozzolanic binder. Moreover, the hydrated phases (straetlingite, ettringite and hemicarboaluminate) were not detected. This demonstrates that the pozzolanic reaction of our binder was limited when associated with hemp shives in the hempcrete mixtures. This limitation could be attributed to the solution of the polysaccharide extractives and the degradation products of alkaline attack leading to delay the setting of binder [DIQ12, GOV04, SED07 & SEM02] or to lack of water to favour the pozzolanic reaction.

An: Anatase   **P**: Portlandite   **Ca**: Calcite   **Q**: Quartz   **Et**: Ettringite   **Hc**: Hemicarboaluminate   **St**: Straetlingite
C2: C_2S **Ce**: Cellulose   **Hy**: Hydrogarnet

Figure 4.17: The XRD analyses of binders and hempcretes at 28 days

For the CB hempcretes, the results in Figure 4.17 showed that the portlandite peaks on diagrams of both C and CP hempcretes were similar to each other and lower than those of commercial binder, and small peaks of C_2S were visible. These observations show a slight reduction of hydration reaction of C_2S in presence of hemp shives. For hydration products, the only difference between commercial binder paste and hempcrete is the absence of hemicarboaluminate phases in the later. This is consistent with an inhibition of pozzolanic reaction due to hemp shiv soluble extractives or to lack of water because of

water absorption of hemp shives. A small peak of Ettringite was observed on the diagrams of both hempcretes at $2\theta = 10.48^{o}$ as in the one of the commercial binder.

Because the thermogravimetric analyses of four hempcretes (S2, SP1, SP2 and SP3) were similar to each other, we only showed the TGA curves of SP1 hempcrete in order to be easy to compare with those of SP4 hempcrete in Figure 4.18 below.
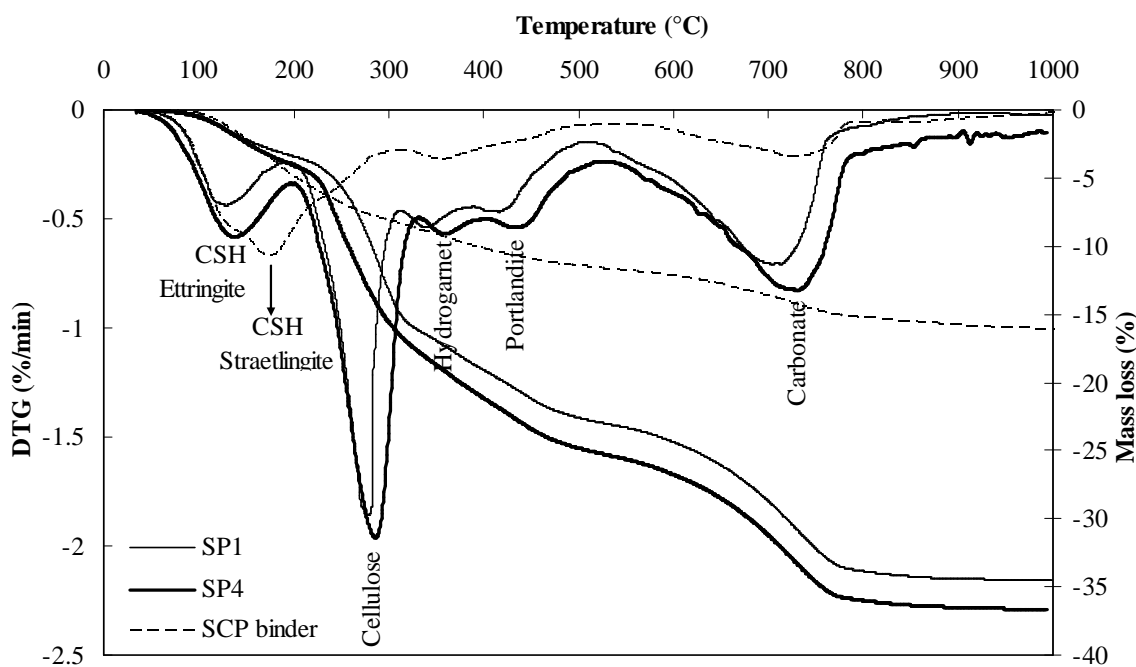
Figure 4.18: TGA curves of pozzolanic binder and pozzolanic hempcretes at 28 days

Figure 4.18 shows the thermogravimetric analyses of SP1 and SP4 hempcretes and our pozzolanic binder at 28-day age. It can be seen that the peak of portlandite decomposition of hempcretes on the hempcretes curves was bigger than that on the analysis of pure binder. Moreover, Straetlingite was not visible, while its decomposition peak was clearly observed in the TGA curves of pure pozzolanic binder. These observations confirmed the results of XRD and lead to conclusion of the partial inhibition of pozzolanic reaction in presence of hemp shives, which may be due to the interaction between mineral species and the soluble polysaccharide extractives from hemp shiv. Moreover, the higher carbonate rate of hempcretes in comparison with that of pozzolanic binder can be attributed to the carbonation of residual portlandite during conservation process of hempcretes.

For the hydration products, this figure also indicates that the peak of C-S-H dehydration of SP4 hempcrete predominated over that of SP1 hempcrete, this can explain

the better hydration of pozzolanic binder during conservation process of hempcretes, and thus the better mechanical properties of SP4 hempcrete.

This figure also shows that cellulose peaks were evidently visible at around 280° because the powder samples contained high content of hemp shiv powder, which is consistent with a previous study [KOS83]. The thermogravimetric analysis results of previous studies on cellulose indicated that the thermal chemical degradation of cellulose occurred from $200 – 300^oC$ depending on heating rate [MAG10b, MOO11 and POL13]. This was confirmed by this study: the TG curves on Figure 4.18 showed the thermal chemical degradation of cellulose occurred from around 220^oC.

In conclusion, the XRD and TGA analyses on the powder samples of hempcretes demonstrated the important difference of mineralogical characteristics among hempcretes. These results showed the limitation of binder hydration in hempcrete mixtures, which colud be attributed to the solution of the polysaccharide extractives and the degradation products of alkaline attack. The XRD analyses indicated that Ettringite was detected on diagrams of CB hempcretes, while it was not visible on pozzolanic hempcrete diagrams, this could confirm the much higher mechanical properties of CB hempcretes against those of pozzolanic hempcretes.

On the other hand, the TGA analyses confirmed the best hydration of pozzolanic binder in SP4 hempcrete against other pozzolanic hempcretes, which could explain the highest mechanical properties of SP4 hempcrete in comparison with other pozzolanic hempcretes.

In the next parts, we will present the measurements of thermal conductivity of these hempcretes to evaluate the thermal insulation of these materials.

4.7 Thermal conductivity

In this study, the thermal conductivity tests were performed on three samples for each hempcrete mixture. This test was realized for both humid samples and dry samples after 90-day age. The samples that reached the constant mass (the change in mass of the sample was less than 0.1% between two weightings 24 hours apart) at 20^oC and 65% RH, are called humid samples. The samples that were dried in an oven at $50°C$ until the constant mass, were called dry samples. The test method and the parameters of the test were presented in the second chapter.

The thermal conductivity of hempcrete was measured according to parallel direction ($\lambda_{//}$) and perpendicular direction ($\lambda_{\perp}$) with the compaction direction. The measurements were performed on the 5-cm-thick samples.

The results of thermal conductivity measurements for hempcrete samples are presented in Table 4.6 and Figure 4.19 below.

Table 4.6: Thermal conductivity hempcretes

Samples	ρ_{dry} (kg/m³)	ρ_{90} (kg/m³)	Dry state			Humid state		
			$\lambda_{\perp}$ (W/m/K)	$\lambda_{//}$ (W/m/K)	$\lambda_{\perp}/\lambda_{//}$	$\lambda_{\perp}$ (W/m/K)	$\lambda_{//}$ (W/m/K)	$\lambda_{\perp}/\lambda_{//}$
Untreated hempcretes								
S1	371.4	-	0.095	0.080	1.18	-	-	-
S2	539.9	556.0	0.122 ± 0.002	0.108 ± 0.001	1.13	0.132	0.115	1.15
C	572.9	619.0	0.137 ± 0.003	0.111 ± 0.001	1.24	0.142	0.121	1.18
Treated hempcretes								
SP1	552.6	560.0	0.127 ± 0.002	0.106 ± 0.001	1.19	0.137	0.117	1.17
SP2	549.3	559.0	0.124 ± 0.001	0.106 ± 0.001	1.17	0.135	0.118	1.15
SP3	551.9	588.0	-	0.099	-	-	0.103	-
SP4	549.7	557.2	-	0.101	-	-	-	-
CP	598.2	631.7	0.147 ± 0.002	0.125 ± 0.001	1.17	0.159	0.126 ± 0.004	1.31
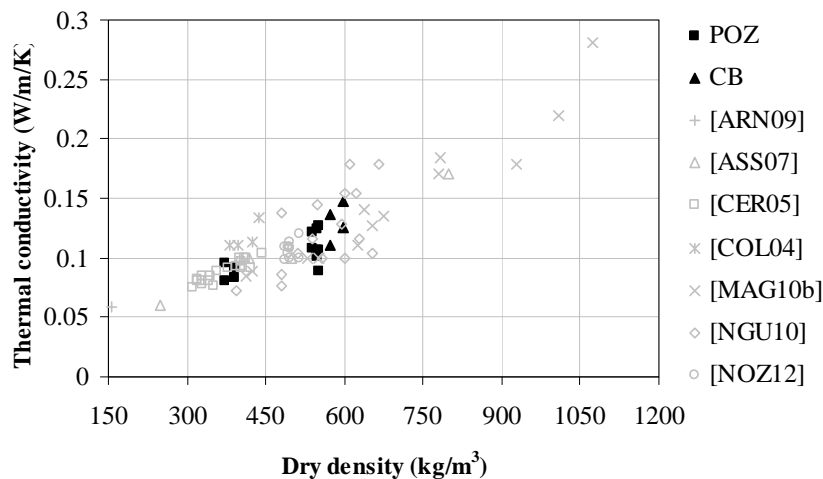
Figure 4.19: Thermal conductivity of dry hempcretes vs dry density

In generally, our results confirmed that the thermal conductivity of hempcretes was low and within the range of values found in the literature, as presented in Figure 4.19. These results also confirmed the difference of thermal conductivity of hempcretes between two directions ($\lambda_{\perp}$ and $\lambda_{//}$). The $\lambda_{\perp}$ to $\lambda_{//}$ ratio was from 1.10 to 1.24 for dry hempcretes and

from 1.15 to 1.31 for humid hempcretes, which confirmed the influence of compaction direction on the thermal conductivity of hempcretes being consistent with previous studies [NGU10, NOZ12, PIC11].

For the influence of density, Figure 4.19 confirmed that the higher the dry density of hempcrete is, the higher the thermal conductivity will be, which is consistent with the results in literature presented in paragraph 1.5.6.1 in first chapter.

In regard to the influence of relative humidity, the thermal conductivity of hempcrete samples conserved at 65% RH condition was insignificantly higher (around from 1.01 to 1.1 times) than that of dry hempcrete samples. This study was also consistent with the studies in literature (1.5.6.3in first chapter).

As far as the binder nature is concerned, our measurements showed that the thermal conductivity of pozzolanic hempcretes is lower than that of CB hempcretes due to the lower dry density of pozzolanic hempcretes in comparison with CB hempcretes in spite of the same fresh density each other. On the other hand, the thermal conductivity of both kinds of hempcretes is accordant with the relation between dry density and thermal conductivity of hempcrete in literature (Figure 4.19). Thus, although the thermal conductivity of commercial binder is 1.3 times higher than that of pozzolanic binder (paragraph 3.4 in chapter 3), the binder nature did not directly influence the thermal conductivity of hempcretes.

For the influence of hemp shiv treatment, we remark that it is insignificant. Untreated and treated hempcretes have similar thermal conductivity for both humid and dry samples.

In conclusion, the thermal conductivity of both pozzolanic and CB hempcretes was low and in the range of values found in the literature. This study confirmed that the thermal conductivity of hempcretes directly depends on dry density and direction of compaction, and indirectly depends on binder nature, while the influence of other factors (the relative humidity and hemp shiv pre-treatment) is insignificant.

4.8 Conclusion

This chapter presented the mechanical properties and thermal conductivity of the untreated and treated hempcretes using the optimal pozzolanic binder developed in this study in comparison with those of the hempcretes using commercial binder.

For the pre-treatment of hemp shives, the principle advantage was water absorption capacity reduction of the treated hemp shives against the untreated hemp shives. Moreover, the method of hemp shiv pre-treatment of SP3 and SP4 hempcretes was much simpler than that of previous studies. However, the pre-treatment hemp shives insignificantly influenced the mass loss of the hempcretes.

In regard to mechanical properties, the results demonstrated that the mechanical properties of the hempcretes using pozzolanic binder were fairly good and comparable with the results found in literature, especially treated hempcretes which improved considerably the modulus of the hempcretes. This study indicated that SP4 hempcrete has not only the best mechanical properties, but could also be applicable in large scale production because of the simple hemp shiv pre-treatment method and storage of treated hemp shives. Moreover, the XRD and TGA analyses confirmed the limitation of binder pozzolanic reaction in the hempcrete mixtures. TGA results showed the much higher C-S-H quantity of SP4 binder against that of other pozzolanic hempcretes, and the mechanical properties of SP4 binder are much higher than others. XRD results only indicated ettringite formation on diagrams of CB hempcretes, which can explain the much better mechanical performances of hempcretes using commercial binder against that of pozzolanic hempcretes.

The thermal conductivity of hempcretes was fairly low and comparable with the results of previous studies. This study confirmed the direct influence of dry density and the compaction direction, the indirect influence of binder nature, and the insignificant influence of other factors (the relative humidity and hemp shiv pre-treatment) on the thermal conductivity of hempcrete.

In conclusion, the pozzolanic hempcrete – SP4 mixture could be applied for industrial production for prefabricated building components with its superior mechanical properties and low thermal conductivity as well as the simple hemp shiv pre-treatment method and storage of treated hemp shiv.

GENERAL CONCLUSION
AND FUTURE WORK

Globally, the aim of this study was to develop a new building material made of a new pozzolanic binder and hemp shives, which satisfies the criterions of an eco-materials. The work under the scope of the research consists of two major parts: development of new pozzolanic binders and the hempcrete using our pozzolanic binder, which was divided into four chapters.

In the literature review chapter, we recalled the concept of sustainable development. From this standpoint in construction area, this chapter illustrated how necessary to replace conventional building materials by eco-materials. It also indicated that the hempcrete made of mineral binders and hemp shives needs to be developed to use for the thermal insulation wall because it not only has a good thermal insulation and low cost, but also environmental-friendly.

For mineral materials, this chapter pointed that flash metakaolin (MK) is one of the best eco-materials because its production consumes far less energy than Portland cement and emits a little CO_2 amount. Moreover, natural hydraulic lime and slaked lime are also considered as eco-materials in comparison with Portland cement. Thus, this chapter brought us to choose flash metakaolin, natural hydraulic lime – NHL3.5 and slaked lime to develop two kinds of pozzolanic binders. On the other hand, glycerol carbonate, potassium sulphate and superplasticizer were also used to improve the mechanical strength at early age and reduce the shrinkage of these binders.

For plant aggregates, these materials combine several environmental benefits: they are local and renewable resources, they are carbon neutral and its embodied energy is usually low. Previous works permitted us to select hemp shives because they were eco-materials and available in Toulouse (in our case); moreover, they had a low cost and a good thermal insulation. This chapter also indicated that it is necessary to develop new methods for hemp shiv pre-treatment, so that it is not only simple, but also has a good effect on reducing of the water absorption capacity of hemp shives.

In the second chapter, we described the methods used in this study, and characterized mineral and plant raw materials.

For mineral raw materials, chemical and mineralogical characteristics of natural hydraulic lime - NHL3.5, slaked lime and MK were characterized by X-ray diffraction and thermogravimetric analyses. These analyses allowed us to calculate the content of $Ca(OH)_2$

containing in NHL3.5 and slaked lime in order to determine the optimal content of two pozzolanic binders (between NHL3.5 or slaked lime and MK). Additionally, we introduced the characteristics of the mineral and organic admixtures (K_2SO_4 and glycerol carbonate respectively) as well as the superplasticizer.

For the hemp aggregates, we characterized physical properties of hemp shives: bulk density, thermal conductivity, water absorption and particle size distribution. Our results confirmed that hemp shives are light weight (bulk density is 110.9 ± 0.7 kg/m^3), very low thermal conductivity (0.0580 ± 0.0004 W/m/K – it is comparable to traditional loose-fill insulation materials). Moreover, we also confirmed the great capacity of water absorption of this material, which is comparable with that in literature. Particle size distribution (PSD) of hemp shives were measured by two methods: mechanical sieving and image analysis methods. We remarked that PSD of hemp shives according to mechanical sieving method depends on vibration time and sample weight, while it does not depend on vibration frequency. The image analysis method, using ImageJ software, measured many parameters of the hemp particles (area, perimeter, length, width, etc.), which is considered as an advantage of this method in comparison with mechanical sieving method.

The third chapter presented our results for new pozzolanic binders. It was divided into two parts: optimization of raw material contents for two pozzolanic binders (from NHL3.5 or slaked lime and MK) and influence of glycerol carbonate and K_2SO_4 admixtures on the properties of the pozzolanic binders.

In the first part, we optimized the mineral materials for two control pozzolanic binders (HM and SM) based on their mechanical strengths: HM binder reaches the highest mechanical strength at early age, nevertheless the SM binder is the most efficient after 28 days. The mineral material content of these two control binder are determined by weight as follows: the first (HM) included 50% NHL3.5 and 50% MK, the second (SM) included 30% slaked lime and 70% MK. Moreover, thanks to using very high content of flash metakaolin, both of HM and SM binders are very interesting in the areas of the economics and the sustainable development in the construction.

In the other parts, we studied the influence of glycerol carbonate and K_2SO_4 admixtures on the properties of the pozzolanic binders.

For the mechanical properties, our results showed that glycerol carbonate decreased the compressive strength, while K_2SO_4 improved significantly strength of the binders

especially at early age. The binders containing both glycerol carbonate and K_2SO_4 (SCP and HCP) had the highest strength. Moreover, at early age (2 days), the strength of HP, HCP, SP and SCP binders was comparable with that of Portland cement paste. In comparison with commercial binder (CB), the strength of our binders with slaked lime (SP and SCP) was 1.3 to 1.5 times higher, while HCP binder's strength was about 1.2 times higher at 2 and 7 days, but approximately 1.1 to 1.2 times lower at 28 and 49 days.

For shrinkage reducing effect, our measurements confirmed that glycerol carbonate reduces significantly the shrinkage of the pastes (HC and SC), while the shrinkage-reducing effect of K_2SO_4 (for HP and SP pastes) showed the best results. We also illustrated that the binders containing both of glycerol carbonate and K_2SO_4 (HCP and SCP) presented the similar shrinkage-reducing effect with the binders containing K_2SO_4 admixture (HP and SP) respectively.

The results of calorimetric test showed that glycerol carbonate retarded, while K_2SO_4 encouraged the hydration reaction of the binders; moreover, the hydration reaction of the binders containing both admixtures was also encouraged. This can explain the significant improvement of strength of the binders containing K_2SO_4 (HP and SP) as well as of the binders containing both admixtures (HCP and SCP) right at early age and the decrease of strength of the binders containing glycerol carbonate (HC and SC).

The mineralogical analyses by XRD and TGA confirmed different influences of glycerol carbonate or/and K_2SO_4 on the mineralogical characteristics of the binders. The presence of glycerol carbonate in HC and SC binders increased the formation of calcium hemicarboaluminate and contributed to form vaterite, whereas neither calcium hemicarboaluminate nor vaterite can contribute to the development of strength of HC and SC binders. In contrast, the presence of K_2SO_4 in binders leads to forms ettringite, which can explain the significant strength-enhancing effect on the binders (HP, HCP, SP and SCP). Moreover, the incorporation of both glycerol carbonate and K_2SO_4 in binders (HCP and SCP) could slightly increase ettringite formation because glycerol carbonate increases pH; therefore, the HCP and SCP binders' strength was slightly higher than that of HP and SP binders respectively.

Furthermore, the thermal conductivity measurements of the binders showed that our binders (HCP and SCP) had lower thermal conductivity against CB binder, lime binders and Portland cement paste. This illustrated that our binders are able to contribute to

increase thermal insulation of the insulating building materials using them, for example, plant concrete in general and hempcrete in particular.

On the other hand, the properties of mortars used our binders (HCP and SCP) and a commercial binder (CB) illustrated that three mortars had good fresh properties, which might compare with those of Portland cement mortar. The mechanical properties of mortars used our binders (SCP and HCP) were better than those of CB mortar, except the compressive strength at 90 days (CB mortar's strength is higher than HCP mortar's), in which the mechanical properties of SCP mortar were the best.

This chapter concluded that our binders (HCP and SCP) could be applied for fabrication of hempcrete because both of them had the best mechanical performance for the NHL3.5-MK and the SL-MK binders respectively, and the significant shrinkage-reducing effect. Moreover, they also presented the low conductivity and the suitability for economic criterion and sustainable development in construction area.

In the last chapter, we presented the hemp shiv pre-treatment, the mechanical properties and thermal conductivity, and mineralogical analyses of different hempcretes formulated with the binders previously selected.

For the pre-treatment of hemp shives, a new method for pre-treatment of hemp shives, with two conditions of conservation of treated hemp shives, was applied. The method with the conservation condition in normal room (for Treated-2 hemp shives) was much simpler than previous methods in literature, and the Treated-2 hemp shives absorbed much less water than the untreated hemp shives.

Hempcretes using our pozzolanic binder had good mechanical properties, which can be compared with the results in literature. We illustrated that the strength-enhancing effect of treated hempcretes was significant against untreated hempcrete, in which the hempcrete used Treated-2 hemp shives (SP4) had the best mechanical properties in comparison with other pozzolanic hempcretes (the strength and modulus of treated hempcretes were around 1.5 times higher than those of untreated hempcretes). However, the mechanical properties of this hempcrete were much lesser than those of hempcretes using commercial binder, which could be attributed to hemp particles causing a negative influence on the development of the pozzolanic reaction.

Moreover, the XRD and TGA analyses showed the limitation of binder hydration in the hempcrete mixtures, which may be due to the solubilisation of the polysaccharide

extractives and the degradation products of alkaline attack. The TGA result indicated that the higher quantity of C-S-H of SP4 hempcrete against that of other pozzlanic hempcretes could explain the much higher mechanical properties of SP4 hempcrete. Furthermore, a peak of ettringite was detected on the diagrams of CB hempcretes, which could explain the much higher mechanical properties of CB hempcretes in comparison with those of pozzolanic hempcretes.

This chapter also showed that the thermal conductivity of both pozzolanic hempcretes and CB hempcretes was fairly low and comparable with the results of previous studies. Our measurements could confirm that the thermal conductivity of hempcretes was directly influenced by dry density and the compaction direction, and indirectly influenced by binder nature, while it was insignificantly influenced by other factors (the relative humidity and hemp shiv pre-treatment).

Thus, this chapter concluded that the SP4 hempcrete used our pozzolanic binder is applicable to prefabricate building components for thermal insulation wall because its mechanical properties and thermal conductivity are fairly good, and the hemp shiv pre-treatment method and storage of treated hemp shives are much simpler than those in literature.

Finally, in our study, we have developed two kinds of pozzolanic binders used glycerol carbonate and potassium sulfate, which not only improve the mechanical strength and significantly reduce shrinkage but also are considered as eco-binders thanks to high contents of flash metakaolin. One of them is applied for fabrication of hempcrete with hemp shives. This hempcrete presents fairly good mechanical and thermal properties in comparison with previous studies.

FUTURE WORK

In continuation of present research work, we propose other important directions concerning both binder and hempcrete as following:

The hydration of this new pozzolanic binder should be analyzed the hydration phases in the system $CaO-SiO_2-Al_2O_3-CaSO_4-CaCO_3-H_2O$ in the presence of glycerol carbonate and potassium sulfate. In order to improve flexural strength of this binder, hemp fiber reinforcement also needs to be studied to use for coating and shotcrete.

The interaction between our binders and hemp shives is very important to study the influence of the soluble extractives from hemp shives on the hydration of binder when they associate each other in hempcrete fabrication. I would be interesting to reach the optimal method of hemp shiv pretreatment to improve the mechanical properties of hempcrete because the positive strength-enhancing effect of treated hemp shives was confirmed in this study.

For the properties of hempcrete, this study showed good mechanical properties of our pozzolanic hempcrete at 28 days, especially treated hempcrete, and their good thermal conductivity at 90 days, in which hempcrete samples were conserved in indoor condition ($20^{o}C$, 65% RH). Thus, the long term behaviors of this hempcrete is necessary to be studied, its durability needs to be assessed, and accelerated aging protocols need to be elaborated in order to endorse its application in construction. Furthermore, the hygrothermal and acoustic properties of this hempcrete also need to be studied in order to confirm the moderation of the indoor humidity variations as well as the acoustic insulation of this material.

Additionally, the numerical models should be developed to predict the hygrothermal performances of hempcrete.

Finally, it will be necessary to carry out an analysis of the life cycle of this hempcrete to clarify if this material could be in accordance with the sustainable development in the construction filed.

CONCLUSION GENERALE

Globalement, l'objectif de cette étude était de développer un nouveau matériau de construction composé d'un nouveau liant pouzzolanique et de chènevotte de chanvre, qui satisfait aux critères d'éco-matériau. Les travaux dans le cadre de cette étude sont divisés en deux parties principales : développement de nouveaux liants pouzzolaniques et développement de bétons de chanvre utilisant notre liant pouzzolanique. Le manuscrit a étéprésenté en quatre chapitres.

Dans le chapitre *État de l'art*, nous avons rappelé le concept de développement durable. Pour le secteur de la construction, ce chapitre démontre la nécessité de remplacer les matériaux de construction traditionnels par des éco-matériaux. Il est également indiqué que le béton de chanvre fait de liants minéraux et de chènevotte a encore besoin d'être développé et en particulier pour des murs devant présenter une bonne isolation thermique parce qu'il a non seulement un bon comportement thermique et un faible coût, mais aussi un respect de l'environnement.

Pour les matériaux minéraux, ce chapitre a souligné que le métakaolin flash (MK) est l'un des meilleurs éco-matériaux, car sa production consomme beaucoup moins d'énergie que celle du ciment Portland et émet peu de CO_2. En outre, la chaux hydraulique naturelle et la chaux éteinte sont également considérées comme des éco-matériaux en comparaison avec le ciment Portland. Ainsi, ce chapitre nous a amené à choisir le métakaolin flash, la chaux hydraulique naturelle - NHL3.5 et la chaux éteinte pour développer deux types de liants pouzzolaniques. D'autre part, le carbonate de glycérol, le sulfate de potassium et le superplastifiant ont été également retenus pour améliorer la résistance mécanique au jeune âge et réduire le retrait de ces liants.

Pour les granulats végétaux, ces matériaux combinent plusieurs avantages pour l'environnement : ils sont locaux et les ressources sont renouvelables, ils sont neutres en carbone et leur énergie intrinsèque est généralement faible. Des travaux antérieurs nous ont permis de sélectionner la chènevotte parce qu'il s'agit d'un éco-matériau disponible à Toulouse (dans notre cas) ; en outre, elle a un faible coût et a de bonne propriétés thermiques. Ce chapitre a montré également qu'il est nécessaire de développer de nouvelles méthodes de pré-traitement de la chènevotte, les plus simples possible, de manière à réduire la capacité d'absorption d'eau de chènevotte.

189

Dans le deuxième chapitre, nous avons décrit les méthodes utilisées dans cette étude, et caractérisé les matières premières minérales et végétales.

Pour les matières premières minérales, les caractéristiques chimique et minéralogique de la chaux hydraulique naturelle - NHL3.5, de la chaux éteinte et du MK ont été déterméees par diffraction de rayons X et analyses thermogravimétriques. Ces analyses nous ont permis de calculer le teneur en $Ca(OH)_2$ contenu dans la chaux hydraulique et dans la chaux éteinte afin de déterminer le teneur optimale des deux liants pouzzolaniques (entre NHL3.5 ou la chaux éteinte et MK). En outre, nous avons présenté les caractéristiques des adjuvants minéraux et organiques (K_2SO_4 et carbonate de glycérol) ainsi que du superplastifiant.

Pour les particules de chènevotte, nous avons caractérisé plusieurs propriétés physiques de la chènevotte : la densité en vrac, la conductivité thermique, l'absorption d'eau et la granulométrie. Nos résultats ont confirmé que la chènevotte est légère (densité en vrac de 110,9 $\pm$ 0,7 kg/m^3), avec une très faible conductivité thermique (0,0580 $\pm$ 0,0004 W/m/K, comparable à celle des matériaux isolants en vrac). En outre, nous avons également confirmé la grande capacité d'absorption d'eau de ce matériau, comparable à celle donnée dans la littérature. La granulométrie (PSD) de la chènevotte a été mesurée par deux méthodes : par tamisage mécanique et par analyse d'image. Nous avons remarqué que le PSD de la chènevotte avec la méthode de tamisage mécanique dépend du temps de vibration et du poids de l'échantillon, mais ne dépend pas de la fréquence de vibration. L'analyse d'image, effectuée avec le logiciel ImageJ, a permis de mesurer de nombreux paramètres des particules de chènevotte (aire, périmètre, longueur, largeur, *etc.*), ce qui est considéré comme un avantage en comparaison avec la méthode de tamisage mécanique.

Le troisième chapitre, consacré à la présentation de nos résultats pour les nouveaux liants pouzzolaniques, a été divisé en deux parties : l'optimisation de la teneur en matières premières pour les deux liants pouzzolaniques (NHL3.5 ou chaux éteinte et MK) et l'influence des adjuvants (carbonate de glycérol et K_2SO_4) sur les propriétés de ces liants pouzzolaniques.

Dans la première partie, nous avons optimisé les matériaux minéraux pour deux liants témoins (HM et SM) en fonction de leurs résistances mécaniques : le liant HM atteint la plus haute résistance mécanique au plus jeune âge, alors que le liant SM est le plus efficace après 28 jours. Les teneurs massiques de ces deux liants témoins sont de 50%

190

de NHL3.5 et 50% de MK pour le premier (HM et de 30% de chaux éteinte et 70% de MK pour le deuxième (SM). Ainsi, grâce à l'utilisation d'une très haute teneur en métakaolin flash, les deux liants (HM et SM) sont très intéressants dans les domaines de l'économie et du développement durable pour la construction.

Dans la deuxième partie, nous avons étudié l'influence de carbonate de glycérol et du K_2SO_4 sur les propriétés des liants pouzzolaniques.

Pour les propriétés mécaniques, nos résultats ont montré que le carbonate de glycérol diminue la résistance en compression, tandis que le K_2SO_4 améliore significativement la résistance en compression, en particulier aux très jeunes âges. Les liants contenant à la fois le carbonate de glycérol et le K_2SO_4 (SCP et HCP) présentent les plus hautes résistances. En outre, aux très jeunes âges (2 jours), la résistance en compression des liants HP, HCP, SP et SCP est comparable à celle du ciment Portland. En comparaison avec le liant commercial (CB), la résistance en compression de nos liants avec la chaux éteinte (SP et SCP) est de 1,3 à 1,5 fois plus élevé, tandis que la résistance en compression du liant HCP est environ 1,2 fois supérieure à 2 et 7 jours, mais environ 1,1 à 1,2 fois inférieure à 28 et 49 jours.

Concernant l'effet de ces produits sur la réduction des variations dimensionnelles, nos mesures ont confirmé que le carbonate de glycérol réduit significativement le retrait des pâtes (HC et SC), mais l'effet de réduction du retrait du K_2SO_4 (pour les pâtes HP et SP) est plus important. Nous avons également montré que les liants contenant à la fois le carbonate de glycérol et le K_2SO_4 (HCP et SCP) ont un effet semblable aux liants contenant seulement du K_2SO_4 (HP et SP).

Les résultats des essais en calorimétrie adiabatique ont montré que le carbonate de glycérol a un effet retard, tandis que le K_2SO_4 favorise la réaction d'hydratation des liants ; en outre, la réaction d'hydratation des liants contenant les deux adjuvants est également favorisée. Ceci peut expliquer l'amélioration significative de la résistance mécanique des liants contenant du K_2SO_4 (HP et SP) et des liants contenant les deux adjuvants (HCP et SCP) aux très jeunes âges ainsi que la diminution de la résistance des liants contenant le carbonate de glycérol (HC et SC).

Les analyses minéralogiques par DRX et ATG ont confirmé les différentes influences du carbonate de glycérol et/ou du K_2SO_4 sur les caractéristiques minéralogiques

191

des liants. La présence de carbonate de glycérol dans les liants HC et SC augmente la formation de l'hémicarboaluminate de calcium et contribue à former de la vatérite, ces composés ne contribuant pas au développement de la résistance des liants HC et SC. En revanche, la présence de K_2SO_4 dans les liants conduit à la formation d'ettringite, ce qui peut expliquer l'effet d'amélioration significative de la résistance sur les liants (HP, HCP, SP et SCP). L'incorporation simultanée du carbonate de glycérol et du K_2SO_4 dans les liants (HCP et SCP) semble augmenter légèrement la formation d'ettringite du fait que le carbonate de glycérol augmente le pHce qui expliquerait la meilleure résistance des liants HCP et SCP par rapport à celle des liants HP et SP.

En outre, la mesure de conductivité thermique des liants a montré que nos liants (HCP et SCP) avaient une très faible conductivité thermique par rapport au liant commercial CB, à la chaux ou au ciment Portland. Cela montre que nos liants sont en mesure de contribuer à augmenter l'isolation thermique des matériaux de construction qui les utilisent, par exemple, avec les bétons végétaux en général et le béton de chanvre en particulier.

Enfin, les propriétés à l'état frais des mortiers confectionnés avec nos liants (HCP et SCP) sont bonnes et comparables avec celles d'un mortier de ciment Portland. Les propriétés mécaniques des mortiers utilisant le liant SCP sont meilleures que celles du mortier CB, à l'exception de la résistance en compression à 90 jours (la résistance du mortier CB est plus élevée que celle du mortier HCP), alors que les propriétés mécaniques du mortier SCP restent les meilleures.

Ce chapitre permet de conclure que nos liants (HCP et SCP) pourraient être appliqués pour la fabrication de béton de chanvre parce qu'ils ont de meilleures performances mécaniques que les liants NHL3.5-MK et SL-MK, et ont un bon effet de réduction du retrait. En outre, ils présentent une faible conductivité et restent performants sur les critères économique et du développement durable dans e domaine de la construction.

Dans le dernier chapitre, nous avons présenté le pré-traitement de la chènevotte, les propriétés mécaniques, la conductivité thermique et les analyses minéralogiques de différentes formules de bétons de chanvre avec les liants sélectionnés précédemment.

Pour le pré-traitement de la chènevotte, une nouvelle méthode de pré-traitement avec deux conditions de conservation des chènevottes traitées, a été appliquée. La méthode de conservation en condition ambiante (chènevotte traitée-2) s'avère beaucoup plus simple que les méthodes citées dans la littérature, et cette chènevotte traitée-2 absorbe beaucoup moins d'eau que la chènevotte non traitée.

Le béton de chanvre utilisant notre liant pouzzolanique a obtenu de bonnes propriétés mécaniques, qui peuvent être comparées avec les résultats de la littérature. Nous avons montré que les propriétés mécaniques du béton de chanvre utilisant la chènevotte traitée étaient significativement plus élevées que celles du béton de chanvre utilisant la chènevotte non traitée. Le béton de chanvre utilisant la chènevotte traitée-2 (SP4) présente les meilleures propriétés mécaniques en comparaison avec d'autres bétons de chanvre pouzzolaniques (la résistance et le module de béton de chanvre utilisant la chènevotte traitée étaient environ 1,5 fois plus élevés que ceux des bétons de chanvre utilisant la chènevotte non traitée). Cependant, les propriétés mécaniques de ces bétons sont restées plus faibles que celles du béton de chanvre utilisant le liant commercial ? Ceci pourrait être attribuée aux particules de chènevotte qui provoquent une influence négative sur le développement de la réaction pouzzolanique.

Les analyses par DRX et ATG ont confirmé la limitation de l'hydratation du liant pouzzolanique dans le béton de chanvre, qui peut être due à la solubilisation des polysaccharides e et aux produits de dégradation de l'attaque alcaline. Les résultats de l'ATG ont montré une plus grande quantité de C-S-H dans le mélange SP4 par rapport aux autres mélanges ce qui pourrait expliquer les propriétés mécaniques très élevées du mélange SP4. En outre, un pic d'ettringite a été détecté sur les diagrammes des mélanges C et CP, ce qui pourrait expliquer les propriétés mécaniques très élevées de ces mélanges en comparaison avec celles des autres mélanges.

Ce chapitre montre également que la conductivité thermique des deux types de bétons de chanvre était assez faible et comparable avec les résultats des études précédentes. Nos mesures confirment que la conductivité thermique du béton de chanvre est directement influencée par la densité sèche et le sens de compactage, et indirectement influencée par la nature du liant, les autres facteurs (humidité relative et prétraitement de chènevotte) ayant un effet négligeable.

Ainsi, ce chapitre a permis de conclure que le béton de chanvre SP4 utilisant notre liant pouzzolanique peut servir à fabriquer des éléments de construction préfabriqués pour des murs présentant une bonne isolation thermique parce que ses propriétés mécaniques et sa conductivité thermique sont assez bonnes, et que la méthode de prétraitement de la chènevotte et de stockage de la chènevotte traitée est beaucoup plus simple que celles décrites dans la littérature.

Enfin, dans le cadre de notre étude, nous avons développé deux types de liants pouzzolaniques utilisant du carbonate de glycérol et du sulfate de potassium, qui non seulement améliorent la résistance mécanique et réduisent le retrait, mais sont également considérés comme des éco-liants grâce à une haute teneur en métakaolin flash. L'un d'entre eux est parfaitement applicable pour la fabrication du béton de chanvre. Ce béton présente de bonnes propriétés thermiques et mécaniques en comparaison avec la bibliographie.

PERSPECTIVES

Dans le cadre de la poursuite des travaux de recherche, nous proposons d'autres directions importantes concernant les liants et le béton de chanvre:

L'hydratation de ce nouveau liant pouzzolanique doit être analysée par des diagrammes de phase inhérents au système CaO-SiO_2-Al_2O_3-$CaSO_4$-$CaCO_3$-H_2O que l'on a en présence de carbonate de glycérol et de sulfate de potassium. Afin d'améliorer la résistance en flexion de ce liant, le renfort par des fibres de chanvre doit être également étudié pour une utilisation comme enduit epo pour du béton projeté.

L'interaction entre nos liants et la chènevotte est très importante et il convient d'étudier l'influence des produits extractibles solubles de la chènevotte sur l'hydratation du liant pour améliorer la fabrication du béton de chanvre. Il serait intéressant de parvenir à une méthode optimale du prétraitement de la chènevotte pour améliorer les propriétés mécaniques du béton de chanvre compte tenu de l'effet positif de la chènevotte prétraitée démontrée dans cette étude.

Pour les propriétés du béton de chanvre, cette étude a montré de bonnes propriétés mécaniques pour les bétons de chanvre utilisant nos liants pouzzolaniques à 28 jours, en particulier les bétons de chanvre avec la chènevotte prétraitée, et leur bonne conductivité thermique à 90 jours, dans lequel les échantillons ont été conservés en conditions contrôlées ($20^{o}C$, 65% HR). Le comportement de ce béton de chanvre à long terme reste à étudier, sa durabilité doit être évaluée, et une procédure de vieillissement accéléré doit être élaborée afin de démontrer son application dans le domaine de la construction. En outre, les propriétés hygrothermique et acoustique de ce béton doivent être également étudiées afin de confirmer la limitation de la variation d'humidité intérieure ainsi que l'isolation acoustique de ce matériau.

En outre, les modèles numériques devraient être mis au point pour prévoir les performances hygrothermiques du béton de chanvre.

Enfin, il sera nécessaire de procéder à une analyse du cycle de vie de ce produit fini afin de conclure sans équivoque sur la conformité avec le développement durable dans la construction de ce nouveau matériau.

References

STANDARDS

NF EN 196-1 Methods of testing cement - Determination of strength

NF EN 196-9 Heat of hydration - Semi-adiabatic method

NF EN 459-1 Building lime Part 1 Definitions, specifications and conformity criteria

NF EN 480-2 Admixtures for concrete, mortar and grout, Test method's - Determination of setting time

NF P18-452 Measuring the flow time of concrete and mortar using workability meter

[AGG11] E. Aggelakopoulou, A. Bakolas & A. Moropoulou (2011). Properties of lime–metakolin mortars for the restoration of historic masonries. *Applied Clay Science*. Vol. 53, pp. 15 -19

[AGR13] http://www.cd2e.com/eco_materiaux/fiche?id_mat=142&type=consultation

[AMZ12] S. Amziane & L. Arnaud (2012). Bio-aggregate-based Building Material. ISTE Ltd and John Wiley & Sons, Inc.

[APP03] G. Appa Rao (2003). Investigations on the performance of silica fume-incorporated cement pastes and mortars. Cement and Concrete Research. Vol. 33, pp. 1765–1770

[ARA05] M. Arandigoyen, J.L. Pérez Bernal, M.A. Bello López and J.I. Alvarez (2005). Lime-pastes with different kneading water- Pore structure and capillary porosity. *Applied Surface Science*. Vol. 252, pp. 1449–1459

[ARG10] Argeco (2010). Fiche Technique argicem

[ARN08] L. Arnaud (2008). Synthèse des connaissances sur les bétons et mortiers de chanvre.

[ARN09] L. Arnaud (2009). Comparative study of hygrothermal performances of building materials. 11th international conference on non-conventional materials and technologies (NOCMAT2009). Bath, United Kingdom

[ARN12] L. Arnaud, E. Gourlay (2012). Experimental study of parameters influencing mechanical properties of hemp concretes. *Construction and Building Materials*. Vol. 28, pp. 50-56

[ASS07] Association Construire en Chanvre (2007). Construire en chanvre: Règles professionnelles d'éxécution. *Fédération Française du Bâtiment*.

[AST11] Saint-Astier (2011). Batichanvre - Fiche Technique

[BAK06] A. Bakolas, E. Aggelakopoulou. A. Moropoulou and S. Anagnostopoulou (2006). Evaluation of pozzolanic activity and physicomechanical characteristics in metakaolin-lime pastes. *Journal of Thermal Analysis and Colorimetry*. Vo1 84. p157-163

[BAN07] M. Bandres (2007). Synthèse de solvants et plastifiants d'origine naturelle selon une démarche d'éco-conception. *Thèse de doctorant. Institut National Polytechnique de Toulouse.*

[BEN08] A. Benazzouk, O. Douzane, K. Mezreb, B. Laidoudi, M. Quéneudec (2008). Thermal conductivity of cement composites containing rubber waste particles: Experimetal study and modelling. *Construction and Building Materials*. Vol. 22, pp. 573 - 579

[BEN12a] E. Benhelal, G. Zahedi, E. Shamsaei & A. Bahadori (2012). Global strategies and potentials to curb CO2 emissions in cement industry. *Journal of Cleaner Production*. Vol 51. Pp 142-161

[BEN12b] E. Benhelal, G. Zahedi & H. Hashim (2012). A novel design for green and economical cement manufacturing. *Journal of Cleaner Production*. Vol 22. Pp 60-66

[BIC05] C. Bich (2005). Contribution à l'étude de l'activation thermique du kaolin: évolution de la structure cristallographique et activité pouzzolanique. *Thèse de doctorant, INSA de Lyon*

[BIL11] N. Billong, U.C. Melo, E. Kamseu, J.M. Kinuthia, D.Njopwouo (2011). Improving hydraulic properties of lime-rice husk ash binder with metakaolin. *Construction and Building Materials*. p2157-2161

[BIN12] S. Bin & L. Jun (2012)**.** Building Energy Effeciency Polisies in China. Global Buildings Performance Network

[BOU12] Bourgogn Conseil Régional (2012). Etat des lieux des connaissances actuelles sur le Fonctionnement Hygrothermique des matériaux biosourcés. *Document Technique C&B*. Ministère de l'Écologie du Développement durable et de l'Énergie

[BPI11] Buildings Performance Institute Europe (2011). Europe's Buildings under the Microscope

[BRA12] A. Brasa and F. M. A. Henriques (2012). Natural hydraulic lime based grouts - The selection of grout injection parameters for masonry consolidation. *Construction and Building*. Materials, 26, p. 135-144,2012.

[BRO01] J. J. Brooks, M. A. Megatjohari (2001). Effect of metakaolin on creep and shrinkage ofconcrete. *Cement and Concrete Composites*. Vol.234, pp. 495-502

[BRU87] G. H. Brudtland (1987). Report of the World Commission on Environment and Development: Our Common Future.

[BRU08] P. Bruijn (2008). Hemp Concretes, Mechanical Properties using both Shives and Fibres. *Licentiate thesis. Swedish University of Agricultural Sciences*

[BRU09] P. B. Bruijn, K. H. Jeppsson, K. Sandin and C. Nilsson (2009). Mechanical properties of lime–hemp concrete containing shives and fibres. *Biosystems Engineering*. Vol. 03, pp. 474 – 479

[BRU13] P. De Bruijn & P. Johansson (2013). Moisture fixation and thermal properties of lime–hemp concrete. Construction and Building Materials. Vol. 47, pp. 1235–1242

[BUR08] A. U. Buranov and G. Mazza (2008). Lignin in straw of herbaceous crops. *Industrial Crops and Products*. Vol. 28, pp. 237–259

[CAB00] J. Cabrera1, R. M. Frías (2000). Mechanism of hydration of the metakaolin lime water system.

[CAR09] F. A. Cardoso, H. C. Fernandes, R. G. Pileggi, M. A. Cincotto, V. M. John. Carbide lime and industrial hydrated lime characterization. *Powder Technology*, Volume 195, Issue 2, 25 October 2009

[CAS07] F. Cassagnabere (2007). Produits prefabriques en beton file vers l'amelioration des performances du materiau pour mieux gerer le procede de production, *Thèse de doctorant. Université de Toulouse*

[CAS09] F. Cassagnabère, G. Escadeillas and M. Mouret (2009). Study of the reactivity of cement/metakaolin binders at early age for specific use in steam cured precast concrete. *Construction and Building Materials*. Vol. 23, pp 775–784

[CAS13]. F. Cassagnabère, P. Diederich, M. Mouret, G. Escadeillas and M. Lachemi (2013). Impact of metakaolin characteristics on the rheological properties of mortar in the fresh state. *Cement & Concrete Composites*. Vol. 37, pp. 95–107

[CER05] V. Cerezo (2005). Propriétés mécaniques, thermiques et acoustiques d'un matériau à base de particules végétales: Approche expérimentale et modélisation théorique. *Thèse de doctorant de l'ENTPE*

[CER06] R. Cerny, A. Kunca, V. Tydlita, J. Drchalova and P. Rovnanikova (2006). Efcect of pozzolanic admixture on mechanical, thermal and hygrocproperties oflime plasters. Construction and Building Materials. Vol. 20, pp. 849–857

[CHA08] J. Chamoin, F. Collet, S. Pretot (2008). Optimisation de bétons de chanvre projeté et moulé – Caractérisation du matériau de référence. *Rencontre de l'AUGC 2008, Nancy 4-6 juin*

[CLE05] J.H. Clements, K. Darragas & H.P. Klein (2005). Alkylene and glycerin carbonate compositions as sodium silicate curing accelerator catalysts. *Huntsman Petrochemical Corporation*. WO 2005042430.

[COL04] F. Collet (2004). Caractéristique hydrique et thermique de matériaux de génie civil à faibles impacts environnementaux. *Thèse de Doctorat de l'INSA de Rennes*.

[COL08] F. Collet, Marjorie Bart, Laurent Serres, Jacques Miriel (2008). Porous structure and water vapour sorption of hemp-based materials. *Construction and Building Materials*. Volume 22 (2008) 1271-1280

[COL12] Collet, F. and S. Pretot (2012). Experimental investigation of moisture buffering capacity of sprayed hemp concrete. *Construction and Building Materials*. Vol. 36, pp. 58–65

[COL13] F. Collet, S. Pretot and C. Lanos (2013). Performance hydrique de bétons de chanvre- effet de l'enduit sur leur capacité de régulateurs hydriques. *31èmes Rencontres de l'AUGC, E.N.S. Cachan*

[COL13a] F. Collet, J. Chamoin, S. Pretot and C. Lanos (2013). Comparison of the hygric behaviour of three hemp concretes. *Energy and Buildings*. Vol. 62, pp. 294–303

[CON07] A. B. Constatinos, G. G. Athina, G. Elena, M. Sevastianos, S. Yiannis and P. L. Dimitris (2007). European residential buildings and empirical assessment of the Hellenic building stock, energy consumption, emissions and potential energy savings. *Building and Environment*. Vol. 42, pp. 1298 – 1314

[COR99] C. Cordier (1999). Caractérisation thermique et mécanique des bétons de chanvre. Rapport de stage de fin d'études. Ecole doctorat MEGA. Vaulx-en-Velin : ENTPE

[COU84] R. S. P. Coutts & P. Kightly (1984). Bonding in wood fibre-cement composites. *Journal of Materials Science*. Vol 19 3355-3359

[COU03] L. Courard, A. Darimont, M. Schouterden, F. Ferauche, X. Willem & R. Degeimbre (2003). *Cement and Concrete Research*. Vol. 33, pp. 1473 – 1479

[CYR11] M. Cyr & G. Escadeillas (2011). Normalisation du métakaolin : pourquoi, comment? *XXIXe Rencontres Universitaires de Génie Civil*. Tlemcen, 29 au 31 Mai 2011.

[DAM10] B. L. Damineli, , F.M. Kemeid, P.S. Aguiar & V.M. John (2010). Measuring the eco-efficiency of cement use. *Cement & Concrete Composites*. Vol 32 555–562

[DEA11] C. C. Dean, , J. Blamey, N.H. Florin, M.J. AlJeboori & P.S. Fennell (2011). The calcium looping cycle for CO2 capture from power generation, cement manufacture and hydrogen production. *Chemical Engineering Research and Design*. Vol 89 836-855

[DEM03] R. Demirboga (2003). Influence of mineral admixtures on thermal conductivity and compressive strength of mortar. *Energy and Buildings.* Vol. 35. Pp 189-192

[DES11] www.dessine-moi-une-maison.fr

[DIQ12] Y. Diquélou (2012). Interface granulats de chanvre - matrice minérale. *Technique Construction Chanvre - Sens, INRA – UMR FARE Reims* .

[DIN99] I. Dincer (1999). Environmental impacts of energy. Energy Policy. Vol 27 845-854

[DOM06] N. Domede (2006). Méthod de requalificatioo des ponts en maçonnerie. *Thèse doctorant. INSA-Toulouse.*

[DON12] R. Dong, H. Lu, Y. Yu, Z. Zhang (2012). A feasible process for simultaneous removal of CO2, SO2 and NOx in the cement industry by NH3 scrubbing. *Applied Energy*. Vol 97 185–191

[EIR06] R. Eires, J. P. Nunes, R. Fangueiro, S. Jalali and A. Camões (2006). New eco-friendly hybrid composite materials for civil construction. *European Conference on Composite Materials*. Biarritz, France

[ELF08] S. Elfordy, F.Lucas, F.Tancret, Y. Scudeller, L. Goudet (2008). Mechanical and thermal properties of lime and hemp concrete "hempcrete" manufactured by a projection process. *Construction and Building Materials.* Volume 22 2116-2123

[EIR] R. Eires, JP. Nunes, R. Fangueiro, S. Jalali, A. Camões. New eco-friendly hybrid composite materials for civil construction.

[ESC06] G. Escadeillas (2006). Les éco – matériaux dans la construction: Enjeux et perspectives. *Septième édition des journées scientifiques du Regroupement francophone pour la recherche et la formation sur le béton.* Toulouse, France pp. 56 – 65

[ESC12] G. Escadeillas, V. T. Nguyen, S. Julien & J. P Tardy (2012). Ciment pouzzolanique pour traitement de sol

[EVR08] A. Evrard (2008). Transient hygrothermal behaviour of Lime-Hemp Masterials. *Thèse doctorant. Ecole Polytechnique de Louvain*

[EUR11] European Commission (2011). Reducing the environmental impact of building materials

[FOR06] C. Fortes-Revilla, S. Martínez-Ramírez & M. T. Blanco-Varela (2006). Modelling of slaked lime–metakaolin mortar engineering characteristics in terms of process variables. *Cement & Concrete Composites*. 458 – 467

[FRI02] R. M. Frías & J. Cabrera (2002). Influence of MK on the reaction kinetics in MK/lime and MK-blended cement systems at 20°C. *Cement Concrete Research*. Vol. 31, pp. 519-527.

[FRI03] R. M. Frías & M.I. Sánchez de Rojas (2003).The effect of high curing temperature on the reaction kinetics in MK/lime and MK-blended cement matrices at 60°C. *Cement Concrete Research*. Vol. 33, pp. 643-649

[FRI06] R. M. Frías (2006). Study of hydrated phases present in a MK–lime system cured at 60°C and 60 months of reaction. *Cement Concrete Research*. Vol. 36, pp. 827-831

[GAR04] E. Gartner (2004). Industrially interesting approaches to ''low-CO2'' cements. *Cement and Concrete Research*. Vol 34 1489–1498

[GIE97] D. J. Gielen (1997). Building Materials and CO_2 - Western European emission reduction strategies

[GLE07] P. J. P. Gleize, M. Cyr and G. Escadeillas (2007). Effect ofmelakaolin on autogenousShrinkage of cementpaste. *Cement and Concrete Composite*. Vol. 29, pp. 80-87

[GLE11] P. Glé, E Gourdon, L. Arnaud (2011). Acoustical properties of materials made of vegetable particles with several scales of porosity. *Applied Acoustics*.

[GOV04] A. Govin, (2004). Aspects physico – chimiques de l'interation bois – ciment – Modification de l'Hydratation du ciment par le bois. *Thèse de doctorant. Ecole Nationale Supérieure Des Mines De Saint Etienne et Université Jean Monnet De Saint Etienne.*

[GUA06] A. F. Gualtieri, A. Viani & C. Montanari (2006). Quantitative phase analysis of hydraulic limes using the Rietveld method. *Cement Concrete Research*. 36, 401-406

[IGA09] C. Igathinathane, L.O. Pordesimo, E.P. Columbus, W. D. Batchelor and S. Sokhansanj (2009). Sieveless particle size distribution analysis of particulate materials through computer vision. *Computers and Electronics in Agriculture.* Vol. 66, pp. 147–158

[ITA07] Italcementi Group (2007). Sustainable Development Report

[IZA10] A. Izaguirre, J. Lanas and J.I. Álvarez (2010). Ageing of lime mortars with admixtures: Durabilityand strength assessment. *Cement and Concrete Research*. Vol. 40, pp. 1081–1095

[IZA11] A. Izaguirre, J. Lanas and J.I. Álvarez (2011). Characterization of aerial lime-based mortars modified by the addition of two different water-retaining agents. *Cement & Concrete Composites*. Vol. 33, pp. 309–318

[KAK00] G. Kakali, S. Tsivilis, E. Aggeli & M. Bati (2000). Hy dartion products of C3A, C3 S and Portland cement in the presence of $CaCO_3$. *Cement and Concrete Research*. Vol. 30, pp. 1073-1077

[KHA96] J. M. Khatib and S. Wild (1996).Pore size distribution of metakaolin paste. *Cement and Concrete Research*. Vol. 26, pp. 1545-1553

[KHA98] J. M. Khatib and S. Wild(1998).Sulphate Resistance of Metakaolin Mortar. *Cement and ConcreteResearch*. Vol. 28, pp. 83–92

[KHA05] J. M. Khatib, J. J. Hibbert (2005). Selected engineering properties of concrete incorporating slag and metakaolin. *Construcfion and Building Materials*. Vol. 19, pp. 460-472

[KHA08] M. Khazma, N. Hajj, A. Goullieux, R.M. Dheilly & M. Queneudec (2008). Influence of sucrose addition on the performance of a lignocellulosic composite with a cementious matrix. Composites. Vol. 39, 1901–1908.

[KOB11] N. Kob, Huntsman & Aisa Sendijarevic, N. Lathia and T. Polymers (2011). Application Glycerine Carbonate in Novel one-Component Polyurethane Blocked Systems

[KOS83] M. Kosik, I. Surina, L. Lapcik, I. Rucka, and V. Reiser (1982). Thermolytic reaction of cellulose I. Dehydration reaction of cellulose. Chem. Zvesti. Vol. 37, 843 – 850.

[KOS06] S. Koseoglu, Glycerol Production and Utilization, Practical Short Courses on Biodiesel : Market, Trends, Chemistry and Production

[KUM06]M. K. Kumaran (2006). A Thermal and moisture property database for common building and insulation materials. National Research Council Canada, Ottawa, Ontario K1A 0R6, Canada

[KYD11] E. H. Kadri, S. Kenai, K. Ezziane, R. Siddique, G. De Schutter (2011). Influence of MK and silica fume on the heat of hydration and compressive strength development of mortar. *Applied Clay Science*. Vol. 53, pp. 704–708

[KYO97] Kyoto Protocol to the United Nations Framework Convention on Climate Change.

[LAN03] J. Lanas and J. I. Alvarez (2003). Masonry repair lime-based mortars: Factors affecting the mechanical behavior. *Cement and Concrete Research*. Vol. 33, pp. 1867–1876

[LAN04] J. Lanas, J. L. Pérez Bernal, M.A. Bello, J.I. Alvarez Galindo (2004). Mechanical properties of natural hydraulic lime-based mortars. *Cement and Concrete research*. p2191-2201

[LAN05] J. Lanas, R. Sirera and J.I. Alvarez (2005). Mechanical properties of masonry repair dolomitic lime-based mortars. *Thermochimica Acta*. Vol. 429, pp. 219–226

[LAW06] R. M. Lawrence, T. J. Mays, P. Walker, D. D'Ayala (2006). Determination of carbonation frofiles in non-hydraulic lime mortars using thermogravimetric analysis. *Thermochimica acta*. Vol. 444, p179-189

[LAW07] R. M. Lawrence, T. J. Mays, S. P. Rigby, P. Walker and D. D'Ayala (2007). Effects of carbonation on the pore structure of non-hydraulic lime mortars. Cement and Concrete Research. Vol. 37, pp. 1059–1069

[LIN02] P. Linger, J. Mussig, H. Fischer and J. Kobert (2002). Industrial hemp (Cannabis sativa L.) growing on heavy metal contaminated soil- fibre quality and phytoremediation potential. *Industrial Crops and Products*. Vol. 16, pp. 33–42

[LOR08] Loreti Group (2008). Greenhouse gas emission reductions from blended cement production. California Climate Action Registry

[LOT08] B. Lothenbach, G. L. Saout, E. Gallucci & K. Scrivener (2008). Influence of limestone on the hydration of Portland cements. *Cement and Concrete Research*. Vol. 38, pp. 848-860

[MAA10] O. A. Martinez-Aguilar, P. Castro-Borges, J. I. Escalante-García (2010). Hydraulic binders of Fluorgypsum–Portland cement and blast furnace slag, stability and mechanical properties. *Construction and Building Materials*. Vol. 24. pp 631–639

[MAG08] C. Magniont, G. Escadeillas, C. O. Multon, Pascale De Caro (2008). Effects of incorporation of glycerol carbonate and flax fibres into a pozzolanic matrix

[MAG10a] C. Magniont, G. Escadeillas, C. Oms-Multon & P. De Caro (2010). The benefits of incorporating glycerol carbonate into an innovative pozzolanic matrix. *Cement Concrete Research*. Vol. 40, pp. 1072-1080

[MAG10b] C. Magniont (2010). Contribution à la formulation et à la caractérisation d'un écomatériau de construction à base d'agroressources. *Thèse de doctorant*, *Université de Toulouse*

[MAG12] C. Magniont, , G. Escadeillas, M. Coutand & C. Oms-Multon (2012). Use of plant aggregates in building ecomaterials. *European Journal of Environmental and Civil Engineering*. Vol. 16, pp. 17-33

[MAL00] V. M. Malhotra (2000). Role of supplementary cementing materials in reducing greenhouse gas emissions. In: Gjorv OE, K. Sakai, editors. Concrete technology for a sustainable development in the 21st century. E&FN SPON; p. 226–235.

[MAR10] M. C. Martín-Sedeño, A.J.M. Cuberos, A.G. De la Torre, G. Álvarez-Pinazo, L.M. Ordónez, M. Gateshk, M.A.G. Aranda (2010). Aluminum-rich belite sulfoaluminate cements Clinkering and early age hydration. *Cement and Concrete Research*. Vol 40. Pp 359–369

[MEI06] A. Meier, E. Bonaldi, G.M. Cella, W. Lipinski, D. Wuillemin (2006). Solar chemical reactor technology for industrial production of lime. *Solar Energy*. Vol 80 1355–1362

[MER07] G. Mertens, P. Madau, D. Durinck, B. Blanpain and J. Elsen (2007). Quantitative mineralogical analysis of hydraulic limes by X-ray diffraction. *Cement and Concrete Research*. Vol. 37, pp. 1524–1530

[MOH06] B. J. Mohr, J. J. Biernacki & K. E. Kurtis (2006). Microstructural and chemical effects of wet-dry cycling on pulp fiber-cement composites. *Cement and Concrete Research*. Vol 36 1240–1251.

[MON08] P. Monreal, L. B. M. Mamboundou, R. M. Dheilly & M. Quéneudec (2008). Evaluation de l'efficacité des traitements physicochimiques sur la performance de composites cimentaires lignocellulosiques confectionnés à partir de pulpes de betterave. ORGAGEC' 0 8. Université de Picardie - Jules Verne

[MON11] P. Monreal, L. B. M. Mamboundou, R. M. Dheilly & M. Quéneudec (20011). Effects of aggregate coating on the hygral properties of lignocellulosic composites. Cement & Concrete Composites. Vol. 33, 301–308.

[MOO11] R. J. Moon, A. Martini, J. Nairn, J. Simonsen & J. Youngblood (2011). Cellulose nanomaterials review: structure, properties and nanocomposites. *Chem. Soc. Rev.*, Vol. 40, pp. 3941–3994

[MOS06] J. Mosquerma, B. Silva, B. Prieto and A. Ruiz-Herrere (2006).Addition of cement tolime-based mortars: Effect on pore structure and vapor transport. *Cement and Concrete Research*. Vol. 36, pp. 1635-1642

[MOU09] P. Mounanga, P. Poullain, Guy Bastian, Patrick Glouannec, Hamid Khelifi (2009). Influence de la composition et du mode de mise en oeuvre sur le développement des propriétés mécaniques du béton de chanvre. *Rencontres de l'AUGC 2009, Sait Malo 3-5 juin*

[MUR83] M. Murat (1983). Hydration reaction and hardening of calcined clays and related minerals. I. Preliminary investigation on metakaolinite. *Cement and concrete research*. Vol. 13, pp. 259 - 266

[MSE] Agir pour une économie locale respectueuse des hommes et de l'environnement. Ecolodel, MATERIAUX ET SOLUTIONS ECOLOGIQUES (*http://www.ecolodeve.fr/Chanvre.html*)

[MUS10] J. Mussig (2010). Industrial Applications of Natural Fibres - Structure, Properties and Technical Applications. *A John Wiley and Sons, Ltd., Publication*

[NEV11] A. M. Neville (2011). Properties of Concrete – Fifth edition

[NGU06] T. H. Nguyen (2006). Influence de sous produits organiques d'origine d'agricole sur les caractéristiques d'usages des mortiers. *Mémoire du Master de Recherche de l'INSA Toulouse, Université de Toulouse*

[NGU10] T. T. Nguyen (2010). Contribution à l'étude de la formulation et du procédé de fabrication d'éléments de construction en béton de chanvre. *Thèse de doctorant*. *Université de Bretagne – SUD*

[NOR05] Nordisk Innovations Center (2005). Moisture Buffering of Building Materials. *Department of Civil Engineering, Technical University of Denmark.*

[NOZ12] V. Nozahic (2012). Vers une nouvellement démarche de conception des bétons de végétaux lignocellulosiques basée sur la compréhension et l'amélioration de l'interface liant/ végétal application à des granulats de chènevotte et tige de tournesol associés à un liant ponce/ chaux". *Thèse de doctorant. Université Blaise Pascal*

[NOZ12a] V. Nozahic, S. Amziane, G. Torrent, K. Saïdi and H. De Baynast, (2012). Design of green concrete made of plant-derived aggregates and a pumice–lime binder. *Cement & Concrete Composites*. Vol. 34, pp. 231-241

[OEC03] H. Takahiko (2003). Environmentally Sustainable Buildings Challenges and Policies. *Organisation for Economic Co-operation and Development*

[PAY12] J. Payá, M. V. Borrachero, J. Monzó, L. Soriano, M. M. Tashima (2012). A new geopolymeric binder from hydrated-carbonated cement. *Materials Letters*. Vol. 74, pp. 223–225

[PIC11] V. Picandet (2011). Biomaterials & Binders for Construction: European workshop in Darmstadt

[PIC12] V. Picandet, P. Tronet & C. Baley (2012). Caractérisation granulométrique des chènvottes. *XXXe Rencontres AUGC-IBPSA Chambéry, Savoie.*

[PER07] C. Perlot & Patrick Rougeau (2007). Intérêt des métakaolins dans les bétons

[POL13] M. Poletto, V. Pistor and A. J. Zattera (2013). Structural Characteristics and Thermal Properties of Native Cellulose

[PRI06] L. Price, S. De La Rue Du Can, J. Sinton & E. Worrell (2006). Sectoral Trends in Global Energy Use and GHG Emissions. *Lawrence Berkeley National Laboratory*

[RAF11] S. Rafat, & I.K. Mohammad (2011). Supplementary Cementing Materials. *Engineering Materials*

[RAM00] T. Ramlochana, M. Thomasa and K. A. Gruber (2000). The effect of metakaolin on alkalisilica reaction in concrete. *Cement and ConcreteResearch.* Vol. 30, pp. 339-344

[RAT13] R. V. Ratiarisoa (2013). Valorisation de résidus végétaux issus de la distillation de plantes aromatiques régionales pour la réalisation d'agromatériaux innovants. Rapport de Stage – Master 2 Recherche

[RIO09] C. A. Rios, C.D. Williams, M. A. Fullen (2009). Hydrothermal synthesis of hydrogarnet and tobermorite at 175°C from kaolinite and metakaolinite in the CaO–Al2O3–SiO2–H2O system: A comparative study. *Applied Clay Science.* Vol.43, pp. 228–237.

[ROD05] C. Rode, R. Peuhkuri, K. K. Hansen, B. Time, K. Svennberg, J. Arfvidsson and T. Ojanen (2005). Nordtest project on moisture buffer value of materials. *AIVC Conference "Energy performance regulation", Brussels, September 21-23, 2005*

[ROE04] S. Roesl, J. Carmeliet & H. Hens (2004). Interlaboratory Comparison of Hygric Properties of Porous Building Materials. *Journal of Thermal Envelope and Building Sience.* Vol. 27, pp. 1097 - 1963

[ROK05] G. Rokicki, P. Rakoczy, P. Parzuchowski & M. Sobiecki (2005). Hyperbranched aliphatic polyethers obtained from environmentally begin monomer: glycerol carbonate. Green Chemistry. Vol. 7, pp. 529 – 539

[ROW05] R. Rowell (2005). "Moisture properties," in Handbook Of Wood Chemistry And Wood Composites, R. Rowell, Ed.: CRC Press.

[SAB01] B. B. Sabir, S. Wild and J. Bai (2001). Metakaolin and calcined clays as

pozzolans for concrete: a review. Cement and Concrete Composites. Vol. 23, pp. 441-454

[SAI06] Saint Astier Data (2006). Mineralogy of binders – CO_2 emission of various binders

[SAN11] R. San Nicolas (2011). Approche performantielle des bétons avec métakaolins obtenus par calcination flash. *Thèse de doctorant. Université de Toulouse*

[SAN13] R. S. Nicolas, M. Cyr & G. Escadeillas (2013). Characteristics and applications of flash metakaolins. *Applied Clay Science*. Vol. 83-84, pp. 253 - 262

[SAV02] J. H. Savastano, V. M. John, V. Agopyan & O. Pellegrino Ferreira (2002). Weathering of vegetable fibreclinker free cement composites. Materials and Structures. Vol. 35, 64-68.

[SED07] D. Sedan (2007). Etude des interactions physico-chimiques aux interfaces fibres de chanvre ciment. *Thèse de doctorant. Université de Limoges.*

[SEM02] K. E. Semple, R. B. Cunningham & P. D. Evans (2002). The suitability of five Western Australian mallee eucalypt species for wood-cement composites. *Industrial Crops and Products*. Vol. 16, 89–100.

[SEP10] A. Sepulcre-Aguilar & F. Hernández-Olivares (2010). Assessment of phase formation in lime-based mortars with added metakaolin, Portland cement and sepiolite, for grouting of historic masonry. *Cement Concrete Research*. Vol. 40, 66-76

[SHI00] C. Shi & R. L. Day (2000). Pozzolanic reaction in the presence of chemical activators Part II. Reaction products and mechanism. *Cement Concrete Research*. Vol. 30, 607-613.

[SID12] R. Siddique & R. Bennacer (2012). Use of iron and steel industry by-product (GGBS) in cement paste and mortar. *Resources, Conservation and Recycling*. Vol. 69, pp. 29– 34

[SIL93] P. S. De Silva & F. P. Glasser (1993). Phase relations in the system $CaO-Al_2O_3$-SiO_2-H_2O relevant to metakaolin - calcium hydroxide hydration. Cement and Concrete Research. Vol. 23, pp. 627-639

[STR00] J. Straube (2000). Moisture proreperties of Plaster and Stucco for Strawbale Buildings. Report for Canada Mortgage and Holising Corporation

[TAZ95] E. Tazawa, S. Miyazawa & T. Kasai (1995). Chemical shrinkage and endogenous shrinkage of hydrating cement paste. *Cement and Concrete Research*. Vol. 25, pp. 288-292

[THO05] A. B. Thomsen, S. Rasmussen, V. Bohn, K. V. Nielsen and A. Thygesen (2005). Hemp raw materials: The effect ofcultivar, growth conditions and pretreatment on the chemical composition of the fibres. *Risø National Laboratory Roskilde, Denmark*

[TRA10] A. D. Tran Le (2010). Etude des transferts hygrothermiques dans le beton de chanvre et leur application au batiment. *Thèse de doctorant de l'Université de Reims Champagne-Ardenne*

[TRA10a] A. D. Tran Le, C. Maalouf, T. H. Mai, E. Wurtz, F. Collet (2010). Transient hygrothermal behaviour of a hemp concrete building envelope. *Energy and Buildings*. Vol. 42, pp. 1797–1806

[TRI12] Q. M. Trinh (2012). Utilisation du métakaolin par substitution du ciment dans les applications géotechniques d'injection et de scellement d'ancrage. *Thèse de doctorant, Université de Toulouse*

[TYD12] V. Tydlitát, J. Zákoutsky, M. Schmieder, R. Cerny (2012). Application of large-volume calorimetry for monitoring the early-stage hydration heat development in cement-based composites as a function of w/c. Thermochimica Acta. Vol. 546, pp. 44– 48

[VAL04] I. Valovirta & J. Vinha (2004). Water Vapor Permeability and Thermal Conductivity as a Function of Temperature and Relative Humidity. ASHRAE

[VEJ12] E. Vejmelková, M. Keppert, P. Rovnaníková, Z. Keršner and R. Cerny (2012). Application of burnt clay shale as pozzolanaddition to lime mortar. *Cement & Concrete Composites*. Vol. 34, pp. 486–492.

[VEJ12a] E. Vejmelková, M. Keppert, P. Rovnaníková, Z. Keršner and R. Cerny (2012). Mechanical, fracture-mechanical, hydric, thermal, and durability properties of limeme takaolin plasters for renovation of historical buildings. Construction and Building Materials. Vol. 31, pp. 22–28

[VEL09] A. L. Velosa, F. Rocha and R. Veiga (2009). Influence of chemical and mineralogical composition of metakaolin on mortar characteristics. *Acta Geodyn Geomater*. Vol. 153, pp. 121-126

[VER12] T. Verdier (2012). Valorisation de granulats végétaux dans un matériau de construction à matrice minérale. *Master thesis, Université de Toulouse*

[VIC99] C. Vick (1999). Adhesive bonding of wood materials, "in Wood handbook: wood as an engineering material. Vol. 113, W. U. F. S. Madison, Ed.: General technical report FPL.

[VIG96] M. R. Vignon, D. Dupeyre and C. Garcia-Jaldon (1996). Morphological characterization of steam-exploded hemp fibers and their utilization in polypropylene-ased composites. *Bioresource Technology*. Vol. 58, pp. 203-215.

[VOL02] F. A. Vollenbroek (2002). Sustainable development and the challenge of innovation. Journal of Cleaner Production. Volume 10 pp. 215–223

[UNC92] United Nations Conference on Environment and Development (1992). The Rio Declaration on Environment and Devenlopment

[UNC12] United Nations Conference on Sustainable Development (2012)

[UNE07] United Nations Environment Programme (2007). Buildings and Climate Change

[USG04] United State Green Building Council (2004). Building and Climate Change

[WIL98] S. Wild, J.M. Kinuthia, G.I. Jones & D.D. Higgins (1998). Effects of partial substitution of lime with ground granulated blast furnace slag (GGBS) on the strength properties of lime-stabilised sulphate-bearing clay soils. *Engineering geology*. 51, 37-53.

[ZIM05] Zimmermann, M., H.-J. Althaus & A. Haas (2005). Benchmarks for sustainable construction- A contribution to develop a standard. Energy and Buildings. Vol. 37, pp. 1147–1157